Chlorine Metallurgy—Part I

By W. J. KROLL

(*Consultant, Corvallis, Oregon, U.S.A.*)

OBJECTIONS to the use of chlorine or of chlorides in metal winning are often held by orthodox metallurgists for apparently sound reasons, one of the chief arguments being the corrosion of equipment. This point of view has not hindered the production of magnesium, calcium, lithium, sodium and cerium from their chlorides. With the development of new materials of construction, the corrosion problem is, or can be, minimized. Plastics and perhaps titanium and zirconium will permit elimination of some of the corrosion troubles. Thus the prospects of chlorine metallurgy have brightened.

The uses of chlorine or chlorides in metallurgy are many. Anhydrous chlorides may have to be made as a raw material for the production of metals by reduction with other more electronegative elements, or by fusion electrolysis. Iron may have to be extracted from low-grade nickel, chromium, aluminium or titanium ores for reasons of beneficiation. Alloy constituents may have to be removed with chlorine or with chloride fluxes and since the reactions involved lead mostly to equilibria, i.e. to mixed metals, alloys can also be made by reaction of metals with chlorides. The considerable drop in the price of chlorine in the last twenty years now permits applications of this reagent of which many metallurgists are not yet aware.

In their present state of underdevelopment, thermodynamics[1] are only of little help to the chlorine metallurgist and mistakes are being made by the over-confident use of thermal data. For instance, in aqueous solutions the affinity of nickel for chlorine is higher than that of copper; in a fused bath it is reversed[2], although publications and textbooks do not take notice of this fact[3]. Frequently the thermochemist is a poor chemist and he ignores the many unforeseen side reactions that take place, depending on the temperature. The reaction of HCl with FeO, for instance, described in a few lines in one report[3] took six publications and over 100 pages to be cleared up by another author[4] because of some temperature areas for the formation of hydrated products, of FeOCl and because of valency changes. The most important fact, left out entirely by the thermochemists, which is, however, essential to the metallurgist, is the "ignition" temperature or the knowledge of rates for a given temperature. While admittedly many factors interfere in the determination of these data especially the activity of the surfaces, even crude information would help in appraising the practical value of certain reactions. Many metals with a higher chlorine affinity have, against expectations, a higher ignition temperature in chlorine, and, based on this fact, the metal with the lower affinity might be removed without touching the other metal. Table I gives a general idea of ignition temperatures of oxide versus chlorine reactions as found in the literature. Reaction rates at various temperatures are also given by the authors referred to[5-7].

Most of the reactions of this Table are, at least to some degree, reversible (see below, equation 4). It may be noticed that NiO starts reacting at a lower temperature than Fe_2O_3 and Cb_2O_5 below Ta_2O_5. The order of decreasing chlorine attack on various oxides has been given by Barrett[8] as follows:—

$$Fe_2O_3 \rightarrow Cr_2O_3 \rightarrow MgO \rightarrow CaO \rightarrow TiO_2 \rightarrow ZrO_2 \rightarrow Al_2O_3 \rightarrow SiO_2$$

Similar ignition temperature data have been given for the chlorination of oxides in presence of carbon[5]. The reaction start depends evidently on various, especially physical, factors, which explains the sometimes considerable variations found by various authors.

Basic Reactions

The chemistry of chlorine metallurgy can be summarized in a few equations. A number of anhydrous chlorides can be prepared from aqueous solutions by crystallization or desiccation, but with many other chlorides hydrolysis takes place, which may also lead to oxychloride or basic salt formation.

This can be expressed by the following equations:—

1. Hydrolysis:
   - *a.* Metalchloride + $H_2O \rightleftharpoons$ Metal Hydroxide + HCl
   - *b.* Metalchloride + $H_2O \rightleftharpoons$ Metal Oxychloride + HCl

The reaction 1 *b* is especially disturbing in the production of anhydrous magnesium[9,10] and cerium chloride from aqueous solutions. Since there is an equilibrium involved, it is possible to shift the reaction to the left by passing excess hydrochloric gas over the oxychloride, whereby anhydrous chloride is obtained.

Some anhydrous chlorides cannot be obtained at all from the aqueous solutions or from oxychlorides even in the presence of excess HCl, as for instance $AlCl_3$, BeCl, and ZrCl. These

TABLE I—OXIDES VERSUS CHLORINE. REACTION START

Oxide	Temp. of React. Start in °C.	Compound formed	Reference
ZnO	150; 350	Chloride	24
PbO	200	Chloride	24
CdO	450	Chloride	24
Fe_2O_3	400; 500; 525	Chloride	5, 14, 24
Al_2O_3	1250; 800; 1000; 850	Chloride	5, 6, 7, 14
Cr_2O_3	500	Chloride	5, 6
MoO_3	300; 500	Oxychlor	6, 7
WO_3	500; 750	Oxychlor	6, 7
V_2O_5	550	Oxychlor	7
NiO	200	Chloride	5, 6
BeO	600; 1000	Chloride	7, 14
TiO_2	850	Chloride	7
Ta_2O_5	>1200	Chloride	7
Cb_2O_5	900	Chloride	7
B_2O_3	>900	Chloride	7
U_3O_8	950	Oxychlor	7
SiO_2	>1200	Chloride	8, 14
MnO	250	Chloride	6
CoO	250	Chloride	6
MgO	350	Chloride	22

are prepared by the Oerstedt[11] method of oxide chlorination in the presence of carbon, as expressed by the equation.

2. Reduction chlorination:

$$MeO + 2\,C + Cl_2 \rightleftharpoons MeCl_2 + CO/CO_2$$

In a much broader conception of the same idea other elementary reducing agents, such as sulphur, or hydrogen, or combined ones such as CO, CH_4 can be used in mixture with chlorine. The latter may even be directly tied up with reducing agents in the form of compounds, which have to be broken up to transfer their chlorine and to bind oxygen. These are, for instance: HCl, NH_4Cl, $SiCl_4$, S_2Cl_2, BCl_3, CCl_4, $SOCl_2$[12a] and $COCl_2$. The reactions relating to the oxide-chloride exchanges will be discussed later.

In the presence of excess chlorine, CO forms phosgene within the temperature stability range of the latter, i.e. up to about 700°C. The ratio CO/CO_2 of the waste gases depends on the temperature, on the excess of carbon used and on the thickness of the layer through which CO_2 will filter in contact with unreacted carbon with which it reacts according to:—

3. Carbon monoxide formation:

$$C + CO_2 \rightleftharpoons 2\,CO.$$

The reaction is reversible and proceeds to the left at about 500°C. in the presence of catalysts. It is therefore of no practical value to discuss whether the reaction No. 2 takes place with predominant CO or CO_2 evolution. The composition of the gases varies with the location in the chlorinator from which they are taken. In some cases the exhaust gases may be very rich in CO_2 especially when the bed used is shallow, and when the chlorination takes place at low temperature. With phosgene as chlorinating agent the exit gases are practically free from CO, the reduction proceeding to the end point with formation of carbon dioxide.

The chlorination product is not necessarily an anhydrous chloride. Oxychlorides of various elements may also form, as for instance those of W, V and Mo, and these will be further reduced only in the presence of excess reducing agent and chlorine. The stability of such oxychlorides under these conditions has only partially been investigated. The complete removal of oxygen from vanadium oxychloride is a difficult task.

The physical state of the chlorides obtained has considerable bearing on the success of the chlorination. With volatile chlorides such as those of Zr, Ti and Be the elimination of the reaction product is easy since it is gaseous and it can be collected as liquid or solid in a condenser of some kind. If fused at the chlorination temperature, the chlorides impregnate the reaction mixture as do $MnCl_2$ and $MgCl_2$, and then only chlorination of porous briquettes, on a bed of carbon, which permits percolation by excess chlorine, leads to success. The fused salts can be tapped. With chromium oxide, the multivalency causes considerable trouble[12b,12c] because of the various melting and boiling points of the chlorides formed. $CrCl_2$ melts at 824°C. and boils at 1302°C., while $CrCl_3$ starts subliming at about 920°C. Excess chlorine may bring about formation of the unstable $CrCl_4$[13]. To volatilize chromium as $CrCl_3$ a considerable excess of chlorine must be maintained but the formation of $CrCl_4$ is so fast that the batch plugs up with solid dichloride, or, when a higher temperature is used, it fuses and impregnates the batch to such an extent that the surface accessible to the chlorine is greatly reduced. Therefore the temperature has to be brought up to above 1000°C. while maintaining a considerable excess of chlorine, to inhibit the dissociation of any trichloride formed and to chlorinate up the dichloride which impregnates the batch. The chloride formed in this way is mostly trivalent.

Free silica is not chlorinated in the presence of carbon except above 1200°C.[14,8]. However, silica tied up as silicate, for instance in clay[15] or in zircon[16], readily chlorinates together with the oxide with which it is associated.

In any chlorination of oxides side reactions must be expected; of these, many concern exchanges between oxides and chlorides. These can be derived directly from the equilibria between chlorine and oxides, as expressed by the following equations:—

4. Chlorine versus oxides:

$$MeO_y + \frac{x}{2}\,Cl_2 \rightleftharpoons MeCl_x + \frac{y}{2}\,O_2$$

(see Table I)

5. Chlorides versus oxides:

$$Me_xCl_2 + Me_yO \rightleftharpoons Me_yCl_2 + Me_xO$$

(see Table II).

Both reactions are reversible. This means that relation 4 permits the production of chlorine with oxygen as well as oxygen with chlorine, using chloride or oxide respectively as a reagent. These exchanges depend largely upon temperature. Typical examples of the oxidation of chlorides are those of HCl[17,18], $FeCl_2$[19], $CrCl_2$ as well as that of the chlorides of Si[20], Al, Zr, Sb, Zn, Be, B, Cd, Co, Ni, V, Mo, Mg[21,22]. All these chlorides are oxidized with air or oxygen at elevated temperature.

A new titanium pigment industry, based on the oxidation of titanium tetrachloride is in the making. This will free the titanium pigment industry from the use of sulphur. Silicon tetrachloride can be burned in oxygen by a similar process[20] as shown in a report on German industries.

Equation 4 is important in the production of anhydrous, oxide-free $ZrCl_4$ and $BeCl_2$, since both chlorides, when exposed to air at their condensation temperature, revert partly to oxide and chlorine. It also plays a role in chloridizing roasting, copper oxide among other oxides being chlorinated by free chlorine, generated within the batch[23]. Zinc oxide can also be attacked directly by chlorine[24].

Reaction 5 has already been mentioned above, in connection with chlorides of a reducing character. When the base metal forming the chloride is also a good reducing agent, this chloride may act like a combined chlorinating and reducing agent. For instance HCl reduces and chlorinates MgO[10], TiCl and BCl_3 attack

TABLE II—OXIDES VERSUS CHLORIDES

Oxide	Chloride	References	Oxide	Chloride	References
CuO	$SiCl_4$	27	Al_2O_3	BCl_3	25
BeO	same	27			
MgO	same	27; *a*	SiO_2	BCl_3	25
CaO	same	27; *a*			
ZnO	same	27	SiO_2	$ZrCl_4$	26
B_2O_3	same	27			
TiO_2	same	27	SiO_2	$ThCl_4$	26
SnO_2	same	27	SiO_2	$BeCl_2$	*d*
Cr_2O_3	same	27	SiO_2	NaCl	8
MoO_3	same	27	ZnO	$MnCl_2$	25
MnO_2	same	27	ZnO	$FeCl_3$	25; *e*
Fe_2O_3	same	27	MgO	$PbCl_2$	*e*
			CuO	$PbCl_2$	*e*
Al_2O_3	same	27	MgO	$ZnCl_2$	*e*
			PbO	$SnCl_2$	*f*
NiO	same	27	BaO	$NiCl_2$	*g*
			BaO	AgCl	*g*
Fe_2O_3	$TiCl_4$	*b*	BaO	$PbCl_2$	*g*
			BaO	TlCl	*g*
CaO	$TiCl_4$	*a*	CaO	$FeCl_3$	*a*
CaO	$NiCl_2$	*c*	CaO	$MgCl_2$	*a*
V_2O_5	$CaCl_2$	35	CaO	$ZnCl_2$	*a*
			CaO	$SnCl_4$	*a*
			MgO	$AlCl_3$	*a*

(*a*) C. Daubree: *Comptes Rendus* 1853; 39, 135. (*b*) C. Pascaud. loc. cit, 1951 231, 1232. (*c*) H. J. M. E. Clerc. *Fr. Pat.* 36,617, 1929 addition 669,109, 1928. (*d*) H. A. Sloman. *J. Inst. Met.*, 1932, 49, 377. (*e*) E. A. Ashcroft. *U.S. Pat.*, 1,388,086, 1921. *id* and J. Swinburn. *Trans. Amer. Electrochem. Soc.*, 1904, 6, 80. *id. U.S. Pat.* 695126, 1902. E. Zielinski. *Chem. Abs.* 1934, 28, 437 and *Arch Erzbergbau Erzaufbereit* 1931, 1, 31. G. G. Urazov *Chem Abs.*, 1936, 30, 8109. A. Bagdasarian. *U.S. Pat.* 1,671,003, 1925. (*f*) G. Behr. *Metals Technology, Secondary Metals' Symposium*, October, 1943, AIME. (*g*) J. A. Hedvall, E. Garping, N. Lindekrantz and L. Nelson: *Z. anorg. Chem.*, 1931, 197, 399.

quartz[25,26]. $SiCl_4$, which is always present in the chlorination of siliceous ores, is also an excellent chlorinating agent for a great many oxides[27] and it may be classified among the group of reducing and chlorinating reagents, such as $COCl_2$, which work according to the principle of equation 2. Table II gives a number of such exchanges, as quoted in the literature. The more common ones taking place between NaCl, $CaCl_2$, $MgCl_2$ - have been omitted. It may be deduced from this Table how complex is the chemistry in the various levels of a chlorinator in which ores and mixtures of oxides are being treated, especially when by-products such as $SiCl_4$ and $AlCl_3$ are formed.

Relation 5 does not always yield a pure chloride. Sometimes an oxychloride is produced, whenever such compound is stable enough within the given temperature range. On the other hand new oxide double compounds can also be produced either between the elements involved, or with the oxides of one of these; the latter resulting in a switch of valency. This happens frequently with iron, which readily produces Fe_3O_4 from its trivalent chloride.

The reaction between silica and NaCl[8] does not yield $SiCl_4$ but free chlorine because of the formation of sodium silicate. This will be discussed below.

Oxide-chloride equilibrium reactions can be pushed one way by side reactions brought about by the addition to the reaction mixture of an oxidic radical, generally of an acid nature, capable of forming a strongly exothermic double compound with the new oxide formed. As such one may use: SiO_2, SO_3, P_2O_5, CO_2 or even Al_2O_3, which latter is amphoteric. These radicals may be already tied up in some way, as for instance in silicates, phosphates and carbonates and, provided this tie is not a strong one, it can be split. This means that silicate ores can be used instead of free silica which is important in the treatment of siliceous ores, which are usually hard to process. Chloridizing roasting can be expressed by the following typical equations:—

6. Assisted oxide-chloride exchange[28,29,30,31,32]:

a. $MeO + SiO_2 + CaCl_2 = MeCl_2 + CaO.SiO_2$

b. $MeO + SO_2 + \frac{1}{2}O_2 + 2\,NaCl = MeCl_2 + Na_2SO_4$

Whether the one or the other equation has to be used, depends mainly on the temperature and on the method of recovery of the chloride. This can either be extracted from the reaction cake by leaching, eventually with the help of solvents (sodium thiosulphate for AgCl), or it can be volatilized at high temperature. Reaction 6 *b* is not well adapted to chloridizing volatilization (except to that of platinum and gold[33], which takes place at low temperature) because the charge would melt. Silica is commonly used as an addition in chloridizing volatilization, according to relation 6 *a*, in combination with an alkaline earth metal chloride because of the rather high melting point of the silicate formed. This permits driving off the chlorides before fusion takes place, either because their boiling point is reached, or because they are carried off by partial pressure of their vapour in the furnace gases.

Chloridizing roasting, according to equation 6 *b*, operates with cheap pyrites as a source for sulphur. Other sulphides are usable as well. Naturally, since SO_3 has to be formed, oxidizing conditions have to prevail over the batch. This may cause losses of such chlorides as are readily oxidized, but, on the other hand, it also holds down chloride formation of some elements which would have to be extracted and separated from the cake by wet methods. Sodium sulphate is formed in the chlorination, which salt is thermally very stable. If calcium chloride were used instead of NaCl, calcium sulphate, which is still more stable, would be obtained, since sodium chloride does not react with it.

The fusibility of sodium sulphate-chloride mixtures interferes frequently with the chloridizing roasting, because the exchange of the batch with the chlorine of the furnace atmosphere is reduced by impregnation. The origin of this chlorine must be explained. It results from the reaction of sodium chloride with air and SO_2 according to:—

7. Chlorine generation:

$2\,NaCl + SO_2 + O_2 = Na_2SO_4 + Cl_2$.

This reaction has repeatedly been proposed, especially in wartime, for the production of chlorine by plain chemistry, without having to produce sodium hydroxide as a by-product of an aqueous electrolysis. Other radicals such as SiO_2, Al_2O_3 and even CO_2 also liberate chlorine by the mechanism of equation 7 and may replace $SO_2 + O_2$. In the presence of water vapour hydrochloric acid gas is obtained, the oxygen needed to form sodium sulphate being partly taken from the water, as shown by the relation:—

8: $2\,NaCl + SO_2 + \frac{1}{2}O_2 + H_2O = Na_2SO_4 + 2\,HCl$.

This equation is the basis of the old Hargreaves process of hydrochloric acid production. The presence of HCl in chloridizing roasting may cause trouble because of corrosion and formation of hydrolyzed condensates.

Naturally, when oxidizing pyrites in the presence of metal oxides, various sulphates can be formed, as for instance those of iron, copper, nickel and lead, the thermal stability of which is important in so far as most sulphates can be extracted by aqueous methods. Thermal stability can be expressed approximately as follows in decreasing order, for medium temperatures:—

$CaSO_4$, $MgSO_4$, $PbSO_4$, Ag_2SO_4, $MnSO_4$, $CoSO_4$, $NiSO_4$, $ZnSO_4$, $CuSO_4$, $FeSO_4$.

These sulphates react with excess sodium chloride (or calcium chloride) producing sodium (or calcium) sulphate and anhydrous chlorides. The reactions of the sulphates of Mg, Al, Fe, Zn, Mn, Cu, Ni, Pb with sodium chloride have been described in the literature[34,35].

The kind of ores, to which chloridizing roasting applies, is not well defined. Usually this method is recommended for silicate or sulphide ores containing lithium, gold, silver, platinum, lead, copper, zinc, arsenic and antimony. Zinc ores behave erratically. Arsenic and antimony are volatilized. Neither zircon nor beryl are attacked by $CaCl_2$ or $MgCl_2$ nor do these chlorides react with BeO and ZrO_2 up to 1000°C.

The reversibility of reaction 4 is usually overlooked by metallurgists. The oxidation of chlorides by air or oxygen, which is conditioned largely by temperature, may be expressed in increasing order for red heat roughly as follows:—

$AgCl$, Hg_2Cl_2, $PbCl_2$, $CdCl_2$, $CaCl_2$, $LiCl$, $MnCl_2$, Cu_2Cl_2, $ZnCl_2$, $SnCl_2$, $NiCl_2$, $FeCl_2$, $MgCl_2$, $CrCl_2$, $SnCl_4$, $TiCl_4$, $ZrCl_4$, $AlCl_3$, $SiCl_4$.

In industrial furnaces using chloridizing roasting, conditions are usually oxidizing because of the presence of O_2, CO_2, H_2O in the combustion gases and only the most stable chlorides can be prevented from being oxidized as are those of Ag, Pb, Zn, As, Sb and Cu and only the oxides of these metals are chlorinated. Platinum and gold chlorides dissociate at relatively low temperatures but can be volatilized even in air, since both metals, as well as silver, form no stable oxides[33]. Gold chloride is said to be stabilized by other chlorides and its dissociation can be held back by maintaining a large excess of chlorine over the batch[36]. Chlorination of oxidized platinum-nickel-copper ores with $NaNO_3$ and NaCl is reported[33]. The operation takes place at 600°–700°C. and the ores are leached afterwards. Iron and nickel chloride are not usually found in large quantities in the reacted product if there is not a large excess of chlorine in the furnace atmosphere since their oxidation by furnace gases is usual in the standard industrial furnaces such as rotary kilns or Wedge furnaces. Chlorination of oxides or oxidation of chlorides may sometimes proceed only half way, with formation of oxychlorides (W, Mo, V).

If the chloridizing takes place in complete absence of air, for instance in a vacuum or in a neutral gas, these chlorides can be prevented from being oxidized and can be reclaimed[37,38] as shown by some patents concerning iron extraction from low grade ores[39].

Chloridizing roasting may be followed by aqueous extraction, eventually with the use of specific solvents such as sodium thiosulphate and cyanide. Otherwise the chlorides, if sufficiently volatile, can be driven off

(*Continued on page 252*)

experience in dealing with the foundry problems and advising the clients of an important producer of aluminium and backed by the well-known Neuhausen Research Laboratories. A large number of neat and instructive drawings, photographs and graphs illustrate the description.

There is no doubt that this book will be very useful to the average aluminium foundryman, both the beginner and the slightly more experienced worker.

The reviewer may be permitted to mention some points which struck him as likely to produce slightly distorted ideas in the mind of the inexperienced reader.

In dealing with sorting of aluminium scrap, it would seem necessary to emphasize more strongly the severe limitations of the very interesting new methods of eddy current test (Wirbelstrom-Verfahren) and measurement of electrolytic potential. As the properties measured are not only dependent on the alloy composition but also strongly influenced by heat-treatment, every case of application of these methods needs individual examination. There will remain only a very limited number of really useful applications.

On p. 117 the author makes a statement which could produce the impression that one cannot expect a remelt alloy to be resistant to weather or sea water, to have really high mechanical properties or to take a good anodic coating. The author probably does not intend to produce exactly this impression, but it would be useful to state clearly that the alloying industry has proved capable of producing very high quality material meeting exacting aircraft specifications and certainly permitting the use of suitable alloy types in exposure to weather, sea water and to exacting mechanical conditions along with metal alloyed from virgin aluminium.

In dealing with fluxes the reviewer is not in agreement with the author's emphasis on the solubility of alumina in cryolite. There is no indication that this feature has any significant influence under the conditions under which fluxes work in the foundry. Fluxes completely free from fluorides have been, and are being, used with complete success in separating alumina from liquid aluminium and there is every indication that the surface tension is responsible for the flux lifting the alumina film bodily from the liquid metal surface and enveloping it in liquid flux.

The important effect of gas content in remedying shrinkage and hot-shortness defects in thin walled castings of certain alloys merits more emphasis than it receives in the book. This remedy is in world-wide use mostly applied secretly and with a guilty conscience. The sooner this game of hide-and-seek stops and gives room to an open and well-controlled procedure, the better for both the founder and the user of castings.

These criticisms of detail do not alter the very favourable impression the reviewer obtained from the reading of Mr. Irmann's book.

E. S.

Chlorine Metallurgy—*Continued from page 245*

at their boiling point or even at lower temperature by their partial pressure in the exit gases. SiO_2 is used in this case instead of SO_2+O_2 as a reagent to boost the reaction because of the higher temperature needed for volatilization of the chlorides. This method has been recommended, for instance, for the production of lithium chloride from spodumen using calcium chloride as carrier for the chlorine[40]. A vacuum has been proposed for the same purpose[41,37].

Despite the fact that chloridizing roasting and volatilization is a very old process, and that it has been tried by many metallurgists, its use is, at present, very limited. The main reason is the corrosive nature of the chlorides and the difficulty of accurate control of the tricky chemistry concerned. Chloridizing roasting is bound to make progress once suitable furnaces can be built which permit operation in the absence or with controlled amounts, of oxygen[38]. Present-day rotary kilns and Wedge or Herreshof furnaces are entirely unsuitable for this purpose because of the reaction of the chlorides with furnace gases.

Selective reduction of one of the oxides of the ore may permit separation by subsequent chlorination with elementary chlorine which attacks only the reduced metal. To be successful strict temperature limits must be observed in the reduction as well as in the chlorination step (see equation 4).

(To be continued)

References

[1] H. Villa; *J. Soc. Chem. Ind.*, 1950, 69, supplement, 9.
[2] W. J. Kroll; Canadian Patents 441,144 and 441,145, 1947.
[3] H. Kellogg; *Trans. A.I.M.E.*, 1950, 188, 862.
[4] H. Schaefer; *Z. anorg. Chem.*, 1949, 259, 53, 75; *id., loc. cit.*, 1949, 259, 265; *id., loc. cit.*, 1950, 261, 142; *id., loc. cit.*, 1949, 260, 127; *id., loc. cit.*, 1949, 260, 279; *id. loc. cit.*, 1951, 264, 230.
[5] P. S. Lebedev; *Moscow Inst. Refer. Chem. Alot.*, 1936, 30, 2886.
[6] P. Wahsmut; *Z. ang. Chem.*, 1930, 43, 98.
[7] W. Kangro and R. Jahn; *Z. anorg. Chem.*, 1933, 210, 325.
[8] L. R. Barrett, F. H. Clews and A. T. Green; *Brit. Ceramic Soc.*, 1942, 41, 197; *id.* Gas Research Board Copyright Publ. No. 2, 1940.
[9] C. M. Shigley; *Trans. A.I.M.E.*, 1949, 281, 59.
[10] W. Moldenhauer; *Z. anorg. Chem.*, 1906, 51, 369; Gmelin's "Handbuch der anorganischen Chemie," Magnesium, System No. 27, 112.
[11] Oerstedt; *Pogg Ann*, 1825, 5, 132.
[12a] H. Hecht; *Z. anorg. Chem.*, 1947, 254, 37; *id.* and G. Jander, H. Schlapman; *loc. cit.* 1947, 254, 255.
[12b] C. G. Maier: Bur of Mines Bul. 463, 1942; *id.* U.S. Pat. 2,133,997, 1939; *id.* U.S. Pat. 2,133,998, 1939.
[12c] J. E. Muskatt and Pittsburgh Glass Company; U.S. Pat. 2,185,218, 1940; *id.* U.S. Pat. 2,240,345, 1941; *id.* U.S. Pat. 2,311,458, 1943; *id.* U.S. Pat. 2,325,192, 1943; *id.* U.S. Pat. 2,311,459, 1943; *id.* U.S. Pat. 2,349,747, 1944.
[13] H. A. Doerner; Bureau of Mines Tech. Paper 577, 1937.
[14] V. Spitzin; *Z. anorg. Chem.*, 1930, 189, 337.
[15] A. M. McAfee; *Chem. Met. Eng.*, 1929, 36, 422.
[16] W. J. Kroll, A. W. Schlechten and L. A. Yerkes; *Trans. Electrochem. Soc.*, 1946, 89, 263.
[17] K. C. Rule; Fiat Final Report 833. PB 37,782.
[18] W. M. Grosvenor and J. Miller; U.S. Pat. 2,206,399, 1940.
[19] Ph. Galmiche; *Ann. Chim.* (12), 1948, 3, 243.
[20] C. H. Love and F. H. McBerty; Fiat Final Report 743, 1946, PB 22,624.
[21] I. E Muskat; U.S. Pat. 2,333,948, 1943.
[22] W. Moldenhauer; *Z. anorg. Chem.*, 1906, 51, 373.
[23] von Kothny; *Metallurgie*, 1911, 8, 389.
[24] C. G. Maier; *Eng. and Min. Journ.*, 115 (23), 51.
[25] L. Troost and P. Hautefeuille; *Ann. Chim. Phys.*, 1846, 7, 476; *Comptes Rendus*, 1872, 57, 1819.
[26] W. Fischer, G. Gewehr and H. Winchen; *Z. anorg. Chem.*, 1939, 242, 162.
[27] G. Rauter; *Liebigs Annalen*, 1892, 270, 235.
[28] F. R. Hieman; *Metall u. Erz*, 1930, 27, 474.
[29] A. L. Engel and H. J. Heinen; Bureau of Mines R.I. 4612, 1949; *id.*, Bureau of Mines R.I. 4582, 1950.
[30] S. A. Lyon and O. C. Ralston; Bureau of Mines Bull. 157.
[31] D. M. Liddell; "Handbook of Nonferrous Metallurgy," Part II, McGraw Hill Editors, 1945, 527, 665.
[32] Th. Varley; Bureau of Mines R.I. 2247, 1921.
[33] C. Goetze; *Metall u. Erz.*, 1932, 29, 313.
[34] Gmelin's "Handbuch der anorganischen Chemie," Verlag Chemie, 1928, System No. 21, Natrium, 538.
[35] G. Gin; *Trans. Amer. Electrochem. Soc.*, 1909, 16, 422.
[36] Th. Varley, E. P. Barrett, C. C. Stevenson and R. H. Bradford; Bureau of Mines Bull. 211, 1923.
[37] H. de Wet Erasmus; U.S. Pat. 2,490,184, 1949.
[38] S. Ganelin; U.S. Pat. 396,740, 1921.
[39] M. H. Caron; French Pat. 965,786, 1950.
[40] F. Fraas and O. C. Ralston; Bureau of Mines Report No. 3344, 1937.
[41] H. de Wet Erasmus; U.S. Pat. 2,561,439, 1951.

Chlorine Metallurgy—Part II

By W. J. KROLL

(*Consultant, Corvallis, Oregon, U.S.A.*)

(*Continued from* METAL INDUSTRY, *September* 26, 1952)

WITH multivalent metals, the various chlorides formed possess different degrees of thermal stability, as expressed by their tendency to dissociate, to "disproportionate" or to react with other elements and compounds. Some of the chlorides become progressively weaker with increasing temperature and dissociate with liberation of chlorine. Others are stable only within definite temperature limits and they form only at elevated temperatures by dissolving more of the element of which they are constituted. Conversely this element is precipitated by "disproportioning" on cooling. While the higher chlorides display more the properties of chlorine, resembling in that respect peroxides which act more like oxygen, the lower chlorides have more the character of the element dissolved in them.

Higher chlorides may be represented by the prototypes: $CrCl_3$, $CuCl_2$, VCl_4 and $FeCl_3$. Lower ones are, for instance, $TiCl_2$ and AlCl.

Typical reactions of higher chlorides, which involve only the loose last chlorine atom, can be performed with $FeCl_3$. For instance CO reacts with this compound as follows[5]:—

9. Phosgene formation.

$$CO + 2\ FeCl_3 = 2\ FeCl_2 + COCl_2.$$

Phosgene, which is obtained, is known to be itself a weak compound. This shows how little is required to detach the last chlorine atom from $FeCl_3$.

As a matter of fact, $FeCl_3$ can be used instead of chlorine to bring about the chlorination of oxides in the presence of carbon with the "nascent" chlorine which it readily gives off, as shown in the next equation:—

10. Chlorination with $FeCl_3$:

$$2\ MgO + 4\ FeCl_3 + C = 2\ MgCl_2 + 4\ FeCl_2 + CO_2.$$

Naturally this loose chlorine atom can be used also to react with more iron or with some other metals, which it chlorinates very actively; or it may attack and chlorinate various compounds as shown by the equations:—

11. $Fe + 2\ FeCl_3 = 3\ FeCl_2$

12. $2\ FeCl_3 + Cu_2S = 2\ FeCl_2 + 2\ CuCl + S.$

The back reaction of iron crystals deposited at the cathode in the fusion electrolysis of iron chlorides in a carrier salt with $FeCl_3$, formed at the anode, reduces the current efficiency considerably (see equation 11). Similar conditions prevail in the titanium and zirconium chloride electrolysis.

While $TiCl_4$ is much more stable than $FeCl_3$, its last chlorine atoms can also be knocked off with other elements, with alloys, compounds or with titanium itself whereby lower titanium chlorides are obtained. This is shown[42] by the following equations which include also $TiCl_3$:—

13. $3\ TiCl_4 + Ti \rightleftharpoons 4\ TiCl_3$

14. $2\ TiCl_3 + Ti \rightleftharpoons 3\ TiCl_2$

15. $TiCl_4 + Ti \rightleftharpoons 2\ TiCl_2.$

These are reversible reactions and conversely titanium metal can be precipitated from the lower compounds under certain conditions of temperature. $TiCl_3$ is the more stable of the two compounds formed, but it decomposes at 450°C. as follows:—

16. $2TiCl_3 \rightleftharpoons TiCl_2 + TiCl_4.$

Since the temperature areas of these reactions overlap, mixed chlorides are usually obtained and the pure compounds are difficult to make. The trichloride is violet, the dichloride is black and pyrophoric. It is doubtful whether the latter has ever been produced in the pure state and the products obtained are always contaminated with titanium, probably because $TiCl_2$ "disproportionates" under certain conditions of cooling according to equations 14 and 15. The temperature areas of formation or decomposition have only vaguely been determined. Formation of $TiCl_3$, according to equation 13, takes place at about 600°C. in a pressure tube. $TiCl_2$ forms at 850°C. in a pressure tube but dissociates completely in a vacuum at the same temperature, as indicated in equation 15. Titanium production methods, based on this chemistry, have been proposed.

While the nature of these lower chlorides is fairly well established this was not so with many others until a short time ago. It is a fact, known for many years, that the metals Ba, Ca, Sr, Mg, Na, K, Zn, Cd, Pb and others dissolve in their own chlorides, and formation of lower chlorides of the $TiCl_2$ type was suspected. When cooling, the "sub-chloride" of the metal dissolved precipitates out as a fog. This phenomenon was well described by Lorenz[43] in the fusion electrolysis of chlorides. Fog formation was intensified by the presence of moisture or oxides in the bath, which made coalescing of the precipitate more difficult. Recently Cubiciotti[44] put the formation of these lower chlorides in doubt, and claimed that the metals in question dissolve as such in the salts. He established the equilibrium diagrams of such chloride-metal mixtures, of which the one concerning $Ba/BaCl_2$ is reproduced as Fig. 1. He gave the following solubility Table for various metal chloride mixtures:—

TABLE III—SOLUBILITY OF VARIOUS METALS IN THEIR CHLORIDES

Metal	Solubility Mol per cent	Temperature in °C
Mg	1·2	900
Ca	16·0	900
Sr	20 appr.	900
Ba	30	900
Zn	10^{-4}	500
Cd	16	650
Ce	33	?
K	1	?

The fact that barium dissolves to a very large extent in its chloride makes it impossible to produce this metal by fusion electrolysis. Addition of other salts, such as NaCl, lowers the solubility and fog formation, as shown by Lorenz. It may be noticed that barium metal also dissolves barium chloride. If the metal could be produced from its chloride, the separation from this salt might prove quite difficult. This

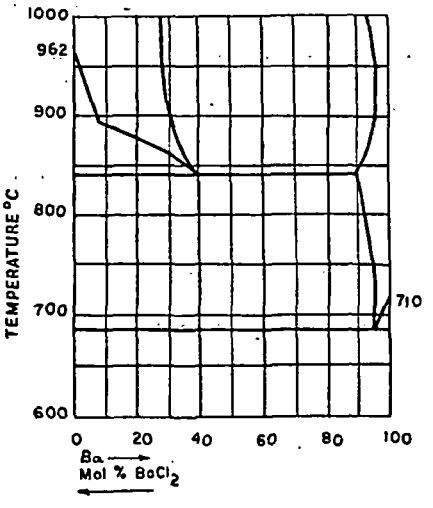

Fig. 1—Equilibrium diagram $BaCl_2/Ba$. See ref. 44

also concerns electrolytic calcium. In getters, chlorine is a poison.

A curious observation was made years ago by Peczalski[45], who discovered that solid copper dissolves many fused chlorides such as those of Ba, Ca, Na, K, Mg, Fe and Al. A kind of copper-salt alloy is formed in this way and the copper is disintegrated. On dissolving in water, copper powder is obtained. Whether this is caused by the formation of an unknown lower copper chloride, or by the mechanism described by Cubiciotti would be worth investigation.

The use of aluminium subchloride in the extraction of aluminium from scrap has been proposed, and this case may therefore be examined also. This new field of metallurgy was opened in 1939 by Wilmore[46] who stated in a patent that aluminium can be volatilized at 1000°C. *in vacuo*, when heated in mixture with AlF_3. The formation of aluminium subchlorides had been mentioned before by a number of authors[47] but Klemm[48] first brought some more definite proof about the existence of such compounds.

When gaseous $AlCl_3$, which compound sublimes at 182·7°C. and melts at 190°C. under a pressure of 2 atmospheres, is passed over pure aluminium in the absence of air, at high temperature, aluminium is carried over in the condensate together with the chloride. The condensate obtained after cooling is constituted, as shown by X-ray analysis, of highly dispersed aluminium in pure $AlCl_3$. The mechanism of this "catalytic distillation" can be represented by the relation:

17. $AlCl_3 + 2\,Al \rightleftharpoons 3\,AlCl$

Similar results have been obtained with the other aluminium halogenides. A summary of the literature of this case is given in the bibliography[46,49,50,51,52,53,54,55]. Weiss[54] found that the AlCl content of the gases obtained when passing $AlCl_3$ over aluminium at atmospheric pressure is 52 per cent at 1000°C., 86 per cent at 1100°C. and 98 per cent at 1200°C. At such temperatures the vapour pressure of aluminium metal is much too low to cause any evaporation. Weiss[54] calculates the energy required to carry over one kilo of aluminium as monochloride to amount to 1·78 kilowatt-hours. Gross[49,50] estimates the heat of formation of AlCl at minus 11·58 Calories, the compound being endothermic. Foster[53] establishes the existence of AlCl by spectrographic methods. Similar, volatile lower aluminium compounds such as AlO and AlS have been described.

The separation of the condensate obtained from the aluminium may take place by evaporation of the $AlCl_3$ at low temperatures, or by fluxing it with other chlorides such as NaCl or KCl. Ardalverk[55] proposes direct high temperature dissolution of aluminium scrap with fluxes, containing $AlCl_3$, separation of the AlCl bearing salts from the undissolved foreign metals by decantation at high temperature, cooling and decantation of the aluminium from the flux. Klemm[56] uses a vacuum in his experiments.

Lower chlorides are powerful reducing agents, since they contain excess metal in readily available form. They are frequently pyrophoric and usually unstable in air. They attack a great many refractories, which they reduce, and with metals they cause alloy formation as shown by Gross[50] and others according to:—

18. $9\,AlCl + 2\,Fe \rightleftharpoons 2\,FeAl_3 + 3\,AlCl_3$

19. $3\,AlCl + Cu \rightleftharpoons CuAl_2 + AlCl_3$.

With graphite, Al_4C_3 is formed. Lower chlorides may be useful in brazing and welding fluxes.

Direct reduction of $AlCl_3$ to subchloride by other metals may explain the plating observed even in such cases, when the affinities of aluminium and that of the reducing agent are far apart ($AlCl_3$ + Fe or Cu). Intermetallic compound formation favours the breaking up of the subchloride formed.

Aluminium trichloride attacks a great many refractories as shown in Table II. This, as well as the alloy formation described makes it very difficult to put catalytic distillation into practice[49,50] as far as the container and heating means are concerned. This is even worse for the production of titanium from $TiCl_3$.

Gross[51] in a patent extends the subchloride idea to other metals and he very broadly claims that similar separations can be obtained by formation of BCl, CoCl, FeCl, NiCl, SnCl, GeCl and TiCl. It had been observed[52] that in treating Fe-, Si- and Cu-bearing aluminium with $AlCl_3$ there was an appreciable and unexplainable volatilization of these elements. Whether such lower chlorides exist, will have to be established by further experiments.

Valency Changes and Sulphide Reactions

In reactions of chlorides of multivalent metals with oxygen or with oxides there is frequently a shift of valencies, as can be shown by the following examples[57,58,59,60]:—

20. $2\,SnCl_2 + O_2 \rightleftharpoons SnCl_4 + SnO_2$

21. $6\,FeCl_2 + 1\tfrac{1}{2}O_2 \rightleftharpoons 4\,FeCl_3 + Fe_2O_3$[61].

Sulphide ores would appear to be well suited for chlorination with elementary chlorine[62,63,64,65,38] since they react at very low temperature. The simplicity of this operation has been stressed by Ashcroft[62,66] who also used carrier salts as solvent within which the chlorination of the powdered sulphide took place. This is important in case the chloride formed sublimes. The operation can be conducted in such a way, that elementary sulphur is liberated but excess chlorine produces S_2Cl_2, which can be burned with air for recovery of sulphur as SO_2. In some cases, however, the chlorination of sulphides leads to complications in the condensation, when the chloride produced has a boiling point close to that of S_2Cl_2, as has been observed in the chlorination of titanium sulphide[65].

Exchanges of sulphides with chlorides[67,38,68] are also recorded in the literature, as for instance those between barium oxide and the chlorides Ag, Pb, Cu, Ni and Ti[62]. Silver chloride reacts with zinc sulphide, producing silver sulphide and zinc chloride[67].

The equilibrium ruling exchanges between anhydrous chlorides and hydrogen sulphide have been studied by Jellineck[70] in a few examples. The equation:—

22. $MeCl_2 + H_2S \rightleftharpoons MeS + 2\,HCl$

is reversible, and anhydrous chlorides could be made by reaction of a sulphide with gaseous hydrochloric acid. Pure titanium and zirconium sulphide can be made by reaction of the tetrachlorides with H_2S.

Sulphide chlorination may permit selective extraction of some metals but this has been little investigated. Fink[71], for instance, selectively extracts iron from bauxites by first sulphidizing the iron with elementary sulphur and chlorinating the material afterwards. Sulphur does not attack alumina, silica nor titanium oxide. In the subsequent chlorination, however, some silicon, titanium and aluminium chloride is produced by chlorination with S_2Cl_2, resulting from the action of the chlorine on iron sulphide.

Purification and Separation Methods for Chlorides

Specific methods for the purification of crude $TiCl_4$, $ZrCl_4$ and $BeCl_2$ are used commercially. Iron chloride contained can be reduced with hydrogen from the trivalent to the divalent form; thus its volatility is greatly reduced and separation is made possible[72]. Fractionation of volatile chlorides in a heated condenser has repeatedly been tried. The $AlCl_3/FeCl_3$ separation by distillation has not been successful because of mixed crystal formation[73]. Reduction of the $FeCl_3$ with aluminium powder is recommended before the sublimation is started. Fractionation in solid form is difficult because of the heat gradient existing in the solid deposit between the outer condenser wall and the condensing inner surface. The growing thickness of the deposit interferes with the heat flow and constant temperature conditions cannot be easily maintained. Also heat dissipation in the axis of the condenser is uneven, most of the heat being given off at the entry of the metal vapours. Fractionation of solid deposits is in its infancy and much will have to be done to improve existing methods. Vanadium, contained in titanium tetrachloride, can be separated by reduction with H_2S or with copper powder; in this way less volatile vanadium compounds are formed[74]. The oxide usually contained in zirconium tetrachloride can be separated by subliming[16].

The possibility of using anhydrous chlorides, which are liquid at room temperature ($SiCl_4$, BCl_3, CCl_4[75], $SnCl_4$, PCl_5, $TiCl_4$) as a solvent for the purifi-

cation or extraction of other chlorides has received little attention. Tarasenkov[76] suggests using $TiCl_4$ as a solvent for $TaCl_5$ with the object of separating this chloride from $CbCl_5$, in which the latter is not soluble.

Chloride separations of multivalent elements can sometimes be obtained by reducing to a lower valency, and the lower chloride so obtained being less volatile can be separated by evaporation of the more volatile constituent. This has been done successfully by Schaefer[75] who reduced selectively $CbCl_5$ contained in mixed crystals with $TaCl_5$ to the less volatile tetrachloride, and separated both chlorides by distillation.

Another method of separation of closely related chlorides is by way of tagging them with another inorganic compound, which forms a complex with them. This methed has been used by Van Arkel[77] for the separation of Hf and Zr. The mixed chlorides are distilled with addition of PCl_5, which complexes both of them but brings about sufficient differentiation in the boiling points to permit fractionation.

(To be continued)

References

42 Gmelin's "Handbuch der anorganischen Chemie," Verlag Chemie, 1951, System No. 41, Titan, 93, 189.
43 R. Lorenz; "Elektrolyse geschmolzener Salze." Knapp Editor Halle, 1905.
44 D. Cubiciotti and C. D. Thurmond; *J. Amer. Chem. Soc.*, 1949, **71**, 2149; Part 3, 4119; *id.*, *J. Amer. Chem. Soc.*, 1952, **74**, 1198.
45 Th. Peczalski; *Comptes Rendus*, 1925, **181**, 463; *loc. cit.*, 1926, **182**, 516.
46 Wilmore; U.S. Pat. 2,184,705, 1939.
47 Gmelin's "Handbuch der anorganischen Chemie," Verlag Chemie, System No. 35, Aluminium. Teil B(1), 163.
48 W. Klemm, E. Voss and K. Geisberger; *Z. anorg. Chem.*, 1948, **256**, 15; W. Klemm and E. Voss; *loc. cit.*, 1943, **251**, 233.
49 Ph. Gross; Roy. Inst. Paper No. 14, 1949. Institute of Min. and Metall. Symposium on Refining Non-Ferr. Metals, July meeting, 461; discussion 470.
50 Ph. Gross, C. S. Campbell, P. J. C. Kent and D. L. Levy; *J. Faraday Soc.*, 1948, 4; discussion 206.
51 Ph. Gross; U.S. Pats. 2,470,305 and 2,470,306, 1949.
52 A. S. Schneider and W. Schmidt; *Z. Metallkunde*, 1951, **42**, No. 2, 43.
53 L. M. Foster, A. S. Russell and C. N. Cochran; *J. Amer. Chem. Soc.*, 1950, **72**, 2580.
54 P. Weiss; *Z. Erzberbau Metallhuttenwesen*, 1950, **3**, 241.
55 Aktieselskabet Ardal Verk; British Pat. 635,318, 1950.
56 W. Klemm, E. Voss and K. Geisberger; *Z. anorg. Chem.*, 1948, **256**, 15; W. Klemm and E. Voss; *loc. cit*, 1943, **251**, 233.
57 E. W. Comstock and Westcott; U.S. Pat. 1,552,786, 1922; R. C. Rowe; *Canad. Mining J.*, 1938 (April), 181.
58 J. O. Betterton and Ch. N. Waterman; U.S. Pat. 2,043,573, 1936.
59 J. O. Betterton and A. J. Phillips; U.S. Pat. 2,043,574, 1936.
60 G. Behr; Metals Technology, Secondary Metals Symposium. 1943 (Oct.), A.I.M.E.
61 Gmelin's "Handbuch der anorganischen Chemie," Verlag Chemie, 1932, System No. 59, Eisen, Teil B, 191.
62 E. A. Ashcroft; U.S. Pat. 1,388,086, 1921; *id.* and J. Swinburn; *Trans. Amer. Electrochem. Soc.*, 1904, **6**, 80. *id.*, U.S. Pat. 695,126, 1902. E. Zielinski; *Chem. Abstr.*, 1934, **28**, 437, and *Arch. Erzbergbau Erzaufbereit*, 1931, **1**, 31. G. G. Urazov; *Chem. Abstr.*, 1936, **30**, 8109. A. Bagdasarian; U.S. Pat. 1,671,003, 1925.
63 R. G. Knickerbocker, C. H. Gorski, H. Kenworthy and A. G. Starliper; *Trans. A.I.M.E.*, 1949, **185**, Metals Branch, 785.
64 H. Borchers; *Metall u. Erz.*, 1936, **16**, 435.
65 J. G. Potter; *Eng. and Min. J.*, 1924, **117**, 646.
66 Anon.; *Eng. and Min. J.*, 1926, **121**, 690.
67 V. Tafel; *Lehrbuch der Metallhuttenkunde*, Hirzel editors, Leipzig, 1927, **1**, 118.
68 G. G. Urazov and M. A. Sokolova; *Chem. Abstr.*, 1946, **40**, 2728.
69 J. A. Hedvall, E. Garping, N. Lindekrantz and L. Nelson; *Z. anorg. Chem.*, 1931, **197**, 399.
70 K. Jellinek and G. von Podjaski; *Z. anorg. Chem.*, 1928, **171**, 261.
71 C. G. Fink; *Trans. Electrochem. Soc.*, 1938, **74**.
72 W. J. Kroll, W. F. Hergert and L. A. Yerkes; *Trans. Eletrochem. Soc.*, 1950, **97**, 305.
73 W. Klemm; "Fiat Review German Science 1939-1946." Dietrich'sche Verlags Buchhandlung 1948. Part I, Inorganic chemistry, 34.
74 C. K. Stoddard and E. Pietz; Bur. of Mines Rep. No. 153, 1947.
75 H. Schaefer; *Z. anorg. Chem.*, 1951, **266**, 140, 151.
76 D. N. Tarasenkov and A. V. Komadin; *Chem. Abstr.*, 1941, **35**, 2381.
77 Gmelin's "Handbuch der anorganischen Chemie;" Verlag Chemie, 1941. System No. 43, Hafnium, 19.

Aluminium Sheathed Cables—*Continued from page 267*

or smaller tube and fitting the appropriate set of straightening rollers at the feeding end. The tubes, it may be noted, are manufactured in a standard range of sizes rising in steps of $\frac{1}{8}$ in. up to 1 in. diameter and in steps of $\frac{1}{4}$ in. above this diameter.

It should be emphasized that although—as mentioned earlier—there are two plants, identical in design and installed side by side, they are completely independent of each other in operation. The time taken for each plant to complete a sheathing operation varies somewhat with different types of cable, but a general indication of productive capacity can be given by the average output per plant which is 3,000 to 4,000 yards of power cable in a 10-hour shift.

Galvanizing

A MEETING of the Hot Dip Galvanizers Association was held in London on Tuesday last for representatives of the leading British general galvanizing firms to discuss Papers prepared for the recent International Conference on Hot Dip Galvanizing held at Düsseldorf which was organized by the Zinc Development Association. **Mr. H. T. Eatwell** (G. A. Harvey and Co. (London) Ltd.), Chairman of the Association, opened the meeting by referring to the improvements in zinc supplies since the last general meeting early in the year. **Mr. R. L. Stubbs** (Director of the Zinc Development Association) explained that the U.K. galvanizers had been hit harder than those anywhere else by the zinc crisis, which had led to severe rationing and the prohibition of many uses of zinc coatings—a policy others had regarded as shortsighted in view of the waste of steel it entailed; no other country had enforced end-use restrictions on zinc coatings.

Talking about the design of galvanizing baths, **Mr. E. M. Wilson** (of Henry Hope and Sons Ltd.) emphasized the need for continuous working to reduce costs and described how the baths and equipment should be constructed to allow a faster throughput of work. Because of the greater ease of control, gas is now replacing coke-firing for the heating of galvanizing baths.

Stressing the need for economy now that raw material and labour costs were so high, **Mr. F. C. Braby** (of Fredk. Braby and Co., Ltd.) suggested how best the problem could be attacked. He referred to the co-operative work of the Association which had contributed much to a reduction in the output of zinc residues, an economy which had no detrimental effect on the quality of the galvanized product.

Introducing a Paper by Mr. A. T. Baldwin, one of the four American delegates to the International Conference, **Mr. R. W. Bailey** (of the Z.D.A.) referred to Mr. Baldwin's pioneer work on the study of galvanizing fluxes, which has also enabled galvanizers to reduce their metal losses. This kind of scientific research on the fundamentals of galvanizing was very rare 20 years ago but its value was now generally appreciated.

Discussing the galvanizing of cast iron, which often presents difficulties to the smaller jobbing galvanizers, **Mr. Montgomery** (of Fredk. Braby and Co., Ltd.) explained the metallurgical differences between cast iron and steel and showed how, through understanding them, the galvanizing problems could be overcome. He thought that mechanical shot blasting was by far the best way to prepare castings for dipping. **Mr. Chivers** (of the Z.D.A.) talked about the disposal of used pickle liquors and explained briefly why it was no longer permissible to discharge them direct into sewers or rivers.

APPLICATIONS OF CHLORINE AND CHLORIDES IN METAL WINNING

Chlorine Metallurgy—Part III

By W. J. KROLL

(Consultant, Corvallis, Oregon, U.S.A.)

(Continued from METAL INDUSTRY, October 3, 1952)

WHEN reducing chlorides with metals or with hydrogen and when chlorinating ores, chlorinated by-products are obtained, which, for economic reasons, must be returned after conversion to the constituents, to obtain a closed cycle. Reduction of such chlorides with more electronegative elements produces anhydrous chlorides, such as those of Al, Mg, Na, Ca of which only the last three could be fully brought back in the cycle by fusion electrolysis, since the aluminium chloride electrolysis is not yet commercially practicable. As to the calcium electrolysis it is far too costly in its present state because of high power consumption caused by the use of a contact cathode. Magnesium and sodium are outstanding, due to the ease with which they can be reclaimed from their chlorides.

Hydrochloric acid beneficiation is a problem of first importance in the reduction of anhydrous chlorides with hydrogen. Two solutions are offered, which were both put into practice during the last war. The first is combustion of HCl with oxygen[17] in a KCl/$FeCl_3$ bath at 450°C., according to a modified Deacon's Process which yields chlorine and water vapour. The waste gas from the oxidation is passed through S_2Cl_2 which does not react with moisture and thus the chlorine gas is stored as SCl_2. It can be liberated by heating, whereby sulphur monochloride is regenerated. A pilot plant capable of producing 50 tons of chlorine a day was in operation along these lines in Germany[17]. The other reclaiming process for hydrochloric acid is the aqueous electrolysis[78]. This requires a large amount of electric energy and capital investment is high.

Whether reclaiming the HCl by way of the electrolysis of $CuCl_2$ with liberation of chlorine and oxidation of the HCl/CuCl solution of the cathode compartment as proposed by Low[79] will be possible on an industrial scale has yet to be seen. A low power consumption is claimed for this method.

Byproduct anhydrous iron di- and trichloride could be reclaimed by reaction with oxygen. In the Westcott-Comstock process[57] pyrites are chlorinated with chlorine to form sulphur and $FeCl_3$. The $FeCl_3$ is oxidized with air, and the chlorine obtained is returned in the cycle. Rotary kilns are used in this operation. It is questionable whether the Fe_2O_3-Fe_3O_4 formed in the last operation can be easily removed from the kiln. No commercial installation has yet been put in operation but pilot plant operation seems to show the way. The chlorination of Fe_2O_3 has been studied by Galmiche[19]. It appears that the oxidation of $FeCl_3$, which is the first member of the equilibrium equation:—

23. $4\,FeCl_3 + 3\,O_2 \rightleftharpoons 2\,Fe_2O_3 + 6\,Cl_2$

is largely temperature conditioned, $FeCl_3$ being fairly stable at 1000°C. in oxygen while it is readily decomposed at lower temperatures. Unfortunately, the rates of oxidation become very low at 500°C. at which temperature sintering of the Fe_2O_3-Fe_3O_4 obtained could be held down. The best rates are found at about 750°C., where the oxygen efficiency may reach 75 per cent. Under these conditions, however, the oxide produced already sinters heavily.

Kangro[80] proposed using this reaction to extract iron from low grade iron ores and it could apply also to iron removal from bauxite, clay, ilmenite and low grade nickel and chromium ores, by heating these above 1000°C. in chlorine, cooling the waste ($FeCl_3$ + O_2) gases down to lower temperatures to bring about a back reaction of the oxygen present, originating from the iron oxide, with the iron trichloride. The chlorine reclaimed could be recycled. No refractories could be found permitting operation under such conditions. Preheating the chlorine to the required temperatures without using electricity constitutes another difficult task. Reclaiming chlorine from waste $FeCl_3$ is a problem of world importance, which will have to be solved some day.

The treatment of by-product $FeCl_3$ in order to make it pay a part of the cost of chlorination in the form of iron, iron oxide, pigment or chlorine, might be achieved by various other means besides those already indicated above. The fusion electrolysis, in a carrier salt, because of the double valency of iron, presents great difficulties. Aqueous electrolysis is successful only from a divalent bath[81] which can be produced by reaction of the trivalent solutions obtained at the anode with pre-reduced ore. The most interesting method, however, is that of Sintermetallwerk Berghaus[82] in which $FeCl_2.2H_2O$ is reduced with hydrogen at 650°C. and the hydrochloric reclaimed, after its elimination from the waste gas mixture with water, by dissolution of iron scrap and precipitation of the aqueous $FeCl_2$ formed as $FeCl_2.2H_2O$ with hydrochloric gas, bubbled into the solution. The hydrogen evolved in the scrap iron treatment is used again in the reduction of the hydrated chloride. This process was put into operation on pilot plant scale on the basis of 20 tons a day but details are lacking. While Berghaus employs iron scrap for reclaiming aqueous HCl, a cycle in which hydrochloric gas would be returned through an aqueous electrolysis could be proposed as well.

Oxygen added or present in the chlorination brings about more general exchanges between this gas and various chlorides formed, which may break down to oxide with liberation of chlorine as shown in reaction 4 (METAL INDUSTRY, September 26, p. 244). Air, when added to the chlorine used to chlorinate oxide/carbon mixtures, helps to maintain the temperature in the apparatus. However, it introduces also many new complications. The batch, because of the various temperatures to which it is subjected along the vertical axis of the chlorinator and due to back reaction with the numerous chlorides which are produced in all chlorinations, varies in its composition on different levels. CO_2 forms CO with excessive carbon which reacts with higher chlorides such as $FeCl_3$, $CuCl_2$, and $CrCl_3$, forming $COCl_2$ and lower metal chlorides as shown previously.

The volatile by-product chlorides such as $SiCl_4$, $TiCl_4$, $AlCl_3$, react in the higher zones with iron oxide. These chlorides have even been proposed to de-iron the ore in a preliminary step[83]. Calcium and magnesium oxides, when chlorinated, impregnate the charge with fused chlorides which inhibit chlorination. Eutectics may form between the chlorides. With sufficient air addition production of such chlorides could be held down. Magnesium chloride, being fairly volatile, frequently contaminates the condensate. It can be understood that the chemistry in an ore chlorinator is quite complex, and differs very much from the over-simplified presentation given by Maier[84] for the chlorination of chromites.

Chlorination of Low Grade Chromites

Among the proposed chlorinations are those of low grade chromites and

lateritic nickel ores. The commercial requirements for ferrochrome prescribe the use of a chromite with a chromium to iron ratio of at least 3:1. The elimination of iron from the low grade ores to bring them up to standard is therefore imperative and chlorination would seem to be one of the best chemical methods suggested for this purpose. Work done by Maier[84], Muskat[85] and Grutzner[86] (I. G. Farbenindustrie) throws enough light on these methods to evaluate the difficulties involved.

Maier avoids batch impregnation by fused chlorides and "filming," by the use of quartz pebbles as carrier for the ore/carbon mixture, and as a heat ballast. This also permits easy percolation with excess chlorine, as required to inhibit $CrCl_2$ formation and $CrCl_3$ dissociation. The addition of air, which he recommends, holds back to some extent the formation of $MgCl_2$, but its action on the oxygen sensitive chlorides such as $CrCl_3$-$FeCl_3$-$CrCl_2$-$FeCl_2$ must be difficult to control. The condensed product contains usually at least 4 per cent $MgCl_2$, carried over by partial pressure in the waste gases. Redistilling of the condensate in a $HCl+Cl_2$ atmosphere, and fractionating does not permit clean separation with good recoveries. Washing of the $CrCl_3$ with water, in which this compound, when pure, is insoluble, does not succeed because of the presence of catalysts, such as $FeCl_2$ and $CrCl_2$, which cause dissolution of the chromium trichloride. Maier's experiments were made only on a laboratory scale with quartz tubes. His results do not permit transposition to industrial requirements.

Muskat[85] worked with a shaft type chlorinator, operated at 1000-1200°C. in the exhaust gases, to which excess chlorine was added, to avoid $CrCl_3$ dissociation, oxygen was mixed with the chlorine to control the temperature of the batch, which contained excess carbon. Results are described only in patent specifications and they might be subject to doubt.

Grutzner[86] goes into his difficulties in detail. He chlorinated a peat moss chromite mixture in a large, shaft type commercial chlorinator on a coke bed, heated with electricity. The volatilization of chromium and iron chlorides was comparatively easy, despite the occasional formation of ferro-chrome, but condensation of the chlorides presented many serious problems. A stationary condenser failed. A rotary one, which was heated so as to provide a heat gradient from 600-400°C. to avoid $FeCl_3$ condensation, was not too successful and the condensate analyzed 92 per cent $CrCl_3$ only, besides iron and 6 per cent $MgCl_2$. Accretions of dense chloride, probably agglomerated with $MgCl_2$, were the main trouble. Grutzner suggested the use of a scraper, but it would be difficult to find a suitable material of construction fulfilling the requirements in such a corroding and hot medium. In none of the discussed cases have chlorine efficiencies been recorded, which are certainly low. None of the investigators attempted selective chlorination of the iron and their final decision was to separate the mixed iron and chromium chloride condensates obtained in a following fractionation step.

The difficulty of removing large quantities of iron by selective reduction of the ore without losing chromium is shown by the work of Boericke[87] who proved that if only 60 per cent of the iron is reduced at 1200°C., 3 per cent of the chromium is extracted with the iron by sulphuric acid leaching. In the chlorination of pre-reduced chromite where $FeCl_3$ acts as a chlorinating agent, the chromium losses are much higher.

The considerable difficulties of chromite/carbon chlorination could greatly be reduced by using comminuted high carbon ferrochrome as starting material. This would eliminate the interference of magnesia and consequent chlorine losses. This grade of ferrochrome can be obtained by arc furnace methods at reduction efficiencies of 90-95 per cent. Chlorination of powdered high carbon ferrochrome[88] at temperatures not in excess of 500°C. permits separation of the iron, as $FeCl_3$ from the less volatile $CrCl_3$ formed, but it is questionable whether the narrow temperature limits permissible could be maintained in commercial chlorinators in spite of the admixture of sand, which the patents recommend, considering the highly exothermic nature of the process.

Chlorination of Low Grade Nickel Ores

Lateric low grade nickel ores, which contain the oxide of this element mostly as hydrosilicate, vary widely in their composition in different geographic locations especially as to the iron, magnesia and silica contents. This indicates that a method of beneficiation that might apply to one kind of ore could not possibly be used universally to all other ore compositions.

Nickel and iron dichloride sublime or boil at 973° and 1023°C. respectively. Iron dichloride melts at 670°C. while the trichloride melts at 282° and distils at 315°C. Fractionation of nickel dichloride from iron trichloride would therefore appear possible.

Nickel could be reduced selectively[89,90] but some iron has to be reduced with it, otherwise the nickel recoveries are too low. A following chlorination step and subsequent aqueous extraction would permit recovering the nickel by aqeuous or thermal methods, as suggested by some patents[89]. Tafel[91] obtained on a laboratory scale an 80 per cent nickel extraction from Frankenstein ores after reducing selectively at 1000°C. and chlorinating at 250°C. Higher nickel recoveries can be obtained only when reducing also larger quantities of iron, and Losev[92] prefers therefore complete chlorination of the ore. This, for the extraction of a 1·5 per cent nickel iron ore of given composition, would require the use of 35·5 tons of chlorine per ton of nickel produced[92].

Nickel oxide can be chlorinated directly with elementary chlorine or with chlorine plus 1 per cent SCl_2 but the recoveries are low[93]. Chloridizing roasting is recommended in a number of patents[94] among which some suggest keeping oxygen out of the reaction zone[39,37]. As shown here, the beneficiation of low grade nickel ores by chlorination is mainly a problem of chlorine recovery from the by-product chlorides such as $FeCl_3$, $MgCl_2$ and $SiCl_4$[95].

Chlorination on Industrial Scale

Only the outstanding features of industrial chlorination will be discussed. The direct production of anhydrous chlorides from chlorine and oxide-carbon mixtures is applied to the following oxidic substances: bauxite, zircon sand, zirconium oxide, rutil, titanium pigment, magnesium oxide. The chlorination of alloys or metals is performed with zirconium cyanonitride, titanium carbide, silicon[96], iron[97] and aluminium metal. The industrial use of phosgene for the chlorination of ores has been put into practice in Germany.

The aluminium chloride from bauxite problem has been solved by McAfee[15]. A German plant using phosgene for the chlorination of bauxite is fully described in various reports[98,99,100,101] It seems that nevertheless aluminium chloride is now made preferably by chlorination of the metal[102].

The production of $ZrCl_4$ from zircon is well described by Berty[96]. The ore has to be ground to 200 mesh, which causes considerable wear of the equipment. The recoveries are low, because of a carry-over of chloride with the waste gases. Better results were obtained by Gilbert[103] with zirconium oxide. The electrically heated chlorinator permits better control of the temperature than the German model. The equipment used by the I.G. Farbenindustrie for chlorinating titanium oxide or rutil is shown in the Berty report previously mentioned. The production of magnesium chloride for the fusion electrolysis, starting from a magnesia is presented in a Fiat report[100].

Silicon chloride has been made by chlorination of SiC at 1200°C.[104]. At present it is preferable to use high grade silicon metal as starting material and the I.G. Farbenindustrie operates in a water-cooled iron tube[96]. Once the silicon starts burning, it continues to do so even inside a water jacket. Provision has to be made to eliminate residues, for instance by means of a helix. The production of titanium chloride from carbide as well as that of $ZrCl_4$ from cyanonitride[105] is a simple operation because the reaction is self-sustaining. The recoveries are high and the equipment is small for a given output compared with the chlorination of oxide. Titanium

chloride production from oxide as practised in Germany is also described by Berty[96].

Beryllium chloride has been produced in the U.S.A. by chlorination of oxide carbon mixtures in quartz tubes. In Germany a large brick-lined chlorinator, which was heated internally by electricity, has been used for the same purpose[106].

Reductions with Metals

Equilibrium reactions between metallic reducing agents and chlorides have various purposes. The first may be the production of a pure metal; the second if any alloy is used, purification and elimination of obnoxious constituents; the third may aim at producing alloys of the reducing agent with the base metal of the chloride to be reduced; the fourth may be the obtaining of a valuable anhydrous chloride for further use; the fifth, the purification of a raw chloride. Examples which may be taken for each case are: the production of zirconium by reduction of the chloride with sodium, the elimination of lead from tin-lead alloys by reaction with tin chloride, the introduction of manganese in aluminium by reaction of the latter with $MnCl_2$, usually in a flux, the production of manganese chloride by reaction of ferro manganese with iron dichloride and the purification of fused zinc chloride with pure zinc. It is apparent that quite a multiplicity of reactions is possible.

Volatile chlorides may be stabilized in non-reacting carrier salts or fluxes and metallic reagents may be confined in a carrier metal, which does not participate in the exchanges that take place. The physical state of the reactor may be gaseous, liquid and solid. Reactions of gaseous potassium metal with chlorides are frequently mentioned in old references. Gaseous zirconium chloride is now used in the production of zirconium. The most common case is the one where metals and salts are both liquid, but the case where the metal is solid may be examined more carefully, since until now it has been almost neglected. Platings obtained on solid metals by the use of gaseous or liquid chlorides are common, as those of zinc, aluminium, boron, silicon, tin, nickel, chromium and copper on iron[107,108,109,110,111,112,113,114,115,45]. The penetration may easily reach a few tenths of a millimetre. Supposing that, instead of compact metal, a fine powder were used to react with a chloride, it is evident that various alloy powders could be obtained, which might find important uses in powder metallurgy. Or, with a powdery reducing agent of high chlorine affinity, complete precipitation of the element of the chloride could be brought about. Finally it might be possible to extract a valuable constituent from a comminuted, usually brittle, alloy by reaction with a cheap chloride, to produce a useful new chloride. Reactions of that kind naturally underlie the law of mass reaction, but in the first place, diffusion into and out of the metal particles dominates the time factor. The reaction may take place in a flash or explosion as for instance the one between magnesium powder and most heavy metal chlorides, or it may be more slow as is the one between powdered ferro manganese and $FeCl_2$. There is also a composition-time factor to be considered since the first particles precipitated have a different composition from the last ones, which diffusion tends to equalize.

So far it has been assumed that the chloride would be perfectly anhydrous and free of oxide. This condition is difficult to achieve because, according to equations 1 and 4, oxygen is readily introduced in the fused salts by reaction with air and humidity. Even water dissolves as such in some fused chlorides, mainly in the hygroscopic ones ($LiCl$, $CaCl_2$, $ZnCl_2$), as is shown by the fact that when aluminium is introduced in fused calcium chloride a lively hydrogen evolution takes place. This is usually not observed with fused $NaCl$, which, however, shows an alkaline reaction in water after cooling, indicating a displacement of chlorine by oxygen.

Dissolutions of oxides in chlorides may be misleading in reduction experiments because the oxide present might be reducible, while the chloride is not. This can be shown with aluminium as a reducing agent. It is not capable of reducing $CaCl_2$ but forms an Al/Ca alloy in a CaO-bearing $CaCl_2$ bath. This compound dissolves large quantities of the oxide[116].

Oxide elimination from a fused bath can be performed by equation No. 2 by bubbling chlorine in the melt in the presence of carbon, or by using a reducing chlorinated compound such as HCl, or CCl_4. With volatile chlorides, which form no readily boiling oxychlorides, distillation or subliming is the standard practice for oxide elimination ($ZrCl_4$, $BeCl_2$, $TiCl_4$). In the fusion electrolysis with a carbon anode, conditioning and deoxidation of the bath take place by running the cell for a while before real production starts.

(To be continued)

References

78 W. C. Gardiner; Fiat Report 832, PB 33,219, 1946. *id.*, PB 44,185-69.

79 F. S. Low; U.S. Pat. 2,468,766, 1949.

80 W. Kangro and R. Flugge; *Z. Elektrochemie*, 1929, **35**, 189.

81 W. J. Granberg; *Iron Age*, 1947, **161**, No. 26, 70.

82 Sintermetallwerk Berghaus; PB 17391, 1944.

83 C. Pascaud; *Comptes Rendus*, 1951, **231**, 1232.

84 C. G. Maier; Bur. of Mines Bull. 463, 1942; *id.*, U.S. Pat. 2,133,997, 1939; *id.*, U.S. Pat. 2,133,998, 1939.

85 I. E. Muskat and Pittsburgh Glass Company; U.S. Pat. 2,185,218, 1940; *id.*, U.S. Pat. 2,240,345, 1941; *id.*, U.S. Pat. 2,311,458, 1943; *id.*, U.S. Pat. 2,325,192, 1943; *id.*, U.S. Pat. 2,311,459, 1943; *id.*, U.S. Pat. 2,349,747, 1944.

86 Grutzner and I.G. Farbenindustrie; PBL Report 70,446—5090-5112 (Report No. 564, 1939); *id., loc. cit.*, 73,693—2615-2628 (Report dated 1931).

87 F. S. Boericke and W. M. Bangert; Bur. of Mines R.I. 3817, 1945; *id.*, Bur. of Mines R.I. 3813, 1945; *id.*, Bur. of Mines R.I. 3847, 1946.

88 I.G. Farbenindustrie; German Pat. 514,571, 1927; 529,806, 1931; and 624,425, 1936.

89 Ch. Hart; U.S. Pat. 2,030,867 and 2,030,868, 1936.

90 E. H. Brown and S. J. Brorick; U.S. Pat. 2,067,874, 1937.

91 V. Tafel and G. Lampe; *Metallwirtschaft*, 1937, **16**, 721.

92 K. J. Losev; *Chem. Abstr.*, 1942, **36**, 5447.

93 I. S. Morozof, G. G. Urazow and A. N. Efremov; *Chem. Abstr.*, 1939, **33**, 9272.

94 C. R. Hayward; *Chem. and Met. Eng.*, 1922, **22**, 261.

95 D. P. Bogatskij; *Chem. Abstr.*, 1945, **39**,, 2951; *loc. cit.* 1946, **40**, 4632.

96 F. H. McBerty; Fiat Final Report 774, 1946.

97 Ph. Balz; PB 46,984.

98 Cios Report, Item 22, File 27, 31.

99 J. G. Kern; PB 485, 1945.

100 J. W. Livingston; PB 951, 1945.

101 Gruber; PB 41,424.

102 Ch. A. Thomas, M. B. Moshier, H. E. Morris and R. W. Moshier; "Anhydrous Aluminium Chloride." Reinhold Pub. Co., 1941, 864.

103 H. L. Gilbert and W. W. Stephens; *J. Met.*, 1952, **4**, 733.

104 O. H. Hutchins; *Trans. Electrochem. Soc.*, **35**, 309.

105 W. J. Kroll, C. T. Anderson, H. P. Holmes, L. A. Yerkes and H. L. Gilbert; *Trans. Electrochem. Soc.*, 1948, **94**, 1.

106 G. Jaeger; *Metallwissenschaft u. Technik*, 1950, **4**, 183.

107 A. Sanfourche; *Comptes Rendus*, 1926, **183**, 791.

108 E. Podzus; *Z. anorg. Chem.*, 1917, **99**, 123.

109 B. W. Gonser and E. E. Slowter; *Met. Ind.*, 1938, **52**, 473.

110 E. D. Martin; Dissertation, Nancy, France, 1924.

111 G. Becker, E. Hertel and C. Kastner; *Z. Physikal. Chem.*, 1936, **177**, 213.

112 E. Vigouroux; *Comptes Rendus*, 1905, **141**, 828; *loc. cit.*, 1906, **142**, 635, 1270.

113 C. F. Powell, I. E. Campbell and B. W. Gonser; *Trans. Electrochem. Soc.*, 1948, **93**, 258.

114 E. A. Beidler, C. F. Powell, I. E. Campbell and L. F. Yntema; *J. Electrochem. Soc.*, 1951, **98**, 21.

115 I. E. Campbell, C. F. Powell, D. H. Nowicki and B. W. Gonser; *Trans. Electrochem. Soc.*, 1949, **96**, 318.

116 B. Neumann, C. Kroeger and H. Juttner; *Z. Elektrochem.*, 1935, **41**, 725.

first book was virtually unobtainable for years. In 1943 a reproduction by Photo-Lithoprint was made in the United States of America, and so permitted the circulation of copies in scientific circles to a limited extent.

Now we have this new book, "Einführung in die Festkörperchemie", which supplements and largely replaces the earlier book. It opens with a most valuable section on the historical development of the chemistry of solids, pointing out that Faraday was one of the founders by his observations on diffusion in metals, that Roberts-Austin carried out the first planned research which gave an example of particle transport in solid matter when he investigated the diffusion of gold in lead, and that J. W. Cobb enunciated his "Theory of solid reactions" in 1910 as a result of his researches in glass technology in which he had shown that mineral silicate formation could take place at temperatures which were well below those necessary to produce a molten phase. Tamman and his co-workers showed that metal reactions in the solid state could provide a new and large chapter on the reactibility of solids. It became apparent that true reactions in the solid state were to be looked upon as a general phenomenon that could take place at quite low temperatures and that the ability to enter into such reactions was a general property of matter. The main body of the book comprises five major divisions. Chapter 1 deals with the building of solid bodies, (2) with the kinetics of the solid state, (3) with reaction in the solid state, (4) with some examples of the practical significance and application of solid-body chemistry. A perusal of this particular chapter provides a broad vision of the tremendous extent of the field and its importance in industry and technology. From powder metallurgy and powder ceramics, through geochemical and petrological syntheses, the question of crystal modification in pigments, problems in the manufacture of porcelain and other branches of the ceramic industry: all these and much more are comprised in this solid-body chemistry. The fifth and last section of the book consists of a most valuable "Atlas of Powder Reactions," in which the elements are arranged according to their grouping in the periodic system and their inorganic compounds in the order in which they usually appear in text-books, oxides-carbonates-chlorides etc. The components of reactions are given, then the product of the reaction. Next follow the temperature at which reaction is just traceable by a stated analytical method, and then the temperature at which reaction appears to be complete. Then the percentage of yield and temperature, and other data with literature references in practically every case. Finally there is the index of literature, a name and a subject index. References in the text of the book are given at the foot of the page.

H. W. G.

APPLICATIONS OF CHLORINE AND CHLORIDES IN METAL WINNING

Chlorine Metallurgy—Part IV

By W. J. KROLL

(*Consultant, Corvallis, Oregon, U.S.A.*)

(*Continued from* METAL INDUSTRY, *October* 10, 1952)

TO facilitate understanding and to broaden present knowledge of chlorine affinities, a few of the author's experiments have been collected in Table IV. Similar experiments [117] have been performed before, particularly by Tamman[118] who reduced various chlorides. In some of his experiments he used a solid metal powder as reducing agent.

In general a chloride in a fused carrier salt of 60:40 per cent KCl/NaCl was reacted for ½ hour in a closed graphite crucible with the stoichiometric amount of a reducing agent mostly in solid, 100 mesh powder form. The melt was stirred every 5 minutes. In such operations, sampling of the reaction products is difficult and reliable data could only be obtained from the salt analysis, the metal powder obtained after leaching frequently being too oxydized and inhomogeneous. Approximate metal balances were obtained, provided the salt did not vaporize. These simple experiments are only a first approach but they give a general idea of the affinities.

The arrows below the equations show the direction of the equilibrium, established by the weight percentage of the reducing agent found in the reacted salts relative to its input. Dotted arrows indicate that the experiment does not disclose the true direction of the equilibrium, because the salt formed was partly volatilized and weights could not be obtained. Mostly equilibria were found and the metal precipitated was an alloy powder. Whenever the equilibrium swings strongly in one direction, metal separations with chlorides or chlorine are possible especially with the following alloys:

Zn from FeZn with $FeCl_2$
Cu from CuNi with $NiCl_2$[2]
Fe from FeNi with $NiCl_2$
Fe from FeCu with CuCl
Pb from PbCu with CuCl
Zn from ZnCu with CuCl.

Manganese zirconium alloys can be made by reaction of Mn with $ZrCl_4$. The cobalt copper, silver nickel, aluminium iron, tin copper and aluminium zirconium affinities are not too far apart, so that alloys could be obtained. Separations could be performed both ways by shifting the concentration of the reaction salts. This can be done by aqueous and by pyrometallurgical methods. For instance the salts can be dissolved in water and separated by known procedures, based on solubility or affinity, for recycling. According to Vogel[119], the separation of cuprous chloride, obtained by exchange of chlorides with copper bearing alloys under the conditions shown above, is relatively easy because of its low solubility in water, when air is absent. On the other hand, it is known that NaCl, $CaCl_2$, $FeCl_3$ and many other chlorides solubilize cuprous chloride in water. However, a concentrated solution of NaCl dissolves 16·9 per cent CuCl at 90°C. and only 8·9 per cent at 11°C. Volatilization of one of the salt bath constituents by chlorination to the form of a higher, more volatile chloride is also possible in some instances, as will be shown below in the case of tin chloride. Precipitation of one salt constituent as oxide within the fused bath is sometimes possible by selective oxidation with air.

Even in the many cases where the reaction of chlorides with metals is orientated the less desired way (for instance $TiCl_4 + Fe$), platings or alloys could still be obtained. Higher temperatures have a considerable influence on the equilibrium as well as on the diffusion in the solid state. In certain instances the ignition temperature may not have been reached in the author's experiments. (Run No. 15, W + CuCl). As shown by runs 8 and 9, silver has a comparatively high affinity for chlorine, and that of lead for this element exceeds that of copper. (Run 13). Intermetallic affinities influence the equilibria considerably as seen from the fact that iron reduces aluminium chloride.

Having thus introduced the reader to the principles of chloride reductions by other metals, the most interesting data regarding similar reactions,

TABLE IV—METAL-CHLORIDE DISPLACEMENT REACTIONS

Run No.	Reaction	Input Composition	Temper. °C	Analysis Salt per cent	Analysis Metal per cent	Per cent of reducing agent in salt	Observation
1	$Zn+FeCl_2=ZnCl_2+Fe$ →	500 KCl/NaCl 252 $FeCl_2$ 131 Zn	650	Zn = 14·7 Fe = 1·4	Fe = 80·9 Zn = 9·0	85	Equil
2	$2\,Cu+NiCl_2=2\,CuCl+Ni$ →	500 KCl/NaCl 131 $NiCl_2$ 126 Cu	700	Cu = 15·1 Ni = 0·7	Cu = 21·7 Ni = 75·5	76	Equil.
3	$Co+2\,CuCl=CoCl_2+2\,Cu$ →	500 KCl/NaCl 198 CuCl 59 Co	650	Cu = 8·9 Co = 4·3		51	Equil.
4	$Fe+NiCl_2=FeCl_2+Ni$ →	500 KCl/NaCl 131 $NiCl_2$ 56 Fe	650	Fe = 7·0 Ni = 0·2	Ni = 90·4 Fe = 5·6	80	Equil.
5	$Fe+2\,CuCl=FeCl_2+2\,Cu$ →	500 KCl/NaCl 200 CuCl 56 Fe	650	Fe = 5·8 Cu = 1·3		72	Equil.
6	$Co+FeCl_2=Fe+CoCl_2$ ←	500 KCl/NaCl 126 $FeCl_2$ 59 Co	650	Fe = 7·7 Co = 1·2		13	Equil.
7	$Zn+MnCl_2=Mn+AnCl_2$ ←	500 KCl/NaCl 126 $MnCl_2$ 65 Zn	600		Mn = 0·1	trace	Equil.
8	$2\,Ag+NiCl_2=2\,AgCl+Ni$ ←	125 KCl/NaCl 12·5 $NiCl_2$ 21·5 Ag	650	Ag = 5·5 Ni = 0·8		36	Equil.
9	$Ag+CuCl=AgCl+Cu$ ←	125 KCl/NaCl 24·7 CuCl 27 Ag	650	Ag = 1·0 Cu = 8·5		6	Equil.
10	$Pb+FeCl_2=PbCl_2+Fe$ ←	500 KCl/NaCl 126 $FeCl_2$ 207 Pb			Pb = 100		No reaction
11	$Si+2\,FeCl_2=SiCl_4+2\,Fe$ - - - →	500 KCl/NaCl 252 $FeCl_2$ 84 Si	900	Si = 1·0 Fe = 11·5	Fe = 51·5 Si = 48.2	3·8	Equil. Fuming Loss
12	$2\,Al+3\,FeCl_2=2\,AlCl_3+3\,Fe$ - - - →	500 KCl/NaCl 189 $FeCl_2$ 27 Al	700	Fe = 3·6 Al = 1·1	Al = 5·5	28	Equil. Fuming Loss
13	$Pb+2\,CuCl=PbCl_2+2\,Cu$ →	500 KCl/NaCl 198 CuCl 207 Pb	600	Pb = 21·9 Cu = 2·5		73	Equil.
14	$Sn+2\,CuCl=SnCl_2+2\,Cu$ ←	500 KCl/NaCl 198 CuCl 118 Sn	650	Cu = 8·5 Sn = 6·7		40	Equil.
15	$W+5\,CuCl=WCl_5+5\,Cu$						No reaction
16	$2\,W+5\,NiCl_2=2\,WCl_5+5\,Ni$ ←	500 KCl/NaCl 282 $NiCl_2$ 92 W	650	W = 0·45		4	Equil.
17	$2\,Zn+ZrCl_4=2\,ZnCl_2+Zr$ ←	500 KCl/NaCl 233 $ZrCl_4$ 130 Zn	700	Zn = 1·6		9	Equil.
18	$4\,Al+3\,ZrCl_4=4\,AlCl_3+3\,Zr$ ←	500 KCl/NaCl 233 $ZrCl_4$ 36 Al	650	Al = 0·8		17	Equil.
19	$2\,Mn+ZrCl_4=2\,MnCl_2+Zr$ →	500 KCl/NaCl 233 $ZrCl_4$ 110 Mn	650	Mn = 10·1		68	Equil.
20	$4\,Cu+ZrCl_4=4\,CuCl+Zr$ ←	500 KCl/NaCl 233 $ZrCl_4$ 254 Cu	700	Cu = 0·5		2	Equil.
21	$2\,Fe+ZrCl_4=2\,FeCl_2+Zr$ ←	500 KCl/NaCl 233 $ZrCl_4$ 110 Fe	700	Fe = 1·1		12	Equil.
22	$Ti+ZrCl_4=TiCl_4+Zr$ ←	500 KCl/NaCl 233 $ZrCl_4$ 48 Ti	700	Ti = 1·0		16	Equil.
23	$2\,Sn+ZrCl_4=2\,SnCl_2+Zr$ ←	500 KCl/NaCl 233 $ZrCl_4$ 237 Sn	700	Sn = 0·05		trace	

usually in the fully liquid state, have been gathered from the literature in Table V, which has to be explained. Complete reduction (column 4) means that a mixture, adjusted in the accurate stoichiometric proportions of the equation, leaves none of the reducing agent behind after the reaction is over, and that no alloys form with it. Some reactions do not go to completion, because the reducing agent has so high an affinity for the metal precipitated, that it partly subtracts itself from the reaction by alloying. Equilibria may go far to one side or the other. Those that proceed only half way or so may be especially adaptable to being displaced to one or the other side by shifting the concentration of the salts. An excess of the reducing agent alloys with the precipitated metal if there is any tendency to alloy. Reactions between Cu, Fe and $ZnCl_2$ help in establishing metallic surfaces when soldering with $ZnCl_2$ fluxes.

The siliconizing of iron has acquired some importance, thanks to the work of Ihrig[120]. The reaction of $SiCl_4$ also takes place with other iron group metals such as chromium and nickel, and alloys are obtained.

A most interesting reaction, because of the principle involved, is the one between silicon, sodium chloride and calcium oxide[121], shown in the following relation:—

24. $4\,NaCl + 4\,CaO + Si \rightleftharpoons SiO_2.2\,CaO + 4\,Na + 2\,CaCl_2.$

This is really a summary of three separate reactions, namely:—

25. $2\,NaCl + CaO \rightleftharpoons CaCl_2 + Na_2O.$
26. $2\,Na_2O + Si \rightleftharpoons SiO_2 + 4\,Na.$
27. $2\,CaO + SiO_2 \rightleftharpoons SiO_2.2\,CaO.$

The equilibrium 25 yields Na_2O, which is reduced by silicon (26); the orthosilicate formation (27), which is also used in chloridizing volatilization, (see equation 6*a*) helps here in the same way, shifting the equilibrium to the right. The affinity of silicon for chlorine is far too low to permit direct reduction of the sodium chloride. However, its affinity for oxygen is high enough to make it a suitable reducing agent for sodium oxide, which is supplied by the equilibrium 25, between CaO and NaCl. Since sodium is continuously removed by volatilization, sodium oxide by reduction, equation 25 can be brought to completion. This method does not apply, however, to the reduction of LiCl with silicon, this chloride being too volatile. This process for producing sodium is quite convenient since it can be operated with cheap equipment at only 800°C. in a vacuum, and no chlorine is liberated, it being only shifted as indicated in equation 25 from the sodium to the calcium. This avoids the handling of chlorine gas.

Barium chloride is not reduced by sodium beyond BaCl, the monochloride. The existence of such salts has recently been doubted[44] but no barium metal can be made that way, nor by fusion electrolysis.

Considering the low chlorine affinity of antimony and arsenic, their plating on many metals from their chlorides is possible[122], but the usefulness of such deposits is rather doubtful. Hot

TABLE V—METAL-CHLORIDE DISPLACEMENT REACTIONS

Reducing Agent	Chloride	No Reduction To Metal	Complete Reduction	Equilibrium†	Alloy Formation
Na, K, Rb, Cs	NaCl, KCl, RbCl, CsCl *a.*			*	*
	$CaCl_2$, $SrCl_2$			*	*
Na, K, Rb, Cs	$BaCl_2$	*			
Na, K, Rb, Cs	$TiCl_4$, $ZrCl_4$, $MnCl_2$, $CrCl_3$, $SiCl_4$,		*		
Na, K, Rb, Cs	$ThCl_4$, UCl_4, $CeCl_3$, $BeCl_2$, $MgCl_2$, $AlCl_3$		*		
Na, K, Rb, Cs	LiCl			*	*
Ca, Sr, Ba	$CaCl_2$, $BaCl_2$ $SrCl_2$, $CeCl_3$, $AlCl_3$, $PrCl_3$			*	*
Ca	$NdCl_3$			*	*
Ca	$ZrCl_4$, $TiCl_4$, $ThCl_4$, $SiCl_4$, $AlCl_3$		*		
Ca	UCl_4, $MnCl_2$		*		
Ca	$BeCl_2$, $MgCl_2$, $CrCl_3$		*		
Ca	$SmCl_3$, $EuCl_3$. *b.*	*			
Mg	$AlCl_3$, $BeCl_2$, $MnCl_2$, $CrCl_3$, $TiCl_4$		*		
Mg	$TaCl_5$, $CbCl_5$, UCl_4, VCl_3, $ThCl_4$		*		
Mg	LiCl, $CeCl_3$, $ZrCl_4$			*	*
Zn	$InCl_3$, $PbCl_2$, Cu_2Cl_2, $SiCl_4$		*		
Zn	$FeCl_2$, $CdCl_2$, $SnCl_2$, $ZrCl_4$			*	*
Fe	$AlCl_3$, $SiCl_4$, $TiCl_4$, $ZrCl_4$, $MoCl_5$			*	*
Fe	$NiCl_2$, $CoCl_2$, $SnCl_2$, Cu_2Cl_2			*	*
Al	BCl_3, $BeCl_2$, $ZrCl_4$, $TiCl_4$, $MnCl_2$, $FeCl_2$			*	*
Pb	$SnCl_2$, $BiCl_3$, $SbCl_3$, $AsCl_3$, Cu_2Cl_2, $CdCl_2$			*	*
H_2	$FeCl_2$, $CoCl_2$, $NiCl_2$, $CrCl_2$, $MoCl_5$			*	
	$ZnCl_2$, Cu_2Cl_2, $PbCl_2$, AgCl			*	
Mo, W, Cr	$SiCl_4$, $NiCl_2$			*	*
Mn	$CrCl_2$, $ZrCl_4$			*	*
	$ZnCl_2$	*			
Ag	Cu_2Cl_2, $NiCl_2$			*	*
Co	$FeCl_2$, Cu_2Cl_2			*	*
Cu	$NiCl_2$, $SnCl_2$, $ZrCl_4$, $SiCl_4$			*	*
Ti	$ZrCl_4$			*	*
Sn	$ZrCl_4$			*	*

†"Equilibrium" means that measurable quantities of reducing agent are distributed in the chloride and metal phase.
(*a*) A. E. Van Arkel. *"Reine Metalle"* J. Springer, Berlin 1939, 88.
(*b*) F. H. S. Spedding. *J. Amer. Chem. Soc.* 1952, 74, 2783.

TABLE VI—HYDROGEN REDUCTION OF CHLORIDES AND HYDROGEN ASSISTED PLATINGS WITH CHLORIDES

Chloride	Reduction to Metal	Metal Plating on	Reference
$AlCl_3$		Fe	124
$TiCl_4$		Fe	124
BCl_3		Fe	124
CCl_4		Fe	124
VCl_4		Fe	124
UCl_4		Fe	124
WCl_6		Fe	124
$MoCl_5$		Fe	124
PCl_3	*		131
CCl_4	*		131
$SnCl_4$	to $SnCl_2$		131
$SbCl_3$	*		131
$TiCl_4$	to $TiCl_3$		131
$TaCl_5$	*		125
$FeCl_2$	*		126, 133, 134
$CuCl$	*		126
$ZnCl_2$	*		126
$PbCl_2$	*		126
$CrCl_2$	*	Mo	115, 131
$MgCl_2$	*		128, 129
$MnCl_2$	*		5
$NiCl_2$	*		5
BCl_3	*	Mo, W	115, 127
$SnCl_4$		Fe, Cu, Zn	109
$TaCl_5$		Fe, Ni, Cu	115, 133
$MoCl_5$		Fe etc.	114
$AgCl$			*a*
$SiCl_4$		Mo	115
$AlCl_3$	*		129

(*a*) M. Jouniaux. *Comptes Rendus* 1899, 129, 883. *Ioc. cit.* 1901, 132, 1270.

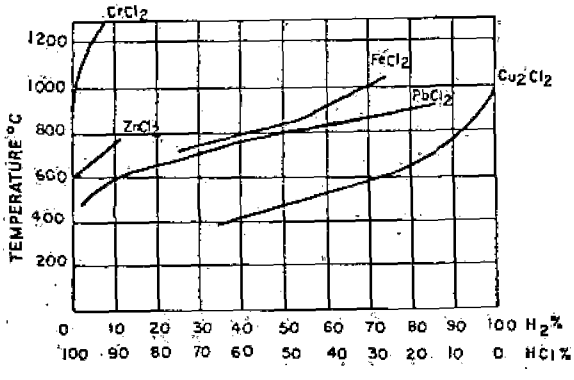

Fig. 2—Equilibrium pressure of hydrogen over the chlorides of Cr, Zn, Fe, Pb, and Cu

iron parts may be heavily attacked by the chlorides of these elements.

Carbon tetrachloride is a slightly exothermic compound, which breaks down quite readily when brought into contact with hot metals. Zinc powder[123] mixed with CCl_4 was used in the first world war as a fog producer. Iron powder is attacked by CCl_4 a little above 200°C. Reactions of this compound with the metals Al, Mn, Cu, Sn, Pb and As are described[123]. More active metals, such as magnesium or calcium, react explosively.

Hydrogen Reduction

This case is exceptional because the chloride produced is volatile (HCl) and it can be removed continuously from the reaction zone, which permits easy shifting of the otherwise very unfavourable equilibrium. Thus platings on other metals, or pure metals can be obtained[45,109,113,114,115,124]. They have been suggested for platings on many metals, mostly alloyed, and concern deposits of Ta[125], Si, Cr, B, Mo, Sn, Co, Ni as well as compounds of various elements (see Table VI).

Hydrogen reduction of chlorides for metal winning is recommended by many authors and the most careful investigation of this subject is that of Bagdasarian[126], who reduced $PbCl_2$, $AgCl$, $CuCl$, $FeCl_2$ and $CrCl_2$, and Maier[84], who worked with chromium chloride. Recently the Germans[82] used this method to make iron powder from the chloride.

Very exothermic chlorides can be reduced by hydrogen only at extremely high temperature, as can be obtained in the arc[127,128,129,130]. At lower temperature, with plurivalent elements, there is usually formation of lower chlorides. Meyer[131] reduced PCl_3, $SnCl_2$, $AsCl_3$, $TiCl_4$, CCl_4, VCl_4, BCl_3, $SbCl_3$ in the chlorine-hydrogen torch in absence of air but he only reached a temperature of about 1000°C. He could produce in this way elementary carbon and phosphorus. Titanium tetrachloride was reduced to trichloride. The well known experiments of Weintraub[127], who reduced BCl_3 with hydrogen in an arc and obtained pure boron, show the influence of the temperature. Quenching the outgoing gases, to avoid back reaction, is essential. Table VII gives the main references concerning hydrogen reduction of chlorides.

When passing hydrogen over the less exothermic chlorides, reduction can be obtained at reasonably low temperature. The equilibrium concentration of hydrochloric gas for a given temperature, as found by Bagdasarian[126] in the reduction of the chlorides of Zn, Cu, Pb, and Fe and those determined by Maier[84], are given in Fig. 2. It shows that the reduction of the chlorides is favoured by higher temperatures. In the reaction of chromium chloride with hydrogen[132] the equilibrium HCl concentration is only 0·075 per cent at 800°C., which is to say, that the hydrogen excess needed is very large. Since this gas has to be cooled for the elimination of the HCl contained, the thermal economics of this method are questionable. With the reduction of $FeCl_2$ the conditions are much more favourable[133,126], since the HCl equilibrium pressure is about 50 per cent at 800°C. The reduction must, of course, be performed at temperatures low enough, so that no sintering of the batch takes place, if one wants to obtain a powder. Fusion of the chloride may also interfere with the reduction.

The elimination of the HCl from the waste gases is a problem which can be solved by various methods. Maier uses activated carbon between the temperatures of −70 and 310°C. Diepschlag[134] condenses the HCl in concentrated $CaCl_2$ solution from which it can be liberated by boiling. Berghaus dissolves it in water.

High purity metal powders can be obtained by this method. However, it has not reached the commercial stage for any of the other metals referred to.

Ammonia gas is a much more efficient reducing agent for anhydrous chlorides than is plain hydrogen.

TABLE VII—COMMERCIAL APPLICATIONS OF CHLORIDE REACTIONS

	Reaction	Reference
1	Dezincing lead with chlorine or $PbCl_2$	*a*
2	Elimination of lead from lead-tin alloys with $SnCl_2$	*b, c, d, e, f, g, h, i*
3	Producing calcium-lead from sodium-calcium chloride and CaC_2 in presence of lead	*j*
4	Separating indium from zinc bearing lead with $PbCl_2$	*k*
5	Separating lead from Bi/Pb with $BiCl_3$ or chlorine	*l*
6	Producing rubidium and cesium by vacuum reduction of the chlorides with calcium	*m*
7	Chromizing and siliconizing iron with chromium or silicon chloride	111, 120
8	Introducing manganese in magnesium and aluminium by reaction with $MnCl_2$ in a flux	
9	Introducing zirconium in magnesium and aluminium by reaction with $ZrCl_4$ in a flux	*n*
10	Production of silicon by reduction of $SiCl_4$ with Zn	*o*
11	Reduction of $ZrCl_4$ with magnesium	16
12	Reduction of $ZrCl_4$ with sodium	72
13	Reduction of $TiCl_4$ with magnesium	*p*
14	Reduction of $TiCl_4$ in a flux with sodium	*q*

(*a*) J. O. Betterton. *A.I.M.E. Tech. Pub.* 504, 1933. (*b*) W. Savelsberg. *Metallboerse* 1932 22, 801,865,897. (*c*) R. Lorenz and G. Schulz. *Z. anorg .Chem.* 1928, 170, 320. (*d*) W. Jander and H. Striebich. *Z. Elektrochemie* 1937, 43, 193. (*e*) F. Koerber and W. Oelsen. *Mitt K. Wil. Inst. Eisen-Forsch* 1932, 14, 119. (*f*) R. Perrin. *U.S. Pat.* 2,356,529, 1944. (*g*) American Metal Co. *Brit. Pat.* 632,839, 1950. (*h*) N. V. Billiton. *Brit. Pat.* 631,784, 1949. (*i*) E. H. Jones. *Inst. Min. Metallurgy*, 1949, 347. Discussion 1950, 363. (*j*) J. O. Betterton. *U.S. Pat.* 1,941,534 and 1,941,535, 1930. J. Siegens and O. Roder. *U.S. Pat.* 2,290,296 1943. H. R. Williams, *Bios Final Report* 883, *PB* 63882. (*k*) Y. E. Lebedev. *U.S. Pat.* 2,433,770, 1947. (*l*) Cerro de Pasco, T. H. Donahue. *U.S. Pat.* 1,778,292, 1930. W. C. Smith, *U.S. Pat.* 1,870,388, 1932. W. C. Smith and P. Mack. *U.S. Pat.* 1,816,388, 1932. (*m*) A. E. Van Arkel. "*Reine Metalle*" J. Springer, Berlin, 1939, 88. (*n*) E. F. Emley, *J. Inst. Met.* 1949, 75, 481. (*o*) D. W. Lyon, C. M. Olson and E. D. Lewis. *Trans. Electrochem. Soc.* 1949, 96, 359. (*p*) W. Kroll. *Trans. Electrochem. Soc.* 1940, 78, 35. (*q*) J. S. Smatko. *Fiat Report* 798, Pb 31, 246, 1946.

Ammonium chloride is produced, which can be recycled by standard methods. The reaction goes straight to ammonium chloride and no excess ammonia is needed. With iron group metals[135] nitrides are formed, which, as far as iron nitride is concerned, can be denitrided with hydrogen in a second step to recover part of the nitrogen contained in the form of ammonia. Iron powder made by ammonia reduction of chloride may contain 4·5 per cent N_2 before denitriding. Zirconium and titanium chloride also give nitride when heated with ammonia but these nitrides are stable. The corrosive properties of ammonium chloride may interfere with the development of such methods.

References

117 S. D. Nicholas; *Nature*, 1932 (Aug.), 581.

118 G. Tammann; *Z. anorg. Chem.*, 1924, **133**, 267.

119 Fr. Vogel; *Metall. u. Erz.*, 1932, 29, 411.

120 H. K. Ihrig; *Metal Progress*, 1938, 33, 367.

121 W. J. Kroll; U.S. Pat. 2,465,730, 1949.

122 Gmelin-Kraut; "Handbuch der anorgan. Chemie." Winters Universitaets Buchhandlung, 3 (2), 498.

123 E. Berger; *Comptes Rendus*, 1920, **171**, 29.

124 N. Paravano and C. Mazetti; *Rec. Trav. Chim. Pays Bas*," 1923, 42, 821.

125 W. G. Burgers and J. L. M. Basart; *Z. anorg. Chem.*, 1934, **216**, 223.

126 A. B. Bagdasarian; *Trans. Amer. Electrochem. Soc.*, 1927, 51, 449.

127 E. Weintraub; *Trans. Amer. Electrochem. Soc.*, 1909, **16**, 165. *J. Ind. Eng. Chem.*, 1911, 3, 299.

128 K. Ebner; U.S. Pat. 2,224,041, 1940.

129 O. Kubaschewsky; PB 37,109.

130 L. D. Jaffee and R. K. Pitler; *Trans. A.I.M.E.*, 1950, **188**, Metals Branch, 1396.

131 F. Meyer; *Ber. Deutsch Chem. Ges.*, 1912, 45, 2548; 1913, 47, 1036.

132 C. G. Maier; Bur. of Mines Bull. 436, 1942; *id.*, U.S. Pat. 2,341,844, 1942.

133 W. Kangro and E. Petersen; *Z. anorg. Chem.*, 1950, **261**, 157.

134 E. Diepschlag and H. Meissner; *Z. anorg. Chem.*, 1941, 245, 409.

135 W. J. Kroll; U.S. Pat. 2,441,770, 1948.

(*To be continued*)

Aluminium Plating

A PROCESS for electrodepositing aluminium at room temperatures has been developed by the U.S. National Bureau of Standards. Dense and ductile deposits are obtained from a plating bath containing an ethyl ether solution of anhydrous aluminium chloride and either lithium hydride or lithium aluminium hydride. Current densities range from 2 amps/dm² (for thick deposits) to 5 amps/dm². The bath is prepared and used in a glass plating vessel with a tightly fitting polyethylene lid. Anodes of aluminium rod pass through the lid and the objects to be plated are introduced and removed through a central hole which is kept closed with a rubber stopper.

Cathode and anode efficiencies are approximately 100 per cent. Deposits 0·05 in. thick have been prepared and thicker deposits should be possible if sharp edges are shielded to prevent treeing.

STANDARD SPECIFICATIONS

Raw Copper. B.S. 1035-40, 1172-4 *and* 1961 : 1952. *Price* 4*s.* 0*d.*

THE Institution has just issued in one booklet the following 10 standards for raw copper :—

B.S.1035—Cathode copper.

B.S.1036—Electrolytic tough pitch high conductivity copper.

B.S.1037—Fire refined tough pitch high conductivity copper.

B.S.1038—99·85 per cent tough pitch copper, conductivity not specified.

B.S.1039—99·75 per cent tough pitch copper, conductivity not specified.

B.S.1040—99·50 per cent tough pitch copper, conductivity not specified.

B.S.1172—Phosphorus de-oxidized non-arsenical copper.

B.S.1173—Tough pitch arsenical copper.

B.S.1174—Phosphorus de-oxidized arsenical copper.

B.S.1861—Oxygen-free high conductivity copper.

This includes revised editions of B.S. 1035-40 first issued in 1942, revised editions of B.S.1172-4 published separately in 1944, and a new specification B.S.1861 for oxygen-free high conductivity copper.

Apart from amending the upper limit for phosphorus in B.S.1172 and B.S.1174, only minor changes have been made to both the earlier series but, in some cases the number of significant figures quoted for the limits has been altered so that the correct degree of accuracy is implied.

Reference Tables for Platinum/Rhodium v *Platinum. Thermocouples.* (*B.S.*1826). *Price* 7*s.* 6*d.*

Reference Tables for Nickel/Aluminium v *Nickel/Chromium Thermocouples.* (*B.S.*1827). *Price* 6*s.* 0*d.*

THESE reference tables are for use in converting thermocouple voltages into the equivalent measured temperatures and in defining the relation between impressed e.m.f. and scale reading for pyrometers which indicate temperature directly.

The tables for platinum-rhodium *v* platinum thermocouples are based on the tables formulated by the National Physical Laboratory, which have been the basis of reference in the United Kingdom for many years.

The tables for nickel/aluminium *v* nickel/chromium thermocouples are based on the tables formulated by the National Bureau of Standard of America, since no other tables are in common use in the United Kingdom.

The tables specify the e.m.f./temperature relations for the thermocouples in four ways, as follows: (a) millivolts: degrees C; (b) degrees C.: millivolts; (c) millivolts: degrees F.; (d) degrees F.: millivolts. Reference tables for copper-*v* constantan thermocouples are in preparation and further tables may be issued in due course.

APPLICATIONS OF CHLORINE AND CHLORIDES IN METAL WINNING

Chlorine Metallurgy—Part V

By W. J. KROLL

(*Consultant, Corvallis, Oregon, U.S.A.*)

(*Continued from* METAL INDUSTRY, *October* 17, 1952)

EXCHANGES of salts with alloys result from many of the reactions mentioned in Table V (METAL INDUSTRY, October 17, 1952) whenever an alloy precipitate is obtained. Therefore one may quite as well start the exchange with an alloy. Calcium carbide may be considered as such. Its activity is due to its calcium content and the carbon is only a carrier for calcium, which normally takes no part in the reaction. For some time great expectations were held for the calcium carbide reduction of oxide-chloride mixtures[136], which gave in a flash a liquid bath with high metal recoveries. These concerned the reductions of the chlorides of Pb, Ag, Cu and Ni which were self-sustaining. Cu and Mn were obtained as prills; Zn boiled off and Sn recoveries were low. In a vacuum, CaC_2 reacts with $MgCl_2$[137] and magnesium metal distils off. Many similar vacuum reactions are possible especially with NaCl but sometimes the carbon affinity of the metal reduced makes such processes impossible as is the case with the mixture $LiCl + CaC_2$. Naturally the carbon liberated in the reaction alloys with the metal produced if the latter has any affinity for carbon. The large amount of calcium oxide contained in the carbide (25 per cent or more) and the high price of this reagent make its use doubtful.

Aluminium carbide has been proposed for the production of various metals with aluminium chloride as a by-product[138].

With calcium carbide as a reducing agent for a chloride and with a metallic solvent to collect the metal reduced one can produce cheap alloys. For instance a mixture of calcium carbide and sodium chloride heated in the presence of lead yields a lead-sodium alloy and calcium chloride is liberated. Since, however, there is also a chemical exchange between sodium-lead and calcium chloride, as shown below, one can also produce in this way calcium-lead alloys by taking care of a large excess of calcium chloride or by reacting the sodium lead obtained in a second step with excess $CaCl_2$. The carbide process is the method employed to-day[139,140,141] for producing a cheap calcium-lead master alloy for debismuthizing lead[142]. The calcium carbide is stirred into lead which is covered with a $CaCl_2$/NaCl flux by means of a mechanical mixer. Alloys with 5 per cent Ca can be made that way[140]. The carrier metal idea was used by Caron[143] a century ago. He reacted sodium-lead alloy with barium chloride and produced sodium chloride and barium-lead. By renewing the barium chloride layer[143], sodium can be "washed" out completely. This method was used in Germany[143] on a large scale after the first world war to produce lead-calcium bearing alloys. While the fusion electrolysis of calcium chloride with lead cathode requires one week to produce a 2·5 per cent lead-calcium alloy[144], the same alloy could be obtained by sodium exchange in only a few minutes. Other carrier metals may be zinc, bismuth and tin, but the most efficient one is lead. It is probably not quite inert since its intermetallic affinity for either sodium or calcium differs and the higher calcium affinity for lead may bring about a shifting towards preferential calcium reduction, not observed if lead is is absent.

As shown by Rinck[145], the reaction between sodium metal and calcium chloride leads to a sodium-calcium alloy with a sodium content of 17 per cent at 850°C. The metals are only partly miscible in the fused state and calcium forms with sodium, a eutectic which melts at 710°C. with 11 per cent Na. The 17 per cent sodium-calcium alloy is in equilibrium with a salt mixture of $CaCl_2$/NaCl containing 71 per cent $CaCl_2$ at 850°C. By reacting this alloy with more calcium chloride the equilibrium can be shifted so that pure calcium is obtained. This "all liquid" operation can be performed in a counter current. The calcium obtained is free of nitrogen but it is contaminated with a little chloride.

Cheap magnesium-calcium alloys with 25 per cent Ca can easily be made by reduction of $CaCl_2$ with sodium in the presence of magnesium, in an inert gas atmosphere. The alloy obtained contains a few tenths of 1 per cent of sodium, which can be removed by a vacuum treatment at elevated temperature.

Rinck studied also the equilibrium between sodium and potassium chloride[145] and he could produce in that way Na/K alloys of any desired composition. By using an excess of KCl, pure potassium can be obtained.

A valuable alloy constituent may be extracted from a carrier metal with the object of producing an expensive chloride. Cheap medium carbon-ferromanganese can, for instance, be reacted with $FeCl_2$ and $MnCl_2$[146]. This salt can be cleanly separated from the metal sponge in a vacuum at 800°C. and a high purity product is obtained. Silicon-zirconium with 37 per cent Zr and 8 per cent Fe, which is cheap, can be reacted with $FeCl_2$[147]. The reaction is self-sustaining and $ZrCl_4$, besides small quantities of $SiCl_4$, are driven off very rapidly. The gas can be bubbled through a bath of fused KCl/NaCl, which collects the $ZrCl_4$ only, $SiCl_4$ not being soluble. The zirconium bearing salt can afterwards be reduced with magnesium to produce zirconium powder. The efficiency of this very rapid process is about 60 per cent of the zirconium present in the alloy. Ferro-zirconium cannot be used for the same purpose because it does not react with $FeCl_2$, the intermetallic compound being too strong.

A survey of the commercial applications of chloride reactions is given in Table VII. Of these only the deleading of lead-tin alloys will be considered, because of the principles involved.

Eliminating Lead

It is frequently easier to separate metals in their chloride phase than in the alloys. This is typified in the so-called "Goldschmidt" process for deleading tin. Savelsberg[148] discussed this method, in which the alloy is reacted with fused $SnCl_2$. Essentially the equilibrium reaction described by Lorenz[149], Jander[150] and Koerber[151] is used. Tin dichloride is reacted close to the melting point of the alloy, at about 250°-260°C. and the slag is withdrawn and treated with chlorine to drive off all divalent tin as $SnCl_4$. This compound is condensed, then reacted with tin to produce pure dichloride, which is returned in the cycle. Shifting of the tin dichloride concentration in the salt is thus accomplished by way of the tin tetrachloride, which can be separated from the lead chloride slag because of its volatility. The equipment used is described in various patents[152,153,154,155,156]. By the same process lead can be removed from 10 per cent babbit alloys[60]. Similar ideas have been proposed for the elimination of Pb, Zn and Fe from a copper bath by injection of $SnCl_2$[157].

The mixed lead-tin chloride slag obtained by the Goldschmidt process

can be de-tinned by oxidation[60] according to:—

28. $SnCl_2 + 2\,PbO = SnO_2 + Pb + PbCl_2$.

The lead chloride is fumed off in a reverberatory furnace. A vacuum retort would certainly be more convenient for this purpose.

This reaction is the base of many propositions to remove tin from lead with a lead chloride flux in an oxidizing medium[58,59,158]. The lead chloride flux can also be used as a means to introduce Cu, Sb, As in lead, by way of the oxides of these metals[159].

Chloride Fluxes

The solubility of oxides is generally not as high in chlorides as in fluorides which latter also have the reputation of releasing the oxide film on metal particles so that they can coalesce. Besides this, any chlorides entrapped in the metal may cause severe local corrosion after solidification which trouble is not found with fluorides. The relatively easy fusibility of chlorides compared with that of fluorides and the lower cost brought about their general use as alloying and melting fluxes for aluminium and magnesium castings[160]. Frequently mixtures of chlorides and fluorides are used, and difficulties are encountered by formation of new compounds with a high melting point and halogen exchanges. For instance magnesium may react with alkali fluorides forming magnesium fluoride which is difficult to fuse. Exchanges between salt constituents[161] may also take place and it is supposed, for instance, that calcium fluoride reacts to some extent with magnesium chloride forming magnesium fluoride and calcium chloride.

Alloying fluxes may contain $MnCl_2$, $CrCl_2$ or $ZrCl_4$. The introduction of zirconium by way of such fluxes is quite tricky[162] and efficiencies are usually low, because some precautions which refer to the nature of this metal and of its chloride are omitted. Commercial $ZrCl_4$ is usually contaminated with more than 2 per cent oxide and free water which is held at the hydrolyzed surface of the particles. This moisture is liable to form a thin oxide film on any reduced zirconium particles and then their dissolution in the metal becomes almost impossible. Furthermore, operation in the presence of air combined with the usual stirring introduces more oxide as well as nitride, to which the chlorides may fasten, causing corrosion of the solidified metal[162]. The zirconium recoveries by this method are very variable and frequently do not exceed 25 per cent, while reduction of zirconium chloride with magnesium under inert gas usually approaches 100 per cent. The use of resublimed dense chloride, held under the surface of the bath, or a flux made out of such chloride, would certainly permit the improvement of the zirconium yields.

The degassing of aluminium which contains mostly hydrogen[163,164] is obtained by bubbling various gases and volatile chlorides through the bath, for instance, chlorine, CCl_4, higher chlorinated carbon compounds, $TiCl_4$, BCl_3, $AlCl_3$ and others. For magnesium, chlorine[165] is the more common reagent. If in both cases hydrogen is to be removed by chemical reaction, it is evident that most of the reagents mentioned will not perform since gas reactions need time. It is doubtful whether the hydrogen would react with chlorine or CCl_4 considering that the gas is dissolved in the metal and the surface and reaction time offered by the reacting gas is too short to bring about rapid elimination. This appears also from the fact that $AlCl_3$, which does not react with hydrogen at the temperature of operation, is considered to be a good hydrogen cleanser. Also back reaction of any HCl formed with aluminium would certainly limit the effectiveness of the procedure. It is therefore most probable that the hydrogen, as well as other gases, if present, are eliminated only by partial pressure in the cleansing gas and in the gaseous reaction products. Using $TiCl_4$ and BCl_3 as cleanser, some reduction of these compounds by the bath takes place which dissolves the metals reduced, forming high melting compounds. These may be beneficial as grain control agents[166].

Lead chloride may be used for the cleansing of various metals, instead of chlorine, which latter Betterton used to de-zinc lead[167]. In this case, lead chloride can also be used. Lebedeff[168] eliminates indium from lead with this reagent. Cerro de Pasco used chlorine to eliminate lead contained in bismuth[169], but bismuth chloride can be used as well. Zinc reacts the same way.

Gold is being freed of copper and silver by chlorination[170]. Magnesium can be removed from aluminium with an $AlCl_3$ flux.

(To be continued)

References

136 L. M. Bullier; German Pat. 118,177, 1901; B. Neumann; *Chem. Zeit.*, 1900, **24**, 1013.
137 C. Matignon; *Comptes Rendus*, 1921, **172**, 381.
138 L. Burgess; U.S. Pat. 1,321,281, 1919.
139 J. O. Betterton; U.S. Pat. 1,941,534 and 1,941,535, 1934; J. Siegens and O. Roder; U.S. Pat. 2,290,296, 1943; H. R. Williams; Bios Final Report 883, PB 63,882.
140 J. O. Betterton; U.S. Pat. 1,941,534 and 1,941,535, 1934.
141 W. Kroll; German Pat. 381,049, 1923.
142 W. Kroll; *Metall u. Erz.*, 1922, **19**, 315; *id.*, U.S. Pat. 1,707,059, 1929; J. O. Betterton and Lebedeff; *Trans. A.I.M.E.*, 1936, **121**, 205.
143 H. Caron; *Comptes Rendus*, 1859, **38**, 440; W. Kroll; German Pat. 382,077, 1923.
144 C. L. Mantell; "Industrial Electrochemistry," McGraw Hill, New York, 1940, 448.
145 E. Rinck; *Comptes Rendus*, 1930, **191**, 404; 1931, **192**, 1378; 1932, **1**, 395.
146 W. J. Kroll and F. E. Bacon; U.S. Pat. 2,452,665, 1948.
147 W. J. Kroll and F. E. Bacon; U.S. Pat. 2,443,253, 1948.
148 W. Savelsberg; *Metallboerse*, 1932, **22**, 801, 865, 897.
149 R. Lorenz and G. Schulz; *Z. anorg. Chem.*, 1928, **170**, 320.
150 W. Jander and H. Striebich; *Z. Elektrochemie*, 1937, **43**, 193.
151 F. Koerber and W. Oelsen; *Mitt. K. W. Inst. Eisen-Forsch.*, 1932, **14**, 119.
152 R. Perrin; U.S. Pat. 2,356,529, 1944.
153 American Metal Co.; British Pat. 632,839, 1950.
154 N. V. Billiton; British Pat. 631,784, 1949.
155 E. H. Jones; *Inst. Min. Metallurgy*, 1949, 347; discussion, 1950, 363.
156 J. O. Betterton and A. J. Phillips; U.S. Pat. 2,113,643, 1938.
157 A. J. Murphy and G. T. Callis; British Pat. 558,287, 1943.
158 Th. D. J. Metuchen and J. C. Reinhardt; U.S. Pat. 2,043.575, 1936.
159 W. T. Butcher; U.S. Pat. 2,097,560, 1937.
160 A. W. Brace; *Met. Ind.*, 1945, **66**, 274.
161 M. G. Raeder; *Z. anorg. Chem.*, 1933, **210**, 145.
162 E. F. Emley; *J. Inst. Metals*, 1949, **75**, 481.
163 W. R. Opie and N. J. Grant; *Trans. A.I.M.E.*, 1950, **188**, 1237.
164 H. A. Sloman; *J. Inst. Metals*, 1945, **71**, (Part 7), 391.
165 R. S. Bush and E. G. Bobalek; *Trans. A.I.M.E.*, 1947, **171**, 261.
166 C. H. Mahoney, A. L. Tarr and P. E. Le Grand; *Trans. A.I.M.E.*, 1945, **161**, 328.
167 J. O. Betterton, A.I.M.E. Tech. Pub. 504, 1933.
168 Y. E. Lebedev; U.S. Pat. 2,433,770, 1947.
169 Cerro de Pasco and T. H. Donahue; U.S. Pat. 1,778,292, 1930; W. C. Smith; U.S. Pat. 1,870,388, 1932; W. C. Smith and P. Mack; U.S. Pat. 1,816,388, 1932.
170 A. H. Cleave and P. W. Bond; *Eng. Min. Journ. Press*, 1923 (Feb. 3), 236.

Correspondence

Metal Whiskers

Correspondence is invited on all subjects of interest to the non-ferrous metal industry. The Editor accepts no responsibility either for statements made or opinions expressed by correspondents in these columns

TO THE EDITOR OF METAL INDUSTRY

SIR,—I am sorry that my friend Mr. Fullman read into my casual reference to the scarcity in this country of an early issue of a rather young American technical journal any reflection on the excellent services provided by his own and other libraries. I would take it for granted that he could supply a copy; and in fact he did so. I intended only to imply that the journal is not one which is yet seen regularly by most metallurgists in this country—and so to excuse my somewhat tardy discussion of a Paper published nearly a year ago.

Recorder II.

Chlorine Metallurgy—Part VI

By W. J. KROLL

(*Consultant, Corvallis, Oregon, U.S.A.*)

(*Continued from* METAL INDUSTRY, *October* 24, 1952)

INFORMATION is given in Table VIII about the fusion electrolysis of chlorides for metal winning, with the main literature references. A distinction has been made as to the physical state of the metal cathode, whether fused or solid.

The commercial methods applied to Be[106], Mg[171], Na[172], Ce[173], Li[174,175] and Ca[176], will not be considered since they are sufficiently covered by textbooks and literature references[177]. The fusion electrolysis of the chlorides of Al, Pb, Cd and Zn with liquid cathode will, however, be examined.

The production of aluminium with a fused cathode and with $AlCl_3$ in a carrier salt[178] has been taken up again recently[179]. The main problem is stabilization of the volatile chloride in the salt. This proposition is not too promising because of the high temperature involved, compared with solid deposition at the cathode (700° as against 250°C.), and a high energy input is needed to keep the cell hot.

Lorenz[43] studied the deposition of Pb, Sn, Zn, Cd and Bi. With cadmium, metal fog formation was especially disturbing. The most interesting attempts at using the fusion electrolysis for zinc and lead were those of Ascroft and Swinburn[62,66] because they started from the sulphide ores which they chlorinated in a carrier salt. They purified their $ZnCl_2$ electrolyte with zinc, eliminating Ag, Pb and Fe as sludge, after which pure metal could be produced. In the last war the I.G. Farbenindustrie operated an experimental cell with $2\,NaCl.ZnCl_2$ as electrolyte at 6000 amp, 4·5-5 volts and 90 per cent current efficiency[180].

Recently the lead chloride electrolysis has been recommended once more[181]. The sulphide ore, according to this suggestion, is added around the anode where the chlorine liberated takes care of the transformation to lead chloride. FeS, ZnS and silica are said not to dissolve in the bath.

Collecting metals difficult of fusion in a fused metal cathode has been frequently suggested. As such Pb, Sn, Zn and Cd might be used. Pyck[182] recently recommended collecting titanium in a zinc cathode. The choice of suitable metal carriers is limited. Generally the melting point of the alloy rises sharply when high melting point metals are added and the paste formed might be quite difficult to remove from the cell. Also, there might be liquidation and formation of crusts, which necessitates stirring. Separation of the alloy obtained, usually in a vacuum at elevated temperature, presumes that the solvent metal has a low enough boiling point for removal at reasonable temperatures. Similar electrolytic methods, but in an aqueous medium with mercury cathodes, have been quite successful[183] in winning pure metals such as zinc, manganese, chromium, nickel and iron.

Separation of the alloy formed in a double cell, bridged by a pool of this alloy and provided eventually with two different fused electrolytes, has repeatedly been proposed, for instance, to produce sodium with a lead-sodium alloy bridge[184], but without success.

Solid Cathode Deposit

The deposition of solid metal from a fused chloride bath[185,186,187,188,189,190,191,192,193,194,195,196,197,198,199,200,201,202,203] is a much more universal process than electrolysis with a fused cathode, as can be seen from Table VIII. Some metals such as Al, Zn and Ca can be deposited as solid or liquid. Calcium can be obtained in solid form from a $CaF_2/CaCl_2$ electrolyte at a much lower voltage than by the contact cathode method. The temperature margin between the freezing point of the salt and the melting point of the metal is, however, small and this process might be difficult to practise.

The fusion electrolysis with a solid cathode deposit offers some advantages over the fused cathode. Because of the large surface, presented by the dendrites, ohmic losses are reduced; compact metals can be disintegrated at the anode, and collected as metal crystals at the cathode; refining raw metals and separation of alloys can be achieved without having to use a three layer bath; alloy powders can be made either from mixed chlorides, or from alloyed anodes; powders produced by this method, because of their angular shape, have superior properties for use in powder metallurgy. They possess high density, are free flowing and compact easily besides being free of gases.

Chloride electrolytes offer some specific advantages in the deposition of solid metals. They permit lowering the melting point of the bath and running the electrolysis much below the temperatures used with fused metal cathodes. This allows the reduction of the power input and the energy consumption, the radiation losses being under such conditions much lower than usual. The anodic chlorine, obtained in metal winning from chlorides, can be recycled for ore extraction, a decisive advantage over the feed production for the fluoride electrolysis, in which pure oxide must be added in the cell, the latter being extracted from the ores with chemicals, not produced in the electrolytic cycle. All these advantages are outweighed by the fact that removing and reclaiming the metal crystals from the cell and from the cathode deposit is a very difficult problem, at

TABLE VIII—FUSION ELECTROLYSIS OF METAL CHLORIDES

Metal Chloride	Cathode		References
	Fused	Solid	
Be, Mg, Ca, Na, Li	*		177
Ce	*		177
Al	*		177, 179
Pb	*		62, 184, 177, 43, 181
Sn	*		177, 43
Cd	*		177, 43
Zn	*		62, 184, 177, 43, 180
Bi	*		177, 43
Fe		*	201, 202, 198, 177, 43, 187
Ni		*	191, 177, 43, 198, 201, 199
Co		*	177, 43, 191
Cu		*	177, 43, 198
Ag		*	177, 43, 198
Mn		*	177, 43, 187, 198, 188, 189, 190
Zr		*	200
Ti		*	186
Ca		*	Own experiments
Sr		*	Own experiments
Al		*	177, 185, 197a
Be		*	177, 43, 195
V		*	Own experiments
Th		*	193
U		*	194
Cr		*	177, 43, 187, 192

(*a*) V. Engelhardt, "*Handbuch der technischen Elektrochemie*" Akademische Verlags Buchhandlung, Leipzig 1934, III, 384.

least when this has to be done on a big scale. The arrangement of such a cell is shown in Figs. 3 and 4.

In the arrangement of Fig. 3 the crystals are deposited at the bottom of the cell, which is the cathode[204]. In this way anode and cathode rooms are easily separated. This arrangement permits building up a cake of metal dendrites, entrapped in electrolyte, but only to a certain height because of the low electrical conductivity of the agglomerate, which, after reaching a certain length, freezes. The problem of dendrite removal is rather easy in this case, since the whole cell can be dismantled after freezing. Such a method, however, is discontinuous.

A cell, which could be run continuously since the cathode, arranged in the centre, can be lifted out for treatment of the deposit, is shown in Fig. 4. This cell has the disadvantage, compared with the first-mentioned construction, that anode and cathode compartments must be separated by a baffle to avoid attack of the cathode plate by stray chlorine and to collect this gas for further use. This is the normal magnesium cell construction.

Jaeger[196] in his cell for electrolyzing beryllium chloride in a carrier salt, uses the arrangement of Fig. 3, with a nickel crucible, but he deposits the dendrites on the walls from which they are scraped down to the bottom, after partially depleting his bath. The latter is syphoned over to another container for repletion with $BeCl_2$ while the dendrites are pressed and freed of electrolyte, as far as possible, before being submitted to an aqueous treatment. This method, while applicable to small-scale operation as is the beryllium electrolysis, could hardly be used for large tonnages.

Cylindrical cells of the Jaeger type are not practicable on a large scale because of the unequal anode and cathode current density. On plant scale a number of equal size plates will have to be used in a box type cell, and these will have to be lifted out periodically. The dendrite deposit of most metals, except copper, adheres but loosely to the cathode sheet, and the slightest shock causes it to drop off to the cell bottom, where it forms very tough accretions, which are most difficult to remove. It is possible to freeze the deposit to the cathode sheet by using a cooling system within the cathode. This adds to the complications of the already complex cell construction.

The I.G. Farbenindustrie[197] as a means of obtaining a denser deposit in the electrolysis of aluminium chloride, suggests compacting with cylinders of non-conducting material. This might work on a laboratory scale in low temperature electrolytes.

The dendrites are a felty mass of crystals, which entrap usually 80 per cent electrolyte. After removal from the bath preliminary "washing" with fused carrier salts has been suggested. The electrolyte must be squeezed out before submitting the cathode material to the next step of dendrite extraction. Hot pressing permits raising the metal content to more than 50 per cent. However, with very active metals this operation, when performed in air, usually results in burns.

For the extraction of the dendrites contained in the cathode deposit two methods are available: evaporation of the chlorides at high temperature in a vacuum, leaving the slightly agglomerated metal behind, or leaching with water, with the help of some acid.

The former method, used on a large scale in titanium and zirconium production by magnesium reduction of the chlorides, does not permit elimination of foreign particles, if these are not volatile, and all the oxide contained in the electrolyte, in dissolved or suspended form, concentrates in the distillation residue. This rules out this method for oxide sensitive metals such as zirconium and titanium when the electrolyte has to contain oxide for smooth cell functioning.

Aqueous extraction allows separation of entrapped particles by tabling. However, it usually introduces oxides, either because of grinding, or by chemical action of the water on the crystals, or because of the hydrolysis of entrapped electrolyte. This also has some bearing on whether the cell should be operated in batches or continuously. In a cell running continuously with addition of fresh electrolyte the cathode deposit naturally contains salts, which might be easily hydrolyzed on leaching ($BeCl_2$, $TiCl_3$, $ZrCl_2$) this causing oxide contamination of the product. One would think that operation in batches, with complete depletion of the bath and elimination of the salts which hydrolyze, would avoid this drawback. This is true only to a limited degree. The dendrites entrap rich electrolyte at the start of the operation, which is not reduced at the end, even after the carrier salts start decomposing with deposition of active reducing agents, such as sodium, for instance, the action of which extends only to the surface of the cathode deposit. Both methods, continuous and discontinuous as well as depletion or no depletion, have been used in beryllium electrolysis. In any case reclaiming the hydrolyzed products might become a high cost item.

When operating a chloride cell considerable difficulties may be found before the deposition can be started. The bath may foam or froth and the metal obtained may then be mushy and of low quality. Lorenz described this phenomenon well. The cell must first be conditioned. It has been mentioned before that anhydrous chlorides, especially the hygroscopic ones, even in the fused state, retain water which reacts with the first metal deposited at the cathode with hydrogen evolution. The anode also takes part in this cleansing, by reaction of the carbon with water. To speed up the cleansing one may add to the bath such reducing agents which react with water. Furthermore moisture in the air reacts with the fused chlorides at the bath surface according to:—

$$MeCl_2 + H_2O \rightleftharpoons MeO + 2\,HCl$$

(see equation 1).

On damp days cells containing

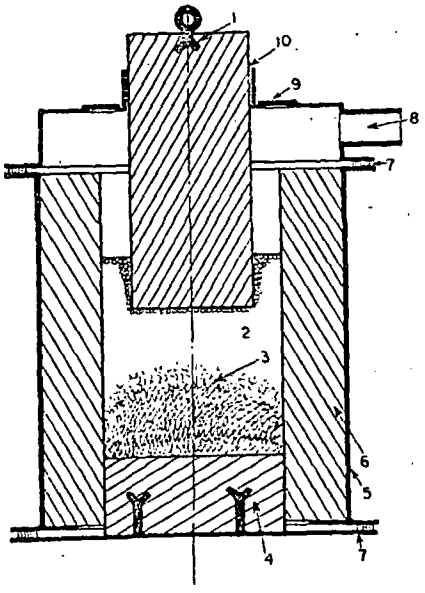

Fig. 3—Arrangement of cell in which anode and cathode are easily separated

1—Graphite anode
2—Electrolyte
3—Dendrite deposit
4—Graphite cathode
5—Iron shell
6—Refractory
7—Insulation
8—Chlorine escape
9—Feeder opening
10—Tight joint

Fig. 4—Arrangement of cell for continuous working

1—Graphite anode. 2—Electrolyte. 3—Dendritic cathode deposit. 4—Cathode sheet. 5—Iron shell. 6—Refractory. 7—Insulation. 8—Chlorine escape. 9—Feeder opening. 10—Tight joint. 11—Refractory baffle. 12—Cathode room. 13—Anode room

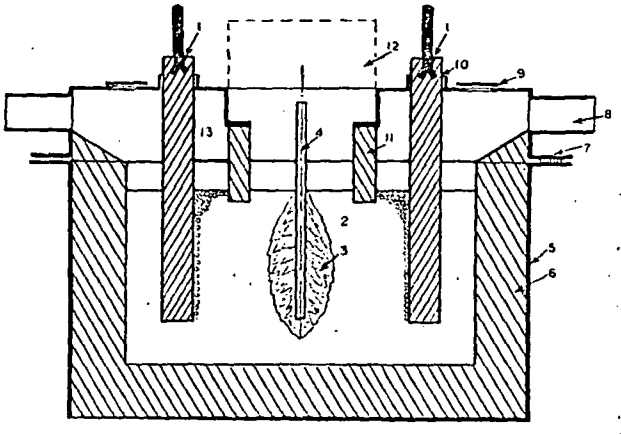

hydroscopic salts are very difficult to operate and production may stop entirely because of interference of moisture from the air. Humidity present in hydroscopic salts also reacts on drying thus introducing oxide.

Another source of oxide is the direct exchange between oxygen of the air and fused chlorides, as shown in equation 4. Metals which are sensitive to oxide will either react with those contained in the bath or will dissolve them. This is facilitated with the dendrites, which present a large reaction surface. On the other hand, there is a continuous reconditioning action of the anode, which results in formation of anhydrous chloride with CO/CO_2 evolution exactly as described in equation 2. Oxide can be eliminated also by artificial means, e.g. by bubbling HCl gas or CCl_4 through the melt.

The delicate reconditioning action of the anode may go too far, in which case the cell develops what is called "anode effect." This phenomenon, which results in a sudden very great increase of the voltage with consequent drop of the amperage, while the anode starts sparking and repulses the electrolyte, is caused by an anodic gas skin, which is almost impervious to the passage of the current. During anode effect some carbon tetrachloride may form within the stability range of temperature for this compound, but the main anodic gas is chlorine with a reduced amount of CO/CO_2. When a little oxide is added to the bath it starts operating again. It has been claimed that chlorine, being negatively charged, is attracted by the anode, which, under certain conditions, it covers with a film. Carbon monoxide and dioxide are said to be positively charged so that they would be repulsed by the anode where they are liberated, thus rupturing the chlorine gas film. However, anode effect has also been observed in cells filled with an oxide electrolyte such as tungstic oxide in a borax bath[205] which invalidates this concept. The necessity of having oxide present in a bath operating with a carbon or graphite anode is especially apparent for a cell running with a fluoride electrolyte, as for instance in the aluminium electrolysis using cryolite. No fluorine is developed in such a cell and the anode gases contain only CO/CO_2 as long as there is no anode effect. Oxide must be added regularly, and the electrolysis proceeds exclusively with consumption of anode carbon. As soon as this oxide is used up, anode effect appears, during which the cell also discharges some CF_4. It has been found that at low temperatures, such as those used in fluorine electrolysis, the anode effect corresponds with the formation of a layer of non-conducting carbon monofluoride[206] at the anode, which is unstable above 400°C. This causes disintegration of the carbon, which then spoils the electrolyte. In the cryolite electrolysis, which works at much higher temperatures, this explanation for the anode effect cannot be upheld. Nor is it valid for the chloride electrolysis in which no such compounds can form. This shows that the anode effect must be attributed to various causes.

While a chloride electrolysis can sometimes be operated in exactly the same way as the cryolite cell works, namely exclusively on account of oxide additions to the bath[207] and no evolution of chlorine, as shown for the magnesium chloride electrolysis, small amounts of oxide must be, and are, present in all chloride cells working at high current density. Since the anode effect depends also on the current density, as has been proved for the aluminium electrolysis in cryolite[208], it could be avoided by increasing the anode surface, for a given current input. Indeed this has been done with the beryllium fluoride electrolysis. Here a circular pot of graphite with internal fins was used as anode to overcome the anode effect. This expedient has limitations, since the graphite is consumed and the fins smooth out. Large production presumes the use of cells with equal size anodes and cathodes and an increase of the anode surface would also augment the radiation area, making it difficult to maintain the cell temperature solely by current input.

The I.G. Farbenindustrie, to avoid anode effect in a chloride bath, recommends the use of a tungsten anode, up to a temperature of 600°C.[197] This kind of anode could not, of course, be employed for large cells.

Some chlorides, such as $FeCl_3$ and $AlCl_3$, disintegrate graphite either by formation of some kind of addition compounds[209] or by production of CCl_4 within the area of temperature within which this compound is stable.

The phenomena at the cathode are not quite as complex as those of the anode. The dendrites grow towards the anode, wherewith the current density decreases very rapidly. Individual crystal branches tend to take more current and grow ahead of others towards the anode, until short circuit takes place, after which the cathode must be removed.

A fluoride cell to which chlorides are added, behaves, if enough chloride is present, like a chloride cell[210,211,42] and chlorine is evolved at the anode. Such electrolytes have been recommended for titanium deposition[42]. Minet[210] used sodium chloride additions to a cryolite bath to produce aluminium. The disadvantages of this cell have been discussed by Haber[211].

(To be concluded)

References

171 Bauer; PB 41,428; PB 49,035-45 and 49,031-49.
172 Anon.;PB 41,132, 41,133. Supp. to Fiat Report 820; PB 44,671.
173 R. Singer; Bios Final Report 400, Item 21, 1946, PB 49.
174 G. T. Motock; Bur. of Mines I.C. 7361, 1946.
175 G. T. Motock; Fiat Final Report 295, 1945.
176 R. M. Hunter; PB 204, 1945 and PB 49,026, 52-56.
177 V. Engelhardt; "Handbuch der technischen Elektrochemie." Akademische Verlags Buchhandlung. Leipzig, 1934. 3. C. L. Mantell; "Industrial Electrochemistry," McGraw Hill Co., New York, 1940. Gmelin's "Handbuch der anorganischen Chemie," System No. 35, Aluminium, and No. 27, Magnesium.
178 V. A. Plotnikov and D. P. Zosimovich; *Chem. Abstr.*, 1937, 31, 4599.
179 H. Grothe and C. A. Piel; *Z. Elektrochemie*, 1950, 54, 210, 216.
180 Messner; PB 41,423.
181 A. D. Turnbull; *Min. and Met.*, 1947, 28, 62.
182 S. C. Pyck; U.S. Pat. 2,558,627, 1951.
183 W. C. Gardiner; Fiat Report 821, 1946, PB 37,994, Duisburger Kupferhutte.
184 E. A. Ashcroft; *Trans. Amer. Electrochem. Soc.*, 1906, 9, 122.
185 A. von Zeerleder; *Trans. Electrochem. Soc.*, 1934, 65, 353.
186 G. D. P. Cordner and H. W. Worner; *Australian J. Appl. Sci.*, 1951. 2, 358. Refer *Comptes Rendus*, 1952, 46, 4927.
187 W. J. Kroll; *Trans. Electrochem. Soc.*, 1945, 87, 551.
188 *id.*, *Trans. Electrochem. Soc.*, 1946, 89, 382; discussion.
189 L. Voltmer; German Pat. 74,959, 1892.
190 Krupp; German Pat. 81,225, 1895.
191 H. J. Blickslager; *Rec. Trav. Chim. Pays Bas*, 1927, 46, 307.
192 Deutsche Gold und Silberscheide Anstalt (H. Nees); German Pat. 709,742, 1941.
193 H. von Wartenberg; *Z. Elektrochemie*, 1909, 15, 866.
194 H. Moissan; *Comptes Rendus*, 1896, 122, 1088.
195 H. S. Cooper; German Pat. 547,620, 1927.
196 G. Jaeger Degussa; U.S. Pat. 2,151,599, 1939.
197 I.G. Farbenindustrie and Brode, Wurster, Buttgenbach; German Pat. 582,568, 1933; 514,125, 1930; 581,310, 1933.
198 A. H. Aten, H. J. den Herzog and L. Westenberg; *Trans. Electrochem. Soc.*, 1925, 47, 265.
199 P. Drossbach; *Z. Elektrochemie*, 1952, 56, 23.
200 V. A. Plotnikov and E. L. Kirichenko; *J. Inst. Metals*, Abstr., 1940, 77, 303.
201 W. Hampe; *Chem. Zeit.*, 1888, 12, No. 11.
202 Vereinigte Stalwerke; German Pat. 582,698, 1933; 580,732, 1931.
203 G. D. P. Cordner and H. W. Worner; *Australian J. Appl. Sci.*, 1951, 2, 358. Refer. *Chem. Abstr.*, 1952, 46, 4927.
204 T. A. Mitchell; U.S. Pat. 2,398,590, 1939.
205 L. Andrieux; *Ann. Chim.*, 1929, 12, 423.
206 W. Rudorff and G. Rudorff; *Z. anorg. Chem.*, 1947, 253, 281; *id.* and U. Hofmann, J. Endell and G. Rueuss; *Z. anorg. Chem.*, 1948, 256, 125.
207 B. Cartwright, L. R. Michels and S. F. Ravitz; Bur. of Mines R.I. 3805, 1945.
208 K. Arndt and H. Probst; *Z. Elektrochemie*, 1923, 29, 330.
209 W. Rudorff and H. Schulz; *Z. anorg. Chem.*, 1940, 245, 121.
210 A. Minet; "Production of Aluminium." Halle.
211 F. Haber; *Z. Elektrochemie*, 1902, 8, 871.

Chlorine Metallurgy—Part VII

By W. J. KROLL

(*Consultant, Corvallis, Oregon, U.S.A.*)

(*Concluded from* METAL INDUSTRY, *October* 31, 1952)

CONSIDERABLE difficulties are experienced when electrolyzing the chlorides of plurivalent metals, such as those of Fe, Cl, Cr, Ti, Zr, Mo, V and others. The anode chlorinates the bath up, the cathode does the opposite, which results in poor current efficiencies. The electrolysis of titanium trichloride[203] in a carrier salt may be taken as an example.

Supposing that $TiCl_3$ can be stabilized in a carrier salt, which fact the author revealed in a memorandum at the Titanium Symposium, November 8-9, 1950, in Washington, D.C., the chlorine evolved at the graphite anode chlorinates some of the lower titanium chloride present in this area, up to the tetrachloride which, being very volatile and insoluble in the bath, escapes with the anodic gases. Similar conditions exist in the tin and iron dichloride[187] fusion electrolysis and losses of $SnCl_4$ and $FeCl_3$ are observed. The titanium trichloride itself reacts with the dendrites, which it dissolves, giving dichloride according to equation 14, which compound forms a diffusion layer around the cathode. Correspondingly the current efficiency is reduced in proportion with this back reaction. Dichloride, once it reaches the anode, is itself chlorinated up to tri- and tetrachloride, thus helping to depolarize the anode. As seen herefrom, it does not matter whether one starts from tri- or dichloride, since after a while the chlorination effect of the anode makes itself felt, bringing the bath up to its stable working composition of mixed di- and trivalent titanium salts. If a start could be made from divalent salt, the current efficiency would be high in the beginning; decreasing with the progress of the chlorinating action of the anode. If titanium tetrachloride was soluble in the bath the current efficiency could be expected to be lower than with a tri- or divalent electrolyte. A larger electrode distance increases the current efficiency to a point because of the reduced mixing action of the anodic chlorine and because of the restricted diffusion of titanium compounds from and to the anode.

Since it is desirable to maintain the low valency condition, and the use of a diaphragm, which would solve this problem, is not possible, the anode might be depolarized. This has been suggested by Nees[192], who injects hydrogen in the anode, made of porous carbon, while electrolyzing chromium chloride in a carrier salt. This amounts practically to reducing the chloride entirely with hydrogen, forming HCl. High purity hydrogen might not be required for depolarizing, which would be an advantage over direct hydrogen reduction. Cordner[203] uses, probably with the same intention, a hydrogen atmosphere. In this process reclamation of the HCl formed becomes a necessity.

Titanium alloy anodes would dissolve in the bath to tri- and dichloride, thus depolarizing automatically. However, the second constituent of the alloy would have to form such chlorinated compounds as do not dissolve in the bath, otherwise they would plate out with the titanium.

At low current densities, titanium dichloride deposits at the cathode. This can be avoided only by operating with a bath that contains little titanium halogenide, to force co-deposition of some active metal of the carrier salt (Na, Ca, Mg, Li, K) which reduces the dichloride to metal. High current density by which the area around the cathode is artificially depleted of titanium chloride, permits similar results being obtained. However, the steadily increasing surface of the dendritic deposit interferes with the intention of maintaining a constant high current density.

As soon as the current is interrupted, the dendrites deposited react rapidly back with the bath and they dissolve with formation of lower chlorides. This is even worse if one tries to mix the crystals with the bath in view of fluidizing them for easy removal from the cell. The product obtained in this case is a very fine powder, mixed with the electrolyte, which can be extracted by wet methods, only with considerable losses.

Production of Aluminium and Manganese

The electrolytic decomposition of $AlCl_3$ and $MnCl_2$ is comparatively easy, because no lower chlorides are formed. The aluminium chloride electrolysis would appear to be attractive; since it can be performed at very low temperatures so that the energy input, required to keep the cell hot, is low. Double aluminium and sodium chloride melts below 200°C. and the cell can be operated at temperatures of this order. The I.G. Farbenindustrie, which experimented with this type of electrolysis, had difficulty with the anodes, made of graphite, which were severely attacked. There seems to be formation of some carbon tetrachloride at this low temperature, resulting in a disintegration of the graphite. Therefore the company tried tungsten anodes which are said to hold out up to 600°C. Soluble anodes of a 13 per cent aluminium-silicon alloy could be refined on pilot plant scale in a bath of $AlCl_3$ in KCl/NaCl (1 : 1 : 1·4 mols.) by the Aluminiumindustrie Neuhausen[212]. Lead chloride was added to the electrolyte to obtain smooth deposits and the aluminium so produced contained 0·2 per cent Pb. The cells had to be closed and the electrolyte was circulated through pipes. The cell voltage could be kept between 0·15 and 0·6 volts. The aluminium chloride electrolysis has a future, since the chloride is easily made and the chlorine obtained in the cell can be recycled. The low power consumption should be an incentive for the development of this process.

The same holds true for the manganese chloride electrolysis in a carrier salt which can be performed at higher current efficiencies and with a lower energy consumption than the aqueous electrolysis. Removal of the cathode deposit in this case as well as in the aluminium chloride electrolysis is one of the main problems to be solved.

Soluble Alloy Anodes

Since the memorable work of Lorenz[43], practically nothing has been done as to the separation of metals and chlorides by fusion electrolysis. This pioneer referred to the separation of Pb/Zn, Pb/Cd/Zn, Ag/Zn, Cu/Zn and Fe/Zn. The author extended this work to the purification of iron and ferro-manganese[187].

In a fusion electrolysis with soluble metal anode the chlorine attacks the anode constituent uniformly. The chlorides formed go either in solution in the bath, or, if volatile ($SiCl_4$, S_2Cl_2, PCl_3) and insoluble at the given temperature, boil off. Carbon in low carbon alloys is not attacked, and floats to the surface of the electrolyte. High carbon alloys behave like plain graphite when used as anodes. In this way a separation of many constituents can be achieved either by leaving them behind in the anode sludge or by volatilizing them as chlorides. Silicon, in a low temperature electrolysis such as that of Al/Si alloys in a NaCl/$AlCl_3$ bath,

which operates below 200°C., remains unattacked in the anode residues[212].

At the cathode the most readily reducible elements deposit first, when the electrolysis starts. This leads to a variation of composition of the bath in which the most electronegative salts accumulate and play the role of a carrier until a limit concentration is reached, where these salts are also decomposed. Their base metal is now co-deposited at the cathode where it may form alloys, if there is any tendency to alloy, with the first deposited metal. Once the bath has reached its equilibrium composition, the same alloy as present at the anode is deposited at the cathode, minus the constituents that form volatile chlorides. This also points the way for producing alloy powders, which can be obtained from mixed chlorides or with soluble alloy anodes provided the bath is adjusted as to its composition for co-deposition. In this way, Blickslager[191] made FeCo and NiCo alloys.

By adjusting the bath composition the electrolysis can be continued without co-deposition of the more electronegative metal, if part of this chloride is systematically extracted from the electrolyte to maintain the correct ratio of the carrier to the decomposable salt. In aqueous electrolysis, too, this is common practice. It can readily be done by treating only the electrolyte, entrapped in the dendrites, which has to be removed anyway. Aqueous methods frequently permit easy separation because of insolubility in water (CuCl)[119]. The salt can also be treated by thermal and chemical methods, as has been shown under the separation methods for tin-lead alloys[148,149,150,151,152,153,154,155]. Chlorination of the fused salts may bring about volatilization of the higher more volatile chlorides.

Separation by precipitation of one of the constituents with oxygen blown into the fused salts might apply to some specific cases (see Table II).

A peculiar way of making alloys has been devised by Andrieux[213]. Metals which form readily fusible eutectics can be used as solid cathodes on which the second, eutectic forming element is deposited. The eutectic runs off the surface and it can be collected on the bottom of the cell. The "icicle" method works well with nickel boride and titanium[214] and beryllium-copper eutectics[215], in which case a fluoride bath must be used. It might be adaptable to chloride electrolytes. Naturally alloy platings can be made the same way[215].

Intermetallic compounds have been produced by Andrieux in a fluoride bath with oxide additions. Similar ideas apply also to the chloride electrolysis[216].

Alloys, fused or solid, can be produced also with a subsidiary soluble anode, switched in parallel with the main anode, but shunted with an adjustable resistance to regulate the rate of dissolution. This anode contains the metal to be co-deposited. Alternatively, chlorides of more electropositive metals than that of the metal deposited at the cathode are fed regularly into the electrolyte. These are reduced by the cathode metal with which they alloy.

The possible uses of the methods described in scrap recovery must be stressed. The separation of zinc and lead from desilverization residues, the separation of ferro-nickel, copper-nickel and copper-silver, the production of copper from brass, of iron from hard zinc, the separation of tin bronzes and recovery of $SnCl_4$ by volatilization from the electrolyte are all within the reach of the electrochemist, provided suitable cells can be constructed.

Conclusion

The reader has been offered a panoramic view of chlorine metallurgy. First its basic reactions were stressed, such as chlorine/oxygen exchanges, equilibria of oxides with HCl, Oerstedts reduction-chlorination and its extension to reduction-chlorination by compounds, the relations ruling oxide/chloride exchanges, which may be assisted by side reactions between a base and an acid, as are used in chloridizing roasting. The importance of oxygen control in chloridizing roasting and in chlorination is emphasized and the possibility of producing pure oxides from chlorides, such as silica and titania by combustion in oxygen is mentioned. Purification methods for chlorides and their separation are discussed as well as the problem of reclaiming by-products such as FeCl, and HCl. The question of higher and lower chlorides and its implication as to phenomena in the chlorinator and for metal winning are discussed. A few examples are given concerning the possible use of chlorine in the beneficiation of low grade ores and the main applications of chlorination in the production of anhydrous chlorides on a commercial scale. The reduction of chlorides with other metals and with alloys, either with fused or with solid reaction products is exemplified and the reduction of chlorides with hydrogen which also concerns platings, is presented. The separation of lead from tin is offered as an example to show how an equilibrium can be shifted one way, and how the reagent, $SnCl_2$, can be reclaimed from the salts by way of chlorination to the more volatile tetraform. A large section is devoted to the fusion electrolysis with special reference to the deposition of metals in solid form. The possibilities of using such methods in metal winning and in alloy refining or production are discussed. The main problems, namely the behaviour of an electrolytic cell operating with fused plurivalent salts, and the removal of cathode deposits from the bath are examined in detail, especially in relation to the possible production of titanium metal. There is a widespread belief that the electrochemistry of fused salts has reached the status of stagnation. It has been shown that, on the contrary, a broad future is open to all those who want to leave the beaten tracks and to pick up again, where the pioneer Lorenz left off forty years ago. If the electrochemists now engaged in developing a fusion electrolysis method for the production of titanium are successful, they will open also the very large field of metal winning and purification with solid cathode deposit, which has been outlined above.

References

212 V. Engelhardt; "Handbuch der technischen Elektrochemie." Akademische Verlags Buchhandlung. Leipzig, 1934, 3.

213 J. L. Andrieux; U.S. Pat. 2,033,172, 1936.

214 H. Fischer; German Pat. 615,951, 1935.

215 H. Fischer and W. Schwan; *Metallwirtschaft*, 1933, 12, 187.

216 J. Koster and R. G. Knickerbocker; Bur. of Mines R.I. 3500, 1940.

Men and Metals

WHEN announcing, in the last issue of this journal, that the City and Guilds of London Institute had decided to establish under its Royal Charter an Insignia Award in Technology, we did not expect that within a few days we should learn of the first presentation of this award.

On Monday last, at Goldsmiths Hall, London, the Duke of Edinburgh, President of the Institute, handed the Insignia Award to **Sir Arthur J. G. Smout.** The award is intended to be a mark of distinction for those who have combined with a sound and adequate knowledge of the fundamental scientific principles of their industry, a capacity for leadership and administration.

Sir Arthur is a past president of the Institute of Metals and a director of Imperial Chemical Industries Limited. During the last war he was prominent in the Ministry of Supply as Director-General of Munitions Production.

AT a recent meeting of the Council of the Gauge and Tool Makers' Association, **Mr. F. W. Halliwell,** M.I.Mech.E., M.I.Prod.E., was re-elected President of the Association for the new session of 1952/53.

Mr. A. L. Dennison, M.I.Prod.E., was elected Chairman of the Association and the two vice-chairmen are **Mr. L. E. Van Moppes** and **Mr. S. J. Harley,** B.Sc., M.I.Mech.E., M.I.Prod.E.

Mr. R. Kirchner, M.I.Mech.E., M.I.Prod.E., was re-elected as honorary treasurer, and the immediate past-chairman, **Mr. H. S. Holden,** M.I.Prod.E., will continue service on the Council of the Association during the new session.

Computational models for ductile and brittle fracture

Lynn Seaman, Donald R. Curran, and Donald A. Shockey

Stanford Research Institute, Menlo Park, California 94025
(Received 21 June 1976)

J. Appl. Phys. 47, No. 11

Computational models of dynamic ductile and brittle fracture are developed for wave propagation in one- and two-dimensional geometries. The model features have been taken mainly from detailed observations of samples partially fractured during impacts, but the functional forms are consistent with theoretical results where applicable. Basic features of the models are the nucleation and growth (hence, the acronym NAG for the models) of voids or cracks, and the stress relaxation resulting from the growing damage. The results of the calculations include number and sizes of cracks, voids, or fragments as a function of position in the material. The NAG analysis presents the nucleation law, determined from experiment, and two growth laws: both growth and nucleation are functions of stress and stress duration. Procedures for treating cracks with a range of sizes and orientation are presented with the method for computing the stress relaxation that accompanies growth of damage. Brittle fracture is essentially anisotropic in actuality and in the model: cracks nucleate and grow as a function of stress normal to their plane, and the stress relaxation is a function of crack opening in the direction of the stress. Criteria are presented for the coalescence of cracks to form fragments and for complete fragmentation. The computational models have been applied to one- and two-dimensional wave propagation problems. The NAG models have been shown to be applicable to several metals, a plastic, and a quartzite, to stress levels from just above threshold to ten times the threshold, and to load durations from 20 nsec to several microseconds. The damage has been computed for stress waves caused by impact, thermal radiation, and explosion.

PACS numbers: 62.50.+p, 44.30.Ni, 44.30.Ea, 62.20.Mk

I. INTRODUCTION

In this paper we describe computational models that we have developed to describe the fracture processes occurring under conditions of projectile impact, air shock loading, deposition of intense thermal radiation (from x-ray, electron-beam, or laser sources), or explosion. The models describe the processes of nucleation of cracks or voids, the growth of these cracks or voids, and the effect of the growing damage on the stress-strain relations. The damage in the models is related only to the stress and stress duration and is therefore independent of the type of loading. The computational models presented here represent a continuation of the development reported in Ref. 1. These models were originally constructed for fracture under one-dimensional impact conditions in which the tensile stress duration was 100 nsec–1 μsec.[2–7] However, the models have now been tested under more general, two-dimensional projectile impacts and under many radiation and explosive-loading conditions. The models have been successfully applied to stress durations as short as 20 nsec and as long as several microseconds. Other researchers have also applied the nucleation and growth method to fracture problems. Stevens, Davison, and Warren[8] reported using a model like our ductile fracture model for single-crystal aluminum. Recently, Davison, Stevens, and Kipp[9] have developed a more elegant treatment of ductile fracture and applied this analysis to an impact in 1145 aluminum.

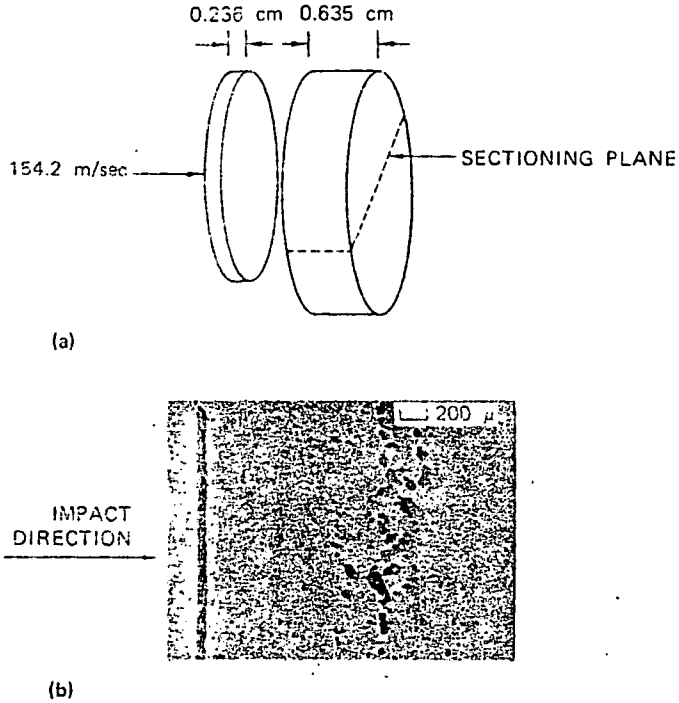

FIG. 1. (a) Impact configuration of a flat plate impact experiment in 1145 aluminum specimen No. 872 and (b) observed ductile fracture damage on a cross section through target.

In the present paper, the fracture phenomena to be treated computationally are first introduced through experimental examples. Then, the model requirements deduced from these observations are listed, and the computational models are presented. Some computed results are given to show the nature of the results.

II. BACKGROUND: OBSERVED FRACTURE PHENOMENA

The experimental data presented here illustrate damage phenomena and provide a common basis for considering damage criteria. Figure 1 is a cross section of an aluminum target plate (0.635 cm thick) that has undergone a planar impact at 154 m/sec by another aluminum plate (0.231 cm thick). Following the compression wave resulting from the impact, rarefaction waves have intersected near the middle of the target plate to cause damage in the form of nearly spherical voids. The damage is spread over a significant portion of the target

ate (about two-thirds of the plate thickness appears in section of Fig. 1), but the heaviest damage is in a narrow zone. Both the number and the size of voids decrease with distance from this zone. This type of damage is termed ductile fracture because of the high ductility (ability to flow) required of the plate material.

An example of brittle fracture is shown in Fig. 2. An Armco iron target was impacted by a flyer plate, which was tapered on the back to provide a varying tensile wave duration across the plate. The damage, which appears as randomly oriented microcracks, varies in proportion to the tensile wave duration. The damage in Fig. 2 is termed "brittle," although the crack growth is much slower than elastic crack velocities, indicating considerable plastic flow at crack tips.

When cracks coalesce, fragmentation occurs, as illustrated in Figs. 3 and 4. Figure 3 is a cross section of a 1.27-cm-diam target of Arkansas novaculite (fine-grained quartz) encased in an aluminum box. The target was impacted by a 0.079-cm-thick Lucite plate at 49.5 m/sec. An identical plate was impacted at 48.9 m/sec, but instead of sectioning it, we performed a wave analysis on the fragments. The resulting fragment groups are shown in Fig. 4. All the fragments are bulky, having six to eight major surfaces. By comparing the results of Figs. 3 and 4, we may deduce that a family of cracks of various lengths and orientations has led to a family of fragments of various sizes.

A sample of full separation is shown in Fig. 5. An aluminum target impacted by a flat plate in a configuration similar to that shown in Fig. 1 has been damaged to the extent that full separation occurred near the center of the target. This full separation appears as a microcrack running through heavily damaged material. Dvorak[10] has pointed out that brittle fracture in polycrystalline material also occurs by the coalescence of small microcracks ahead of the observed microcrack. The microcracks cleave individual grains; these small cracks widen and join to form the main crack.

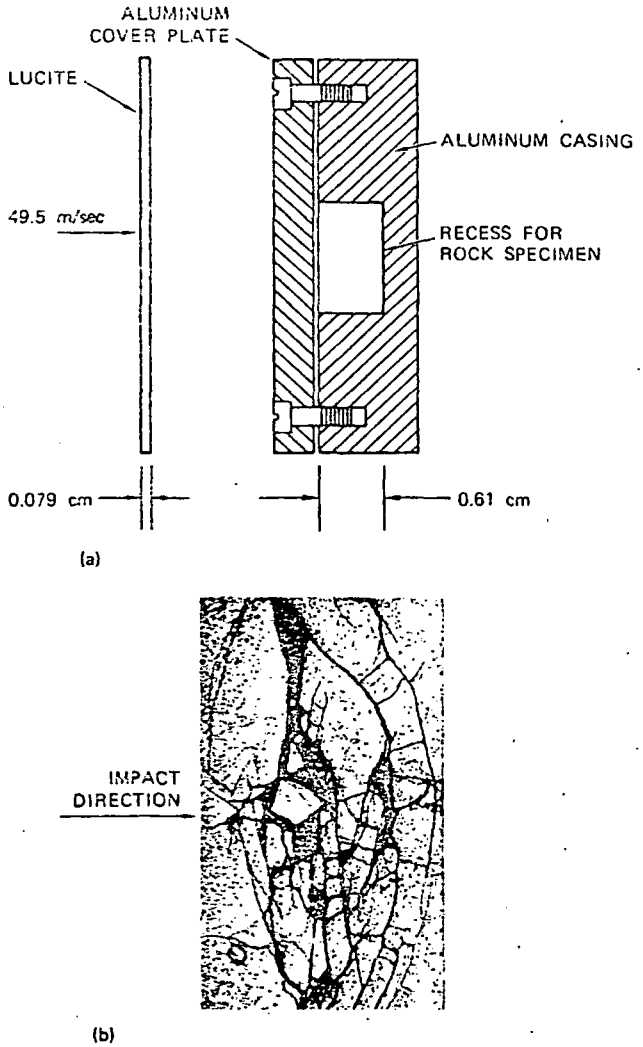

FIG. 3. (a) Configuration of impact experiment and (b) resulting damage on cross section of Arkansas novaculite.

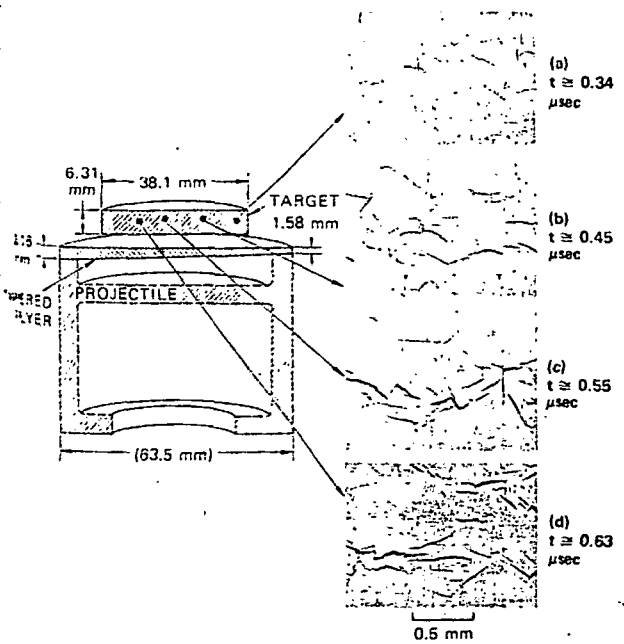

FIG. 2. Configuration of a tapered flyer impact experiment in Armco iron and observed damage on a cross section of the target.

From the review of the typical fracture cases above and from other observations, we have deduced the following:

(i) A range of damage is possible; there is no instantaneous jump from undamaged to fully separated.

(ii) Damage grows as a function of time and the applied stress. Hence, a single stress or strain at any time cannot be expected to characterize the dynamic fracture process. At least, some time-integral quantity (such as impulse) must be used to represent the dynamic strength.

(iii) As the damage occurs, the stiffness of the material decreases; hence, the wave propagation character changes. If the developing damage is not permitted to alter the wave processes in a computational procedure, then subsequent stress histories and damage must be invalid.

(iv) Even incipient damage levels are important, be-

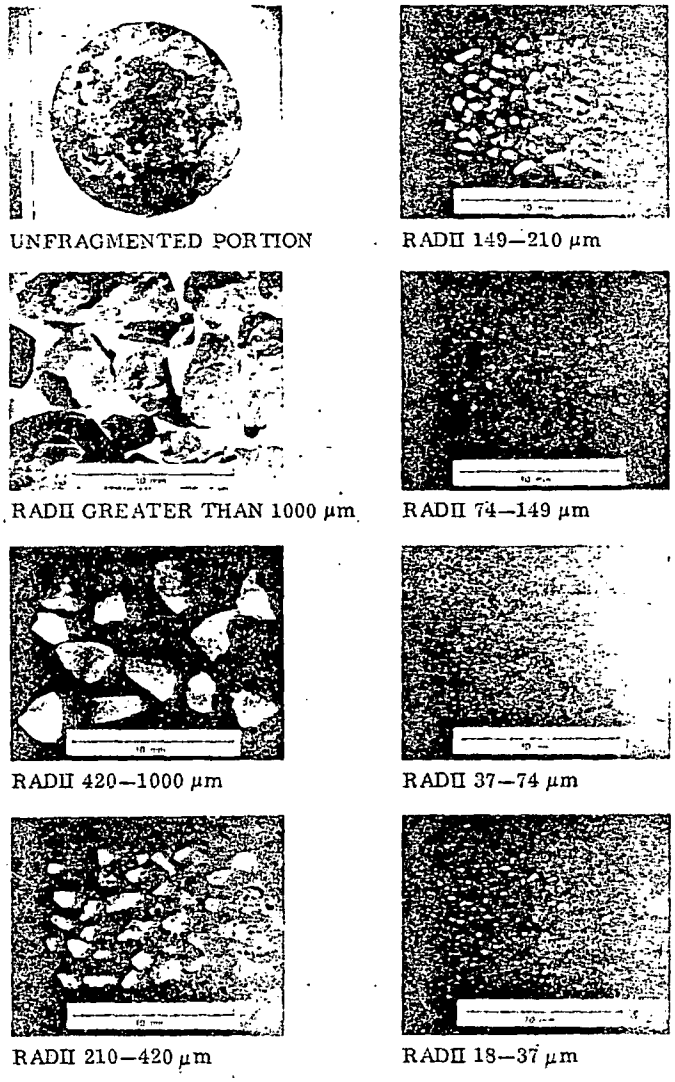

FIG. 4. Photomicrographs of fragments of various sizes from an impact experiment on an Arkansas novaculite target.

cause, while difficult to observe, the voids or cracks may seriously weaken a structure.

While the foregoing features represent experimental observations well enough, it may be possible to simplify or eliminate some of these features for computational purposes.

III. COMPUTATIONAL MODELS FOR FRACTURE

A. Introduction

Our computational models have been constructed to represent fracture and fragmentation in one- and two-dimensional geometries and have been applied to wave propagation problems. The models represent the following phenomena:

Nucleation of cracks or voids as a function of stress level and stress duration.

Growth of cracks or voids as a function of stress.

A range of void or crack sizes at all stages of fracture.

Coalescence of cracks to form fragments.

A range of fragment sizes.

A smooth transition from no damage through fracture to full separation.

These phenomena, which are included in the models, actually provide all the features noted previously in observations of dynamic fracture. Some of the phenomena are fairly well understood, and a few have been treated analytically. Other features, particularly those occurring near full separation, are understood only in broad qualitative terms. Where neither analytical guidance nor experimental evidence was available, estimates of appropriate functions and processes have been made. These estimates were necessary to produce complete models so that full separation could be handled. With complete models available, it may be possible later to reexamine elements of the models and to improve them based on experimental evidence.

The models constructed here are based largely on microscopic observations of material that has reached various stages of fracture. The damage is described by statistical distribution of cracks or voids, not by individual cracks or voids. This level of detail circumvents many of the serious problems encountered in extending microscopic-level theory to the macroscopic level, while enough detail is retained to represent the underlying processes of growth and nucleation.

The computational models represent simplifications of the actual fracture processes. Physically, nucleation may occur by widening of inherent flaws in the material, cracking of hard inclusions, separation along grain boundaries, or by other mechanisms. In the model, however, nucleation means the appearance of the void or crack at an observable and easily identifiable size on photomicrographs at a scale of about 100×. This nucleation occurs in the model as a function of stress and stress duration. After nucleating, the voids or cracks grow (in the model) at a rate dependent on the stress (or stress intensity K_I) level, duration of loading, and

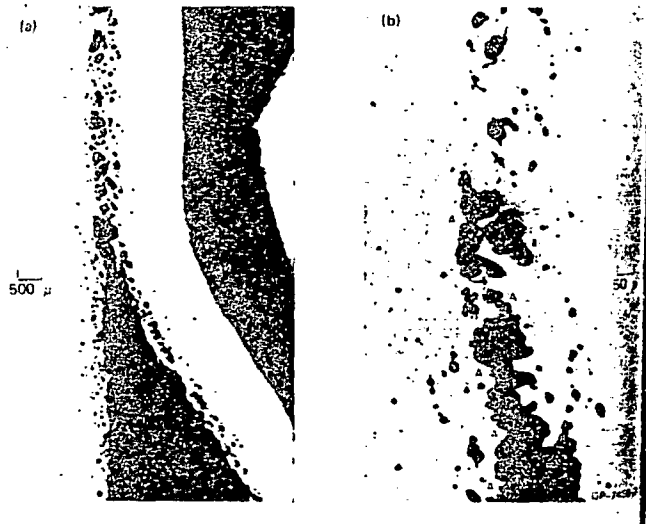

FIG. 5. Ductile cracks. (a) Ductile crack propagation by void coalescence. (b) Tip of ductile crack shown in (a), at higher magnification. Material failure by void coalescence due to necking of the regions separating the voids is apparent near the points marked A.

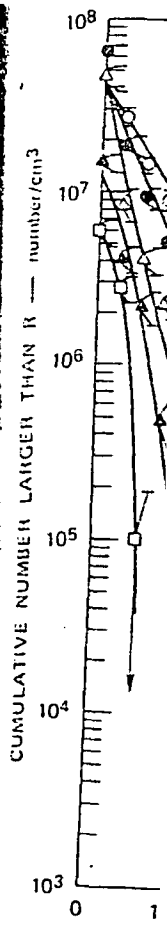

FIG. 6. Observ
face side of the
one-dimensional

the size of the
for the stress
ment of damag

When the nu
cence criterior
oin and to forr
loading, the en
plete separatio
oids continue
exceeds a criti

The two com
models for nuc
subroutines tha
wo-dimensiona
odes. While th
subroutines are
containing the s

The analytica
next.

3. Ductile fractu

The ductile fr
basis of observa
mm² and copper
on polished cros

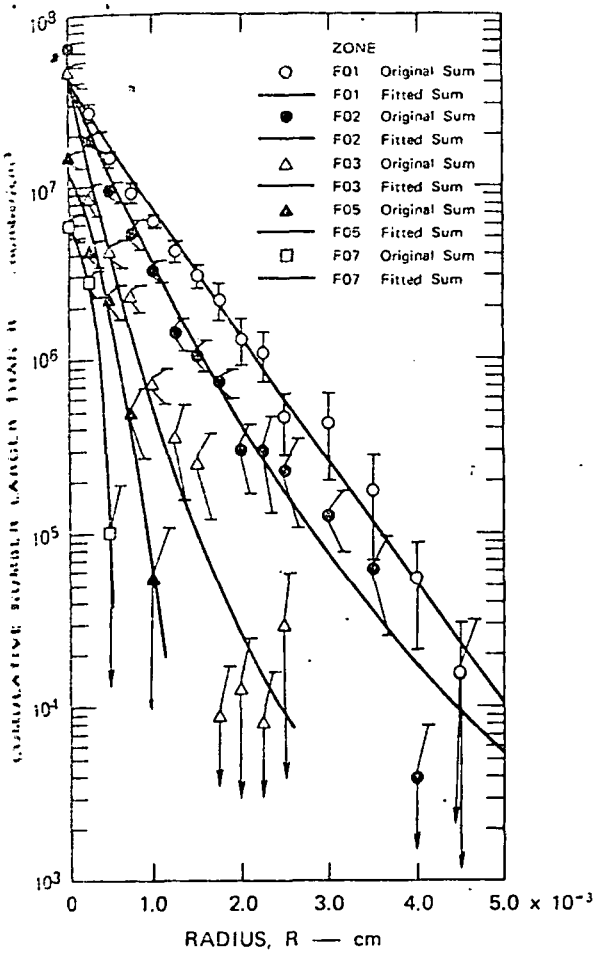

FIG. 6. Observed volume distribution of voids on the free surface side of the spall plane in an OFHC copper target after a one-dimensional impact. Shot S24.

the size of the void or crack. The model also accounts for the stress reduction that accompanies the development of damage.

When the number and size of cracks meet a coalescence criterion in the brittle model, the cracks begin to link and to form isolated fragments. With continued loading, the entire material forms fragments, and complete separation may occur. For ductile fracture, the voids continue to increase in size until the void fraction exceeds a critical value and separation occurs.

The two computational fracture models (termed NAG models for nucleation and growth) are implemented in subroutines that may be readily inserted into one- and two-dimensional Lagrangian wave propagation computer codes. While the material is undergoing fracture, these subroutines are called instead of the usual subroutine containing the stress-strain relations.

The analytical basis for the two models is presented here.

3. Ductile fracture

The ductile fracture model was formulated on the basis of observations of ductile fracture in soft aluminum and copper.[3] These observations, which were made on polished cross sections of targets after impact, showed that the fracture occurred by the nucleation and growth of nearly spherical voids. The observed voids were measured and counted and assembled into number-versus-radius size distributions. These surface distributions were then transformed statistically to volumetric distributions with the BABS1[2] computer program. A sample set of void size distributions is shown in Fig. 6. Curves are given for four depths within the sample; the maximum damage is at the plane F01. All the volumetric distributions obtained with aluminum and copper had a form that could be approximated by the equation

$$N_g(R) = N_0 \exp(-R/R_1), \tag{1}$$

where N_g is the cumulative number/cm^3 of voids with radii larger than R; N_0 is the total number/cm^3 of voids; and R_1 is a parameter of the distribution.

The total void volume is obtained by integrating over the entire distribution:

$$\begin{aligned} V_v &= \frac{4\pi}{3}\int_0^\infty R^3 \frac{dN}{dR}\, dR \\ &= \frac{4\pi}{3}\int_0^\infty R^3 \left(-\frac{N_0}{R_1}\right) \exp\left(-\frac{R}{R_1}\right) dR \\ &= 8\pi N_0 R_1^3. \end{aligned} \tag{2}$$

The void size distribution at any time and at any point can be represented by N_0 and either R_1 or V_v. For computational purposes, N_0 and V_v are selected.

1. Nucleation

Nucleation in the model occurs as the addition of new voids to the existing set. These new voids are presumed to occur in a range of sizes with a size distribution given by Eq. (1). At nucleation, the parameter R_1 equals R_n, the nucleation size parameter (a material constant). The number of voids nucleated is governed by a nucleation rate function that was derived from our work in both ductile and brittle materials:

$$\begin{aligned} \dot{N} &= \dot{N}_0 \exp[(P_s - P_{n0})/P_1] \quad P_s > P_{n0} \\ &= 0, \qquad\qquad\qquad\qquad P \le P_{n0} \end{aligned} \tag{3}$$

where $\dot{N}_0$, P_{n0}, and P_1 are material constants, and P_s is the tensile pressure in the solid material (not the average pressure in the solid and voids). The constant P_{n0} is the threshold for nucleation.

The void volume nucleated in a time interval Δt is found from Eqs. (2) and (3).

$$\Delta V_n = 8\pi \dot{N} \Delta t R_n^3. \tag{4}$$

2. Growth

In the model, damage increases by nucleation of new voids and by growth of the existing voids. In our studies of aluminum and copper, it was found that growth was linearly dependent on the pressure level and current void size, so the growth rate $\dot{R}$ is

$$\dot{R} = [(P_s - P_{g0})/4\eta]\, R \tag{5}$$

where P_{g0} is the threshold pressure for growth, and η is the material viscosity. This is the usual form for a growth law in a viscous material with no strength.

Reference 3 showed that Eq. (5) is accurate for small voids, but for larger radii inertial effects reduce the velocity below that given by Eq. (5). The growth represented by Eq. (5) is spherically symmetric because the void expands equally in all directions. Reference 3 showed that Eq. (5) is an appropriate description of void growth in material with strength undergoing one-dimensional planar flow as well as spherical flow.

The growth of a void during a time interval Δt is obtained by integrating Eq. (5) to obtain the new radius

$$R = R_0 \exp\left(\frac{P_s - P_{s0}}{4\eta}\,\Delta t\right), \tag{6}$$

where R_0 is the radius at the beginning of the time interval. Since every void in the distribution grows by the same exponential factor, even the size parameter R_1 grows according to Eq. (6):

$$R_1 = R_{10} \exp\left(\frac{P_s - P_{s0}}{4\eta}\,\Delta t\right), \tag{7}$$

where R_{10} is the size parameter at the beginning of the time interval. Then the new void volume can also be found from Eqs. (2) and (7):

$$V_v = 8\pi N_0 R_1^3 = V_{v0} \exp\left(3\frac{P_s - P_{s0}}{4\eta}\,\Delta t\right), \tag{8}$$

where $V_{v0} = 8\pi N_0 R_{10}^3$, the void volume at the beginning of the time interval.

The total change in void volume is the sum of the contributions associated with nucleation and growth. Thus, the total void volume at the end of the interval is

$$V_v = V_{v0} \exp\left(3\frac{P_s - P_{s0}}{4\eta}\,\Delta t\right) + \Delta V_n. \tag{9}$$

3. Pressure-volume and stress-volume relations

The stress-strain relations for material undergoing fracture account for the presence of voids. As usual, the stress is separated into pressure and deviatoric components.

The pressure is related to the specific volume and internal energy through a combination of the Mie-Gruneisen equation of state for the solid and a relation between pressure in the solid and average pressure on the porous material. We assume that an average pressure in the solid material can be computed from the specific volume of the solid and the internal energy through use of a small-strain form of the Mie-Gruneisen equation:

$$P_s = C(\rho_s/\rho_0 - 1) + \Gamma\rho_s E, \tag{10}$$

where C is the bulk modulus, Γ is the Gruneisen ratio, E is internal energy, ρ_s is the solid density, and ρ_0 is the initial density of the solid. The pressure computed from Eq. (10) is necessarily an average, because the actual stress states will vary greatly through partially fractured material.

The average pressure on the gross section of the fractured material can now be related to the pressure in the solid components according to a relation derived by Carroll and Holt[11] for porous material:

$$P = P_s\rho/\rho_s, \tag{11}$$

where P is the average pressure on a section and ρ is the average density of the porous material. A combination of Eqs. (10) and (11) relates the average pressure P to the energy E and density ρ.

The deviator stresses are computed by the usual elastic and plastic relations. However, the damage that occurs is presumed to affect both the yield strength and the effective shear modulus of the material. The modulus is reduced as a function of the developing porosity according to the elastic relations of MacKenzie.[12] His formulation, in the present nomenclature, is

$$G = G_0(1 - V_v\rho F), \tag{12}$$

where G is the effective shear modulus, G_0 is shear modulus of the solid, V_v is the specific volume of voids, and

$$F = 5\frac{3C + 4G_0}{9C + 8G_0} = 15\frac{1-\nu}{7-5\nu}, \tag{13}$$

where ν is the Poisson's ratio and C is the bulk modulus of the solid.

The yield strength reduces somewhat more rapidly than the modulus as the porosity increases. Dynamic calculations of void growth[3] indicated that the yield strength should reduce in the following way:

$$Y = Y_0(1 - 4V_v\rho). \tag{14}$$

This expression is used in the fracture subroutine.

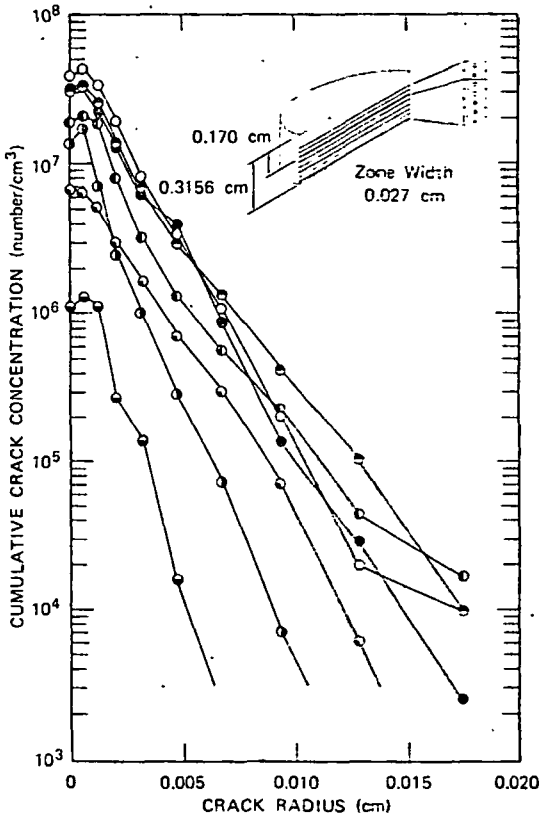

FIG. 7. Crack size distributions in zones near the spall plane in an Armco iron target after a one-dimensional impact. Shot S25.

A simultaneous solution must be obtained for the number of voids, void volume, and pressure; however, the relations between them are highly nonlinear; therefore, an iterative solution procedure was adopted. First, an estimate of the appropriate pressure P_s is made based on a linearization of the relevant equations. Then, a modified regula falsi method is used to obtain the final values of pressure and void volume. Sufficient accuracy is usually obtained with two to five iterations.

C. Brittle fracture

The brittle fracture model was formulated on the basis of observations of fracture in Armco iron,[3,4] beryllium,[4] beryculite,[6] and Lexan polycarbonate[5] (a transparent plastic). Fracture is termed "brittle" in this article whenever the primary damage mode appears as cracks as it did in these materials. This definition contrasts with the more common one which indicates simply a very limited amount of plastic deformation. In many of our "brittle" cases, such as Armco iron, the cracks grow slowly and with extensive adjacent plastic flow. In our impacted targets the cracks were measured for length and angular orientation with respect to the direction of loading. The observed cracks were then organized into groups according to size interval and angle interval. These surface distributions were transformed statistically to volumetric distributions in size and angle with the BABS2[3] computer porgram. For this transformation, it was assumed that the cracks were penny shaped and that the distribution was axisymmetric around the direction of propagation. Figure 7 shows a sample set of crack distributions. Here the angular variation has been suppressed, so the ordinate is the total number of cracks larger than the indicated radius. The volumetric distributions obtained with Armco iron had the exponential form found in Eq. (1) for voids.

For the model calculations, both size distribution and orientation distribution for the cracks, assumed penny shaped, must be considered. These distributions can be characterized by a density function $n(R, \varphi, \psi)$, so that $n(R, \varphi, \psi)\,dR\,d\varphi\,d\psi$ is the number of cracks per unit volume within the size interval R to $R + dR$ and the spherical angle intervals from φ to $\varphi + d\varphi$ and from ψ to $\psi + d\psi$. For the computer calculations, the continuous function n was discretized in φ and ψ and given an analytical form in R:

$$n(R, \varphi_i, \psi_j) = -(N_0^{ij}/R_1^{ij}) \exp(-R/R_1^{ij}), \tag{15}$$

where i and j designate an element in the orientation distribution array; N_0^{ij} is the number of cracks per unit volume in the (ij)th element of the array; and R_1^{ij} is a parameter giving the shape of the crack distribution of the $(ij)^{\text{th}}$ element. The cumulative crack concentration, N_t^{ij}, for each element, is

$$N_t^{ij}(R) = \int_R^\infty n\,dR = N_0^{ij} \exp(-R/R_1^{ij}). \tag{16}$$

The form of Eq. (16) was chosen because it closely matches the observed crack size distributions, typified by those shown in Fig. 7. Each element of the N_0^{ij} and R_1^{ij} matrices is associated with cracks of a specific orientation φ_i and ψ_j at the center of a spherical surface element, as shown in Fig. 8. Cracks with an orientation

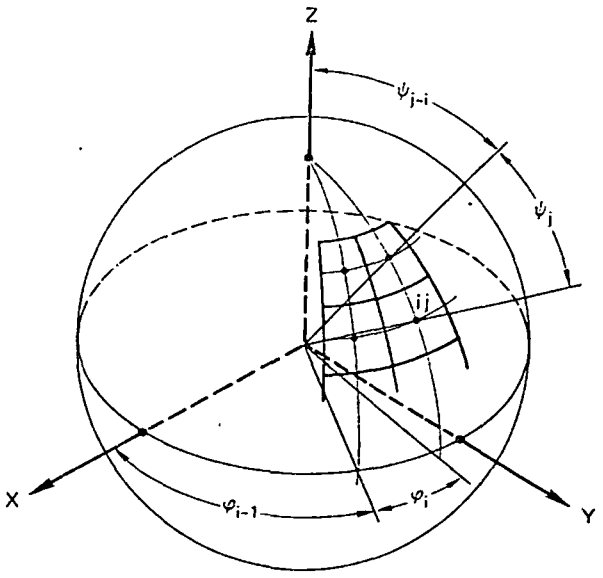

FIG. 8. Definitions of the orientation coordinates for each element of the crack orientation matrix.

φ, ψ cannot be distinguished from those with an orientation $\varphi + 180°$, $180° - \psi$; thus only one hemisphere needs to be represented. For the present calculation only five elements were used: $(\varphi, \psi) = (0°, 90°)$, $(45°, 54.8°)$, $(90°, 90°)$, $(135°, 54.8°)$, and (undefined, 0°). Hence, three elements are in coordinate directions initially, and the other two are in directions which are equiangular to the x, y, and z directions, and the $-x$, y, and z directions.

In two-dimensional axisymmetric or planar flow, the material may rotate in the x-y plane and it is necessary to let the cracks rotate with the material. This rotation of the crack arrays is accounted for by allowing the orientation coordinate in the x-y plane (φ) to rotate with the material. The angular rotation is given by the variable ρ_t. The orientation of the ith row of elements in the x-y plane is then given by

$$\varphi_i = \varphi_{i0} + \rho_t, \tag{17}$$

where φ_i is the current angular position, and φ_{i0} its initial position. At the end of a computation, ρ_t is listed so that the orientation of the ijth element can be related to the fixed x-y grid. The element rotation is independent of the initial orientation of the computational cell and of rotations that the cell undergoes before fracture begins.

1. Crack opening

The opening of cracks, as well as nucleation and growth, is a function of the stress applied normal to the plane of the cracks—neither shear nor torsional distortion of the crack surfaces is considered. In the terminology of fracture mechanics, we are treating only mode-I behavior, and disregarding modes II and III. For two-dimensional problems, in which $\tau_{xz} = \tau_{yz} = 0$, the general expression for this normal stress is

$$\sigma_{\varphi\phi} = \sigma_x l^2 + \sigma_y m^2 + \sigma_z n^2 + 2\tau_{xy} lm, \tag{18}$$

where the direction cosines l, m, and n are related to

φ and ψ as follows:

$$l = \sin\psi\cos\varphi,$$
$$m = \sin\psi\sin\varphi,$$
$$n = \cos\psi.$$

The cracks are presumed to open elastically to the value given by Sneddon and Lowengrub[13]:

$$\delta = [4(1-\nu^2)/\pi E]\, R\,\sigma_{\psi\psi}, \tag{19}$$

where δ is one-half the maximum separation of the crack faces and E is Young's modulus. The crack faces form an ellipsoid with three semiaxes δ, R, and R. Then the volume of a crack is

$$V_{1c} = [16(1-\nu^2)/3E]\, R^3\sigma_{\psi\psi}. \tag{20}$$

The volume of the entire crack distribution is obtained by combining Eqs. (16) and (20) into the following integral:

$$V = \sum_{i,j} V^{ij} = \sum_{i,j} \int V_{1c}\, \frac{d[N_0^{ij}\exp(-R/R_1^{ij})]}{dR}\, dR$$
$$= \frac{32(1-\nu^2)}{E} \sum_{i,j} N_0^{ij} (R_1^{ij})^3\, \sigma_{\psi\psi}^{ij}. \tag{21}$$

This elastic formula may be an accurate representation of the crack opening volume in a few cases where there is little plastic flow. However, for most of the materials and load levels we have considered, there is extensive plastic flow. In fact, in most of our studies, most of the material around the cracks is above the yield stress. When such large-scale plastic flow occurs, Eq. (21) must provide only a low estimate of the actual opening.

2. Crack nucleation

Nucleation in the model occurs as the addition of new cracks to the existing set. These new cracks are presumed to occur in a range of sizes with a size distribution like Eq. (16). At nucleation, the parameter R_1^{ij} equals R_n, the nucleation size parameter (a material constant). The number of cracks nucleated is governed by a nucleation rate function similar to that used for ductile fracture:

$$\dot{N} = \dot{N}_0 \exp[(\sigma_{\psi\psi} - \sigma_{n0})/\sigma_1], \tag{22}$$

where $\dot{N}_0$, σ_{n0}, and σ_1 are fracture parameters and $\sigma_{\psi\psi}$ is the stress normal to the plane of the cracks. This form of nucleation function resembles the relation deduced by Zhurkov[14] for the rate of breakage of atomic bonds. We have found it applicable to ductile materials and also to such diverse brittle materials as Armco iron,[3] beryllium,[4] and polycarbonate.[5] (In beryllium it was found that the deviator stress governs nucleation and not the stress $\sigma_{\psi\psi}$). The new cracks are nucleated with a range of sizes so that the number greater than R is

$$\Delta N_n^{ij} = \dot{N}^{ij}\, \Delta t\, \exp(-R/R_n), \tag{23}$$

where $\dot{N}^{ij}\,\Delta t$ is the total number nucleated in the ijth element, R is the nucleation distribution parameter, and Δt is the time step. The volume of the entire nucleated distribution is obtained by combining Eqs. (21) and (23):

$$V_n = \sum_{ij} V_n^{ij} = \sum_{ij} \int_0^\infty V_{1c}\{d[\dot{N}^{ij}\Delta t\exp(-R/R_n)]\, dR\}/dR$$
$$= [32(1-\nu^2)\Delta t\, R_n^3]/E \sum_{ij} \dot{N}^{ij}\, \sigma_{\psi\psi}^{ij}. \tag{24}$$

If the material is isotropic and under a uniform tensile stress, the probability of crack nucleation is equal in any direction. Then, the number of cracks assigned to each element is proportional to the solid angle subtended by the element. The fraction of the total solid angle for each element is called F_n^{ij}. If the material is not isotropic, F_n^{ij} can be set to reflect the observed flaw orientations.

3. Crack growth

The growth law derived from experimental data on both ductile and brittle fracture is[4]

$$\frac{dR}{dt} = T_1(\sigma - \sigma_{\ell 0})R, \tag{25}$$

where T_1 is a growth coefficient and $\sigma_{\ell 0}$ is the growth threshold stress. Here, $\sigma_{\ell 0}$ is treated as a constant material parameter, but in some cases, it has been taken as the critical stress for crack growth according to fracture mechanics.

$$\sigma_{\ell 0}^* = (\pi/4R)^{1/2} K_{Ic}, \tag{26}$$

where K_{Ic} is the fracture toughness. Since $\sigma_{\ell 0}^*$ is usually very small for impact problems, $\sigma_{\ell 0}$ in Eq. (25) can be taken as a small constant.

When Eq. (25) is integrated over a time step Δt (holding $\sigma_{\ell 0}$ constant), the final value of the radius is

$$R = R_1 \exp[T_1(\bar{\sigma}_{\psi\psi} - \sigma_{\ell 0})\Delta t], \tag{27}$$

where R_1 is the radius at the beginning of the interval and $\bar{\sigma}_{\psi\psi}$ is the average stress in the interval. When Eq. (21) is combined with Eq. (27), the crack volume associated with growth at the end of the time step is

$$V_\ell^{ij} = 32\, N_0^{ij}[(1-\nu)^2/E](R_1^{ij})^3\, \sigma_{\psi\psi}^{ij}\exp[3T_1(\bar{\sigma}_{\psi\psi}^{ij} - \sigma_{\ell 0})\,\Delta t]. \tag{28}$$

The total number of cracks in the ijth element at the end of the time step is

$$N_1^{ij} = N_0^{ij} + \dot{N}^{ij}\Delta t. \tag{29}$$

The total volume V_t^{ij} may be represented as the sum of V_n^{ij} and V_ℓ^{ij} from Eqs. (24) and (28), or the combination of cracks may be described by a single analytical form with N_1^{ij} cracks and a new shape parameter R_2^{ij}:

$$V_t^{ij} = V_n^{ij} + V_\ell^{ij} \tag{30}$$

or

$$V_t^{ij} = 32\, N_1^{ij}\, [(1-\nu^2)/E]\, (R_2^{ij})^3\, \sigma_{\psi\psi}^{ij}. \tag{31}$$

Equating the two expressions for V_t^{ij} provides a means for evaluating R_2^{ij}, the distribution parameter appropriate to the end of the time step:

$$(R_2^{ij})^3 = \{N_0^{ij}(R_1^{ij})^3\exp[3T_1(\bar{\sigma}_{\psi\psi}^{ij} - \sigma_{\ell 0})\,\Delta t] + \dot{N}^{ij}\Delta t\, R_n^3\}/N_1^{ij}. \tag{32}$$

Now the damage at the end of the time step can be completely characterized by two parameters, N_1^{ij} and R_2^{ij}, obtained from Eqs. (29)–(32).

D. Fragmentation model

The fragmentation process envisioned in our model is a natural extension of the brittle fracture process. The brittle fracture process is presumed to occur until some point at which interaction of the cracks becomes signi-

icant and coalescence begins. At this point, the gross stress on the cross section is still approximately equal to the stress in the solid material. The growth and nucleation processes are presumed to continue beyond the beginning of coalescence. Eventually, isolated fragments will occur within the solid material. As these fragments separate, they form voids in the continuous solid material, which cannot support the applied stress. The stress in the remaining solid material must increase to maintain the external tensile stress. The increased stress in the solid will lead to more growth and nucleation of cracks; hence, the final stages before complete fragmentation are cataclysmic and will tend to continue with very little outside encouragement. The crescendo of damage which occurs in our model just before full separation is probably very similar to the damage that actually occurs. This process will tend to emphasize damage in a few regions while allowing adjacent regions to be only slightly fractured.

A relationship between the fragment sizes and the numbers and sizes of the preceding cracks is required to model the fragmentation process. From our observations in both rock and metals, it appears that the fragments are typically chunky objects with an average of six to eight sides, each side probably being produced by one crack. Thus, for large fragments, the crack radius may approximate the fragment radius and the number of fragments may be one-third to one-fourth the number of cracks. Each large fragment contains a great number of uncoalesced small cracks; thus, only some fraction of the small cracks leads to fragments. The small fragments have the same shape as the large fragments. The number of fragments in a size range appears to increase as the size decreases, indicating the fragment-size distributions have a shape similar to crack-size distributions. These observations of actual fragments have been incorporated into the computational model.

The computational model provides (i) a criterion for crack interaction to begin the crack coalescence process; (ii) a criterion for the beginning of fragmentation, i.e., formation of the first isolated chunks; (iii) a criterion for completion of fragmentation; (iv) provision for stress-strain relations for material that is partially fragmented; (v) a method for computing a fragment-size distribution. In describing the model, we first present the method for transforming from cracks to fragments. The criteria and stress-strain relations are then introduced.

1. Formation of the fragment size distributions

A fragment is produced by the intersection of a number of cracks, each crack forming surfaces on two adjacent fragments. Generally, the size of the fragment face will be similar to the size of the cracks that have caused the fragment. In the model, the crack radius is R_c and the fragment size is defined by a radius R_f. The ratio of these radii is γ:

$$\gamma = R_f/R_c, \tag{33}$$

where γ is a number near 1.0. For chunky fragments with a small number of faces, one can relate the number

PARTIAL FRAGMENTATION

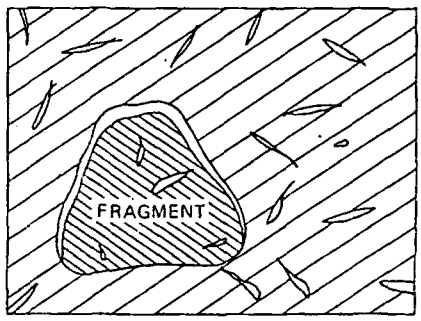

FIG. 9. Schematic depiction of the fragment formation process.

of fragments produced to the number of cracks. The parameter β is defined as

$$\beta = N_f/N_c, \tag{34}$$

where, for example, β is $\frac{1}{4}$ for eight-sided fragments. The fragment size distribution has the same form as the crack size distribution, Eq. (16). Thus,

$$N_f^{ij} = N_{f0}^{ij} \exp(-R_f/R_{f1}^{ij}), \tag{35}$$

where N_f^{ij} and R_{f1}^{ij} are related to N^{ij} and R_1^{ij} through Eqs. (33) and (34). Thus, the fragment size distribution is completely determined from the crack size distribution and the factors β and γ.

The volume v_f of a fragment of radius R_f is

$$v_f = T_f (R_f)^3, \tag{36}$$

where T_f is a coefficient that reflects the shape and number of sides of the fragment. The total volume of fragments can be determined by multiplying the number of fragments of radius R_f $(dN/dR)dR$ from Eq. (16), by the relative volume per fragment, and integrating the result:

$$V_f = T_f \sum_{ij} \int \frac{N_{f0}^{ij}}{R_1^{ij}} \exp\left(-\frac{R_f}{R_{f1}^{ij}}\right) R_f^3 \, dR = 6\beta\gamma^3 T_f \sum_{ij} N_0^{ij} (R_1^{ij})^3. \tag{37}$$

2. Criteria for fragmentation

The transition from slightly cracked to fully fragmented must occur gradually and with no discontinuities. The transition process is assumed to occur as follows: Cracks form and grow initially with little interaction between adjacent cracks. Under continued loading, cracks begin to interact, coalesce, and form fragments that are completely contained in the solid material (Fig. 9). The fragmented material no longer carries any loads, so the stress in the remaining unfragmented material may increase to sustain the external loads. This stress leads to more crack growth and fragmentation until the material is fully fragmented. In our computational model, the early stage of interaction is characterized by the concept of a "crack range," defined as a volume surrounding each crack. When the crack ranges of two cracks overlap, the cracks interact strongly, that is, the subsequent growth velocity and direction of one crack are altered by the presence of the other crack. The crack range is visualized as having a pancake or

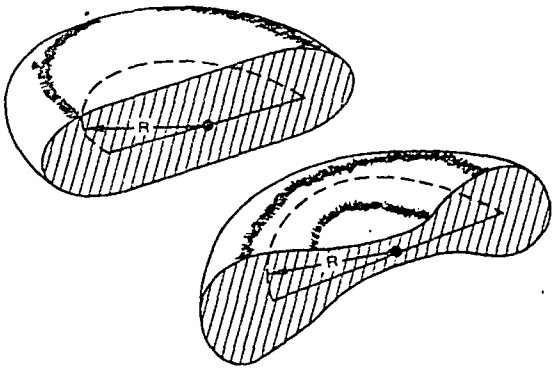

FIG. 10. Possible cross sections and shapes of the crack range surrounding penny-shaped cracks.

doughnut shape, as indicated in Fig. 10. Crack range is a function of the crack size only, and therefore, its volume is

$$V_{cr} = T_c R^3, \tag{38}$$

where T_c is a constant. The magnitude of T_c will depend on the material. For very brittle materials, T_c could be large (say, 20), but for very ductile materials, the value may be near unity. In the computational model, we presume that fragmentation begins when the crack ranges of all the cracks completely fill the volume of the material. The total crack range is derived by summing the ranges for cracks of all sizes and from all crack orientations:

$$V_{cr} = T_c \sum_{ij} \int_{R=0}^{\infty} R^3 \, dN. \tag{39}$$

This integral is like Eq. (24) in which the value of dN from Eq. (16) is inserted. The result is

$$V_{cr} = 6 T_c \sum_{ij} N_0^{ij} (R_1^{ij})^3. \tag{40}$$

The criterion for beginning fragmentation is then

$$V_{cr} = 1. \tag{41}$$

With a criterion for the start of fragmentation, we can now define the process by which the fragments are formed in a way that is physically reasonable and mathematically consistent but nonrigorous. At the completion of fragmentation, the Volume V_f from Eq. (37) is unity. At the beginning of fragmentation, it has a value

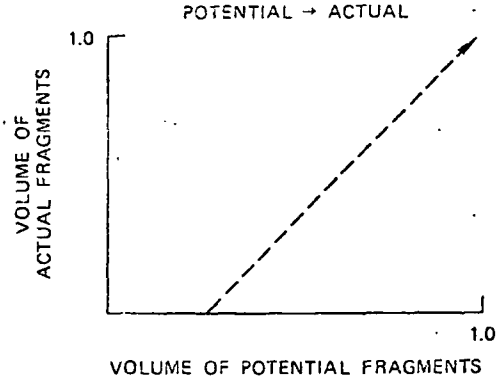

FIG. 11. Proposed relationship of actual fragments to potential fragments.

V^* obtained by solving (37) with the conditions of (40) and (41):

$$V^* = 3\gamma^3 T_f / T_c. \tag{42}$$

Now we define V_f as the potential fragment volume, because there are no fragments until V_f exceeds V^*. The actual fragment volume is computed according to the relation in Fig. 11:

$$V_a^f = \frac{V^f - V^*}{1 - V^*} = 1 - f_u, \tag{43}$$

where f_u is the unfragmented fraction of material. We presume that this same fraction $(1 - f_u)$ pertains to all fragment sizes and orientations, so the actual number of fragments is

$$(N_{f0}^{ij})_a = N_{f0}^{ij} (1 - f_u). \tag{44}$$

3. Stress-strain relations for brittle material

The stress-strain relations for material undergoing fracture and fragmentation account for both the opening of cracks and the voids produced by internal fragments. As usual, the stress is separated into pressure and deviatory components.

The pressure is related to the specific volume and internal energy in the same way as for ductile fracture. For brittle fracture, however, the porosity is the sum of the crack opening volume V_v and the volume of the fragmented material $(1 - f_u)V_s$, where V_s is the specific volume of the solid material. The material in a fragment is treated as having the same specific volume as the remaining solid, which is under stress. The fragment is completely surrounded by solid, as shown in Fig. 9; therefore, the volume associated with the fragment, including the fragment volume at original density and the void around the fragment, is assumed to equal the volume that the fragment would have at the current specific volume of the stressed solid. The deviator stress is computed from an expression which accounts for the anisotropy of damage:

$$\Delta\sigma_h' = 2\dot{G}(\Delta\epsilon_h' - \Delta\epsilon_h'^c), \tag{45}$$

where $\Delta\epsilon_h'$ is the deviator strain (total strain less mean strain) in the h direction, and $\Delta\epsilon_h'^c$ is the deviator strain taken up by changes in the porosity in the h direction. The contribution to $\epsilon_h'^c$ from any element of the crack orientation array is the total crack opening and fragmented volume of the element multiplied by the square of the cosine of the angle between the element and the h direction. As in ductile fracture, the deviator stress from Eq. (45) is modified if yielding occurs.

As for ductile fracture, an iteration procedure is required to solve simultaneously for damage and stresses. Here, however, the initial stress estimate is based simply on a purely elastic-plastic calculation. Damage is then computed based on these stresses. The computed damage leads of stresses from Eqs. (10) and (45). These new stresses serve as estimates for the next cycle. The changes in crack strains $\Delta\epsilon_h^c$ are heavily damped from cycle to cycle to force convergence.

IV. COMPARISON OF CALCULATIONS WITH DATA

Five of the many-simulations of actual experiments

TABLE I. Test configurations for sample fracture computations.

description	No.	Layer	Material	Thickness (cm)	Velocity (cm/sec)
o iron impact	S25	Projectile	Armco iron	0.0038	1.96×10^{4}
		Target	Armco iron	0.3156	• • •
		Gage backing	C7 epoxy	0.5	• • •
sas novaculite	52	Projectile	PMMA	0.079	4.89×10^{3}
t		Front cover	Aluminum	0.157	• • •
		Target	Novaculite	0.610	• • •
		(gap)	• • •	0.002	
		Rear cover	Aluminum	0.152	• • •
red flyer impact					
AR 30	2024-2	Projectile	OFHC copper	taper	3.065×10^{4}
ogeneous		(thickness of 0.2545—0.6355 cm varying over 3.81 cm)			
r steel		Target	XAR 30	1.016	
		Gage backing	PMMA	0.508	• • •
tron-beam	4	(single layer)	S200 beryllium	0.386	[410 J/cm^2]
tion					
aluminum					
t	939	Projectile	1145 aluminum	0.114	1.856×10^{4}
		Target	1145 aluminum	0.318	

rmed during development of the proceding models resented here to indicate some of the variety of ts. The first sample is a flat plate impact in Armco The experimental conditions are given in Table I. mpact produced compressive stresses of about 40 This experiment is one of those from which the re parameters for Armco iron were derived. efore, good correlation is expected. The computed k size distributions for several cells are shown in 12 and compared with several of the experimental tributions (also shown in Fig. 7). The inset of Fig. ows the relative positions of measured zones and putational cells. The total number of cracks and ize distribution on and near the plane of maximum ge is well represented by the computations. The ty of the calculated results appears to diminish distance from this plane.

pact experiments in Arkansas novaculite provide mple of computations which simulated full-frag- tion. For these calculations, the cracks were ted with the observed initial flaw size distribution er than by a nucleation process. Also, the cracks permitted to grow at one-third of the sound speed. resulting fragment size distribution from the com- tions is compared with the measured distribution in 13. The comparison indicates that the fragment distribution can be obtained from our computational el.

r fracture process, there are no large cracks, microcracks. However, large cracks may be ed by the coalescence of small cracks: in such s, our method may be able to simulate the appear- and propagation of large cracks. Such a simulation attempted for a tapered flyer impact listed in Table and shown in Fig. 14. The damage actually occurs as all plane, which proceeds across the plate. The uted progress of this large spall crack is shown g. 15. The final appearance of the crack is com- ed with the computed position in Fig. 16. Hence, there is some hope that large cracks may be treated by this method.

The fourth sample (S200 beryllium) was irradiated by Buck and Shea[15] in an electron-beam machine at a

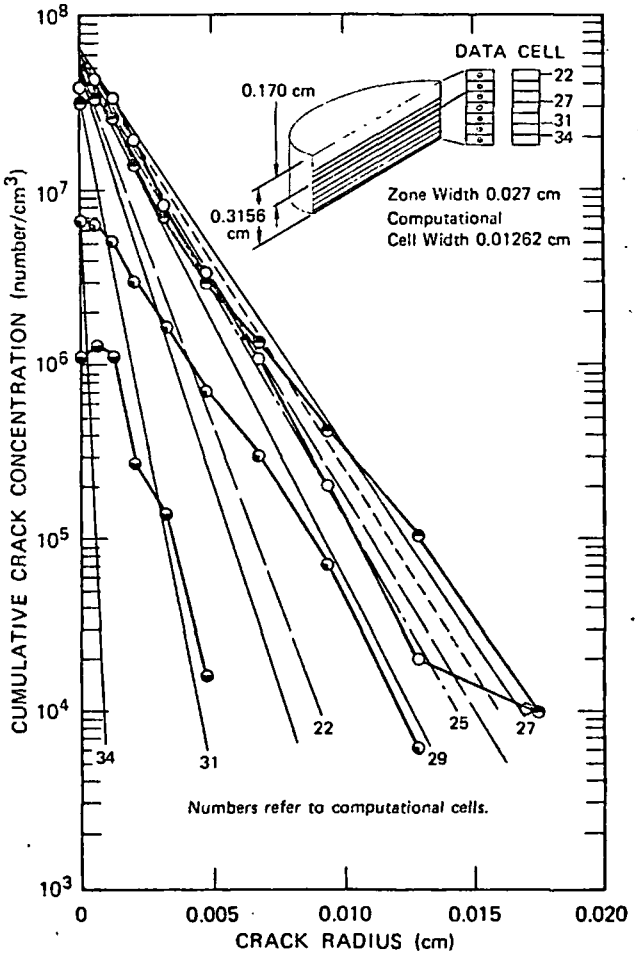

FIG. 12. Computed crack size distributions in Armco iron target: simulation of shot S25.

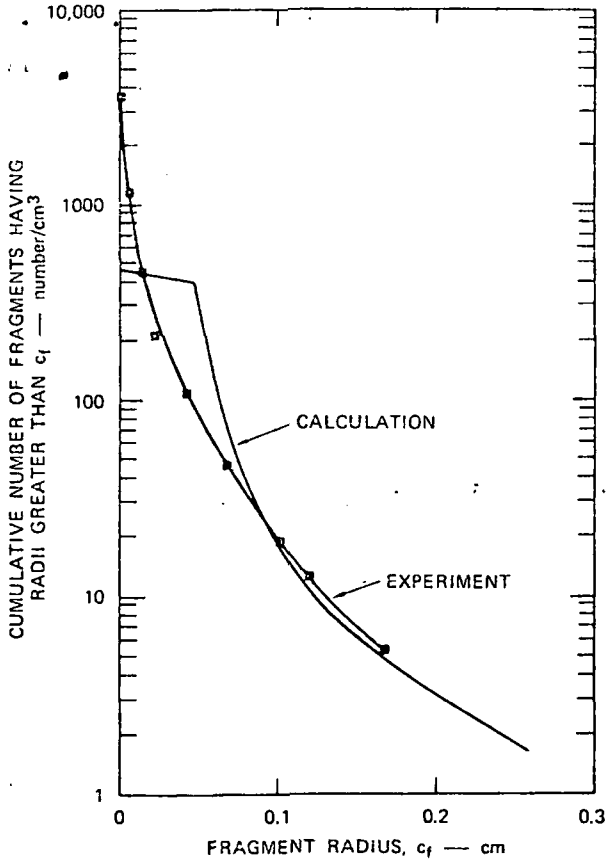

FIG. 13. Comparison of experimental and computed fragment size distributions for experiment 53 in Arkansas novaculite.

fluence of 410± 10% J/cm^2. The distribution of the energy with depth is shown in Fig. 17. The deposition occurred in approximately 50 nsec causing compression throughout the sample. Rarefaction waves generated at the free surfaces met near the specimen center to produce tensions of 0.95 GPa (according to the calculations) and caused an intermediate level of damage. The measured crack size distribution on the plane of maximum damage is shown in Fig. 18, together with three computed curves. The fracture computations use parameters derived from the fracture damage measured by Shockey *et al.*[4] in targets from a series of flat plate impacts conducted by Warnica.[16] The undamaged state of the beryllium was represented by the dislocation dynamics model

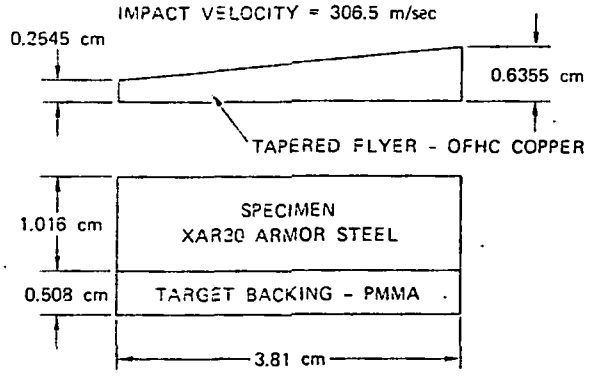

FIG. 14. Configuration for the two-dimensional simulation of fragmentation in a tapered flyer impact.

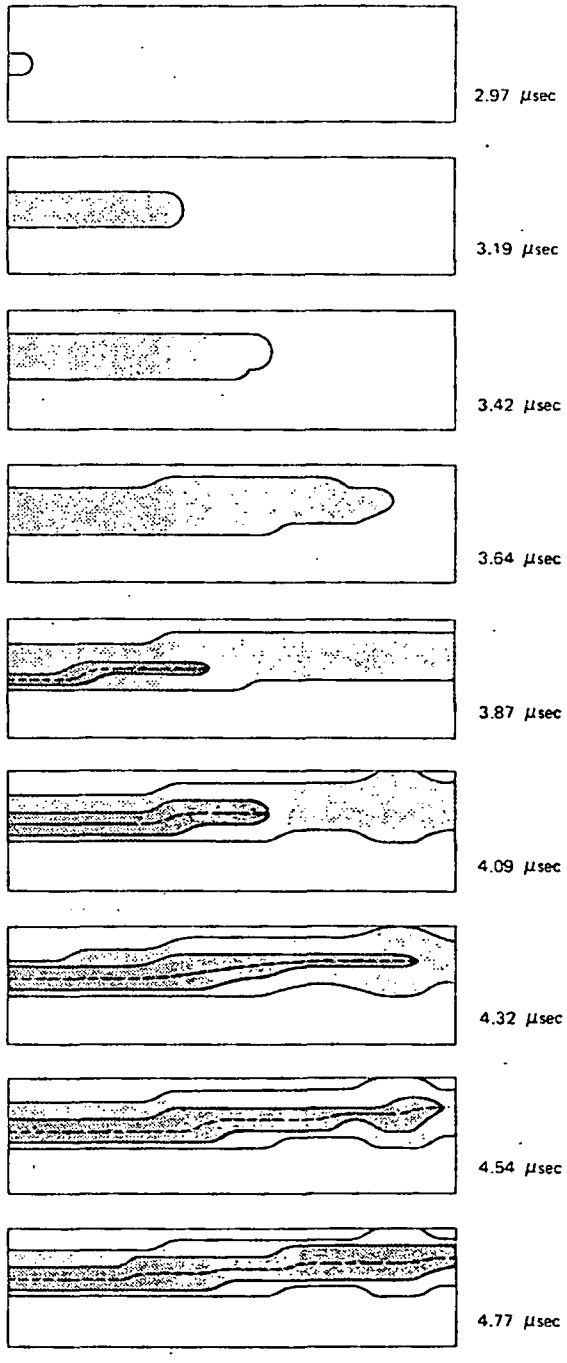

FIG. 15. Sequence of cross sections of XAR30 steel specimens showing progress of fracture and partial fragmentation (light shading) and full fragmentation (dark shading) resulting from a tapered flyer impact: No. 2024-2.

constructed by Read and Cecil.[17] The computed curves thus are predictions of damage in a radiation environment based on data from plate impact: no modifications were made in any aspect of the model to improve the agreement with the measured damage shown in Fig. 18. The observed damage does fall near the computed range, especially for the larger, and therefore more serious, cracks. Evidently, the precision of the fluence measurement is not sufficient to more precisely assess the agreement of the measured and computed damage distributions.

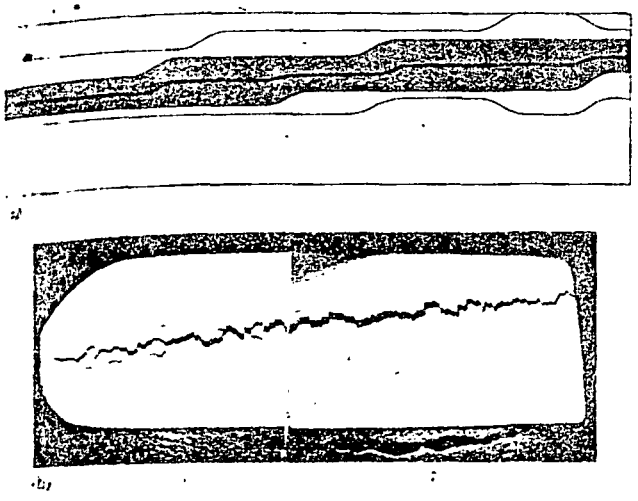

FIG. 16. Comparison of computed and observed damage in a specimen impacted by a tapered flyer. (a) Computed damage on meridian section of XAR30 target. (b) Cross section of XAR30 target showing partial spall.

The measured and computed (at 410 J/cm²) distribution of damage through the specimen is shown in Fig. 19 for three different crack sizes. These curves are obtained by taking points from damage curves (such as in Fig. 18) at various depths in the specimen. The measured numbers of cracks are generally larger than the computed numbers, but the spatial extent of damage is fairly well indicated in the computations.

These four experiments indicate, to some extent, the range of applicability of the NAG model to fracture problems. They show that the brittle model fits experimental data at low damage levels and at full fragmentation, that this microfracturing model can represent the progress of large cracks, and that fracture data from plate impacts can predict damage under thermal radiation.

The fifth experiment is an impact in 1145 aluminum[2] in which ductile fracture reached a damage level of 12%. The comparisons of measured and computed relative void volume and void concentration are shown in Fig. 20. The NAG parameters on which these results are based were able to simulate damage in impacts from 1.0 to

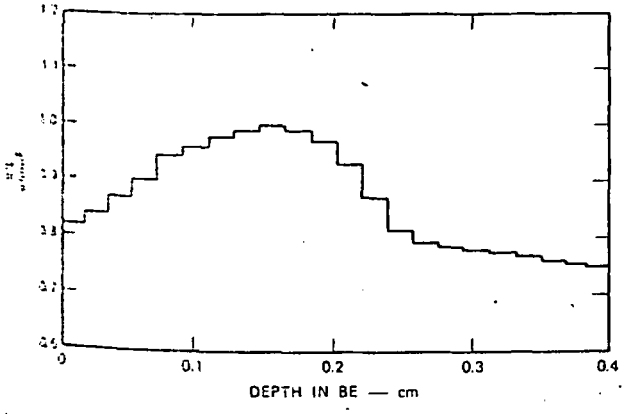

FIG. 17. Normalized depth-dose profile for the electron-beam experiment in S200 beryllium.

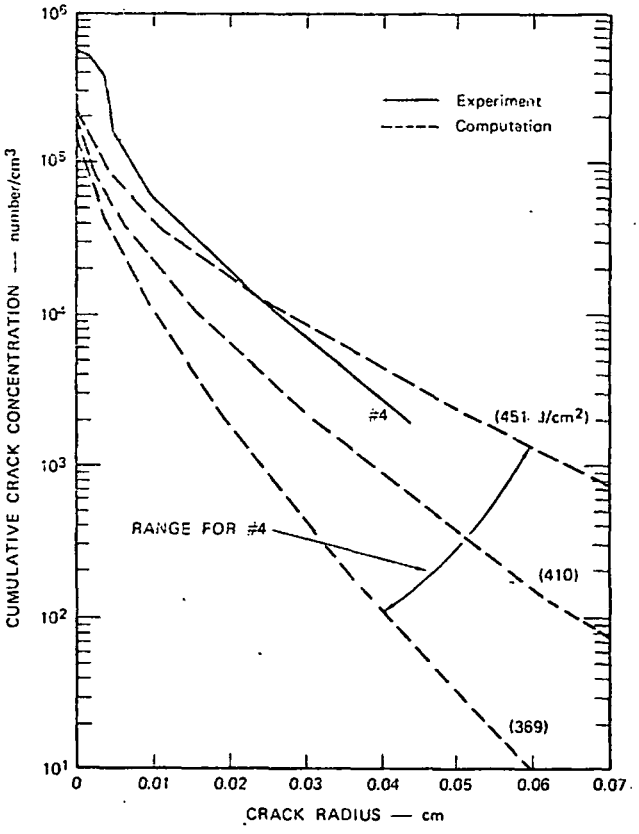

FIG. 18. Comparison of predicted and measured damage distributions curves for the zones of maximum damage in electron-beam specimen 4.

1.4 GPa and ranges of peak damage for 1% to 10% void volume. Thus far, good correlations with the ductile fracture model have been obtained up to about 10% void volume. The ductile fracture with parameters derived from plate impact data has also been successful in predicting damage under thermal radiation.

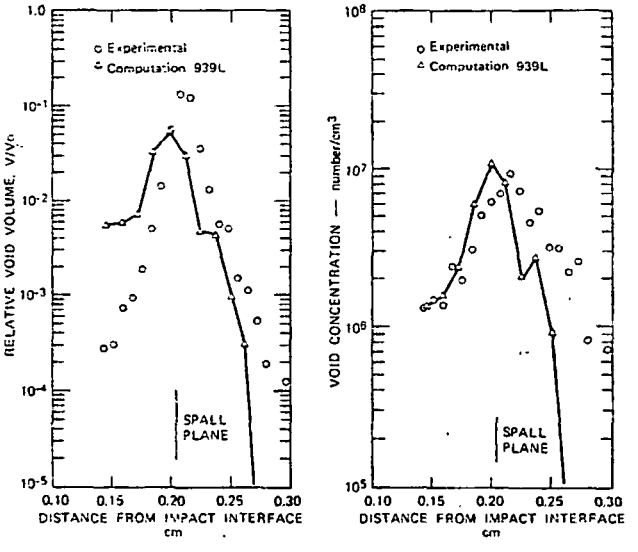

FIG. 19. Comparison of predicted and measured fracture damage as a function of depth into electron-beam specimen 4.

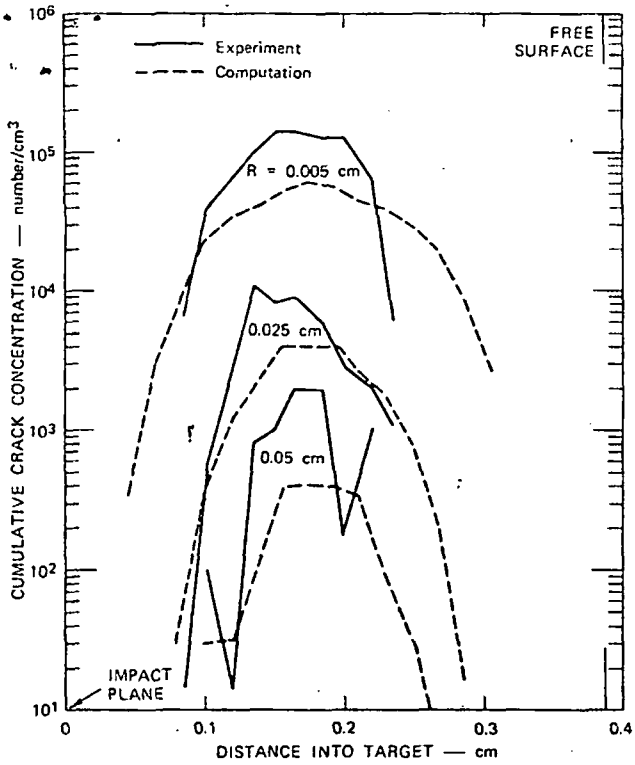

FIG. 20. Computed and observed damage in 1145 aluminum sample after 1.43 GPa impact.

SUMMARY

We have developed computational models af ductile and brittle fracture for wave propagation calculations in one- and two-dimensional geometries. The model features were constructed from detailed observations of the dynamic fracture processes in a wide range of materials, including several metals, a polycarbonate, and a fine-grained quartzite. These observations show the nucleation and growth of voids or cracks; hence, these two processes are represented in the models. The stress-strain relations for material undergoing fracture and the treatment of coalescence and fragmentation are very approximate in the models. In spite of the approximations, the models have been shown to represent fairly well the dynamic fracture processes over a wide range of material types, stress levels, and load durations.

[1]T.W. Barbee, Jr., L. Seaman, R. Crewdson, and D. Curran, J. Mater. 7, 393—401 (1972).
[2]T.W. Barbee, Jr., L. Seaman, and R.C. Crewdson, Technical Report No. AFWL-TR-70-99, Air Force Weapons Laboratory, Kirtland Air Force Base, N.M., 1970 (unpublished).
[3]L. Seaman, T.W. Barbee, Jr., and D.R. Curran, Technical Report No. AFWL-TR-71-156, Air Force Weapons Laboratory, Kirtland Air Force Base, N.M., 1971 (unpublished).
[4]D.A. Shockey, L. Seaman, and D.R. Curran, Final Report No. AFWL-TR-73-12, Kirtland Air Force Base, N.M., 1973 (unpublished).
[5]D.R. Curran, D.A. Shockey, and L. Seaman, J. Appl. Phys. 44, 4025—4038 (1973).
[6]D.A. Shockey, D.R. Curran, L. Seaman, J.T. Rosenberg, and C F. Petersen, Int. J. Rock Mech. Sci. Geomech. Abstr. 11, 303—317 (1974).
[7]D.A. Shockey, D.R. Curran, M. Austin, and L. Seaman, Final Report. for Defense Nuclear Agency, No. DNA 3730F, 1975 (unpublished).
[8]A.L. Stevens, L. Davison, and W.E. Warren, in *Dynamic Crack Propagation*, edited by G.C. Sih (Noordhoff International Publishing, The Netherlands, 1973), p. 37.
[9]L. Davison, A.L. Stevens, and M.E. Kipp, J. Mech. Phys. Solids (to be published).
[10]G.J. Dvorak, in Ref. 8, p. 49.
[11]M. Carroll and A.C. Holt, J. Appl. Phys. 42, 759 (1972).
[12]J.K. MacKenzie, Proc. Phys. Soc. B 63, 2 (1950).
[13]I.N. Sneddon and M. Lowengrub, *Crack Problems in the Classical Theory of Elasticity* (Wiley, New York, 1969).
[14]S.N. Zhurkov, Int. J. Fract. Mech. 1, 311 (1965).
[15]V. Buck and J. Shea, Report No. PIFR 356-1, Air Force Weapons Laboratory, Kirtland Air Force Base, N.M., 1973 (unpublished).
[16]R.L. Warnica, Report No. MSL-68-18, Materials and Structures Laboratory, General Motors Corp., Warren, Mich. 1968 (unpublished).
[17]H.E. Read and R.A. Cecil, Report No. DNA 2845F, Defense Nuclear Agency, Wash., D.C. 1972 (unpublished).

Technology News

From the Bureau of Mines, United States Department of the Interior

Technology News describes tested developments from the Bureau of Mines Research Programs. It is published to encourage the transfer of this information to the minerals industry and its application in commercial practice. Mention of company or product names is for documentation only and does not imply government endorsement of a specific firm or product.

Bureau of Mines research is performed and reported under mandate of the United States Congress.
For a free subscription to Technology News, write to: Technology Transfer Group, Bureau of Mines, 2401 E St., NW, Washington, D.C. 20241.

No. 101, May 1981

Computer Model of In Situ Leaching Hydrology

Objective

Determine the site specific flow behavior of leachants and groundwater during development, production, and restoration phases of an in situ leaching operation.

Approach

A computer program has been developed which simulates the hydrologic activity associated with in situ mining. Various user options enable modeling of many of the site specific geologic conditions and well field specifications that affect the hydrology of solution mining.

How It Works

In situ hydrology is modeled, using a closed-form solution to the three-dimensional, partial differential equation that describes changes in hydraulic head as a result of pumping from leachant injection and recovery wells.

Model capabilities include arbitrary well patterns and pumping schedules, partially penetrating well screens, directionally anisotropic permeability and natural groundwater flow, in either

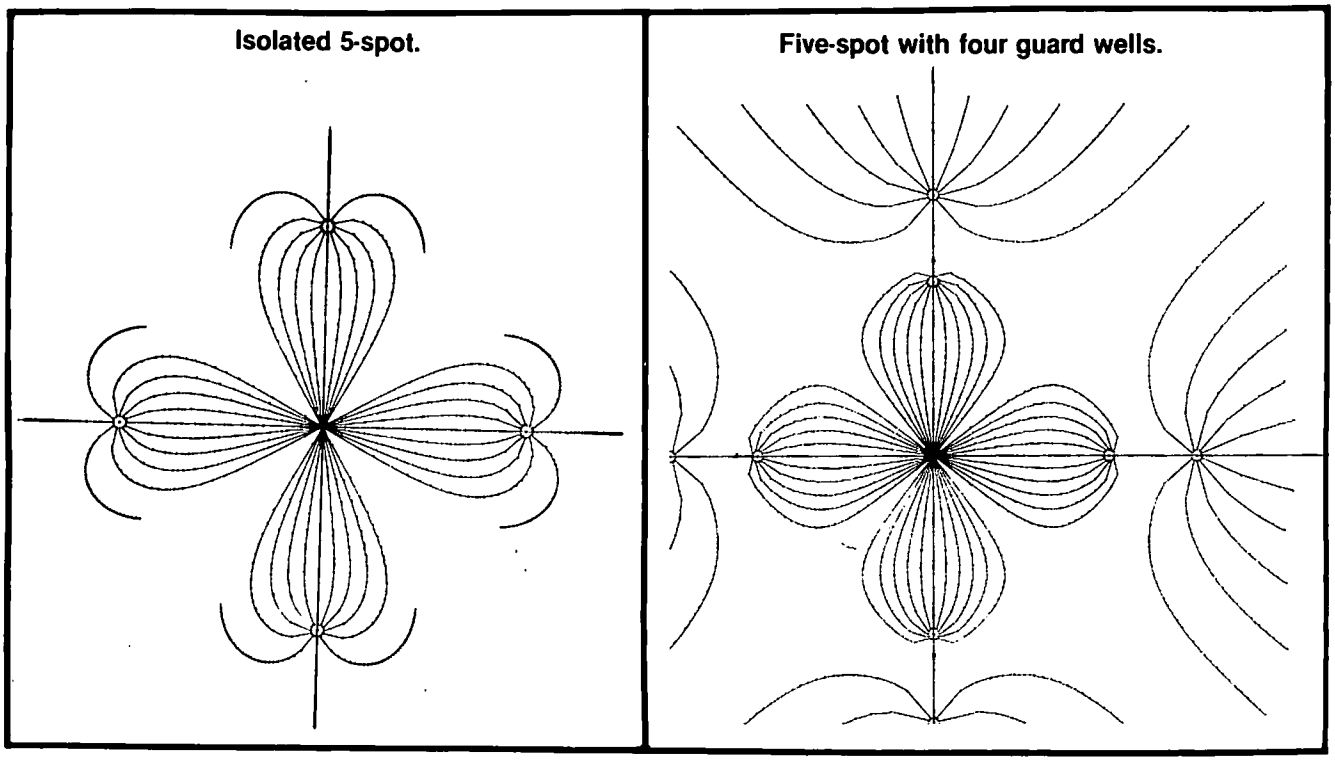

Streamline graphics for various well and pumping configurations.

leaky or nonleaky, confined aquifers and under steady state or time dependent flow conditions.

Model output is presented numerically and graphically. Numeric values are given for (1) hydraulic head, velocity and direction of flow, (2) volume of solution passed between injection and production wells, and volume escaped into the aquifer, (3) production well breakthrough time for each streamline, and (4) areal sweep of a well pattern. Graphic output is used to describe leachant stream flow lines, as shown in the figure.

Test Results

In addition to extensive laboratory testing, the Twin Cities Research Center has closely monitored the application of this model at three different mine sites. At each site the solution breakthrough time and the hydraulic head at observation wells (predicted and actual) were used to "tune" the model. The model was then used satisfactorily to assess suitability of various well configurations and pumping schedules, in terms of fluid dispersion within the ore pod and fluid excursions into the surrounding aquifer. The hydrology of groundwater restoration measures was also simulated.

A computer model of in situ leaching hydrology was developed at the Twin Cities Research Center. The project leader was Robert D. Schmidt.

Patent Status

The United States Department of the Interior is not applying for a patent on this development.

For More Information

Two Bureau of Mines Reports of Investigations are available:
8287—Computer Modeling of Five Spot Well Pattern Fluid Flow During In Situ Uranium Leaching
8479—Computer Modeling of Fluid Flow During Production and Environmental Restoration Phases of In Situ Uranium Leaching

A copy of each can be obtained without charge from Bureau of Mines, Publications and Distribution Division, 4800 Forbes Avenue, Pittsburgh, PA 15213.

To learn more write to:
Technology Transfer Officer
Bureau of Mines
Twin Cities Research Center
5629 Minnehaha Avenue South
Minneapolis, Minnesota 55417

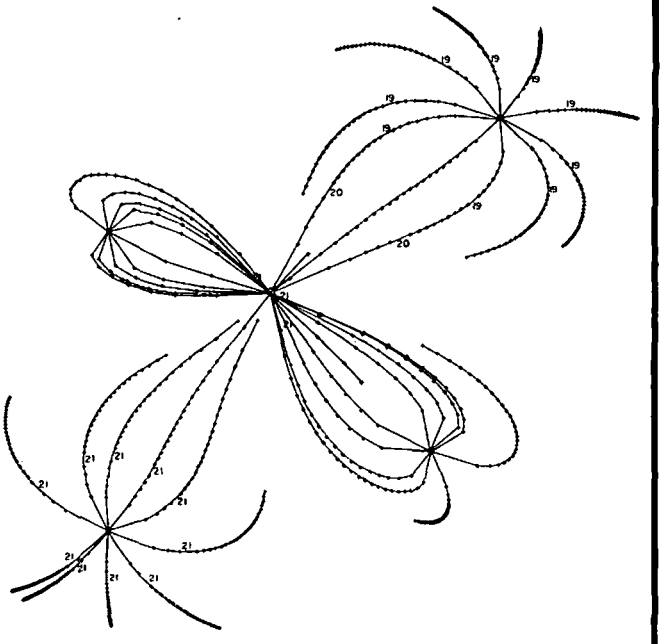

Five-spot pattern with directional permeability.

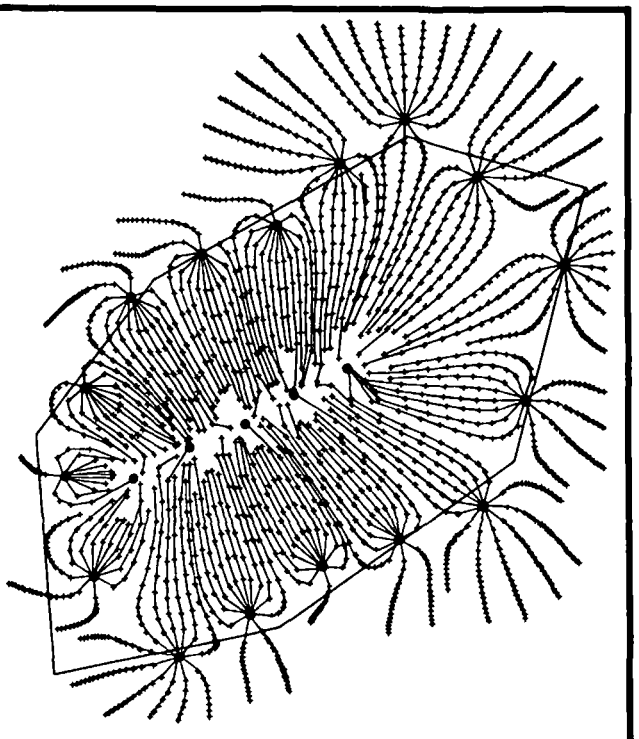

Streamline pattern, fluid excursions.

Report of Investigations 8287

Computer Modeling of Five-Spot Well Pattern Fluid Flow During In Situ Uranium Leaching

By Donald I. Kurth and Robert D. Schmidt

UNITED STATES DEPARTMENT OF THE INTERIOR
Cecil D. Andrus, Secretary

BUREAU OF MINES

This publication has been cataloged as follows:

Kurth, Donald I

Computer modeling of five-spot well pattern fluid flow during in situ uranium leaching / by Donald I. Kurth and Robert D. Schmidt. [Washington] : U.S. Dept. of the Interior, Bureau of Mines, 1978.

76 p. : diagrs. ; 27 cm. (Report of investigations - Bureau of Mines ; 8287)

Bibliography: p. 36-37.

1. Uranium - Metallurgy. 2. Leaching. 3. Uranium mines and mining. I. Schmidt, Robert D., jt. author. II. United States. Bureau of Mines. III. Title. IV. Series: United States. Bureau of Mines. Report of investigations - Bureau of Mines ; 8287.

TN23.U7 no. 8287 622.06173

U.S. Dept. of the Int. Library

CONTENTS

ILLUSTRATIONS

COMPUTER MODELING OF FIVE-SPOT WELL PATTERN FLUID FLOW DURING IN SITU URANIUM LEACHING

by

Donald I. Kurth [1] and Robert D. Schmidt [1]

ABSTRACT

This Bureau of Mines report describes the development and application of a computer model of aquifer hydrology associated with in situ leaching of uranium. The model provides uranium resource developers with a simulation of leachant flow characteristics in a preproduction or pilot five-spot leaching operation.

Various types of aquifers are modeled using closed form solutions of the partial differential equations describing the change in fluid head (pressure) as the leaching operation is carried out.

User-supplied descriptive input consists of aquifer, well, and leachant flow characteristics. Numeric and graphic outputs such as isopressure, isovelocity, and isotime contours are available. A typical application is shown.

INTRODUCTION

In recent years the increased demand for uranium has focused interest on the extraction of uranium from low-grade ore deposits. Current Bureau of Mines research has been directed toward improved uranium extraction using in situ leaching techniques. This report is the most recent effort of the Bureau to provide the mining industry with a means of simulating the hydrological activity in a uranium-bearing aquifer when in situ leaching is underway. The simulated fluid movement that results from user selection of aquifer and well characteristics is given in graphic and numeric forms designed to show the effect of well spacing, input and output flow rates, and other parameter values on the pattern of leachant flow in the aquifer.

The model was developed directly from closed form solutions to the aquifer hydrology partial differential equations of Hantush and Jacob (8, 11)[2] which describe fluid flow in a variety of aquifer types. The model allows the

[1]Mathematician, Twin Cities Mining Research Center, Bureau of Mines, Twin Cities, Minn.

[2]Underlined numbers in parentheses refer to items in the bibliography preceding the appendixes.

simulation of flow resulting from wells partially penetrating an aquifer bounded above by either a leaky or a nonleaky layer. This allows for the determination of differential fluid movement at different levels in the aquifer.

The utility of a computer hydrology model dealing exclusively with a single five-spot in situ well pattern, and providing a detailed description of the basic hydrological parameters associated with leaching, rests, to a large extent, on the suitability of implementing a pilot or experimental five-spot leaching operation prior to developing a full-scale production plant. Most in situ leaching projects begin in this fashion.

The conventional use of five-spot patterns for pilot production is in part due to the effectiveness of this pattern in waterflooding projects of the oil industry. Waterflooding of an oil-bearing formation to boost recovery was introduced in 1924, and it has since become a common industry practice (4). Waterflooding is a two-phase flow process in which, as applied to five-spot patterns, water is pumped into the corner wells and displaces oil in the formation. The oil is then pumped out the center well.

In addition to this established precedent, literature analysis and numerous Bureau discussions with mineral exploration companies involved in leaching projects have revealed that there are still some major problems associated with profitable leaching of uranium. These problems are concentrated primarily in the geochemistry of leaching and involve detrimental chemical interactions between formation rock and leachant solution.

The leachant environment of a single five-spot pilot operation is easily regulated from the standpoint of fluid dispersion and flow rates. Thus, such an operation is better suited than a large production operation to an optimal analysis of site-specific geochemistry problems. The detailed output of the Five-Spot In Situ Leaching program (5-SISL) can assist in the regulation of this leaching environment.

Future Bureau modeling will include an expanded hydrology model capable of simulating a multiple-well, production-type leaching operation and a chemical model of the leaching process. The goal of this effort will be to optimize well and leachant parameter values through computer simulation of the in situ mining process.

WELL-AQUIFER GEOMETRY AND NOMENCLATURE

For this model the input and output wells have been idealized as line sinks or sources (the well radius is not taken into account). Figure 1 shows the arrangement of wells for a conventional five-spot pattern.

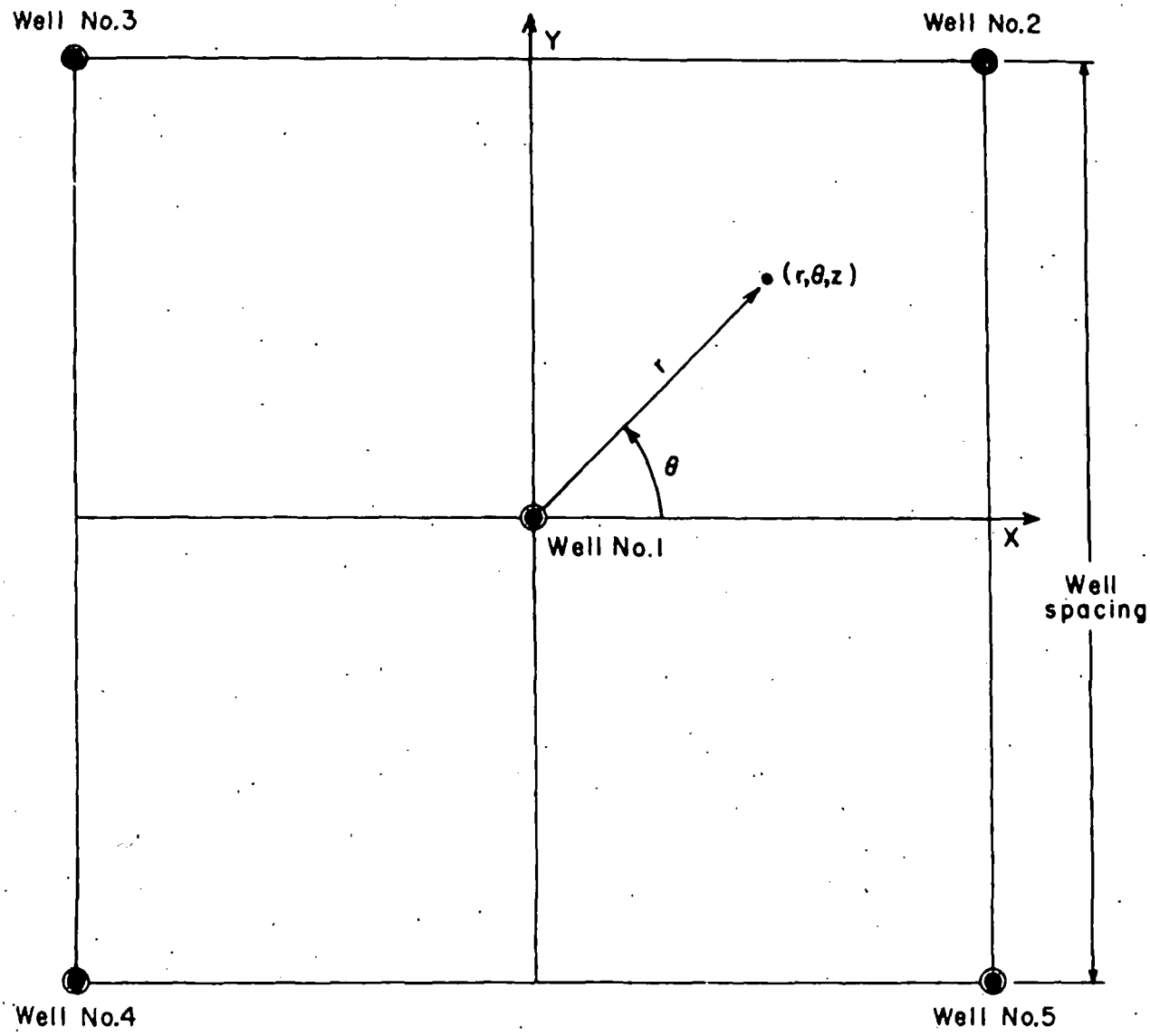

FIGURE 1. - Five-spot well pattern.

A well is constructed to intersect an aquifer, which may be confined or leaky, as shown in the cross section in figure 2. A leaky aquifer is one that is slightly permeable, with the permeability assumed to be totally vertical, from an aquitard layer. An aquitard layer is a semipervious, confining layer that is above or below (usually above) the leaky aquifer.

The definitions and nomenclature presented here apply to the subsequent account of the development of hydrology and drawdown equations. As far as possible these variable names are used in the FORTRAN computer program listed in appendix C. The important variables are as follows:

Δh = change in head (or pressure or drawdown) from the original piezometric surface, in feet.

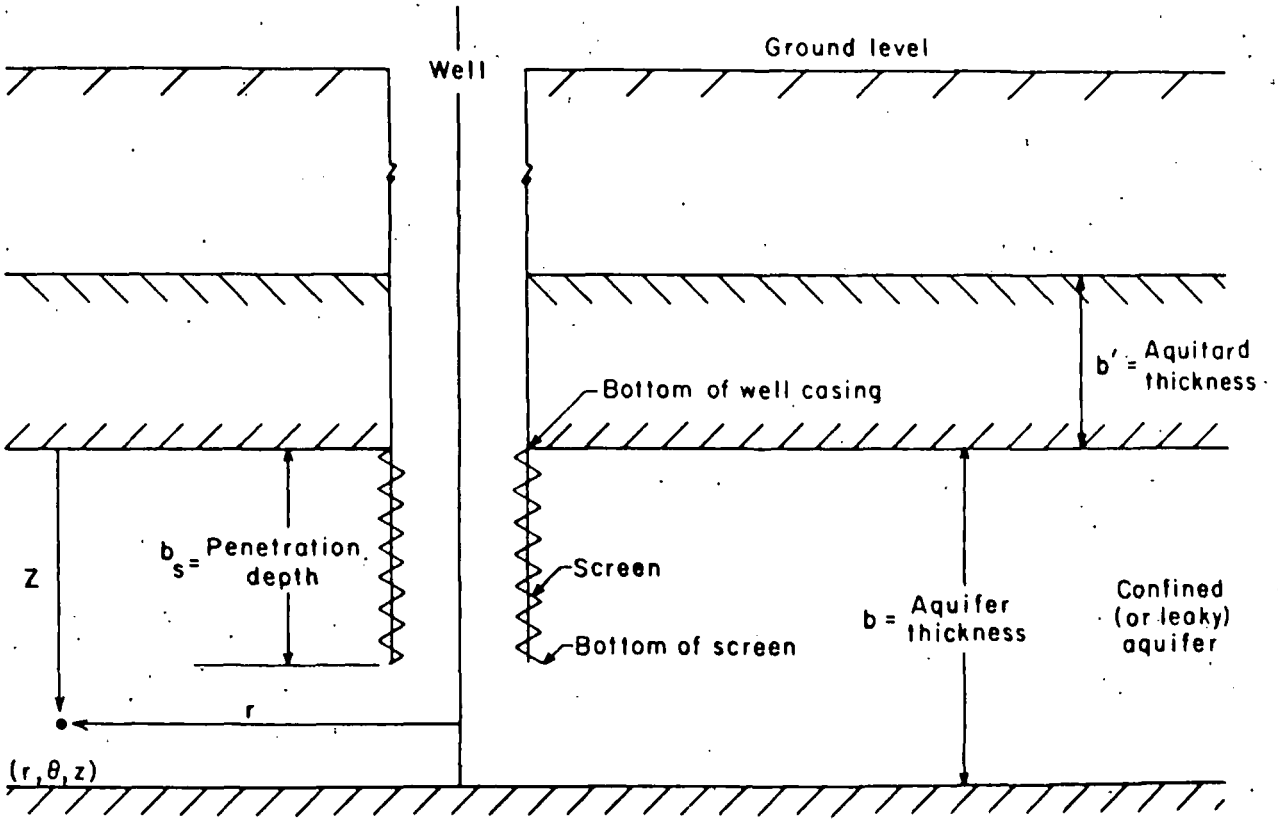

FIGURE 2. - Well-aquifer cross section.

(r,θ,Z) = cylindrical coordinates of the point at which Δh is calculated.

r = radius of the point from the well center, in feet (figs. 1 and 2).

θ = angle in horizontal plane of the point from the X-axis, in degrees (fig. 1). (Note that θ does not appear explicitly in the following equations because of radial symmetry.)

$X = r \cos \theta$.

$Y = r \sin \theta$.

Z = vertical distance of the point (r,θ,Z) from the top of the aquifer, in feet (fig. 2).

t = time interval of evaluation, in hours.

K = aquifer permeability, in feet per second.

K' = aquitard permeability, in feet per second.

b = aquifer thickness, in feet (fig. 2).

b' = aquitard thickness, in feet (fig. 2).

B = leakage factor = $\sqrt{\frac{K \cdot b \cdot b'}{K'}}$, in feet.

γ = specific weight of fluid, in pounds per cubic foot.

α = compressibility of solid "skeleton," in square feet per pound.

β = compressibility of fluid, in square feet per pound.

n = porosity, dimensionless.

Q = input (+) or output (-) flow rate, in cubic feet per second.

r_e = radius of influence (minimum radius at which no head change occurs), in feet.

b_s = depth of penetration (of partially penetrating well) below aquifer top, in feet (fig. 2).

$T = Kb$ = transmissivity, in square feet per second.

$S = \gamma b(\alpha + n\beta)$ = storativity, dimensionless.

HYDROLOGY (LEACHANT FLOW) EQUATIONS

Hantush (8) developed one of the more general models in the leaching hydrology literature. This model describes the time-dependent flow in a leaky aquifer being pumped from a well that only partially penetrates the aquifer. The leaky aquifer with a completely penetrating well, the confined aquifer with a partially penetrating well, the confined aquifer with a completely penetrating well, and steady-state versions of most of these are special cases of Hantush's general model. Stating the general flow problem mathematically, the boundary value problem is given by

$$\frac{\partial^2 \Delta h}{\partial r^2} + \frac{1}{r} \cdot \frac{\partial \Delta h}{\partial r} + \frac{\partial^2 \Delta h}{\partial z^2} - \frac{\Delta h}{B^2} = \frac{\gamma(\alpha + \beta n)}{K} \cdot \frac{\partial \Delta h}{\partial t}, \qquad (1)$$

where

$$\Delta h = \Delta h\ (r,z,t),$$

$$\Delta h\ (r,z,0) = 0,$$

$$\Delta h\ (\infty,z,t) = 0,$$

$$\frac{\partial \Delta h}{\partial z}\ (r,0,t) = 0,$$

$$\frac{\partial \Delta h}{\partial z}\ (r,b,t) = 0,$$

and $$\lim_{r \to 0} 2\pi K r \int_0^b \frac{\partial \Delta h}{\partial r}\, dz = -Q.$$

The numerical analysis approach used in this computer program consists of finding the classical closed form solutions of the partial differential equations developed extensively in the hydrological literature. This method of solution is normally preferable to finite difference or finite element methods because closed form methods generally require less computing time.

Specifically, a finite difference method used to model the relatively simple hydrology of an in situ leaching operation with two space dimensions (x, y) and a time dimension (t) requires calculation of fluid head at more (x, y) grid points than are normally of interest to the analyst. This often results in the inefficient use of data processing facilities. Other researchers, for example, McKee (17), concur with this judgment, although it is not an absolute; for some partial differential equations and boundary conditions, finite difference methods may be more efficient. In the more complex, nonlinear forms of hydrological partial differential equations, finite differences (or finite elements) must be used because of the lack of closed form solutions and in some situations, portions of several methods may be used.

Using a particular closed form solution of the partial differential equation with the method of images and some integration (which brings in the depth of penetration b_s), the following final closed form solution is obtained:

$$\Delta h = \frac{Q}{4\pi K b}\left[W_1\left(u, \frac{r}{B}\right) + \frac{2b}{\pi b_s} \sum_{m=1}^{\infty} \frac{1}{m} \cos\left(\frac{m\pi z}{b}\right) \sin\left(\frac{m\pi b_s}{b}\right) W_1\left(u, \sqrt{\left(\frac{r}{B}\right)^2 + \left(\frac{m\pi r}{b}\right)^2}\right)\right], \qquad (2)$$

where $$u = \frac{\gamma(\alpha + \beta n)}{4K} \cdot \frac{r^2}{t} \quad (3)$$

and $$W_1(u,\lambda) = \int_u^\infty \frac{1}{y} \exp\left(-y - \frac{\lambda^2}{4y}\right) dy. \quad (4)$$

$$W(u) = W_1(u,0) = \int_u^\infty \frac{1}{y} \exp(-y)\, dy. \quad (5)$$

$W_1(u,\lambda)$ and $W(u)$ are the so-called well functions. Since the integral forms of W_1 and W are not convenient for digital computer application, truncated infinite series, which usually converge quite rapidly, are used. These are as follows:

$$W_1(u,\lambda)^{3/} = 2K_o(\lambda) - I_o(\lambda) \cdot W\left(\frac{\lambda^2}{4u}\right) + \exp\left(-\frac{\lambda^2}{4u}\right) \cdot \left[0.5772 + \ln(u) + W(u) - u + u(I_o(\lambda)-1)\left(\frac{4}{\lambda^2}\right) - u^2 \cdot \sum_{\ell=1}^{\infty} \sum_{m=1}^{\ell} \frac{(-1)^{\ell+m}(\ell-m+1)!}{[(\ell+2)!]^2} \cdot \left(\frac{\lambda^2}{4}\right)^m \cdot u^{\ell-m}\right] \quad (6)$$

and $$W(u)^{4/} = -0.5772 - \ln(u) + u - \frac{u^2}{2\cdot 2!} + \frac{u^3}{3\cdot 3!} - + \ldots \quad (7)$$

In the preceding series

0.5772... = Euler's constant,

$K_o(\lambda)$ = modified Bessel function of zeroth order, dimensionless,

and $I_o(\lambda)$ = modified Bessel function of zeroth order, dimensionless.

The following polynomial approximations for $K_o(\lambda)$ and $I_o(\lambda)$ (1) were used for the computer program:

For $0 \leqq \lambda \leqq 3.75$:

$$I_o(\lambda) = 1. + 3.5156229\ (\lambda/3.75)^2 + 3.0899424\ (\lambda/3.75)^4 + 1.2067492\ (\lambda/3.75)^6 + .2659732\ (\lambda/3.75)^8 + .0360768\ (\lambda/3.75)^{10} + .0045813\ (\lambda/3.75)^{12}. \quad \left[|\text{Error}| < 1.6 \times 10^{-7}\right] \quad (8)$$

---

[3] In the program, FUNCTION WU_1 calculates this series only to $\ell = 5$.

[4] In the program, FUNCTION WU calculates this series only to u^5.

For $3.75 \leq \lambda < \infty$:

$$I_0(\lambda) = \lambda^{-1/2} \cdot \exp(\lambda) \cdot \left[.39894228 + .01328592 \ (\lambda/3.75)^{-1} \right.$$
$$+ .00225319 \ (\lambda/3.75)^{-2} - .00157565 \ (\lambda/3.75)^{-3}$$
$$+ .00916281 \ (\lambda/3.75)^{-4} - .02057706 \ (\lambda/3.75)^{-5}$$
$$+ .02635537 \ (\lambda/3.75)^{-6} - .01647633 \ (\lambda/3.75)^{-7}$$
$$\left. + .00392377 \ (\lambda/3.75)^{-8} \right] . \qquad (9)$$
$$\left[|\text{Error}| < 1.9 \times 10^{-7} \right] .$$

For $0 < \lambda \leq 2$:

$$K_0(\lambda) = -\ln(\lambda/2) \ I_0(\lambda) - .57721566 + .4227842 \ (\lambda/2)^2$$
$$+ .23069756 \ (\lambda/2)^4 + .03488590 \ (\lambda/2)^6$$
$$+ .00262698 \ (\lambda/2)^8 + .00010750 \ (\lambda/2)^{10}$$
$$+ .00000740 \ (\lambda/2)^{12} . \qquad (10)$$
$$\left[|\text{Error}| < 1 \times 10^{-8} \right] .$$

For $2 \leq \lambda \leq \infty$:

$$K_0(\lambda) = \lambda^{-1/2} \exp(-\lambda) \left[1.25331414 - .07832358 \ (2/\lambda) \right.$$
$$+ .02189568 \ (2/\lambda)^2 - .01062446 \ (2/\lambda)^3$$
$$+ .00587872 \ (2/\lambda)^4 - .00251540 \ (2/\lambda)^5$$
$$\left. + .00053208 \ (2/\lambda)^6 \right] . \qquad (11)$$
$$\left[|\text{Error}| < 1.9 \times 10^{-7} \right] .$$

Four main aquifer models for head change in a single pumped well are considered in the computer program. These are:

1. Steady-state flow in a confined aquifer (SUBROUTINE SSCONF).
2. Nonsteady-state flow in a confined aquifer (SUBROUTINE TMECONF).
3. Steady-state flow in a leaky aquifer (SUBROUTINE SSLEAKY).
4. Nonsteady-state flow in a leaky aquifer (SUBROUTINE TMELKY).

The formulas for calculating change in head (Δh) used in these subroutines are found in (8) and are special or degenerate cases of equation 1.

All of these models allow for a partially penetrating form of a single well, where the casing ends at the top of the aquifer and the screen runs from the top partway down into the aquifer.

The formula for the steady-confined case is

$$\Delta h = \frac{Q}{2\pi Kb}\left[\ln\left(\frac{re}{r}\right) + \frac{2b}{\pi b_s}\sum_{m=1}^{\infty}\frac{1}{m}\cos\left(\frac{m\pi z}{b}\right)\sin\left(\frac{m\pi b_s}{b}\right)R_o\left(\frac{m\pi r}{b}\right)\right], \quad (12)$$

where $$R_o\left(\frac{m\pi r}{b}\right) = K_o\left(\frac{m\pi r}{b}\right) - K_o\left(\frac{m\pi r_e}{b}\right)\cdot\frac{I_o\left(\frac{m\pi r}{b}\right)}{I_o\left(\frac{m\pi r_e}{b}\right)}.$$

The formula for the nonsteady-confined case is

$$\Delta h = \frac{Q}{4\pi Kb}\left[W(u) + \frac{2b}{\pi b_s}\sum_{m=1}^{\infty}\frac{1}{m}\cos\left(\frac{m\pi z}{b}\right)\sin\left(\frac{m\pi b_s}{b}\right)W_1\left(u,\frac{m\pi r}{b}\right)\right]. \quad (13)$$

The formula for the steady-leaky case is

$$\Delta h = \frac{Q}{2\pi Kb}\left[K_o\left(\frac{r}{B}\right) + \frac{2b}{\pi b_s}\sum_{m=1}^{\infty}\frac{1}{m}\cos\left(\frac{m\pi z}{b}\right)\sin\left(\frac{m\pi b_s}{b}\right)K_o\left(\sqrt{\left(\frac{r}{B}\right)^2 + \left(\frac{m\pi r}{b}\right)^2}\right)\right]. \quad (14)$$

The formula for the nonsteady-leaky case is

$$\Delta h = \frac{Q}{4\pi Kb}\left[W_1\left(u,\frac{r}{B}\right) + \frac{2b}{\pi b_s}\sum_{m=1}^{\infty}\cos\left(\frac{m\pi z}{b}\right)\sin\left(\frac{m\pi b_s}{b}\right)W_1\left(u,\sqrt{\left(\frac{r}{B}\right)^2 + \left(\frac{m\pi r}{b}\right)^2}\right)\right]. \quad (15)$$

Now the solution of equation 1 for Δh in the case of the five-spot (five wells) is easily found by noting that:

$$\Delta h = \pm\Delta h_1 \pm \Delta h_2 \pm \Delta h_3 \pm \Delta h_4 \pm \Delta h_5,$$

where the plus sign is chosen if the well is an input well and the minus sign is chosen if the well is an output well. This additivity of solutions is a

simple but important consequence of the linearity of equation 1; that is, if h_i is a solution of equation 1 and h_j is a solution of equation 1, then $(h_i + h_j)$ is also a solution of equation 1.

The velocity in the x-direction, V_x, and the velocity in the y-direction, V_y, are then easily found from Darcy's law:

$$V_x = -K \frac{\partial \Delta h}{\partial x},$$

and

$$V_y = -K \frac{\partial \Delta h}{\partial y}$$

by calculating the two partials rather than obtaining analytical expressions for them. These are calculated quite simply by replacing the partials with difference quotients.

Finally, streamlines are constructed by integrating the expressions:

$$\frac{dx}{dt} = V_x,$$

and

$$\frac{dy}{dt} = V_y.$$

Again, rather than integrate analytic expressions to obtain further analytic expressions for x and y, the integration is performed with the use of difference approximations, for example,

$$X_{n+1} = X_n + V_n(X_n, Y_n) \cdot (t_{n+1} - t_n),$$

and

$$Y_{n+1} = Y_n + V_y(X_n, Y_n) \cdot (t_{n+1} - t_n).$$

PERMEABILITY CALCULATION FROM FIELD MEASUREMENTS

The objective of the so-called "inverse problem" is to obtain storativity, S, and transmissivity, T, from field measurements of Δh at various times, t, during a drawdown test. Thus, data are taken in the form $(\Delta h_1, t_1)$, $(\Delta h_2, t_2)$, $(\Delta h_3, t_3)$, .., $(\Delta h_n, t_n)$. For a confined aquifer several methods can be used to find S and T, among them Theis' graphical method. The following equivalent method using least squares lends itself to digital computer application.

Using the single well (one operational output well and one observation well), for the nonsteady confined aquifer case, Δh is given by

$$\Delta h = \frac{Q}{4\pi T} \cdot W(u), \tag{16}$$

from equation 13 with $b_s = b$.

If u is small,[6] the first two terms of the W(u) series suffice. Thus,

$$\Delta h \cong \left(\frac{Q}{4\pi T}\right)\left[-.5772 - \ln\left(\frac{Sr^2}{4T}\cdot\frac{1}{t}\right)\right],$$

or
$$\Delta h \cong -\left(\frac{Q}{4\pi T}\right)\left[.5772 + \ln\left(\frac{Sr^2}{4T}\right)\right] + \frac{Q}{4\pi T}\ln(t), \tag{17}$$

or
$$\Delta h \cong A_o + A_1\tau, \tag{18}$$

where
$$\tau = \ln(t) \tag{19}$$

linearizes the equation.

The least-squares solution for A_o and A_1 is found by setting

$$\frac{\partial R}{\partial A_o} = 0 \tag{20}$$

and
$$\frac{\partial R}{\partial A_1} = 0, \tag{21}$$

where
$$R = \sum_{i=1}^{n} (\Delta h_i - A_o - A_1\tau)^2, \tag{22}$$

and solving for A_o and A_1. Solutions from equations 20 and 21 are

$$A_o = \frac{\left(\sum_1^n \Delta h_i\right)\left(\sum_1^n \tau_i^2\right) - \left(\sum_1^n \Delta h_i\,\tau_i\right)\left(\sum_1^n \tau_i\right)}{n\left(\sum_1^n \tau_i^2\right) - \left(\sum_1^n \tau_i\right)^2}, \tag{23}$$

and
$$A_1 = \frac{n\left(\sum_1^n \Delta h_i\,\tau_i\right) - \left(\sum_1^n \Delta h_i\right)\left(\sum_1^n \tau_i\right)}{n\left(\sum_1^n \tau_i\right) - \left(\sum_1^n \tau_i^2\right)^2}. \tag{24}$$

---

[5]After calculating S and T, the user should estimate u using $u = \frac{r^2 S}{4Tt}$, to insure that u is sufficiently small.

Because $A_1 = \frac{Q}{4\pi T}$ (equations 17 and 18), T is given by:

$$T = Q/4\pi A_1 . \tag{25}$$

Substituting expression 25 into A_o as given by equations 17 and 18, gives the following expression for A_o:

$$A_o = -\left(\frac{Q}{4\pi} \cdot \frac{4\pi A_1}{Q}\right) \cdot \left[0.5772 + \ln\left(\frac{Sr^2}{4} \cdot \frac{4\pi A_1}{Q}\right)\right] . \tag{26}$$

Solving equation 26 for S yields

$$S = (Q/\pi r^2 A_1) \cdot \exp(-A_o/A_1 - 0.5772). \tag{27}$$

Permeability, K, and porosity, n, are obtained from T and S by

$$K = T/b, \tag{28}$$

and

$$n = (S - \gamma \cdot \alpha \cdot b)/(\gamma \cdot \beta \cdot b) \tag{29}$$

from the definitions of S and T.

Using the five-spot pattern (five operational wells and one observation well) for the nonsteady confined aquifer case with conservation of flow (ΣQ in = Σ Q out), the model Δh becomes:

$$\Delta h = W(u_o) - 1/4\left[W(u_1) + W(u_2) + W(u_3) + W(u_4)\right] . \tag{30}$$

$$\text{Let } r_i = \sqrt{(x_i \pm s)^2 + (y_i \pm s)^2} . \tag{31}$$

Again, if $u_i = \frac{r_i^2 S}{4Tt}$ is small,[6] the first two terms of the $W(u_i)$ series suffice so that

$$\Delta h = \frac{Q}{4\pi T}\left[-.5772 - \ln\left(\frac{Sr_o^2}{4Tt}\right) + \frac{Sr_o^2}{4Tt}\right]$$

$$-1/4 \cdot \frac{Q}{4\pi T}\left[-.5772 - \ln\left(\frac{Sr_1^2}{4Tt}\right) + \frac{Sr_1^2}{4Tt}\right]$$

$$-1/4 \cdot \frac{Q}{4\pi T}\left[-.5772 - \ln\left(\frac{Sr_2^2}{4Tt}\right) + \frac{Sr_2^2}{4Tt}\right]$$

[6]Work cited in footnote 5.

$$-1/4 \cdot \frac{Q}{4\pi T}\left[-.5772 - \ln\left(\frac{Sr_3^2}{4Tt}\right) + \frac{Sr_3^2}{4Tt}\right]$$

$$-1/4 \cdot \frac{Q}{4\pi T}\left[-.5772 - \ln\left(\frac{Sr_4^2}{4Tt}\right) + \frac{Sr_4^2}{4Tt}\right],$$

or
$$\Delta h = \frac{Q}{4\pi T}\left(-\ln r_o^2 + 1/4 \ln r_1^2 + 1/4 \ln r_2^2 + 1/4 \ln r_3^2 + 1/4 \ln r_4^2\right) + \left(\frac{Q}{4\pi T}\right)\cdot\left(\frac{S}{4T}\right)\cdot\left(r_o^2 - 1/4\, r_1^2 - 1/4\, r_2^2 - 1/4\, r_3^2 - 1/4\, r_4^2\right)\cdot\left(\frac{1}{t}\right), \quad (32)$$

or
$$\Delta h = B_o + B_1 \lambda, \quad (33)$$

where $\lambda = \frac{1}{t}$ is the linearizing transformation.

Clearly B_o and B_1 have the same form as A_o and A_1 (equations 23 and 24) in the single well case; that is

$$B_o = \frac{\left(\sum_1^n \Delta h_i\right)\left(\sum_1^n \lambda_i^2\right) - \left(\sum_1^n \Delta h_i \lambda_i\right)\left(\sum_1^n \lambda_i\right)}{n\left(\sum_1^n \lambda_i^2\right) - \left(\sum_1^n \lambda_i\right)^2}, \quad (34)$$

and
$$B_1 = \frac{n\left(\sum_1^n \Delta h_i \lambda_i\right) - \left(\sum_1^n \Delta h_i\right)\left(\sum_1^n \Delta \lambda_i\right)}{n\left(\sum_1^n \lambda_i^2\right) - \left(\sum_1^n \lambda_i\right)^2}. \quad (35)$$

From the expression for B_o (equations 32 and 33), T is found to be

$$T = \frac{Q}{4\pi B_o}\left(-\ln r_o^2 + 1/4 \ln r_1^2 + 1/4 \ln r_2^2 + 1/4 \ln r_3^2 + 1/4 \ln r_4^2\right). \quad (36)$$

Substituting this expression into the expression for B_1 in equations 32 and 33, S is found to be

$$S = \frac{B_1 Q}{B_0^2 \pi} (-\ln r_0^2 + 1/4 \ln r_1^2 + 1/4 \ln r_2^2 + 1/4 \ln r_3^2 + 1/4 \ln r_4^2)^2 / (r_0^2 - 1/4 r_1^2 - 1/4 r_2^2 - 1/4 r_3^2 - 1/4 r_4^2). \quad (37)$$

Permeability, K, and porosity, n, are obtained from T and S by equations 28 and 29. This procedure is used in SUBROUTINE INVERSE.

COMPUTER PROGRAM DOCUMENTATION

The program documentation is arranged in three sections. The first is devoted to general details which may be helpful to the user of the five-spot model computer program (5-SISL). Various aspects of program development are discussed, as well as the available options. The logical structure of the program is also outlined. The second section summarizes the functions performed by each subroutine. The final section gives a description of the required input parameters and their formats.

Program Development

The 5-SISL program has been designed to be flexible in adjusting to unique field situations and in providing a wide variety and quantity of aquifer hydrology information as output.

The logic of the 5-SISL program develops sufficient generality to accommodate all types of aquifers and a broad range of recovery operations within the basic five-spot well pattern. Generality has been achieved particularly with regard to the spacing of the wells, their characteristics as they relate to the aquifer, and the function of each well in the leaching process.

To evaluate the hydrology, the program uses a horizontal matrix of points specified by the user. Each point is evaluated in terms of the change in head, velocity, and direction of particle flow.

The program provides several user options for describing the nature of the aquifer and its confining beds as well as the time interval since the initiation of pumping these options take the form of four basic models: steady-state confined, nonsteady-state (time dependent) confined , steady-state leaky, and nonsteady-state leaky. Corresponding to these four models are four subprograms. Additional details concerning the applications of SSLEAKY, TMECONF, SSCONF, and TMELKY are contained in the 5-SISL routines section and on flow card 2 of the Input Variables Section.

For each subprogram the penetration depth of the well screen into the aquifer can also be specified (fig. 2). This option can simulate any of the following four disruptions of radial flow that commonly occur in the leaching process.

1. Incomplete penetration of the well screen through the aquifer caused by irregularities in screen placement or aquifer thickness.

2. Buildup of material over time at the bottom of a completely penetrating screen.

3. Blockage of the lower part of the well screen by particles of rust, drilling mud, or other debris caused by improper drilling.

4. Precipitation of minerals on the screen caused by changes in the chemical equilibria in the aquifer.

Pressure and velocity data, as well as derivations such as particle traversal time, can be presented to the user in both graphic and tabular form. Thus, the program contains several options to insure that the hydrology data are available in the form that can best satisfy the requirements of a given pilot uranium recovery operation.

Simplifying Assumptions

The 5-SISL program incorporates certain simplifying assumptions. While some of these are not absolutely warranted, they do permit programing of a less complex nature without significantly reducing the accuracy of results, as verified by the field situation in which they were tested.

First, as mentioned earlier, the program assumes wells are located in a symmetric five-spot pattern. While the program can account for any combination of well input and output fluid volumes, only points in the first quadrant are evaluated. Thus, this quarter five-spot technique necessitates three more 90° rotations of the pattern about the center well to obtain a complete evaluation of points located in all four quadrants of a five-spot pattern having different corner well inputs or outputs.

Second, the program assumes that permeability is isotropic throughout the area of evaluation. Normally, this affects analysis only if the five-spot pattern covers a large area. However, there could be leaching situations in which this would be a definite limitation.

Third, the program assumes that no natural ground waterflow is present. The qualifications and limitations implied by this assumption are similar to those for the permeability assumption.

FORTRAN Versions

The 5-SISL program was written initially in the FORTRAN IV language for a CDC 6600 computer.[7] The default core memory required for execution of the program is 75K octal.

---

[7]Reference to specific equipment (or trade names or manufacturers) is made for identification only and does not imply endorsement by the Bureau of Mines.

Minor revisions of the 5-SISL program may be required to adapt to systems using other FORTRAN versions.

Program Control Structure

The flow of control through the program is shown in figure 3. This flow diagram identifies the procedures that determine the basic parameters associated with the leaching, such as the change in head and velocity at each coordinate of the evaluation matrix. These parameters are then translated into the graphic and numeric output that are more useful to the development of the well field.

A more detailed diagram of the structural relationship that exists between routines that comprise 5-SISL is shown in the two parts of figure 4. Each routine is designed to operate independently (or nearly so) in fulfilling a particular function; consequently, many patterns of control transfer can occur. Program control is transferred to a routine for a specific computation and returned to the calling routine when the required computation has been completed.

Five-Spot In Situ Leaching (5-SISL) Routines

The following is a brief discussion of each routine in program 5-SISL in terms of its contribution to the simulation.

SETUP is a dummy main program. Its primary functions are to control the dimensions of the evaluation matrices and to determine if a drawdown data analysis is needed for an empirical estimate of aquifer permeability before the leaching parameters are evaluated. If permeability and porosity estimates are required, an INVERSE routine makes these estimates from user-supplied drawdown data. If permeability estimates are supplied as input data, the program proceeds to INSITU, the driver routine for 5-SISL.

INSITU is the main control routine. It begins with a call to the data input routine INPT and then calls all the routines that are necessary to meet the user's evaluation requirements. INSITU initiates this data collection process by collecting and maintaining changes in head and velocity measurements for points on the user-specified evaluation matrix. Once these measurements have been computed, INSITU calls streamline evaluation and plotting routines, or contour mapping routines for further development of these basic parameters. INSITU also handles special output file requirements and the omission or addition of special points not on the matrix.

INPT is responsible for input of matrix specifications, output requirements, aquifer characteristics, well penetration data, and depth of analysis within the aquifer.

PARTIAL approximates $\frac{\partial \Delta h}{\partial x}$ and $\frac{\partial \Delta h}{\partial y}$ to be used later in calculating velocity by Darcy's law. This approximation for each value of x and y on the evaluation matrix is accomplished by differencing the Δh values calculated at points intermediate to the grid values.

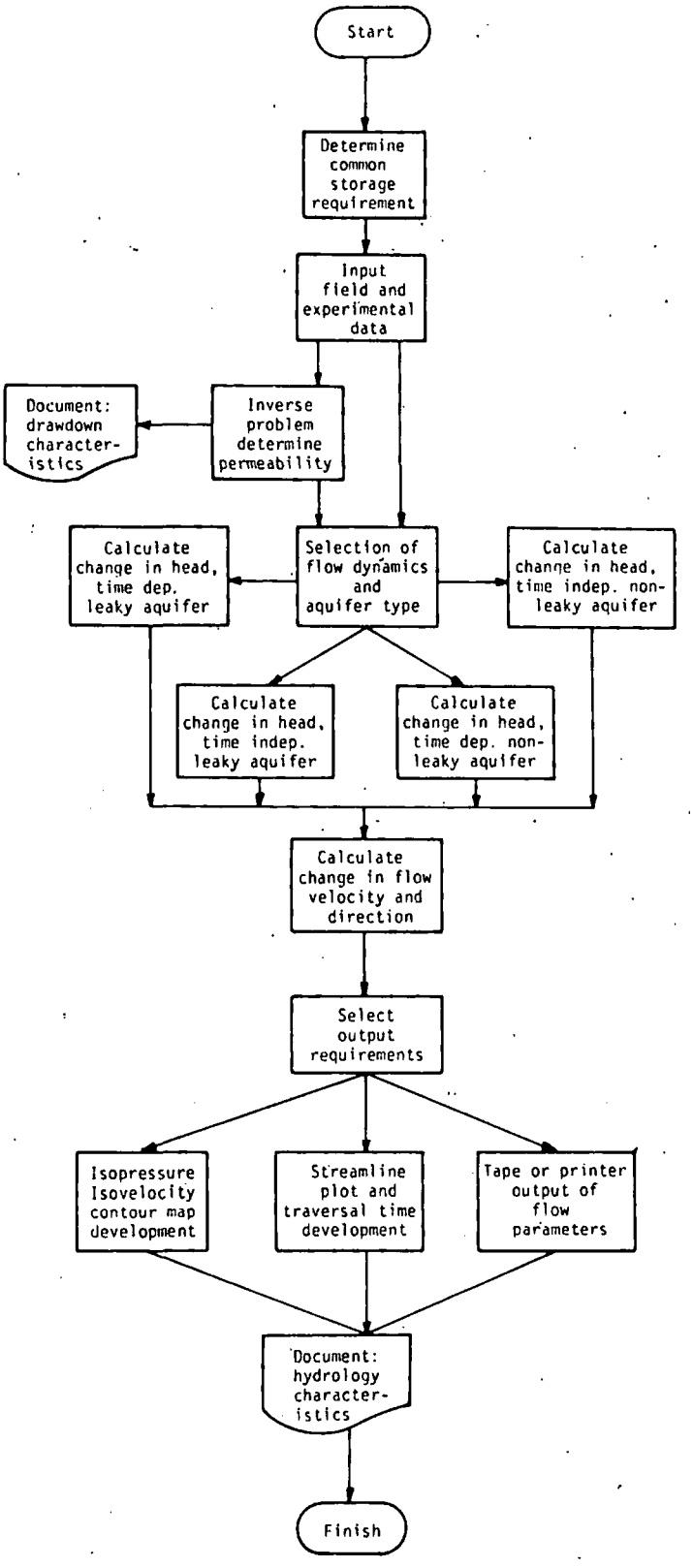

FIGURE 3. - Hydrology model flow of control diagram.

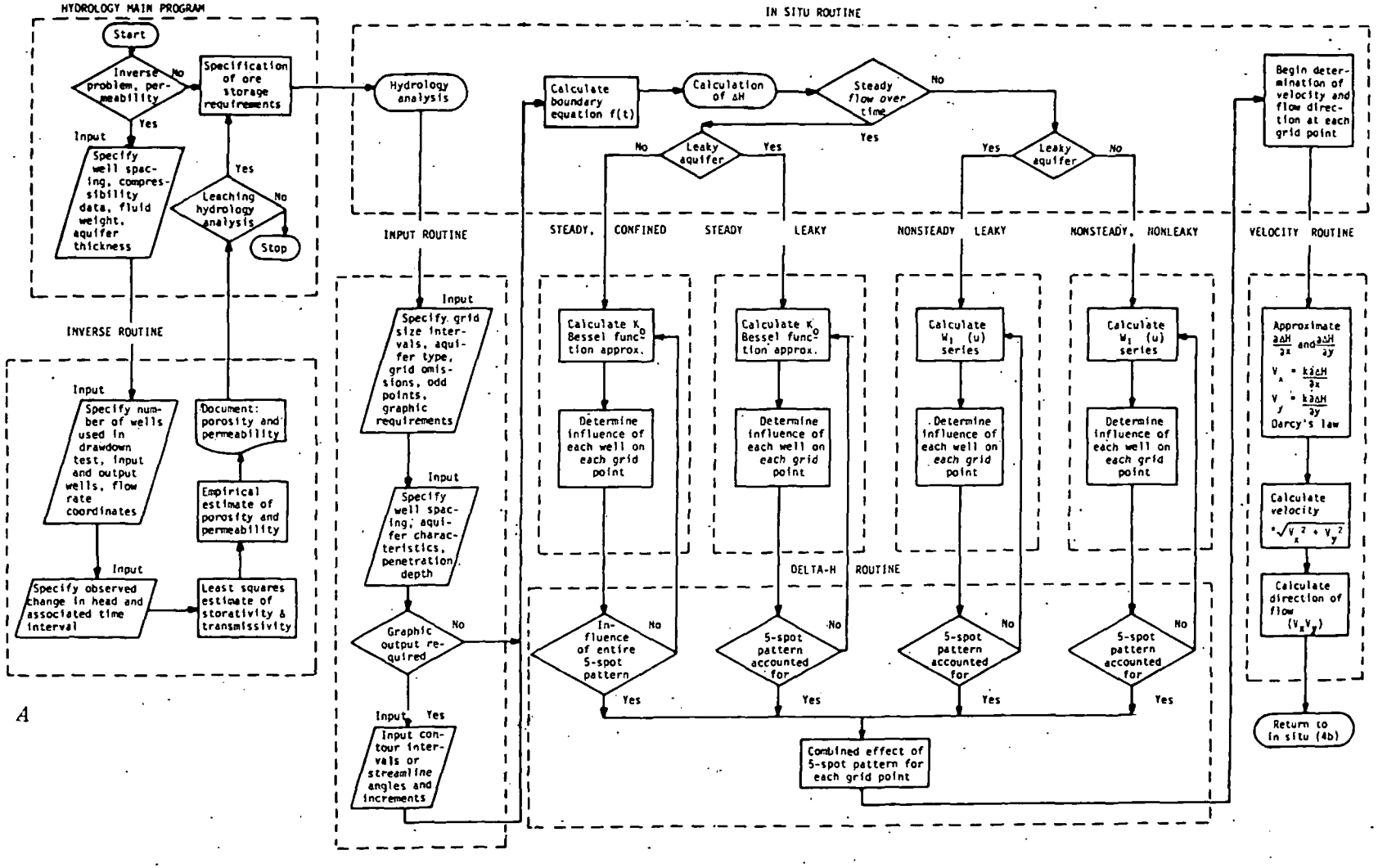

FIGURE 4A. - Hydrology model structural diagram.

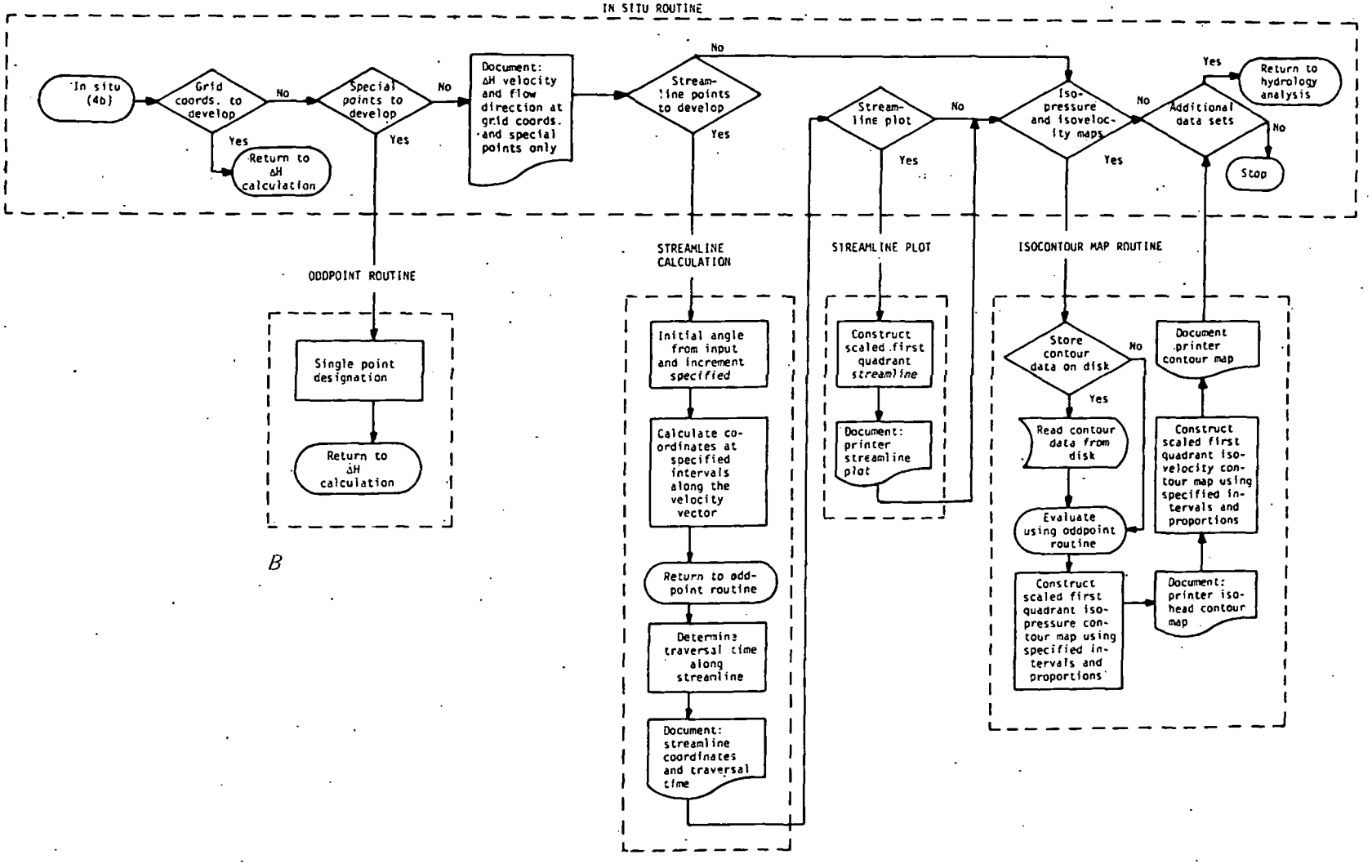

FIGURE 4B. - Hydrology model structural diagram.

VXVY applies Darcy's law to the approximated partials and the aquifer permeability estimate to obtain the velocity of particle flow during the leaching process.

ODDPLOT evaluates points in the aquifer, in terms of pressure, velocity, and direction of flow, that are not on the previously established matrix. This includes special interest points as well as those resulting from streamline evaluation.

WU computes a numerical approximation of the well function given by equation 5. This is used in the determination of Δh, in the time-dependent confined aquifer flow model.

WU1 computes a numerical approximation of the well function given by equation 4. It takes into account the aquifer depth (Z) at which the hydrology analysis is performed, and is used in the calculation of Δh, in the time-dependent leaky aquifer case.

DELTAH accumulates the weighted well functions associated with individual wells in the five-spot pattern. This routine determines the relative importance of each well (input and output characteristics) in terms of its effect on the fluid head at each coordinate of the aquifer matrix. A weighted combination yields the change in head for any point in the aquifer evaluation plane.

SSLEAKY determines the individual well's contribution to Δh, for the case when fluid flow has reached a steady-state condition in the aquifer and the leaching aquifer is slightly permeable from an above confining layer. Each coordinate point which is evaluated using this routine requires five iterations, one for each well. Limits of evaluation on each of the five integrals being approximated are specified by the relative distance of the matrix coordinate from each well.

TMECONF determines the individual well's contribution to Δh for the case when fluid flow parameters have not yet reached a steady-state in the aquifer, and the aquifer is bounded on top by an impervious confining bed.

SSCONF combines the steady-state and confined characteristics from SSLEAKY and TMECONF. This permits steady-state flow evaluation when the aquifer is confined from above.

TMELKY allows a time-dependent flow evaluation in conjunction with an unconfined, leaky layer above the aquifer. Each of these four routines permits a partially penetrating well screen, such that the depth of penetration and resulting impact on complete radial flow is individually specified for each well.

BESSK and BESSI are numerical approximations of I and K Bessel functions which are used in steady-state flow evaluation.

STRMLNE determines points in the aquifer evaluation plane that comprise streamlines or fluid flow directional lines, while the leaching process is underway. This routine references ODDPLOT in determining the direction of particle flow from any given point in the aquifer. The initial angle of particle flow and the incremental unit (in both feet and hours) is sufficient to define both equidistance and equitime streamlines. Streamlines are defined in a horizontal plane within the aquifer. The output from this routine can be the input to PLOTLNE. Alternatively, the user may divert STRMLNE output to an auxiliary file for online storage and use this as input to an independent plotting program.

PLOTLNE constructs printer streamline plots for both equitime interval and equidistance interval versions. While the equidistance interval version can assess the eventual path that leach particles will follow, the equitime plot displays the change in velocity of leach fluid as it traverses a streamline. It also indicates the time required for leach solution to reach a certain point on the aquifer.

INVERSE is used for a drawdown estimate of aquifer permeability. The analysis is appropriate only for a nonsteady-state, confined-aquifer situation. The user can specify either a drawdown test that involves the simultaneous operation of all five wells in the leaching pattern and one or more observation wells, or a single output well and one or more observation wells. Thus field measurements of Δh taken from either arrangement can be input to the INVERSE routine to yield a field estimate of transmissivity and storativity. To obtain good average estimates of S and T over a large horizontal aquifer, drawdown data should be taken from wells at various locations because S and T may differ somewhat from well to well.

ERROR is simply an error processing routine. It is designed to assist the user in locating input-related problems.

CONTOUR develops line-printer contour maps to aid users who do not have more sophisticated mapping programs or facilities available. The routine can produce first quadrant isohead and isovelocity maps. The user specifies the contour value for each line, and the range of values for each specification that will result in a character's being printed on the map.

Input Variables, Definitions, and Format

No.	Variable Name	Card column	Format	Description
				(Assignment card)
1	ASSIGN	1-5	I5	INVERSE program leach analysis option. If ASSIGN ≤0, leach analysis is performed (see Leach Analyses Data Set) with or without calculation of permeability and porosity using INVERSE subprogram. (See drawdown evaluation data set.) If, in addition, permeability and porosity (flow card 4) are equal to zero then |ASSIGN| = the number of observation wells that are used in calculating the average value of permeability and porosity. If ASSIGN >0, only the INVERSE subprogram (Drawdown Evaluation Data Set) is run. In this case ASSIGN = the number of observation wells involved in the drawdown analysis. Approximate aquifer permeability and porosity are obtained by averaging the values obtained for each of the observation wells.

Drawdown Evaluation Data Set

The complete drawdown evaluation data set (four cards) is required only if ASSIGN ≥0. This drawdown analysis is appropriate only for the nonsteady-state, confined aquifer case.

No.	Variable Name	Card column	Format	Description
				(INVERSE card 1)
1	S	1-15	E15.5	S = the X and Y component of the diagonal distance between the center well and each of the 4 symmetric peripheral wells (feet). This is required only if the entire five-spot pattern is in operation during the drawdown test (WELLUSE >0).
2	ALPHA	16-30	E15.5	Compressibility of aquifer solid (ft^2/lb).
3	BETA	31-45	E15.5	Compressibility of fluid (ft^2/lb).
4	GAMMA	46-60	E15.5	Specific weight of fluid (lb/ft^3).
5	B	61-75	E15.5	Thickness of aquifer (feet).

No.	Variable Name	Card column	Format	Description

INVERSE cards 2-4 are required in the leach analysis program (after flow card 8) if no permeability or porosity is specified.

(INVERSE card 2)

1	SAMPLES	1-5	I5	Number of water depth samples taken from each well.
2	WELLUSE	6-10	I5	If WELLUSE = 0, only the center well is used in the drawdown test. The center well is an output well. If WELLUSE = 1 or 2, the entire five-spot pattern is in operation during the drawdown test. If WELLUSE = 1, the corner wells are output wells and the center well is an input well. If WELLUSE = 2, the center well is an output well and the corner wells are input wells.
3	Q	15-30	E15.5	Average output flow rate (ft^3/sec) of fluid during drawdown test. Total input flow must equal total output flow when the entire five-spot pattern is in operation for the drawdown test.
4	X	31-45	E15.5	X coordinate of observation well during drawdown test.
5	Y	46-60	E15.5	Y coordinate of observation well during drawdown test.

(INVERSE card 3)

1	INPUT(1,1)	1-6	F6.0	The depth to the water level in the observation well at a maximum of 12 time points (feet).
2	INPUT(1,2)	7-12	F6.0	
3	INPUT(1,3)	13-18	F6.0	
.	.	.	.	
.	.	.	.	
.	.	.	.	
12	INPUT(1,12)	67-72	F6.0	

No.	Variable Name	Card column	Format	Description
			(INVERSE card 4)	
1	INPUT(2,1)	1-6	F6.0	The time points at which the previous observations (12 maximum) were made. (Time, minutes, is zero at the start of the drawdown test.)
2	INPUT(2,2)	7-12	F6.0	
3	INPUT(2,3)	13-18	F6.0	
	.	.	.	
	.	.	.	
	.	.	.	
12	INPUT(2,12)	67-72	F6.0	

Inverse cards 2-4 are repeated for each observation well in the drawdown test. If ASSIGN >0 (assignment card), the leach analysis data set is not required.

Leach Analysis Data Set

The following data cards are required for in situ leaching fluid flow analysis (ASSIGN ≤0).

No.	Variable Name	Card column	Format	Description
			(Flow card 1)	
1	M1	1-5	I5	Dimension of the first quadrant square matrix over which the flow analysis is performed. $M1^2$ is the number of grid nodes on the matrix that will automatically be evaluated by the program (maximum, M1 = 30).
2	L1	6-10	I5	L1/2 = the total number of streamline points that may be generated for one streamline plot (maximum, L1 = 1,000). Changes to these two variable specifications that are greater than maximum values also require new common storage specifications in SETUP.

No.	Variable Name	Card column	Format	Description
				(Flow card 2)
1	ITOT	1-3	I3	Total number of fluid flow analyses to be made.
2	IRUN	4-6	I3	The number of this leach analysis.
3	AQR	7-9	I3	Leaky or nonleaky aquifer parameter. If AQR = 1, aquifer is nonleaky. If AQR = 2, aquifer is leaky.
4	ITME	10-12	I3	Time dependent or time independent flow parameter. If ITME = 1, flow is assumed to have reached steady-state. If ITME = 2, flow is time dependent. In this case, flow analysis is usually made for the normally short time interval prior to steady-state.
5	NPR	13-15	I3	NPR = auxiliary output file number. File name is TAPE(NPR).
6	NUMODD	16-18	I3	NUMODD = the number of special interest points, if any (not on the $M1^2$ flow matrix), that are to be evaluated.
7	NUMOMT	19-21	I3	NUMONT = the number of points, if any, that are on the flow matrix but are not to be evaluated.
8	XSTART	22-24	I3	XSTART = the X coordinate of the left most grid line of the first quadrant flow evaluation matrix (XSTART $\geq$0).
9	XFINISH	25-27	I3	XFINISH = the X coordinate of the right most grid line of the first quadrant flow evaluation matrix (XFINISH $\geq$ XSTART).
10	YSTART	28-30	I3	YSTART = the Y coordinate of the lowest grid line of the first quadrant flow evaluation matrix (YSTART $\geq$0).
11	YFINISH	31-33	I3	YFINISH = the Y coordinate of the highest grid line in the first quadrant flow evaluation matrix (YFINISH $\geq$ YSTART).

No.	Variable Name	Card column	Format	Description
12	NLINES	34-36	I3	Number of first quadrant fluid flow streamlines to be calculated. $0 \leq$ NLINES ≤ 15. If NLINES = 0, streamline routine is omitted.
13	OUTOPT	37-39	I3	Output specification of fluid flow model. If OUTOPT = -1, leach analysis of grid matrix is skipped. Odd points and streamlines, if specified, are evaluated. Grid data (see OUTOPT = 2) is read from auxiliary NPR file (flow card 2) and used to construct isohead and isovelocity contour maps on printer facilities. This option is designed primarily for convenient inexpensive improvement in the differentiation of contour lines of these maps. If OUTOPT = 1, all output is directed solely to the printer. No auxiliary file is saved. If OUTOPT = 2, grid evaluated points are directed solely to auxiliary file NPR. This option facilitates the use of other plotting and mapping routines. If OUTOPT = 3, grid data and streamline values are directed to both printer and auxiliary NPR file.
14	ITEREND	40-42	I3	Maximum number of iterations allowed in Δh calculation. More iterations are required to evaluate points near the wells. NOTE.--Erratic Δh values may indicate insufficient number of iterations.
15	IPLOT	43-45	I3	Number of streamlines to be shown on first quadrant, streamline printer plot. $0 \leq$ IPLOT ≤ 5. If IPLOT = 0, plotting routine is skipped.

No.	Variable Name	Card column	Format	Description
16	LINES(1)	46-48	I3	LINES(1) = the number of isopressure contour lines to be shown on a first quadrant printer contour map. $-10 \leq$ LINES(1) ≤ 10. If LINES(1) = 0, no contour map is constructed. If LINES(1) <0, then INTRVL (i,1) and PERCNT (j,1) must consist of actual measurements of Δh at which contour values will be accepted and positioned. If LINES(1) >0, then INTRVL (i,1) must consist of proportional distances along the first quadrant input well, output well diagonal. PERCNT (j,1) must consist of a proportion of the Δh value that is calculated at the coordinates specified by INTRVL (i,1). (See isopressure cards 1 and 2).
17	LINES(2)	49-51	I3	LINES(2) has a meaning analogous to LINES(1) for the construction of isovelocity contour maps. $-10 \leq$ LINES(2) ≤ 10. The only difference occurs when LINES(2) >0. Then INTRVL (i,2) must consist of proportional distances along the diagonal from the first quadrant peripheral well to the corner of the fluid flow evaluation matrix. The interpretation of PERCNT (i,2) is analogous to PERCNT (i, 1).
				(Flow card 3)
1	INCRX	1-15	E15.5	INCRX is the increment between X coordinates of the fluid flow evaluation matrix (feet).
2	INCRY	16-30	E15.5	INCRY is the increment between Y coordinates of the fluid flow evaluation matrix (feet).
3	S	31-45	E15.5	S is the X and Y component of the diagonal distance between the center well and each of the four symmetric peripheral wells (feet).
4	B	46-50	E15.5	Thickness of aquifer being leached (feet).
5	GAMMA	61-75	E15.5	Specific weight of leaching fluid (lb/ft^3).

No.	Variable Name	Card column	Format	Description
				(Flow card 7)
1	ALPHA	1-15	E15.5	Compressibility of aquifer solid (ft^2/lb).
2	BETA	16-30	E15.5	Compressibility of fluid (ft^2/lb).
3	Z	31-45	E15.5	The distance, from the top of the aquifer, at which the horizontal x, y matrix of points is evaluated (feet).
4	XINC	46-60	E15.5	X ± XINC is used to approximate $\frac{\partial \Delta h}{\partial x}$. Normally XINC = $\frac{INCRX}{2}$.
5	YINC	61-75	E15.5	Y ± YINC is used to approximate $\frac{\partial \Delta h}{\partial y}$. Normally YINC = $\frac{INCRY}{2}$.
				(Flow card 8)
1	TERM	1-15	E15.5	Termination value for convergent series calculating DELPART(I), the influence of individual wells on each matrix point (range 10^{-5} to 10^{-1}). Points very near the well require more iterations for stable values.

Insert inverse cards 2-4 here if variables 1 and 4 equal 0 on flow card 4. Insert one set of inverse cards for each observation well in the drawdown analysis.

(Leaky aquifer card)

This card is required only in the leaky aquifer case. Variable 4 on flow card 2 = 2.

1	BPRIME	1-15	E15.5	The thickness of the aquifer above the aquifer to be leached (feet).
2	KPRIME	16-30	E15.5	The permeability of the aquifer above the aquifer to be leached (ft/sec).

No.	Variable Name	Card column	Format	Description
				(Steady-state, nonleaky card)
				This card is required only in the steady-state, nonleaky case. Variables 4-5 on flow card 2 both equal 1.
1	RE	1-15	E15.5	Minimum radius of influence about each well outside of which the head does not change significantly (feet). (For default RE = 600 feet, insert blank card.)
				(Omission card)
				Omission card(s) are included only if variable 8 on flow card 2 >0, one card for each omission.
1	OMIT(i,1)	1-10	F10.0	X coordinate of a point of the flow evaluation matrix that is not to be evaluated.
2	OMIT(i,2)	11-20	F10.0	Y coordinate of a point on the flow evaluation matrix that is not to be evaluated.
				(Odd point card)
				Odd point card(s) are included only if variable 7 on flow card 2 >0, one card for each odd point.
1	ODDPT(1,i)	1-10	F10.0	X coordinate of a point off the flow evaluation matrix that is to be evaluated.
2	ODDPT(2,i)	11-20	F10.0	Y coordinate of a point off the flow evaluation matrix that is to be evaluated.
3	ODDPT(3,i)	21-30	F10.0	X increment for approximation of pressure change $\left(\text{normally ODDPT(3,i)} = \frac{\text{INCRX}}{2} \right)$.
4	ODDPT(4,i)	31-45	F10.0	Y increment for approximation of pressure change $\left(\text{normally ODDPT(4,i)} = \frac{\text{INCRY}}{2} \right)$.

No.	Variable Name	Card column	Format	Description
The following two cards are to be included only if variable 13 on flow card 2 >0.				
				(Streamline card 1)
1	DISTME(1)	1-10	F10.0	DISTME(1) >0 causes an equal distance interval, streamline plot to be generated. DISTME(1) = the distance between points of evaluation on the streamline (feet). (The length of individual streamline vectors.)
2	DISTME(2)	11-20	F10.0	DISTME(2) >0 causes an equal time interval, streamline plot to be generated. DISTME(2) = the time interval between points of evaluation on the streamline (hours). (Both variables must be >0 for generation of streamline plots.)
3	RADIUS	21-30	F10.0	This is a radius about each well, at which evaluation of streamlines will begin and end (feet). (A 1- or 2-foot radius is usually practical.)
4	MAXID	31-40	I10	Maximum number of streamline coordinates that may be calculated for any one streamline $\left(\text{MAXID} \leq \frac{L1}{2} \right)$.
				(Streamline card 2)
1	ANGLE(1)	1-5	F5.0	ANGLE(i) specifies the initial angle of each streamline to be calculated. Number of angles = NLINES. If center well is input, 0° < ANGLE(i) < 90°. If peripheral wells are input, 270° < ANGLE(i) < 360° (maximum of 15 angles).
2	ANGLE(2)	6-10	F5.0	
3	ANGLE(3)	11-15	F5.0	
⋮	⋮	⋮	⋮	
15	ANGLE(15)	70-75	F5.0	

No.	Variable Name	Card column	Format	Description

The following two cards are included only if variable 17 on flow card 2 >0.

(Isopressure card 1)

1	INTRVL(1,1)	1-8	F8.0	INTRVL(i,1) represents the intervals at which isohead contour lines are constructed. INTRVL(i,1) can be expressed in terms of proportions of the diagonal distance between the center well and the first quadrant peripheral well, or as the actual Δh values through which contour lines are to be constructed. In the latter case, contour values must be input as negative values.
2	INTRVL(2,1)	9-16	F8.0	
3	INTRVL(3,1)	17-24	F8.0	
⋮	⋮	⋮	⋮	
10	INTRVL(10,1)	72-80	F8.0	

Proportional values are useful when the user has no idea what relevant Δh values will be, prior to map construction. Maximum of 10 contour lines permitted. Number of contour values = LINES(1).

(Isopressure card 2)

1	PERCNT(1,1)	1-8	F8.0	PERCNT(i,1) represents the range of acceptability about INTRVL(i,1). PERCNT(i,1) can be input as a proportion of the Δh value for each INTRVL(i,1), or as an actual Δh value range, in this case PERCNT(i,1) is input as a negative number. The sign of PERCNT(i,1) must coincide with INTRVL(i,1).
2	PERCNT(2,1)	9-16	F8.0	
3	PERCNT(3,1)	17-24	F8.0	
⋮	⋮	⋮	⋮	
10	PERCNT(10.1)	72-80	F8.0	

The following two cards are included only if variable 18 on flow card 2 >0.

(Isovelocity card 1)

1	INTRVL(1,2)	1-8	F8.0	The interpretation of INTRVL(i,2) is analogous to that of INTRVL(i,1) except that proportional distance is a measure of the diagonal distance from the first quadrant peripheral well to the upper right corner of the flow evaluation matrix (that is, the distance between the points (s,s) and (XFINISH, YFINISH).
2	INTRVL(2,2)	9-16	F8.0	
3	INTRVL(3,2)	17-24	F8.0	
⋮	⋮	⋮	⋮	
10	INTRVL(10,2)	72-80	F8.0	

No.	Variable Name	Card column	Format	Description
			(Isovelocity card 2)	
1	PERCNT(1,2)	1-8	F8.0	The interpretation of PERCNT(i,2) is analogous to that of PERCNT(i,1). The sign of PERCNT(i,2) must coincide with INTRVL(i,2).
2	PERCNT(2,2)	9-16	F8.0	
3	PERCNT(3,2)	17-24	F8.0	
⋮	⋮	⋮	⋮	
10	PERCNT(10,2)	72-80	F8.0	

PROGRAM APPLICATION AND VERIFICATION

A field application of 5-SISL was designed to verify some program results and to illustrate the program output. This application is the result of a cooperative agreement between the Bureau of Mines and a private mineral development corporation. A pilot five-spot in situ uranium leaching operation located in the West-Central United States provided the input parameter values.

Appendix A contains the physical records of information that comprise the input for this application. For this example the INVERSE subprogram was used in obtaining permeability and porosity estimates from a drawdown test involving a single observation well. However, only the permeability value obtained was part of the leach analysis data set of this application; the required porosity estimate was taken from core measurement.

Flow analysis output consists of change in head, fluid velocity, and direction of fluid flow for every point on the aquifer evaluation matrix. Printer output for this application also includes well-to-well traversal times for individual streamlines, and two streamline plots, both distance and time incremented versions. A listing of output from this application is contained in appendix B.

Examples of the first quadrant streamline plots, both distance and time incremented versions, are presented in figures B-1 and B-2 of the appendix. Figure B-1 approximates the path of leachant particle movement, at 2-foot intervals, between the center input well and peripheral output wells. Arrows indicate input and output orientation at coordinates (0,0) and (25,25). A time-incremented version of the streamline plot is approximated in figure B-2. Here the increments between plotted points (denoted by asterisks) represent fluid movement in fixed 3-hour time intervals. Numbers plotted on these streamlines indicate no appreciable fluid movement over one or more fixed intervals.

In this application, line printer isopressure and isovelocity contour maps were not developed. Instead, an independent contour mapping routine (SACMS) which used output from the auxiliary (NPR) file was developed.

An isopressure contour map superimposed on a first quadrant streamline plot and a first quadrant isovelocity contour map comprise figures B-3 and B-4.

Verification of this computer model was obtained from two sources. The first compared model prediction and field measurement of the leachant traversal time between input and output wells. The second compared the streamline plots generated by this model with those that have been empirically or analytically described by other researchers.

The correspondence between predicted and observed leachant traversal times was obtained for the pilot five-spot operation mentioned earlier. Given the input parameter values that describe the in situ test site, the model predicted that initial breakthrough of the leachant would occur after approximately 160 hours. This is the traversal time for leachant particles moving along the shortest route, the 45° streamline. Field measurements indicated the initial breakthrough would occur after approximately 120 to 140 hours.

The graphic output from this model was compared with those outputs obtained by DeWiest (4) and by McKee in a proprietary model of leaching hydrology. The fluid streamline patterns associated with the five-spot well arrangement were consistent across all three sources.

DISCUSSION

Some problems were encountered in the development of this program that are related to computational characteristics of the program and sources of required input data. Similar problems may be encountered in other applications of the 5-SISL program.

1. A considerable discrepancy shows up between porosity estimates that were derived from aquifer core samples, and those obtained from drawdown tests conducted at the leaching site. Discussions with other individuals active in the field confirmed that this discrepancy is not uncommon. The field application shown in this report uses a drawdown test estimate of permeability and a core measurement estimate of porosity.

2. The input values of α (compressibility of solid skeleton) and β (compressibility of the fluid) are approximate values found in the literature (5); there is no known practical way of measuring these in situ.

3. Estimates of b (aquifer thickness) and b' (aquitard thickness) were taken from coring data.

4. The radius of influence, r_e, is assumed to be some very large number. Literature estimates typically range from 600 to 2,000 feet (default RE = 600 feet).

5. The various series used tend to converge too slowly for efficient computation when matrix points near the wells are being evaluated. During program development, tests indicated that this occurs when a matrix point is less than 1 foot from either an input or output well; for this reason, the program contains safeguards to prevent an extremely large or infinite, iterative loop in the process of finding convergent values. The user specifies a convergence requirement (TERM) for the individual contributory factor of Δh, along with a maximum number of iterations that can be performed in attempting to achieve this limit (ITEREND); the two prevent the waste of computer time. If points very near the wells are to be evaluated, a small TERM value coupled with a large ITEREND are recommended ($1.\times10^{-5}$, 200). If all matrix points are at least a foot from the well, less stringent requirements are adequate to achieve five decimal place accuracy ($1.\times10^{-1}$, 50). Erratic Δh values for points near the wells indicate that convergence requirements have not been adequate.

This model was developed for uranium leaching applications, specifically to assist in regulation of the aquifer hydrology, so that further attention can be directed toward site-specific geochemistry problems. However, the fluid flow equations involved in this model are applicable to any mineral leaching operation that uses a five-spot pattern of input and output wells.

CONCLUSION

The computer model (5-SISL computer program) described here provides uranium resource developers with a simulation of leachant flow characteristics in a preproduction or pilot five-spot leaching operation.

The model was verified with field measurements and by comparison with similar models developed by other researchers. Input requirements are readily obtainable and the model is supplied with several options for convenient numeric and graphic output. These include various isoparameter contours and streamline plots. A typical application has also been included.

BIBLIOGRAPHY

1. Abramowitz, M., and I. A. Stegun. Handbook of Mathematical Functions. Dover Publishing, Inc., New York, 1964, pp. 228-233, 358-385.

2. Bredehoeft, J. D., and G. F. Pinder. Digital Analysis of Areal Flow in Multiaquifer Ground Water Systems: A Quasi Three-Dimensional Model. Water Resour. Res., v. 6, June 1970, pp. 883-888.

3. Chow, V. T. On the Determination of Transmissibility and Storage Coefficients From Pumping Test Data. Trans. American Geophys. Union, v. 33, June 1952, pp. 397-404.

4. Craig, F. F. The Reservoir Engineering Aspects of Water Flooding. Trans. AIME Inc., New York, Mono. 3, 1971, 135 pp.

5. DeWiest, R. J. Geohydrology. John Wiley & Sons, Inc., New York, 1965, 366 pp.

6. Hantush, M. S. Analysis of Data From Pumping Tests in Leaky Aquifers. Trans. American Geophys. Union, v. 37, December 1956, pp. 702-714.

7. _____. Aquifer Tests on Partially Penetrating Wells. J. Hydraulics Division, Proc. of American Soc. Civil Eng., September 1961, pp. 171-195.

8. _____. Drawdown Around a Partially Penetrating Well. J. Hydraulics Division, Proc. of American Soc. Civil Eng., July 1961, pp. 83-98.

9. _____. Non-Steady Flow to a Well Partially Penetrating an Infinite Leaky Aquifer. Proc. of the Iraqi Scientific Societies, v. 1, January 1957, pp. 10-19.

10. Hantush, M. S., and C. E. Jacob. Non-Steady Green's Functions for an Infinite Strip of Leaky Aquifer. Trans. American Geophys. Union, v. 36, February 1955, pp. 101-112.

11. _____. Non-Steady Radial Flow in an Infinite Leaky Aquifer. Trans. American Geophys. Union, v. 36, February 1955, pp. 95-100.

12. _____. Steady Three-Dimensional Flow to a Well in a Two-Layered Aquifer. Trans. American Geophys. Union, v. 36, April 1955, pp. 286-292.

13. Hantush, M. S., and I. S. Papadopulos. Flow of Ground Water to Collector Wells. J. Hydraulics Division, Proc. of American Soc. Civil Eng., September 1962, pp. 221-244.

14. Jacob, C. E. Radial Flow in a Leaky Artesian Aquifer. Trans. American Geophys. Union, v. 27, April 1946, pp. 198-208.

15. Kipp, K. L. Unsteady Flow to a Partially Penetrating Finite Radius Well in an Unconfined Aquifer. Water Resour. Res., v. 9, April 1973, pp. 448-462.

16. Kirkham, D. Exact Theory of Flow Into a Partially Penetrating Well. J. Geophys. Res., v. 64, September 1959, pp. 1317-1327.

17. McKee, C. W. Private communication, 1977. Available upon request from C. W. McKee, University of Wyoming, Laramie, Wyo., or from R. D. Schmidt, Bureau of Mines, Twin Cities, Minn.

18. Murray, J. M. Ground Water Hydrology. Sec. in Handbook on Principles of Hydrology, ed. by D. M. Gray, Water Information Center, Port Washington, New York, 1973, pp. 6.1-6.56.

19. Neuman, S. P., and P. A. Witherspoon. Theory of Flow in a Confined Two Aquifer System. Water Resour. Res., v. 5, August 1969, pp. 803-816.

20. Williams, R. A., R. Y. Lai, and G. M. Karadi. Non-Steady Flow to a Well With Time Dependent Drawdown. Water Resour. Bull., v. 8, April 1972, pp. 294-303.

21. Yeh, W. G., and G. W. Tauxe. Quasilinearization and the Identification of Aquifer Parameters. Water Resour. Res., v. 7, April 1971, pp. 375-381.

APPENDIX A.--APPLICATION INPUT DATA

DRAWDOWN EVALUATION DATA SET

```
    1                                                                          (ASSIGNMENT CARD)
     25.00000E0      2.57000E-8      2.32000E-8      64.00000E0      13.90000E0  (INVERSE CARD 1)
    5    0      1.44000E-2      25.00000E0      25.00000E0                     (INVERSE CARD 2)
 2.90  3.17  3.33  3.42  3.60                                                  (INVERSE CARD 3)
90.00105.00128.84150.17169.00                                                  (INVERSE CARD 4)
```

LEACH ANALYSIS DATA SET

```
   -1                                                                          (ASSIGNMENT CARD)
   30 1000                                                                     (FLOW CARD 1)
  1  1  1  1  6  0  0  0 10  0 10  5  1 30  5  0  0                           (FLOW CARD 2)
     2.00000E0       2.00000E0       25.00000E0      13.90000E0      64.00000E0 (FLOW CARD 3)
      .28000E0       2.93333E0       1.58465E-4                                (FLOW CARD 4)
    1.78200E-2        .44600E-2        .44600E-2       .44600E-2       .44600E-2 (FLOW CARD 5)
    13.90000E0      13.90000E0      13.90000E0      13.90000E0      13.90000E0 (FLOW CARD 6)
    2.57000E-8      2.32000E-8       3.00000E0       1.00000E0       1.00000E0 (FLOW CARD 7)
    1.00000E-5                                                                 (FLOW CARD 8)
   600.00000E0                                                                 (STEADY STATE NONLEAKY CARD)
      2.0        3.0        1.0        300                                     (STREAMLINE CARD 1)
15.0 20.0 25.0 30.0 45.0                                                       (STREAMLINE CARD 2)
```

APPENDIX B.--APPLICATION OUTPUT DATA

POROSITY AND PERMEABILITY COMPUTED FROM FIELD OBSNS. OF WELL DRAWDOWN

CONFINED AQUIFER CASE

OUTPUT WELL(S) IS/ARE CENTER WELL(S)

MAJOR EFFECT ON OBSN. WELL 1 IS FROM THE CORNER WELL(S).

OBSN. NUMBER	WELL DRAWDOWN	TIME(MIN.)	STORATIVITY	TRANSMISSIVITY	PERMEABILITY	POROSITY
1	.29000E+01	.90000E+02				
2	.31700E+01	.10500E+03				
3	.33300E+01	.12884E+03				
4	.34200E+01	.15017E+03				
5	.36000E+01	.16900E+03				
			.59951E-03	.11294E-02	.81252E-04	.27940E+02

RUN NUMBER 1
CHANGE IN HEAD IS TIME INDEPENDENT
TIME INTERVAL OF EVALUATION IS 0 DAYS 2.933 HOURS
AQUIFER IS NON-LEAKY
INPUT WELL(S) IS(ARE) LOCATED AT CENTER
AVE. INPUT VOLUME OF LEACHING FLUID 7.998 GAL./MIN./WELL
AVE. OUTPUT VOLUME OF LEACHING FLUID 2.002 GAL./MIN./WELL
AVE. PERMEABILITY OF AQUIFER .15847E-03 FT./SEC.
AVE. POROSITY OF AQUIFER .28000E+00
DEPTH OF PENETRATION OF EACH PIPE INTO THE AQUIFER 13.90 13.90 13.90 13.90 13.90 FT.
HEIGHT OF ANALYSIS(Z) IN AQUIFER 3.000 FT.

X CO-ORD (FEET)	Y CO-ORD (FEET)	DRAWDOWN (FEET)	VELOCITY (FEET/SEC.)	DIRECTION OF FLOW (DEGREES)
.20000E+01	0.	.36943E+01	.40028E-03	0.
.40000E+01	0.	.28018E+01	.18609E-03	.12381E-11
.60000E+01	0.	.22800E+01	.12249E-03	0.
.80000E+01	0.	.19101E+01	.91326E-04	0.
.10000E+02	0.	.16240E+01	.72647E-04	0.
0.	.20000E+01	.36943E+01	.40028E-03	0.
.20000E+01	.20000E+01	.32480E+01	.24619E-03	.45000E+02
.40000E+01	.20000E+01	.26581E+01	.16219E-03	.25686E+02
.60000E+01	.20000E+01	.22120E+01	.11546E-03	.18041E+02
.80000E+01	.20000E+01	.18708E+01	.88463E-04	.13946E+02
.10000E+02	.20000E+01	.15983E+01	.71265E-04	.11460E+02
0.	.40000E+01	.28018E+01	.18609E-03	.12381E-11
.20000E+01	.40000E+01	.26581E+01	.16219E-03	.25686E+02

.40000E+01

.40000E+01	.40000E+01	.23553E+01	.12753E-03	.45000E+02
.60000E+01	.40000E+01	.20426E+01	.10071E-03	.33502E+02
.80000E+01	.40000E+01	.17653E+01	.81465E-04	.26564E+02
.10000E+02	.40000E+01	.15266E+01	.67631E-04	.22131E+02
0.	.60000E+01	.22800E+01	.12249E-03	0.
.20000E+01	.60000E+01	.22120E+01	.11546E-03	.18041E+02
.40000E+01	.60000E+01	.20426E+01	.10071E-03	.33502E+02
.60000E+01	.60000E+01	.18324E+01	.85761E-04	.45000E+02
.80000E+01	.60000E+01	.16202E+01	.73055E-04	.36967E+02
.10000E+02	.60000E+01	.14219E+01	.62806E-04	.31417E+02
0.	.80000E+01	.19101E+01	.91326E-04	0.
.20000E+01	.80000E+01	.18708E+01	.88463E-04	.13946E+02
.40000E+01	.80000E+01	.17653E+01	.81465E-04	.26564E+02
.60000E+01	.80000E+01	.16202E+01	.73055E-04	.36967E+02
.80000E+01	.80000E+01	.14596E+01	.64919E-04	.45000E+02
.10000E+02	.80000E+01	.12984E+01	.57689E-04	.39042E+02
0.	.10000E+02	.16240E+01	.72647E-04	0.
.20000E+01	.10000E+02	.15983E+01	.71265E-04	.11460E+02
.40000E+01	.10000E+02	.15266E+01	.67631E-04	.22131E+02
.60000E+01	.10000E+02	.14219E+01	.62806E-04	.31417E+02
.80000E+01	.10000E+02	.12984E+01	.57689E-04	.39042E+02
.10000E+02	.10000E+02	.11674E+01	.52789E-04	.45000E+02

TOTAL NUMBER OF COORDINATES PRODUCED = 27 FOR STREAMLINE NUMBER 1 INITIAL ANGLE OF STREAMLINE = 15.00 DEGREES

TOTAL TIME TO TRAVERSE STREAMLINE = 540.575 HOURS

X CO-ORD	1.93	3.89	5.84	7.80	9.75	11.70	13.64	15.58	17.52	19.44	21.34	23.21	25.04	26.81	28.49
Y CO-ORD	.52	.92	1.35	1.78	2.23	2.68	3.14	3.62	4.13	4.69	5.31	6.01	6.81	7.75	8.83

X CO-ORD	30.05	31.43	32.57	33.40	33.85	33.85	33.35	32.35	30.91	29.14	27.19	26.00
Y CO-ORD	10.09	11.54	13.18	15.00	16.95	18.95	20.88	22.62	24.01	24.94	25.35	26.00

TOTAL NUMBER OF COORDINATES PRODUCED = 24 FOR STREAMLINE NUMBER 2 INITIAL ANGLE OF STREAMLINE = 20.00 DEGREES

TOTAL TIME TO TRAVERSE STREAMLINE = 357.375 HOURS

X CO-ORD	1.88	3.80	5.71	7.63	9.53	11.44	13.34	15.23	17.11	18.97	20.80	22.59	24.31	25.93	27.42
Y CO-ORD	.68	1.24	1.82	2.41	3.01	3.62	4.24	4.89	5.57	6.30	7.11	8.01	9.03	10.20	11.54

X CO-ORD	28.71	29.74	30.43	30.69	30.44	29.64	28.31	26.54	26.00
Y CO-ORD	13.07	14.78	16.66	18.64	20.63	22.46	23.95	24.89	26.00

TOTAL NUMBER OF COORDINATES PRODUCED = 21 FOR STREAMLINE NUMBER 3 INITIAL ANGLE OF STREAMLINE = 25.00 DEGREES

TOTAL TIME TO TRAVERSE STREAMLINE = 260.738 HOURS

X CO-ORD	1.81	3.68	5.54	7.39	9.24	11.08	12.92	14.75	16.56	18.35	20.10	21.78	23.38	24.86	26.17
Y CO-ORD	.85	1.56	2.31	3.06	3.82	4.59	5.37	6.18	7.03	7.93	8.91	9.98	11.18	12.53	14.04

X CO-ORD	27.23	27.97	28.29	28.10	27.33	26.00
Y CO-ORD	15.74	17.60	19.57	21.56	23.40	26.00

TOTAL NUMBER OF COORDINATES PRODUCED = 20 FOR STREAMLINE NUMBER 4 INITIAL ANGLE OF STREAMLINE = 30.00 DEGREES

TOTAL TIME TO TRAVERSE STREAMLINE = 210.503 HOURS

X CO-ORD	1.73	3.52	5.30	7.06	8.85	10.62	12.38	14.13	15.86	17.56	19.21	20.80	22.30	23.67	24.86
Y CO-ORD	1.00	1.89	2.80	3.72	4.65	5.58	6.53	7.50	8.51	9.56	10.69	11.90	13.22	14.68	16.29

X CO-ORD	25.79	26.37	26.51	26.10	26.00
Y CO-ORD	18.06	19.97	21.97	23.92	26.00

TOTAL NUMBER OF COORDINATES PRODUCED = 18 FOR STREAMLINE NUMBER 5 INITIAL ANGLE OF STREAMLINE = 45.00 DEGREES

TOTAL TIME TO TRAVERSE STREAMLINE = 160.004 HOURS

X CO-ORD	1.41	2.83	4.24	5.66	7.07	8.49	9.90	11.31	12.73	14.14	15.56	16.97	18.38	19.80	21.21
Y CO-ORD	1.41	2.83	4.24	5.66	7.07	8.49	9.90	11.31	12.73	14.14	15.56	16.97	18.38	19.80	21.21

X CO-ORD	22.63	24.04	26.00
Y CO-ORD	22.63	24.04	26.00

5 FIRST QUADRANT STREAMLINE(S) PLOTTED WITH THE FOLLOWING DATA
HEIGHT IN AQUIFER 3.00 FT.
INITIAL ANGLE(S) 15.00 20.00 25.00 30.00 45.00 DEGREES
STREAMLINE INCREMENT 2.00 FT.

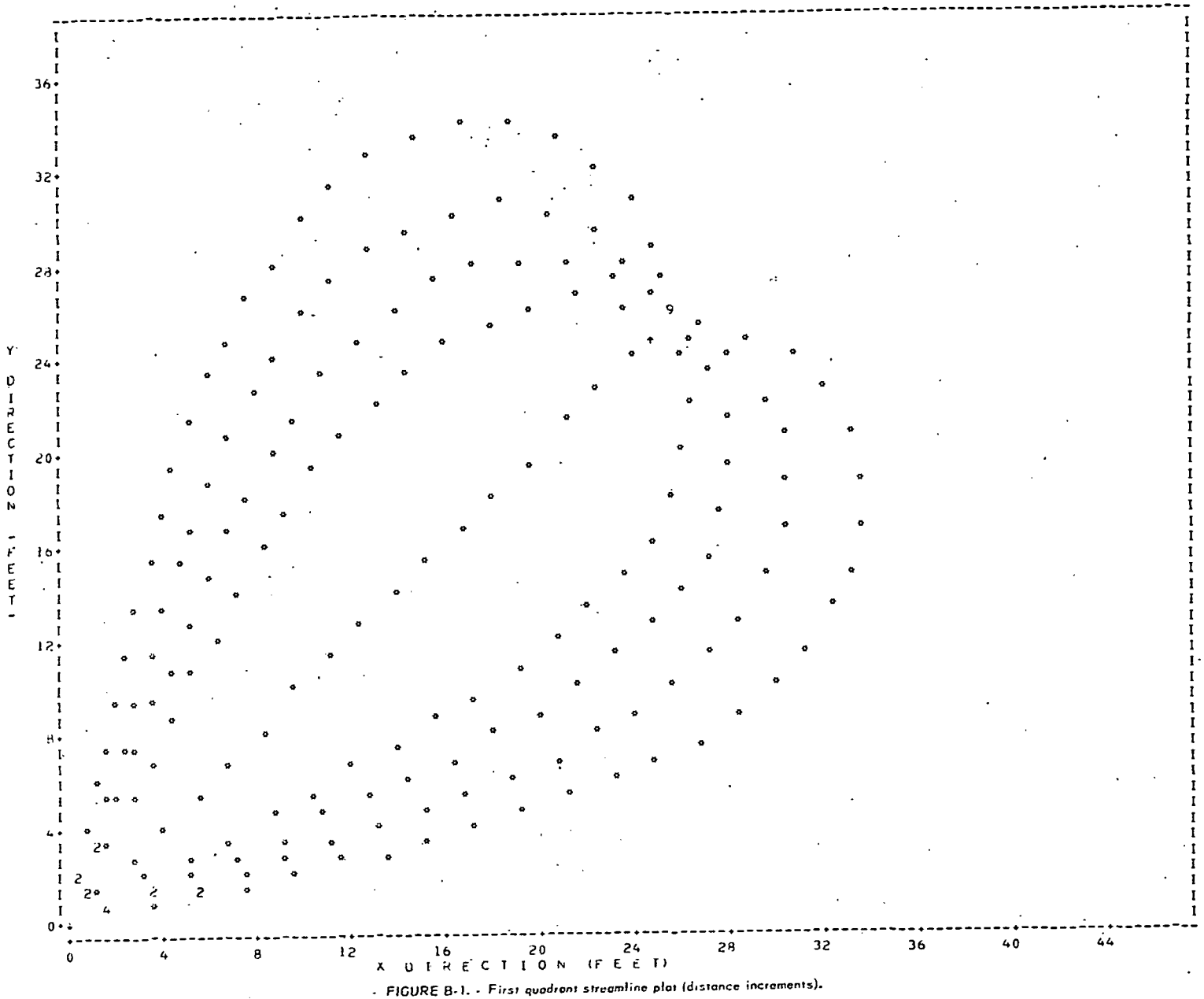

FIGURE B-1. - First quadrant streamline plot (distance increments).

TOTAL NUMBER OF COORDINATES PRODUCED = 152 FOR STREAMLINE NUMBER 1 INITIAL ANGLE OF STREAMLINE = 15.00 DEGREES

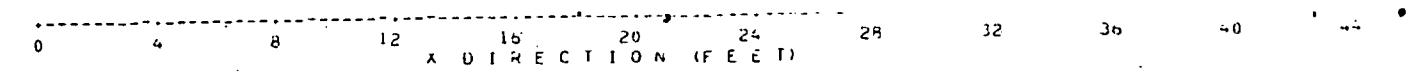

FIGURE B-1. - First quadrant streamline plot (distance increments).

TOTAL NUMBER OF COORDINATES PRODUCED = 152 FOR STREAMLINE NUMBER 1 INITIAL ANGLE OF STREAMLINE = 15.00 DEGREES

TOTAL TIME TO TRAVERSE STREAMLINE = 461.534 HOURS

X CO-ORD	1.93	5.97	7.24	8.27	9.18	10.00	10.74	11.44	12.09	12.70	13.28	13.84	14.37	14.88	15.37
Y CO-ORD	.52	1.34	1.62	1.85	2.05	2.23	2.40	2.56	2.71	2.86	3.00	3.13	3.26	3.39	3.51
X CO-ORD	15.84	16.29	16.73	17.16	17.58	17.98	18.37	18.75	19.12	19.48	19.83	20.17	20.51	20.83	21.15
Y CO-ORD	3.63	3.76	3.87	3.99	4.11	4.22	4.34	4.45	4.57	4.68	4.80	4.91	5.03	5.14	5.25
X CO-ORD	21.46	21.77	22.07	22.36	22.64	22.92	23.19	23.46	23.72	23.98	24.23	24.47	24.71	24.95	25.18
Y CO-ORD	5.37	5.48	5.60	5.72	5.83	5.95	6.07	6.19	6.30	6.42	6.54	6.67	6.79	6.91	7.03
X CO-ORD	25.41	25.63	25.84	26.06	26.26	26.47	26.67	26.86	27.06	27.24	27.43	27.61	27.78	27.96	28.13
Y CO-ORD	7.16	7.28	7.41	7.53	7.66	7.79	7.91	8.04	8.17	8.30	8.44	8.57	8.70	8.83	8.97
X CO-ORD	28.29	28.45	28.61	28.77	28.92	29.07	29.21	29.35	29.49	29.63	29.76	29.89	30.01	30.14	30.26
Y CO-ORD	9.10	9.24	9.38	9.51	9.65	9.79	9.93	10.07	10.21	10.36	10.50	10.64	10.79	10.93	11.08
X CO-ORD	30.37	30.49	30.60	30.70	30.81	30.91	31.01	31.10	31.20	31.29	31.37	31.46	31.54	31.62	31.69
Y CO-ORD	11.22	11.37	11.52	11.67	11.82	11.97	12.12	12.27	12.42	12.57	12.73	12.88	13.04	13.19	13.35
X CO-ORD	31.76	31.83	31.90	31.96	32.02	32.08	32.14	32.19	32.24	32.28	32.33	32.37	32.40	32.44	32.47
Y CO-ORD	13.51	13.66	13.82	13.98	14.14	14.30	14.46	14.62	14.78	14.95	15.11	15.27	15.44	15.60	15.77
X CO-ORD	32.49	32.52	32.54	32.56	32.57	32.58	32.59	32.59	32.60	32.59	32.59	32.58	32.56	32.54	32.52
Y CO-ORD	15.93	16.10	16.27	16.44	16.61	16.78	16.95	17.12	17.29	17.46	17.63	17.81	17.98	18.16	18.33
X CO-ORD	32.50	32.47	32.43	32.39	32.35	32.30	32.25	32.19	32.13	32.06	31.98	31.90	31.81	31.72	31.62
Y CO-ORD	18.51	18.69	18.86	19.04	19.22	19.40	19.58	19.76	19.94	20.13	20.31	20.49	20.68	20.87	21.05
X CO-ORD	31.51	31.39	31.27	31.13	30.99	30.83	30.67	30.49	30.29	30.08	29.85	29.59	29.31	29.00	28.65
Y CO-ORD	21.24	21.43	21.62	21.81	22.00	22.19	22.39	22.58	22.78	22.98	23.17	23.38	23.58	23.78	23.99
X CO-ORD	28.24	27.75													
Y CO-ORD	24.20	24.41													

TOTAL NUMBER OF COORDINATES PRODUCED = 105 FOR STREAMLINE NUMBER 2 INITIAL ANGLE OF STREAMLINE = 20.00 DEGREES

TOTAL TIME TO TRAVERSE STREAMLINE = 320.039 HOURS

X CO-ORD	1.80	5.72	6.98	8.01	8.91	9.72	10.45	11.14	11.78	12.38	12.95	13.50	14.02	14.52	15.01
Y CO-ORD	.68	1.79	2.17	2.49	2.76	3.02	3.25	3.46	3.67	3.87	4.05	4.24	4.41	4.58	4.75
X CO-ORD	15.47	15.92	16.35	16.77	17.18	17.58	17.96	18.34	18.70	19.06	19.40	19.74	20.07	20.39	20.71
Y CO-ORD	4.92	5.08	5.24	5.40	5.56	5.71	5.87	6.02	6.18	6.33	6.48	6.64	6.79	6.95	7.10
X CO-ORD	21.01	21.31	21.61	21.89	22.17	22.45	22.72	22.98	23.23	23.48	23.73	23.97	24.20	24.43	24.65
Y CO-ORD	7.25	7.41	7.56	7.72	7.88	8.04	8.20	8.36	8.52	8.68	8.84	9.01	9.17	9.34	9.51
X CO-ORD	24.87	25.09	25.29	25.50	25.70	25.89	26.08	26.26	26.44	26.62	26.79	26.96	27.12	27.27	27.43
Y CO-ORD	9.68	9.85	10.02	10.20	10.37	10.55	10.73	10.91	11.09	11.28	11.46	11.65	11.84	12.03	12.22
X CO-ORD	27.57	27.72	27.85	27.99	28.12	28.24	28.36	28.48	28.59	28.69	28.79	28.89	28.98	29.06	29.14
Y CO-ORD	12.41	12.61	12.80	13.00	13.21	13.41	13.61	13.82	14.03	14.24	14.45	14.67	14.89	15.10	15.33
X CO-ORD	29.22	29.29	29.35	29.41	29.46	29.51	29.55	29.58	29.61	29.63	29.64	29.65	29.64	29.63	29.61
Y CO-ORD	15.55	15.78	16.01	16.24	16.47	16.71	16.95	17.19	17.43	17.68	17.93	18.18	18.44	18.70	18.97
X CO-ORD	29.58	29.54	29.49	29.43	29.35	29.26	29.16	29.03	28.89	28.72	28.53	28.30	28.03	27.70	27.29
Y CO-ORD	19.23	19.51	19.78	20.06	20.35	20.64	20.94	21.24	21.56	21.88	22.21	22.55	22.90	23.27	23.67

TOTAL NUMBER OF COORDINATES PRODUCED = 80 FOR STREAMLINE NUMBER 3 INITIAL ANGLE OF STREAMLINE = 25.00 DEGREES

TOTAL TIME TO TRAVERSE STREAMLINE = 244.911 HOURS

X CO-ORD	1.81	5.43	6.67	7.68	8.56	9.35	10.07	10.74	11.36	11.95	12.51	13.05	13.56	14.05	14.52
Y CO-ORD	.85	2.23	2.73	3.14	3.50	3.82	4.11	4.39	4.65	4.90	5.14	5.38	5.60	5.82	6.03

TOTAL NUMBER OF COORDINATES PRODUCED = 65 FOR STREAMLINE NUMBER 4 INITIAL ANGLE OF STREAMLINE = 30.00 DEGREES

TOTAL TIME TO TRAVERSE STREAMLINE = 200.842 HOURS

X CO-ORD	1.73	5.09	6.30	7.29	8.14	8.90	9.59	10.24	10.84	11.41	11.95	12.46	12.96	13.43	13.89
Y CO-ORD	1.00	2.67	3.29	3.80	4.24	4.63	5.00	5.34	5.66	5.97	6.26	6.54	6.81	7.08	7.34
X CO-ORD	14.33	14.75	15.17	15.57	15.95	16.33	16.70	17.06	17.41	17.75	18.08	18.41	18.73	19.04	19.35
Y CO-ORD	7.59	7.84	8.08	8.32	8.56	8.80	9.03	9.26	9.49	9.72	9.95	10.18	10.41	10.64	10.87
X CO-ORD	19.64	19.94	20.22	20.50	20.78	21.04	21.31	21.56	21.81	22.06	22.30	22.54	22.77	22.99	23.21
Y CO-ORD	11.10	11.34	11.57	11.80	12.04	12.28	12.52	12.77	13.01	13.27	13.52	13.78	14.04	14.30	14.57
X CO-ORD	23.42	23.63	23.83	24.03	24.22	24.40	24.58	24.75	24.91	25.07	25.21	25.35	25.48	25.59	25.69
Y CO-ORD	14.85	15.13	15.42	15.71	16.01	16.32	16.63	16.95	17.29	17.63	17.99	18.36	18.75	19.15	19.57
X CO-ORD	25.78	25.85	25.90	25.92	25.91										
Y CO-ORD	20.02	20.50	21.02	21.59	22.23										

TOTAL NUMBER OF COORDINATES PRODUCED = 51 FOR STREAMLINE NUMBER 5 INITIAL ANGLE OF STREAMLINE = 45.00 DEGREES

TOTAL TIME TO TRAVERSE STREAMLINE = 158.680 HOURS

X CO-ORD	1.41	3.94	4.93	5.72	6.41	7.02	7.58	8.11	8.59	9.06	9.50	9.92	10.33	10.72	11.10
Y CO-ORD	1.41	3.94	4.93	5.72	6.41	7.02	7.58	8.11	8.59	9.06	9.50	9.92	10.33	10.72	11.10
X CO-ORD	11.47	11.83	12.18	12.52	12.85	13.18	13.50	13.82	14.14	14.45	14.75	15.06	15.36	15.65	15.95
Y CO-ORD	11.47	11.83	12.18	12.52	12.85	13.18	13.50	13.82	14.14	14.45	14.75	15.06	15.36	15.65	15.95
X CO-ORD	16.25	16.54	16.83	17.13	17.42	17.72	18.01	18.31	18.61	18.92	19.23	19.54	19.86	20.19	20.53
Y CO-ORD	16.25	16.54	16.83	17.13	17.42	17.72	18.01	18.31	18.61	18.92	19.23	19.54	19.86	20.19	20.53
X CO-ORD	20.88	21.24	21.63	22.04	22.48	22.97									
Y CO-ORD	20.88	21.24	21.63	22.04	22.48	22.97									

5 FIRST QUADRANT STREAMLINE(S) PLOTTED WITH THE FOLLOWING DATA
HEIGHT IN AQUIFER 3.00 FT.
INITIAL ANGLE(S) 15.00 20.00 25.00 30.00 45.00 DEGREES
STREAMLINE INCREMENT 3.00 HRS.

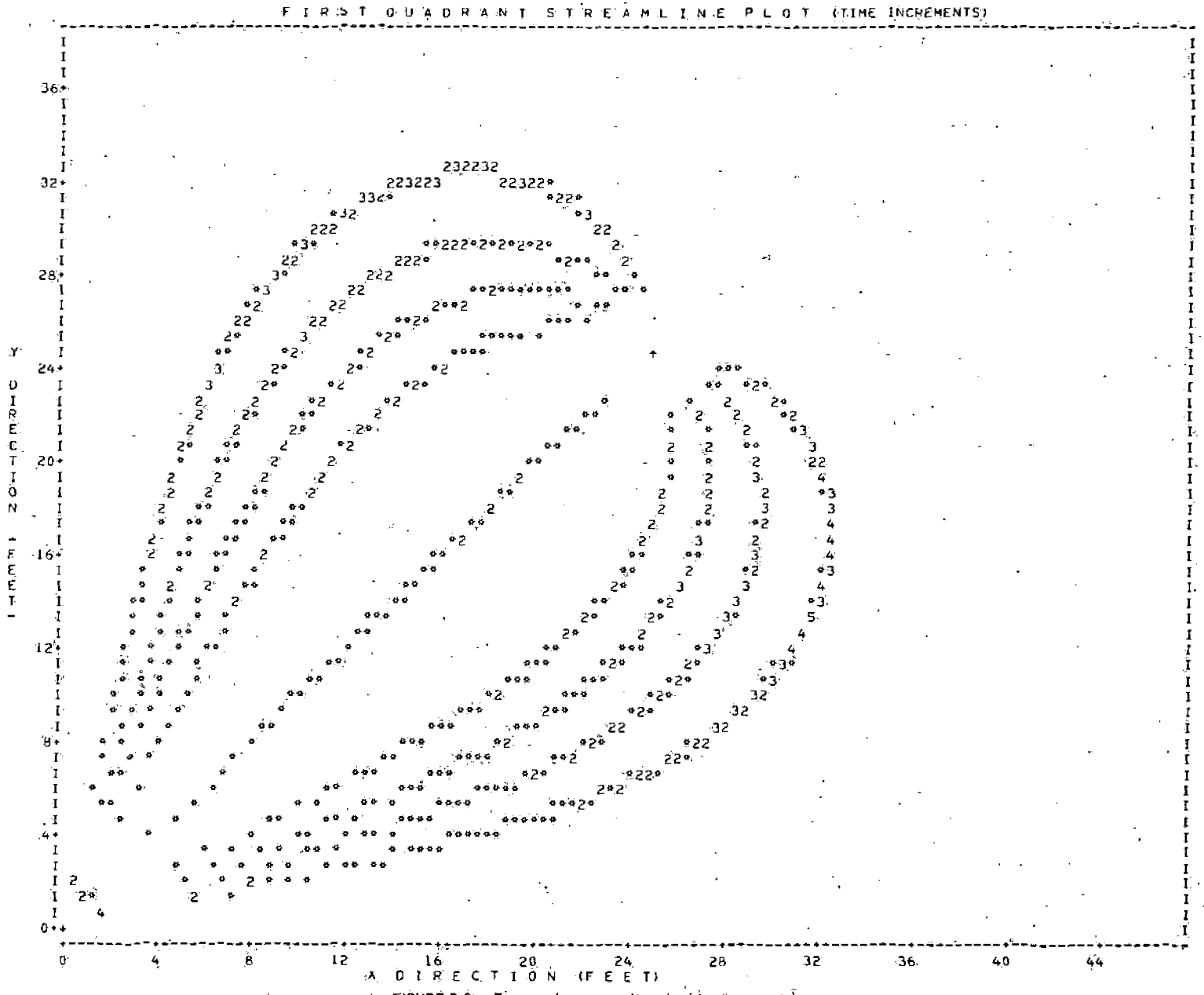

FIGURE B-2. - First quadrant streamline plot (time increments).

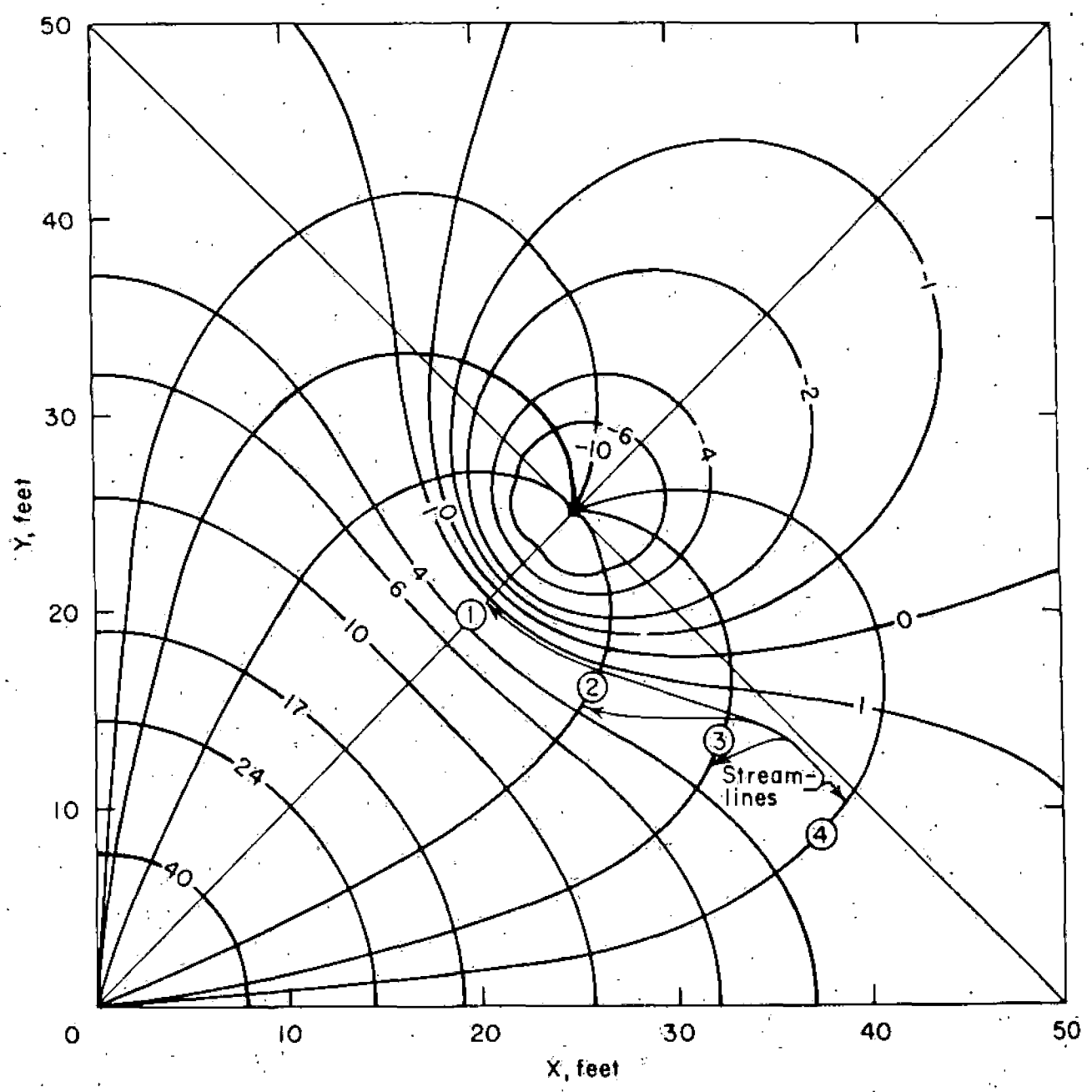

FIGURE B-3. - Isopressure (feet of water) contour map.

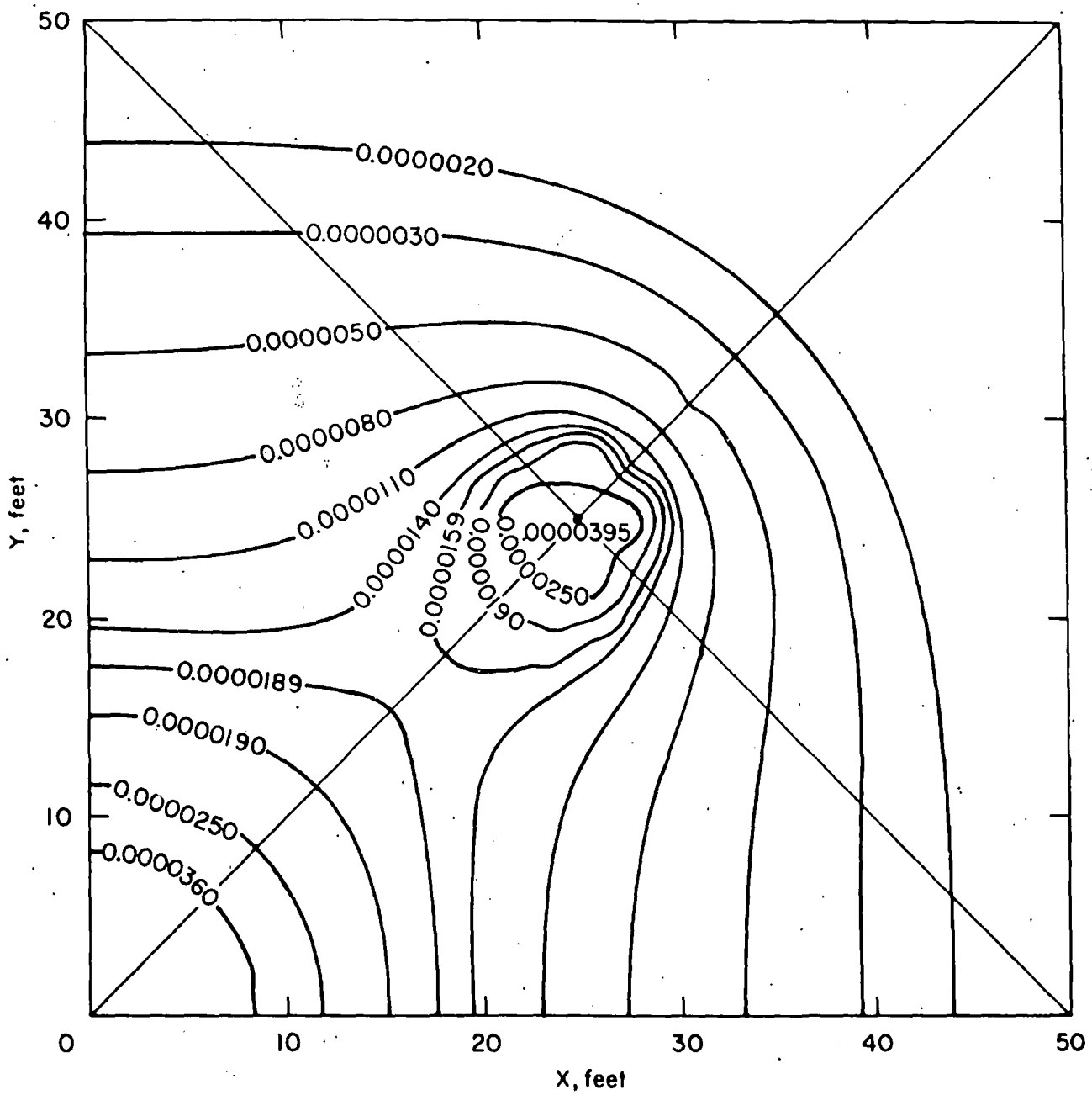

FIGURE B-4. - Isovelocity (feet per second) contour map.

APPENDIX C.--PROGRAM LISTING

```
      PROGRAM  SETUP (INPUT, OUTPUT, TAPE5=INPUT, TAPE12, TAPE6,        SETU  10
     1   TAPE13, TAPE14, TAPE15)                                        SETU  20
      COMMON  /DATA/  PNDEPTH, X, Y, Z, RE                              SETU  30
      COMMON  /CONST/  ITME, NPR, S, B, K, T, T1, T2, GAMMA, N, N2, VT, SETU  40
     1   Q, ALPHA, BETA, N1, K1, SS, SCO, IRUN, ITOT, AQR, BPRIME,      SETU  50
     2   KPRIME, ITEREND, TERM                                          SETU  60
      COMMON / LINES/ ANGLE, RADIUS, NLINES, OUTOPT, MAXID, IPLOT,      SETU  70
     1  DISTME (2)                                                      SETU  80
      COMMON  /CONTR/  LINES (2), PERCNT (10, 2), INTRVL (10, 2)        SETU  90
C                                                                       SETU 100
C     THIS DUMMY MAIN PROGRAM CONTROLS  SIZE OF MATRICES. LARGER        SETU 110
C     MATRICES MAY BE IMPLEMENTED VIA THE READ STATEMENT OR CHANGES     SETU 120
C     TO THE COMMON DIMENSIONS.                                         SETU 130
C                                                                       SETU 140
C***** THIS  PROGRAM EVALUATES THE PARTICLE FLOW PARAMETERS ASSOCIATED  SETU 150
C***** WITH INSITU LEACHING OF URANIUM AT EACH GRID NODE OF A USER      SETU 160
C***** SPECIFIED HORIZONTAL MATRIX OF POINTS AT A SPECIFIED AQUIFER     SETU 170
C***** DEPTH.  CHANGE IN HEAD,VELOCITY OF FLOW,DIRECTION AND STREAMLINE SETU 180
C***** VALUES ARE AVAILABLE FOR OUTPUT.                                 SETU 190
C***** INVERSE DECISION MADE IN MAIN PROGRAM,SPECIFIES PROGRAM CALCUL-  SETU 200
C***** ATION OF AQUIFER PERMEABILITY AND POROSITY.                      SETU 210
C                                                                       SETU 220
      DIMENSION   ANGLE (20), PLOTFLE(1000,3), PNDEPTH (5), Q (5),      SETU 230
     1   THETA (30,30), VRAD (30,30), VX (30,30), VY (30,30), XCOORD    SETU 240
     2  (1000), XLIST (60), XPART (30,30), XYLIST (30,30), YCOORD(1000), SETU 250
     3   YLIST (60), YPART (30,30)                                      SETU 260
      INTEGER     ASSIGN                                                SETU 270
      READ (5,   10)  ASSIGN                                            SETU 280
      IF (ASSIGN .LE. 0)  GO TO 1000                                    SETU 290
      READ (5,   20)  S, ALPHA, BETA, GAMMA, B                          SETU 300
      CALL INVERSE (K, N, S, ALPHA, BETA, GAMMA, B, ASSIGN)             SETU 310
      GO TO 1010                                                        SETU 320
 1000 READ (5,   10)  M1, L1                                            SETU 330
      IF  (L1 .LE. 0)  L1  =  1000                                      SETU 340
      M2  =  2 * M1                                                     SETU 350
      CALL INSITU (M1, M2, L1, XLIST, YLIST, XYLIST, XPART, YPART, VX,  SETU 360
     1   VY, VRAD, THETA, PLOTFLE, XCOORD, YCOORD,ASSIGN)               SETU 370
 1010 CONTINUE                                                          SETU 380
C                                                                       SETU 390
   10 FORMAT  ( 2I5 )                                                   SETU 400
   20 FORMAT  ( 5E15.5 )                                                SETU 410
C                                                                       SETU 420
      END                                                               SETU 430
```

```
C////////////////////////////////////////////////////////////////////////INSI  10
      SUBROUTINE  INSITU (M1, M2, L1, XLIST, YLIST, XYLIST, XPART,      INSI  20
     1   YPART, VX, VY, VRAD, THETA, PLOTFLE, XCOORD, YCOORD, ASSIGN)    INSI  30
C                                                                       INSI  40
C***** SUBROUTINE INSITU ACTS AS THE DRIVER ROUTINE BY CALLING ALL       INSI  50
C***** SUBROUTINES NECESSARY TO MEET SPECIFIED OUTPUT REQUIREMENTS.      INSI  60
C***** OUTPUT  OPTION SPECIFIES PRINTER OR LOGICAL FILE STORAGE FOR      INSI  70
C***** LATER USE AS INPUT DATA TO CONTOUR MAPPING OR PLOTTING PROGRAMS.  INSI  80
C                                                                       INSI  90
      COMMON  /DATA/  PNDEPTH, X, Y, Z, RE                              INSI 100
      COMMON  /CONST/  ITME, NPR, S, B, K, T, T1, T2, GAMMA, N, N2, VT, INSI 110
     1   Q, ALPHA, BETA, N1, K1, SS, SCO, IRUN, ITOT, AQR, BPRIME,      INSI 120
     2   KPRIME, ITEREND, TERM                                          INSI 130
      COMMON  /LINES/  ANGLE, RADIUS, NLINES, OUTOPT, MAXID, IPLOT,     INSI 140
     1   UISTME (2)                                                     INSI 150
      COMMON  /CONTR/  LINES (2), PERCNT (10, 2), INTRVL (10, 2)        INSI 160
      DIMENSION   ANGLE (20), ODDLIST (9,20), ODDPT (4,20), OMIT        INSI 170
     1   (10,2), OUTA (2), OUTB (2), OUTC (2), OUTD (2), OUTE (2),      INSI 180
     2   PLOTFLE (L1,3), PNDEPTH (5), Q (5), THETA (M1,M1), VRAD.       INSI 190
     3   (M1,M1), VX (M1,M1), VY (M1,M1), XCOORD (L1), XLIST (M2), XPARTINSI 200
     4   (M1,M1), XYLIST (M1,M1), YCOORD (L1), YLIST (M2), YPART (M1,M1)INSI 210
      INTEGER     AQR, DAYS, OUT, OUTOPT, SCO, XFINISH, XSTART,         INSI 220
     1   YFINISH, YSTART, ASSIGN                                        INSI 230
      REAL        INCRX, INCRY, K, KPRIME, K1, N, N1, N2                INSI 240
      DATA    OUTA, OUTB, OUTC, OUTD, OUTE / 8HINDEPEND, 8HDEPENDEN,    INSI 260
     1   8HENT     , 8HT       , 8HNON-LEAK , 8HLEAKY   , 8HY       ,   INSI 270
     2   8H        , 8HCENTER  , 8HCORNERS  /                            INSI 280
      PRINT   10                                                        INSI 290
C***********************************************************************INSI 300
C***** CALL TO INPUT ROUTINE IS INIATED HERE.                           INSI 310
 1000 CALL INPT (OMIT, NUMOMT, NUMODD, YSTART, YFINISH, XSTART,         INSI 320
     1   XFINISH, INCRX, INCRY, XINC, YINC, ODDPT, ASSIGN)              INSI 330
      IF (XSTART .LT. 0 .OR. YSTART .LT. 0 .OR. XFINISH .LT. 0 .OR.     INSI 340
     1   YFINISH.LT.0)  CALL ERROR (1)                                  INSI 350
      IF (S .LE. 0)  CALL ERROR (2)                                     INSI 360
      IF (Z .GT. B)  CALL ERROR (7)                                     INSI 370
 1010 IF (ITME .LE. 1)  GO TO 1030                                      INSI 380
 1020 FOFT  =  GAMMA * (ALPHA + N * BETA) / (4. * K * T)                INSI 490
C***** INITIATE COMPUTATION FOR CHANGE IN HEAD,VELOCITY AND             INSI 500
C***** DIRECTION OF LEACHING PARTICLES IN THE AQUIFER.                  INSI 510
 1030 IF (Q(1) .LT. 0.0)  GO TO 1040                                    INSI 520
      IN  =  1                                                          INSI 530
      OUT  =  2                                                         INSI 540
      GO TO 1050                                                        INSI 550
 1040 IN  =  2                                                          INSI 560
      OUT  =  1                                                         INSI 570
 1050 IF (OUTOPT .EQ. -1)  GO TO 1210                                   INSI 580
        DO 1080  IY  =  YSTART, YFINISH                                 INSI 590
        Y  =  - INCRY + INCRY * FLOAT (IY)                              INSI 600
        NN  =  0                                                        INSI 610
          DO 1070  IX  =  IY, XFINISH                                   INSI 620
          REALX = (FLOAT(IX) - 1) * INCRX                               INSI 625
           DO 1070  NM  =  2, 4, 2                                      INSI 630
           NN  =  NN + 1                                                INSI 640
           X  =  REALX - 3. * XINC + NM * XINC                          INSI 650
           IF (X .EQ. 0.0 .AND. Y .EQ. 0.0)  GO TO 1060                 INSI 660
           IF (X .NE. S .OR. Y .NE. S)  GO TO 1070                      INSI 670
 1060      NUMOMT  =  NUMOMT + 1                                        INSI 680
           OMIT (NUMOMT, 1)  =  REALX                                   INSI 690
           OMIT (NUMOMT, 2)  =  Y                                       INSI 700
```

```
            GO TO 1080                                                    INSI 710
 1070       CALL DELTAH (XLIST(NN), FOFT)                                 INSI 720
          CALL PARTX (M1, M2, XLIST, YLIST, XPART, YPART, IX, IY,         INSI 730
     1      XFINISH, YSTART, XINC, YINC)                                  INSI 740
 1080     CONTINUE                                                        INSI 750
C                                                                        INSI 760
C      DETERMINE PARTIAL WITH Y.                                         INSI 770
C                                                                        INSI 780
         DO 1110  IX  =  XSTART, XFINISH                                 INSI 790
         X  =   - INCRX + INCRX * FLOAT (IX)                             INSI 800
         NN  =  0                                                        INSI 810
           DO 1100  IY  =  YSTART, IX                                    INSI 820
           REALY = (FLOAT(IY) - 1.) * INCRY                              INSI 825
             DO 1100  NM  =  2, 4, 2                                     INSI 830
             NN  =  NN + 1                                               INSI 840
             Y  =  REALY - 3. * YINC + NM * YINC                         INSI 850
             IF (X .EQ. 0.0 .AND. Y .EQ. 0.0)  GO TO 1090                INSI 860
             IF (X .NE. S .OR. Y .NE. S)  GO TO 1100                     INSI 870
 1090        NUMOMT  =  NUMOMT + 1                                       INSI 880
             OMIT (NUMOMT, 1)  =  X                                      INSI 890
             OMIT (NUMOMT, 2)  =  REALY                                  INSI 900
             GO TO 1110                                                  INSI 910
 1100        CALL DELTAH (YLIST(NN), FOFT)                               INSI 920
         CALL PARTY (M1, M2, XLIST, YLIST, XPART, YPART, IX, IY,         INSI 930
     1      XFINISH, YSTART, XINC, YINC)                                  INSI 940
 1110    CONTINUE                                                        INSI 950
C                                                                        INSI 960
C      DETERMINE HEAD      CHANGE AT EACH GRID POINT.                    INSI 970
C                                                                        INSI 980
         DO 1140  IX  =  XSTART, XFINISH                                 INSI 990
           DO 1140  IY  =  YSTART, IX                                    INSI1000
           X  =   - INCRX + INCRX * FLOAT (IX)                           INSI1010
           Y  =   - INCRY + INCRY * FLOAT (IY)                           INSI1020
             DO 1120  II  =  1, NUMOMT                                   INSI1030
             IF (X .EQ. OMIT(II,1) .AND. Y .EQ. OMIT(II,2))  GO TO 1140  INSI1040
 1120        CONTINUE                                                    INSI1050
 1130      CALL DELTAH (XYLIST(IX, IY), FOFT)                            INSI1060
 1140      CONTINUE                                                      INSI1070
C                                                                        INSI1080
C     DETERMINE VELOCITY AND DIRECTION AT EACH GRID POINT.               INSI1090
C                                                                        INSI1100
       CALL VXVY (M1, VX, VY, VRAD, THETA, XPART, YPART, XSTART,         INSI1110
     1   XFINISH, YSTART)                                                INSI1120
C*************************************************************************INSI1130
       HRS  =  T / 3600.                                                 INSI1140
       DAYS  =  HRS / 24.                                                INSI1150
       HRS  =  HRS - FLOAT (DAYS) * 24.                                  INSI1160
       IF (Q(1) .LT. 0.0)  QIN  =  ABS (Q (2) + Q (3) + Q (4) + Q (5))   INSI1170
     1   / 4.0                                                           INSI1180
       IF  (Q(1) .GT. 0.0)  QIN  =  Q (1)                                INSI1190
       QOUT  =  ABS (Q(1)) + (ABS (Q(2) + Q(3) + Q(4) + Q(5))) / 4.0 -   INSI1200
     1   QIN                                                             INSI1210
       GALIN  =  ABS (QIN) * 7.4805 * 60.                                INSI1220
       GALOUT  =  ABS (QOUT) * 7.4805 * 60.                              INSI1230
       PRINT   20, IRUN,                                OUTA (ITME), OUTB INSI1240
     1   (ITME), DAYS, HRS, OUTC (AQR), OUTD (AQR), OUTE (IN), GALIN,    INSI1250
     2   GALOUT, K, N, PNDEPTH, Z                                        INSI1260
       PRINT   30                                                        INSI1270
         DO 1150  IX  =  XSTART, XFINISH                                 INSI1280
           DO 1150  IY  =  YSTART, IX                                    INSI1290
```

```
            XYLIST (IY, IX)  =  XYLIST (IX, IY)                          INSI1300
            XPART (IY, IX)  =  XPART (IX, IY)                            INSI1310
            YPART (IY, IX)  =  YPART (IX, IY)                            INSI1320
            VX (IY, IX)  =  VX (IX, IY)                                  INSI1330
            VY (IY, IX)  =  VY (IX, IY)                                  INSI1340
            VRAD (IY, IX)  =  VRAD (IX, IY)                              INSI1350
 1150       THETA (IY, IX)  =  THETA (IX, IY)                            INSI1360
          DO 1200  KK  =  YSTART, YFINISH                                INSI1370
          XK1  =  (FLOAT(KK) - 1.) * INCRY                               INSI1380
            DO 1200  M  =  XSTART, XFINISH                               INSI1390
            XL  =  (FLOAT(M) - 1.) * INCRX                               INSI1400
              DO 1160  II  =  1, NUMOMT                                  INSI1410
              IF (XL .EQ. OMIT(II,1) .AND. XK1 .EQ. OMIT(II,2))  GO TO   INSI1420
     1          1180                                                      INSI1430
              IF (XK1 .EQ. OMIT(II,1) .AND. XL .EQ. OMIT(II,2))  GO TO   INSI1440
     1          1180                                                      INSI1450
 1160         CONTINUE                                                   INSI1460
            IF (OUTOPT .EQ. 2)  GO TO 1190                               INSI1470
 1170       PRINT   40, XL, XK1, XYLIST (M, KK),                         INSI1480
     1        VRAD(M, KK), THETA (M, KK)                                 INSI1490
 1180       IF (OUTOPT .EQ. 1)  GO TO 1200                               INSI1500
 1190       WRITE (NPR,   50)  XL, XK1, XYLIST (M, KK), VRAD (M, KK),    INSI1510
     1        THETA (M, KK)                                              INSI1520
 1200       CONTINUE                                                     INSI1530
C*************************************************************************INSI1540
C***** INITIATE COMPUTATION OF ODDPOINTS NOT ON THE MATRIX,IF REQUIRED.  INSI1550
 1210  IF (NUMODD .LE. 0)  GO TO 1250                                     INSI1560
       CALL ODDPLOT (FOFT, NUMODD, ODDLIST, K, ODDPT)                     INSI1570
       IF (OUTOPT .EQ. 2)  GO TO 1230                                     INSI1580
         DO 1220  NODD  =  1, NUMODD                                      INSI1590
         PRINT   40, (ODDLIST(J, NODD), J=1, 9)                           INSI1600
         IF (ODDLIST(1,NODD) .EQ. ODDLIST(2,NODD))  GO TO 1220            INSI1610
         PRINT   40, ODDLIST (2, NODD), ODDLIST (1, NODD), (ODDLIST(J,    INSI1620
     1     NODD), J=3, 9)                                                 INSI1630
 1220    CONTINUE                                                         INSI1640
       IF (IABS(OUTOPT) .EQ. 1)  GO TO 1250                               INSI1650
 1230    DO 1240  NODD  =  1, NUMODD                                      INSI1660
         WRITE (NPR,   50)   (ODDLIST(J, NODD), J=1, 3), (ODDLIST (J,     INSI1670
     1     NODD), J=8, 9)                                                 INSI1680
         IF (NPR .LE. 10)  GO TO 1240                                     INSI1690
         IF (ODDLIST(1,NODD) .EQ. ODDLIST(2,NODD))  GO TO 1240            INSI1700
         WRITE (NPR,   50)  ODDLIST (2, NODD), ODDLIST (1, NODD),         INSI1710
     1     ODDLIST (3, NODD), ODDLIST (8, NODD), ODDLIST (9, NODD)        INSI1720
 1240    CONTINUE                                                         INSI1730
 1250  CONTINUE                                                           INSI1740
       IF (IABS(OUTOPT) .EQ. 1)  GO TO 1260                               INSI1750
C***** ODDPOINTS ARE NOT USED IN CONTOUR MAP GENERATION.                  INSI1760
       NUMBER  =  (XFINISH - XSTART) *  * 2 + NUMODD                      INSI1770
       PRINT   60, NPR, NUMBER                                            INSI1780
 1260  PRINT   70                                                         INSI1790
C***** INITIATE CALCULATION OF STREAMLINES,IF REQUIRED.                   INSI1800
       IF (NLINES .GT. 0)  CALL STRMLNE (FOFT, K, NPR, INCRX, INCRY, Z,   INSI1810
     1  S, IN, OUT, L1, PLOTFLE, XCOORD, YCOORD)                          INSI1820
       IF (LINES(1) .GT. 0 .OR. LINES(2) .GT. 0)  CALL CONTOUR (INCRX,    INSI1830
     1  INCRY, K, XSTART, XFINISH, YSTART, YFINISH, S, FOFT, Z, M1,       INSI1840
     2  XYLIST, VRAD, OUTOPT, IN, OUT, NPR)                               INSI1850
       IF (IRUN .LT. ITOT)  GO TO 1000                                    INSI1860
       RETURN                                                             INSI1870
C                                                                         INSI1880
   10  FORMAT  ( 1H1  )                                                  INSI1890
```

```
   20  FORMAT  ( 1H1, 30X *RUN NUMBER* 1X, I3 /                          INSI1900
     1                              30X *CHANGE IN HEAD IS TIME* 1X,     INSI1910
     2    2A8 / 30X *TIME INTERVAL OF EVALUATION IS* 1XI5, 1X *DAYS*     INSI1920
     3    1XF6.3, 1X *HOURS* / 30X *AQUIFER IS* 1X2A8 / 30X *INPUT WELL(*INSI1930
     4    *S) IS(ARE) LOCATED AT* 1X, A8 / 30X *AVE. INPUT VOLUME OF LEA*INSI1940
     5    *CHING FLUID* 1X, F8.3, 1X *GAL./MIN./WELL* / 30X *AVE. OUTPUT*INSI1950
     6    * VOLUME OF LEACHING FLUID* 1X, F8.3, 1X *GAL./MIN./WELL* / 30XINSI1960
     7    *AVE. *                                                        INSI1965
     7    *PERMEABILITY OF AQUIFER* 1X, E15.5, 1X *FT./SEC.* / 30X       INSI1970
     8    *AVE. *                                                        INSI1975
     8    *POROSITY OF AQUIFER* 1X, E15.5 / 30X *DEPTH OF PENETRATION OF*INSI1980
     9    * EACH PIPE INTO THE AQUIFER* 1X, 5(2X, F5.2), 1X,  *FT.* / 30XINSI1990
     9    *HEIGHT OF ANALYSIS(Z) IN AQUIFER* 1XF7.3, 1X *FT.* ///  )     INSI2000
   30  FORMAT (1H0,26X,*X CO-ORD*,10X,*Y CO-ORD*,10X,*DRAWDOWN*,11X,     INSI2010
     1 *VELOCITY*,5X,*DIRECTION OF FLOW*,/,28X,*(FEET)*,12X,*(FEET)*,    INSI2020
     2 12X,*(FEET)*,11X,*(FEET/SEC.)*,7X,*(DEGREES)*,//)                 INSI2030
   40 FORMAT (1H0,20X,5(E15.5,3X))                                       INSI2040
   50  FORMAT  ( 5E15.5 )                                               INSI2070
   60  FORMAT  ( 10X *MATRIX CO-ORDINATES,CHANGE IN HEAD,VELOCITY AND D*INSI2080
     1   *IRECTION(ANGLE,DEGREES) OUTPUT ON FILE* I5 / 10X *TOTAL NUMBE*INSI2090
     2   *R OF CO-ORDINATES OUTPUT =* I5 )                             INSI2100
   70  FORMAT  ( 1H1 )                                                  INSI2110
C                                                                        INSI2120
      END                                                               INSI2130
```

```
C////////////////////////////////////////////////////////////////////////INPT  10
      SUBROUTINE  INPT (OMIT, NUMOMT, NUMODD, YSTART, YFINISH, XSTART, INPT  20
     1   XFINISH, INCRX, INCRY, XINC, YINC, ODDPT, ASSIGN)               INPT  30
C***** INPUT MATRIX SPECIFICATIONS,OUTPUT REQUIREMENTS,AQUIFER          INPT  40
C***** CHARACTERISITCS,WELL PENETRATION DATA,DEPTH OF ANALYSIS.         INPT  50
      COMMON  /DATA/  PNDEPTH, X, Y, Z, RE                             INPT  60
      COMMON  /CONST/  ITME, NPR, S, B, K, T, T1, T2, GAMMA, N, N2, VT,INPT  70
     1   Q, ALPHA, BETA, N1, K1, SS, SCO, IRUN, ITOT, AQR, BPRIME,     INPT  80
     2   KPRIME, ITEREND, TERM                                         INPT  90
      COMMON  /LINES/  ANGLE, RADIUS, NLINES, OUTOPT, MAXID, IPLOT,    INPT 100
     1   DISTME (2)                                                    INPT 110
      COMMON  /CONTR/  LINES (2), PERCNT (10, 2), INTRVL (10, 2)       INPT 120
      DIMENSION   ANGLE (20), ODDPT (4,20), OMIT (10,2), PNDEPTH (5), QINPT 130
     1   (5)                                                           INPT 140
      INTEGER     AQR, OUTOPT, SCO, XFINISH, XSTART, YFINISH, YSTART   INPT 150
     1  ,ASSIGN                                                        INPT 155
      REAL        INCRX, INCRY, K, KPRIME, K1, N, N1, N2               INPT 160
      READ (5,   10)  ITOT, IRUN,      AQR, ITME, NPR, NUMODD, NUMOMT, INPT 170
     1   XSTART, XFINISH, YSTART, YFINISH, NLINES, OUTOPT, ITEREND,    INPT 180
     2   IPLOT, LINES                                                  INPT 190
      READ (5,   20)  INCRX, INCRY, S, B, GAMMA, N, T, K, DUM1, DUM2  INPT 200
     1   (Q(I), I=1, 5), PNDEPTH, ALPHA, BETA, Z, XINC, YINC, TERM     INPT 210
      IF  (XINC .LE. 0)  XINC  =  INCRX / 2.                           INPT 220
      IF  (YINC .LE. 0)  YINC  =  INCRY / 2.                           INPT 230
      T  =  T * 3600.                                                  INPT 240
      IF (K .EQ. 0.0 .OR. N .EQ. 0.0)  CALL INVERSE (K, N, S, ALPHA,   INPT 250
     1   BETA, GAMMA, B, ASSIGN)                                       INPT 260
 1000 IF (AQR .GT. 1)  READ (5,   20)  BPRIME, KPRIME                 INPT 270
      IF (AQR .EQ. 1 .AND. ITME .EQ. 1)  READ (5,   20)  RE            INPT 280
      XSTART  =  IFIX (FLOAT(XSTART) / INCRX + 1.0)                    INPT 290
      YSTART  =  IFIX (FLOAT(YSTART) / INCRY + 1.0)                    INPT 300
      XFINISH  =  IFIX (FLOAT(XFINISH) / INCRX + 1.0)                  INPT 310
      YFINISH  =  IFIX (FLOAT(YFINISH) / INCRY + 1.0)                  INPT 320
C***** OMIT INCALCULABLE OR UNWANTED MATRIX COORDINATES HERE.           INPT 330
      OMIT (1, 1)  =  OMIT (1, 2)  =  0.0                              INPT 340
      OMIT (2, 1)  =  OMIT (2, 2)  =  S                                INPT 350
      NUMOMT  =  2 + NUMOMT                                            INPT 360
      IF (NUMOMT .LE. 2)  GO TO 1020                                   INPT 370
        DO 1010  II  =  3, NUMOMT                                      INPT 380
 1010   READ (5,   30)  OMIT (II, 1), OMIT (II, 2)                     INPT 390
 1020 IF (NUMODD) .LE. 0)  GO TO 1040                                  INPT 400
        DO 1030  I  =  1, NUMODD                                       INPT 410
 1030   READ (5,   30)   (ODDPT(J, I), J=1, 4)                        INPT 420
 1040 IF (NLINES .LE. 0)  GO TO 1050                                   INPT 430
      READ (5,   40)  DISTME, RADIUS, MAXID                            INPT 440
      DISTME (2)  =  DISTME (2) * 3600.                                INPT 450
      READ (5,   50)   (ANGLE(I), I=1, NLINES)                         INPT 460
 1050 IF (LINES(1) .LE. 0)  GO TO 1060                                 INPT 470
      READ (5,   60)   (INTRVL(I, 1), I=1, 10), (PERCNT (I, 1), I=1,   INPT 480
     1   10)                                                           INPT 490
 1060 IF (LINES(2) .LE. 0)  GO TO 9999                                 INPT 500
      READ (5,   60)   (INTRVL(I, 2), I=1, 10), (PERCNT (I, 2), I=1,   INPT 510
     1   10)                                                           INPT 520
 9999 RETURN                                                           INPT 530
C                                                                      INPT 540
   10 FORMAT  ( 17I3 )                                                 INPT 550
   20 FORMAT  ( 5E15.5 )                                               INPT 560
   30 FORMAT  ( 4F10.0 )                                               INPT 570
   40 FORMAT  ( 3F10.0, I10 )                                          INPT 580
   50 FORMAT  ( 15F5.0 )                                               INPT 590
   60 FORMAT  ( 10F8.0 / 10F8.0 )                                      INPT 600
C                                                                      INPT 610
      END                                                              INPT 620
```

```
C////////////////////////////////////////////////////////////////////////PART   10
      SUBROUTINE  PARTIAL (M1, M2, XLIST, YLIST, XPART, YPART, IX, IY, PART   20
     1   XFINISH, YSTART, XINC, YINC)                                    PART   30
C***** CALCULATE APPROXIMATIONS OF THE PARTIAL DERIVATIVES HERE         PART   40
C***** TO BE USED LATER IN CALCULATION OF VELOCITY AND DIRECTION OF     PART   50
C***** PARTICLES IN THE LEACHING AQUIFER.                               PART   60
      DIMENSION   XLIST (M2), XPART (M1,M1), YLIST (M2), YPART (M1,M1) PART   70
      INTEGER     XFINISH, YSTART                                       PART   80
      ENTRY PARTX                                                       PART   90
      NM  =   - 1                                                      PART  100
        DO 1000  J  =  IY, XFINISH                                      PART  110
        NM  =  NM + 2                                                   PART  120
 1000   XPART (J, IY)  =   (XLIST (NM + 1) - XLIST (NM)) / (2. * XINC) PART  130
      GO TO 9999                                                        PART  140
      ENTRY PARTY                                                       PART  150
      NM  =   - 1                                                      PART  160
        DO 1010  J  =  YSTART, IX                                       PART  170
        NM  =  NM + 2                                                   PART  180
 1010   YPART (IX, J)  =   (YLIST (NM + 1) - YLIST (NM)) / (2. * YINC) PART  190
 9999 RETURN                                                            PART  200
      END                                                               PART  210


C////////////////////////////////////////////////////////////////////////VXVY   10
      SUBROUTINE  VXVY (M1, VX, VY, VRAD, THETA, XPART, YPART, XSTART, VXVY   20
     1   XFINISH, YSTART)                                                VXVY   30
C***** VELOCITY AND DIRECTION OF FLOW OF PARTICLES IS CALCULATED         VXVY   40
C***** HERE. USED IN DETERMINATION OF STREAMLINES.                       VXVY   50
      COMMON  /CONST/  ITME, NPR, S, B, K, T, T1, T2, GAMMA, N, N2, VT,VXVY   55
     1   Q, ALPHA, BETA, N1, K1, SS, SCO, IRUN, ITOT, AQR, BPRIME,      VXVY   58
     2   KPRIME, ITEREND, TERM                                          VXVY   59
      DIMENSION   THETA (M1,M1), VRAD (M1,M1), VX (M1,M1), VY (M1,M1),  VXVY   60
     1   XPART (M1,M1), YPART (M1,M1)                                   VXVY   70
      INTEGER     XFINISH, XSTART, YSTART                               VXVY   80
      REAL        K, N                                                  VXVY   90
        DO 1010  I  =  XSTART, XFINISH                                  VXVY  100
          DO 1010  J  =  YSTART, I                                      VXVY  110
          IF (XPART(I,J) .EQ. 0. .AND. YPART(I,J) .EQ. 0.)  GO TO 1010 VXVY  120
C     VELOCITY IN X AND Y.                                              VXVY  130
          VX (I, J)  =   - K * XPART (I, J) / N                         VXVY  140
          VY (I, J)  =   - K * YPART (I, J) / N                         VXVY  150
          VRAD (I, J)  =  SQRT (VX (I, J) *  * 2 + VY (I, J) *  * 2)   VXVY  160
          ETA  =  ATAN2 (VY(I, J), VX(I, J))                            VXVY  170
          THETA (I, J)  =  ETA * 180. / 3.141592654                     VXVY  180
 1000     IF (THETA(I,J) .GE. 0.)  GO TO 1010                           VXVY  190
          THETA (I, J)  =  360. + THETA (I, J)                          VXVY  200
          GO TO 1000                                                    VXVY  210
 1010     CONTINUE                                                      VXVY  220
      RETURN                                                            VXVY  230
      END                                                               VXVY  240
```

```
C////////////////////////////////////////////////////////////////////////ODDP   10
      SUBROUTINE  ODDPLOT (FOFT, NUMODD, ODDLIST, K, ODDPT)              ODDP   20
      COMMON  /DATA/  PNDEPTH, X, Y, Z, RE                               ODDP   30
C***** ALL ODDPOINTS (NOT ON THE ESTABLISHED MATRIX) ARE EVALUATED HERE.ODDP   40
C***** INCLUDES POINTS REQUIRED FOR STREAMLINE EVALUATION AS WELL AS    ODDP   50
C*****  OTHER SPECIAL INTEREST POINTS.                                  ODDP   60
      DIMENSION   ODDLIST (9,20), ODDPT (4,20), PNDEPTH (5), XLIST (2),ODDP   70
     1   YLIST (2)                                                      ODDP   80
      REAL        K                                                    ODDP   90
        DO 1020  JJ  =  1, NUMODD                                       ODDP  100
        IF (ODDPT(1,JJ) .EQ. 0 .AND. ODDPT(2,JJ) .EQ. 0 .OR.           ODDP  110
     1    ODDPT(1,JJ) .EQ. S .AND. ODDPT(2,JJ).EQ.S)  CALL ERROR (3)    ODDP  120
        IY  =  1                                                       ODDP  130
        Y  =  ODDPT (2, JJ)                                            ODDP  140
          DO 1000  IX  =  1, 2                                         ODDP  150
          X  =  ODDPT (1, JJ) - 3. * ODDPT (3, JJ) + 2. * FLOAT (IX) * ODDP  160
     1      ODDPT (3, JJ)                                             ODDP  170
 1000     CALL DELTAH (XLIST(IX), FOFT)                                ODDP  180
        CALL PARTX (1, 2, XLIST, YLIST, XPART, YPART, IX, IY, 1, 1,    ODDP  190
     1    ODDPT(3, JJ), ODDPT(4, JJ))                                  ODDP  200
        IX  =  1                                                       ODDP  210
        X  =  ODDPT (1, JJ)                                            ODDP  220
          DO 1010  IY  =  1, 2                                         ODDP  230
          Y  =  ODDPT (2, JJ) - 3. * ODDPT (4, JJ) + 2. * FLOAT (IY) * ODDP  240
     1      ODDPT (4, JJ)                                             ODDP  250
 1010     CALL DELTAH (YLIST(IY), FOFT)                                ODDP  260
        CALL PARTY (1, 2, XLIST, YLIST, XPART, YPART, IX, IY, 1, 1,    ODDP  270
     1    ODDPT(3, JJ), ODDPT(4, JJ))                                  ODDP  280
        CALL VXVY (M1, VX, VY, VRAD, THETA, XPART, YPART, 1, 1, 1)     ODDP  290
        Y  =  ODDPT (2, JJ)                                            ODDP  300
        CALL DELTAH (DELH, FOFT)                                       ODDP  310
        ODDLIST (1, JJ)  =  ODDPT (1, JJ)                              ODDP  320
        ODDLIST (2, JJ)  =  ODDPT (2, JJ)                              ODDP  330
        ODDLIST (3, JJ)  =  DELH                                       ODDP  340
        ODDLIST (4, JJ)  =  XPART                                      ODDP  350
        ODDLIST (5, JJ)  =  YPART                                      ODDP  360
        ODDLIST (6, JJ)  =  VX                                         ODDP  370
        ODDLIST (7, JJ)  =  VY                                         ODDP  380
        ODDLIST (8, JJ)  =  VRAD                                       ODDP  390
 1020   ODDLIST (9, JJ)  =  THETA                                      ODDP  400
      RETURN                                                           ODDP  410
      END                                                              ODDP  420
```

```
C////////////////////////////////////////////////////////////////////////WU    10
      FUNCTION  WU (WUIN)                                                 WU    20
C***** CALCULATION OF WELL DRAWDOWN SOLUTION OF PARTIAL DIFFERENTIAL     WU    30
C***** EQUATION FOR TIME DEPENDENT FLOW IN A NON-LEAKY AQUIFER.          WU    40
C***** REPRESENTED AS CONVERGENT INFINITE SERIES.                        WU    50
      COMMON  /CONST/  ITME, NPR, S, B, K, T1, T2, GAMMA, N, N2, VT, Q,WU    60
     1   ALPHA, BETA, N1, K1, SS, SCO, IRUN, ITOT, AQR, BPRIME, KPRIME  WU    70
      DIMENSION   Q (5)                                                   WU    80
      IF (WUIN .GT. 1.)  GO TO 1010                                       WU    90
 1000 WU  =   - .57721566 + .99999193 * WUIN - .24991055 * WUIN * WUIN WU   100
     1   + .05519968 * WUIN *  * 3 - .00976004 * WUIN *  * 4 + .00107857WU   110
     2   * WUIN *  * 5 - ALOG (WUIN)                                     WU   120
      GO TO 9999                                                          WU   130
 1010 WU  =   (WUIN *  * 4 + 8.5733287401 * WUIN *  * 3 + 18.0590169730WU   140
     1   * WUIN * WUIN + 8.6347608925 * WUIN + .2677737343) / (WUIN *  *WU   150
     2   4 + 9.5733223454 * WUIN *  * 3 + 25.6329561486 * WUIN *  * 2 + WU   160
     3   21.0996530827 * WUIN + 3.9584969228) / (WUIN * EXP(WUIN))       WU   170
 9999 RETURN                                                             WU   180
      END                                                                WU   190


C////////////////////////////////////////////////////////////////////////WU1   10
      FUNCTION  WU1 (J, U, PRT1, PRT2)                                    WU1   20
C***** CALCULATION OF WELL DRAWDOWN SOLUTION OF PARTIAL DIFFERENTIAL     WU1   30
C***** EQUATION FOR TIME DEPENDENT FLOW IN A LEAKY AQUIFER.              WU1   40
      COMMON  /CONST/  ITME, NPR, S, B, K, T, T1, T2, GAMMA, N, N2, VT,WU1   50
     1   Q, ALPHA, BETA, N1, K1, SS, SCO, IRUN, ITOT, AQR, BPRIME,       WU1   60
     2   KPRIME                                                          WU1   70
      DIMENSION   Q (5), U (5)                                            WU1   80
      REAL        K, KPRIME                                               WU1   90
      PRT4  =  PRT2 / U (J)                                               WU1  100
      PRT5  =  EXP ( - PRT4)                                              WU1  110
      PRT6  =  .5772 + ALOG (U(J)) + WU (U (J)) - U (J)                   WU1  120
      PRT7  =  U (J) * ( (BESSI(PRT1) - 1.) / PRT2)                       WU1  130
      PRT10  =  0.0                                                       WU1  140
        DO 1020  L  =  1, 5                                               WU1  150
          DO 1020  M  =  1, L                                             WU1  160
          IPRT8  =  L - M + 1                                             WU1  170
          IPRT9  =  L + 2                                                 WU1  180
          FACT8  =  1.                                                    WU1  190
          FACT9  =  1.                                                    WU1  200
            DO 1000  ICOUNT  =  1, IPRT8                                  WU1  210
 1000       FACT8  =  FACT8 * FLOAT (ICOUNT)                             WU1  220
            DO 1010  ICOUNT  =  1, IPRT9                                  WU1  230
 1010       FACT9  =  FACT9 * FLOAT (ICOUNT)                             WU1  240
 1020     PRT10  =  PRT10 + ((((  - 1) *  * (L + M)) * FACT8) / (FACT9 *WU1   250
     1     * 2)) * (PRT2 *  * M) * (U(J) *  * (L - M))                   WU1  260
      WU1  =  2. * BESSK (PRT1) - BESSI (PRT1) * WU (PRT4) + PRT5 *       WU1  270
     1   (PRT6 + PRT7 - (U(J) *  * 2) * PRT10)                           WU1  280
      RETURN                                                              WU1  290
      END                                                                 WU1  300
```

```
C////////////////////////////////////////////////////////////////////////DELT  10
      SUBROUTINE  DELTAH (DELH, FOFT)                                    DELT  20
C***** DELTAH MAKES A DETERMINATION OF WHICH ROUTINE IS TO BE USED IN     DELT  30
C***** EVALUATING CHANGE IN HEAD.  ALSO DETERMINES THE RELATIVE           DELT  40
C***** IMPORTANCE OF EACH WELL IN THE 5-SPOT PATTERN, IN DETERMINING THEDELT  50
C***** CHANGE IN HEAD AT A GIVEN GRID NODE.                             DELT  60
      COMMON  /DATA/  PNDEPTH, X, Y, Z, RE                               DELT  70
      COMMON  /CONST/  ITME, NPR, S, B, K, T, T1, T2, GAMMA, N, N2, VT,DELT  80
     1   Q, ALPHA, BETA, N1, K1, SS, SCO, IRUN, ITOT, AQR, BPRIME,      DELT  90
     2   KPRIME, ITEPEND, TERM                                          DELT 100
      DIMENSION   DELPART (5), PNDEPTH (5), Q (5), R (5), U (5)         DELT 110
      INTEGER     AQR, SCO                                              DELT 120
      REAL        K, KPRIME                                             DELT 130
      F1  =   (X - S) * (X - S)                                         DELT 140
      F2  =   (Y - S) * (Y - S)                                         DELT 150
      F3  =   (X + S) * (X + S)                                         DELT 160
      F4  =   (Y + S) * (Y + S)                                         DELT 170
      R (1)  =  SQRT (X * X + Y * Y)                                    DELT 180
      R (2)  =  SQRT (F1 + F2)                                          DELT 190
      R (3)  =  SQRT (F1 + F4)                                          DELT 200
      R (4)  =  SQRT (F3 + F2)                                          DELT 210
      R (5)  =  SQRT (F3 + F4)                                          DELT 220
        DO 1000  J  =  1, 5                                             DELT 230
 1000   U (J)  =  FOFT * R (J) *  * 2                                  DELT 240
      IF (ITME .GT. 1)  GO TO 1020                                      DELT 260
      IF (AQR .GT. 1)  GO TO 1010                                       DELT 270
      CALL SSCONF (DELPART, R)                                          DELT 280
      GO TO 1040                                                        DELT 290
 1010 BB = SQRT (K * B * BPRIME / KPRIME)                               DELT 295
      CALL SSLEAKY (DELPART, R, U, BB)                                  DELT 300
      GO TO 1040                                                        DELT 310
 1020  IF (AQR .GT. 1)  GO TO 1030                                       DELT 320
      CALL TMECONF (DELPART, R, U)                                      DELT 330
      GO TO 1040                                                        DELT 340
 1030 BB = SQRT (K * B * BPRIME / KPRIME)                               DELT 345
      CALL TMELKY (DELPART, R, U, BB)                                   DELT 350
 1040  DELH  =  DELPART (1) - DELPART (2) - DELPART (3) - DELPART (4) - DELT 360
     1   DELPART (5)                                                    DELT 370
      RETURN                                                            DELT 380
      END                                                               DELT 390
```

```
C////////////////////////////////////////////////////////////////////////SSLE  10
      SUBROUTINE  SSLEAKY (DELPART, R, U, BB)                           SSLE  20
C***** THIS ROUTINE DETERMINES THE LEACHING PARAMETERS OF TIME INDEP.    SSLE  30
C***** FLOW IN A LEAKY AQUIFER.  PARTIAL PENETRATION OF WELLS INTO       SSLE  40
C***** THE AQUIFER IS SPECIFIED BY PNDEPTH.                             SSLE  50
      COMMON  /DATA/  PNDEPTH, X, Y, Z, RE                              SSLE  60
      COMMON  /CONST/  ITME, NPR, S, B, K, T, T1, T2, GAMMA, N, N2, VT, SSLE  70
     1   Q, ALPHA, BETA, N1, K1, SS, SCO, IRUN, ITOT, AQR, BPRIME,      SSLE  80
     2   KPRIME, ITEREND, TERM                                          SSLE  90
      DIMENSION   DELPART (5), PNDEPTH (5), Q (5), R (5), SUM (5), U    SSLE 100
     1   (5)                                                            SSLE 110
      REAL        K                                                     SSLE 120
      KEY  =  0                                                         SSLE 130
        DO 1000  I  =  1, 5                                             SSLE 140
1000    SUM (I)  =  0.0                                                 SSLE 150
        DO 1060  I  =  1, 5                                             SSLE 160
        C  =  Q (I) / (2. * 3.14159 * K * B)                            SSLE 170
        PRT1  =  R (I) / BB                                             SSLE 180
        IF (PNDEPTH(I) .NE. B)  GO TO 1010                              SSLE 190
        DELPART (I)  =  C * BESSK (PRT1)                                SSLE 200
        GO TO 1060                                                      SSLE 210
1010    IF  (PNDEPTH(I) .LE. 0)  PNDEPTH (I)  =  .0001                  SSLE 220
        SUMN  =  1.0                                                    SSLE 230
1020    ARG  =  SQRT (PRT1 *  * 2 + (SUMN * 3.14159 * R(I) / B) *  * 2)SSLE 240
        PART  =  COS (SUMN * 3.14159 * Z / B) * SIN (SUMN * 3.14159 *   SSLE 250
     1    PNDEPTH (I) / B) * (1. / SUMN) * BESSK (ARG)                  SSLE 260
        SUMN  =  SUMN + 1.0                                             SSLE 270
        SUM (I)  =  SUM (I) + PART                                      SSLE 280
        IF (KEY .GT. 0 .OR. ABS(PART) .LE. TERM)  GO TO 1030            SSLE 290
        IF (SUMN .GT. ITEREND)  GO TO 1040                              SSLE 300
        GO TO 1020                                                      SSLE 310
1030    KEY  =  KEY + 1                                                 SSLE 320
        IF  (ABS(PART) .GT. TERM)  KEY  =  0                            SSLE 330
        IF (KEY .GT. 3)  GO TO 1050                                     SSLE 340
        GO TO 1020                                                      SSLE 350
1040    PRINT   10, SUMN, X, Y, SUM (I), PART                           SSLE 360
1050    DELPART (I)  =  C * (BESSK (PRT1) + 2. * (B / (3.14159 *        SSLE 370
     1    PNDEPTH(I))) * SUM (I))                                       SSLE 380
1060    CONTINUE                                                        SSLE 390
      RETURN                                                            SSLE 400
C                                                                       SSLE 410
   10 FORMAT  ( 10X *SERIES DOES NOT CONVERGE SUFFICIENTLY AFTER * F3.0SSLE 420
     1   * ITERATIONS FOR THE POINT X=* F5.2, 2X *Y=* F5.2 / 10X       SSLE 430
     2   *FINAL SUM =* E15.5 / 10X *FINAL TERM =* E15.5 )               SSLE 440
C                                                                       SSLE 450
      END                                                               SSLE 460
```

```
C////////////////////////////////////////////////////////////////////////TMEC  10
      SUBROUTINE  TMECONF (DELPART, R, U)                                TMEC  20
C***** THIS ROUTINE DETERMINES THE LEACHING PARAMETERS OF TIME DEP.       TMEC  30
C***** FLOW  NON-LEAKY AQUIFER SITUATION. PARTIAL OR TOTAL                TMEC  40
C***** PENETRATION OF AQUIFER IS SPECIFIED.                               TMEC  50
      COMMON  /DATA/  PNDEPTH, X, Y, Z, RE                               TMEC  60
      COMMON  /CONST/  ITME, NPR, S, B, K, T, T1, T2, GAMMA, N, N2, VT,TMEC  70
     1   Q, ALPHA, BETA, N1, K1, SS, SCO, IRUN, ITOT, AQR, BPRIME,       TMEC  80
     2   KPRIME, ITEREND, TERM                                           TMEC  90
      DIMENSION   DELPART (5), PNDEPTH (5), Q (5), R (5), SUM (5), U     TMEC 100
     1   (5)                                                             TMEC 110
      REAL        K                                                      TMEC 120
      KEY  =  0                                                          TMEC 130
      DO 1000  I  =  1, 5                                                TMEC 140
 1000 SUM (I)  =  0.0                                                    TMEC 150
      DO 1060  I  =  1, 5                                                TMEC 160
      C  =  Q (I) / (4.0 * 3.14159 * K * B)                              TMEC 170
      IF (PNDEPTH(I) .NE. B)  GO TO 1010                                 TMEC 180
      DELPART (I)  =  C * WU (U (I))                                     TMEC 190
      GO TO 1060                                                         TMEC 200
 1010 IF  (PNDEPTH(I) .LE. 0)  PNDEPTH (I)  =  .0001                     TMEC 210
      SUMN  =  1.0                                                       TMEC 220
 1020 ARG1  =  SUMN * 3.14159 * R (I) / B                                TMEC 230
      ARG2  =  ARG1 *  * 2 / 4.0                                         TMEC 240
      PART  =  COS (SUMN * 3.14159 * Z / B) * SIN (SUMN * 3.14159 *      TMEC 250
     1   PNDEPTH (I) / B) * (1. / SUMN) * WU1 (I, U, ARG1, ARG2)         TMEC 260
      SUMN  =  SUMN + 1.0                                                TMEC 270
      SUM (I)  =  SUM (I) + PART                                         TMEC 280
      IF (KEY .GT. 0 .OR. ABS(PART) .LE. TERM)  GO TO 1030               TMEC 290
      IF (SUMN .GT. ITEREND)  GO TO 1040                                 TMEC 300
      GO TO 1020                                                         TMEC 310
 1030 KEY  =  KEY + 1                                                    TMEC 320
      IF  (ABS(PART) .GT. TERM)  KEY  =  0                               TMEC 330
      IF (KEY .GT. 10)  GO TO 1050                                       TMEC 340
      GO TO 1020                                                         TMEC 350
 1040 PRINT  10, SUMN, X, Y, SUM (I), PART                               TMEC 360
 1050 DELPART (I)  =  C * (WU (U(I)) + 2. * B / (3.14159 * PNDEPTH      TMEC 370
     1   (I)) * SUM (I))                                                TMEC 380
 1060 CONTINUE                                                           TMEC 390
      RETURN                                                             TMEC 400
C                                                                        TMEC 410
   10 FORMAT  ( 10X *SERIES DOES NOT CONVERGE SUFFICIENTLY AFTER * F3.0TMEC 420
     1   * ITERATIONS FOR THE POINT X=* F5.2, 2X *Y=* F5.2 / 10X         TMEC 430
     2   *FINAL SUM =* E15.5 / 10X *FINAL TERM =* E15.5 )                TMEC 440
C                                                                        TMEC 450
      END                                                                TMEC 460
```

```
C////////////////////////////////////////////////////////////////////////TMEL  10
      SUBROUTINE  TMELKY (DELPART, R, U, BB)                             TMEL  20
C***** LEACHING PARAMETERS OF TIME DEPENDENT FLOW,LEAKY AQUIFER           TMEL  30
C***** SITUATION.  PARTIALLY OR TOTALLY PENETRATING OPTIONS AVAILABLE.    TMEL  40
C     OPTIONS:                                                           TMEL  50
C     PNDEPTH = 0    (TOP OF AQUIFER)                                    TMEL  60
C     PNDEPTH = B/2    (MID AQUIFER)                                     TMEL  70
C     PNDEPTH = B    (BOTTEM OF AQUIFER)                                 TMEL  80
      COMMON  /DATA/  PNDEPTH, X, Y, Z, RE                               TMEL  90
      COMMON  /CONST/  ITME, NPR, S, B, K, T, T1, T2, GAMMA, N, N2, VT,TMEL 100
     1   U, ALPHA, BETA, N1, K1, SS, SC0, IRUN, ITOT, AQR, BPRIME,      TMEL 110
     2   KPRIME, ITEREND, TERM                                          TMEL 120
      DIMENSION   DELPART (5), PNDEPTH (5), Q (5), R (5), SUM (5), U    TMEL 130
     1   (5)                                                            TMEL 140
      REAL         K                                                     TMEL 150
      KEY  =  0                                                          TMEL 160
        DO 1000  I  =  1, 5                                              TMEL 170
 1000   SUM (I)  =  0.0                                                  TMEL 180
        DO 1060  I  =  1, 5                                              TMEL 190
        PRT1  =  R (I) / BB                                              TMEL 200
        PRT2  =  PRT1 *  * 2 / 4.0                                       TMEL 210
        C  =  Q (I) / (4.0 * 3.14159 * K * B)                            TMEL 220
        IF (PNDEPTH(I) .NE. B)  GO TO 1010                               TMEL 230
        DELPART (I)  =  C * WU1 (I, U, PRT1, PRT2)                       TMEL 240
        GO TO 1060                                                       TMEL 250
 1010   IF  (PNDEPTH(I) .LE. 0)  PNDEPTH (I)  =  .0001                   TMEL 260
        SUMN  =  1.0                                                     TMEL 270
 1020   ARG1  =  SQRT (PRT1 *  * 2 + (SUMN * 3.14159 * R(I) / B) *  *    TMEL 280
     1    2)                                                            TMEL 290
        ARG2  =  ARG1 *  * 2 / 4.0                                       TMEL 300
        PART  =  COS (SUMN * 3.14159 * Z / B) * SIN (SUMN * 3.14159 *    TMEL 310
     1    PNDEPTH (I) / B) * (1. / SUMN) * WU1 (I, U, ARG1, ARG2)       TMEL 320
        SUMN  =  SUMN + 1.0                                              TMEL 330
        SUM (I)  =  SUM (I) + PART                                       TMEL 340
        IF (KEY .GT. 0 .OR. ABS(PART) .LE. TERM)  GO TO 1030             TMEL 350
        IF (SUMN .GT. ITEREND)  GO TO 1040                               TMEL 360
        GO TO 1020                                                       TMEL 370
 1030   KEY  =  KEY + 1                                                  TMEL 380
        IF  (ABS(PART) .GT. TERM)  KEY  =  0                             TMEL 390
        IF (KEY .GT. 10)  GO TO 1050                                     TMEL 400
        GO TO 1020                                                       TMEL 410
 1040   PRINT  10, SUMN, X, Y, SUM (I), PART                             TMEL 420
 1050   DELPART (I)  =  C * (WU1 (I, U, PRT1, PRT2) + 2.0 * B /          TMEL 430
     1    (3.14159 * PNDEPTH (I)) * SUM (I))                            TMEL 440
 1060   CONTINUE                                                         TMEL 450
      RETURN                                                             TMEL 460
C                                                                        TMEL 470
   10  FORMAT  ( 10X *SERIES DOES NOT CONVERGE SUFFICIENTLY AFTER * F3.0TMEL 480
     1   * ITERATIONS FOR THE POINT X=* F5.2, 2X *Y=* F5.2 / 10X         TMEL 490
     2   *FINAL SUM =* E15.5 / 10X *FINAL TERM =* E15.5 )                TMEL 500
C                                                                        TMEL 510
      END                                                                TMEL 520
```

```
C////////////////////////////////////////////////////////////////////////SSCO  10
      SUBROUTINE  SSCONF (DELPART, R)                                    SSCO  20
C***** LEACHING SITUATION INVOLVING TIME DEPENDENT FLOW, NON-LEAKY       SSCO  30
C***** AQUIFER. PARTIAL OR TOTAL PENETRATION.                            SSCO  40
C     STEADY STATE FLOW, CONFINED AQUIFER.                               SSCO  50
C     DEPTH OF PENETRATION = PNDEPTH                                     SSCO  60
C                                                                        SSCO  70
      COMMON  /DATA/  PNDEPTH, X, Y, Z, RE                               SSCO  80
      COMMON  /CONST/  ITME, NPR, S, B, K, T, T1, T2, GAMMA, N, N2, VT,SSCO  90
     1   Q, ALPHA, BETA, N1, K1, SS, SCO, IKUN, ITOT, AQR, BPRIME,      SSCO 100
     2   KPRIME, ITEREND, TERM                                          SSCO 110
      DIMENSION   DELPART (5), PNDEPTH (5), Q (5), R (5), SUM (5)       SSCO 120
      REAL        K                                                    SSCO 130
      IF  (RE .EQ. 0.0)  RE  =  600.                                     SSCO 140
      KEY  =  0                                                          SSCO 150
      DO 1000  I  =  1, 5                                                SSCO 160
1000  SUM (I)  =  0.0                                                    SSCO 170
      DO 1070  I  =  1, 5                                                SSCO 180
      C  =  Q (I) / (2. * 3.14159 * K * B)                               SSCO 190
      IF (PNDEPTH(I) .NE. B)  GO TO 1010                                 SSCO 200
      DELPART (I)  =  C * ALOG (RE / R (I))                              SSCO 210
      GO TO 1070                                                         SSCO 220
1010  IF  (PNDEPTH(I) .LE. 0)  PNDEPTH (I)  =  .0001                     SSCO 230
      SUMN  =  1.0                                                       SSCO 240
      BESSFN2  =  1.0                                                    SSCO 250
1020  ARG1  =  3.14159 * R (I) * SUMN / B                                SSCO 260
      ARG2  =  3.14159 * RE * SUMN / B                                   SSCO 270
      BESSFN1  =  BESSK (ARG1)                                           SSCO 280
      IF (BESSFN2 .EQ. 0.0)  GO TO 1030                                  SSCO 290
      BESSFN2  =  BESSK (ARG2) * BESSI (ARG1) / BESSI (ARG2)             SSCO 300
      IF  (BESSFN2 / BESSFN1 .LE. 1.0E - 5)  BESSFN2  =  0.0             SSCO 310
1030  PART  =  COS (SUMN * 3.14159 * Z / B) * SIN (SUMN * 3.14159 *      SSCO 320
     1   PNDEPTH (I) / B) * (1. / SUMN) * (BESSFN1 - BESSFN2)           SSCO 330
      SUMN  =  SUMN + 1.0                                                SSCO 340
      SUM (I)  =  SUM (I) + PART                                         SSCO 350
      IF (KEY .GT. 0 .OR. ABS(PART) .LE. TERM)  GO TO 1040               SSCO 360
      IF (SUMN .GT. ITEREND)  GO TO 1050                                 SSCO 370
      GO TO 1020                                                         SSCO 380
1040  KEY  =  KEY + 1                                                    SSCO 390
      IF  (ABS(PART) .GT. TERM)  KEY  =  0                               SSCO 400
      IF (KEY .GT. 3)  GO TO 1060                                        SSCO 410
      GO TO 1020                                                         SSCO 420
1050  PRINT   10, SUMN, X, Y, SUM (I), PART                              SSCO 430
1060  DELPART (I)  =  C * (ALOG (RE / R(I)) + 2. * B / (3.14159 *        SSCO 440
     1   PNDEPTH (I)) * SUM (I))                                         SSCO 450
1070  CONTINUE                                                           SSCO 460
      RETURN                                                             SSCO 470
C                                                                        SSCO 480
   10 FORMAT  ( 10X *SERIES DOES NOT CONVERGE SUFFICIENTLY AFTER * F3.0SSCO 490
     1   * ITERATIONS FOR THE POINT X=* F5.2, 2X *Y=* F5.2 / 10X        SSCO 500
     2   *FINAL SUM =* E15.5 / 10X *FINAL TERM =* E15.5 )               SSCO 510
C                                                                        SSCO 520
      END                                                                SSCO 530
```

```
C////////////////////////////////////////////////////////////////////////BESS  10
      FUNCTION  BESSK (BESSIN)                                           BESS  20
C                                                                        BESS  30
C     K BESSEL FUNCTION APPROXIMATION.                                   BESS  40
C                                                                        BESS  50
      IF (BESSIN .GE. 2.)   1010, 1000                                   BESS  60
 1000 BESSK  =   - ALOG (BESSIN / 2.) * BESSI (BESSIN) - .57721566 +     BESS  70
     1   .42278420 * ((BESSIN / 2.) *  * 2) + .23069756 * ( (BESSIN /   BESS  80
     2   2.) *  * 4) + .0348859 * ( (BESSIN / 2.) *  * 6) + .00262698 * BESS  90
     3   ( (BESSIN / 2.) *  * 8) + .0001075 * ( (BESSIN / 2.) *  * 10) +BESS 100
     4   .0000074 * ( (BESSIN / 2.) *  * 12)                           BESS 110
      GO TO 1020                                                         BESS 120
 1010 BESSK  =   (1. / (SQRT(BESSIN) * EXP(BESSIN))) * (1.25331414 -    BESS 130
     1   .07832358 * (2. / BESSIN) + .02189568 * ( (2. / BESSIN) *  * 2)BESS 140
     2   - .01062446 * ( (2. / BESSIN) *  * 3) + .00587872 * ( (2. /    BESS 150
     3   BESSIN) *  * 4) - .00251540 * ( (2. / BESSIN) *  * 5) +        BESS 160
     4   .00053208 * ( (2. / BESSIN) *  * 6))                          BESS 170
 1020 CONTINUE                                                           BESS 180
      RETURN                                                             BESS 190
      END                                                                BESS 200


C////////////////////////////////////////////////////////////////////////BESS  10
      FUNCTION  BESSI (BESSIN1)                                          BESS  20
C                                                                        BESS  30
C     I BESSEL FUNCTION APPROXIMATION.                                   BESS  40
C                                                                        BESS  50
      BESSIN  =  BESSIN1 / 3.75                                          BESS  60
      IF (BESSIN1 .LT. -3.75 .OR. BESSIN1 .GT. 3.75)  GO TO 1010         BESS  70
 1000 BESSI  =  1. + 3.5156229 * (BESSIN *  * 2) + 3.0899424 * (BESSIN  BESS  80
     1   *  * 4) + 1.2067492 * (BESSIN *  * 6) + .2659732 * (BESSIN *  *BESS  90
     2   8) + .0360768 * (BESSIN *  * 10) + .0045813 * (BESSIN *  * 12) BESS 100
      GO TO 1020                                                         BESS 110
 1010 BESSI  =   (EXP(BESSIN1) / SQRT(BESSIN1)) * (.39894228 +          BESS 120
     1   .01328592 * (BESSIN *  * ( - 1)) + .00225319 * (BESSIN *  * ( -BESS 130
     2   2)) - .00157565 * (BESSIN *  * ( - 3)) + .00916281 * (BESSIN * BESS 140
     3   * ( - 4)) - .02057706 * (BESSIN *  * ( - 5)) + .02635537 *     BESS 150
     4   (BESSIN *  * ( - 6)) - .01647633 * (BESSIN *  * ( - 7)) +      BESS 160
     5   .00392377 * (BESSIN *  * ( - 8)))                              BESS 170
 1020 CONTINUE                                                           BESS 180
      RETURN                                                             BESS 190
      END                                                                BESS 200
```

```
C////////////////////////////////////////////////////////////////////////STRM  10
      SUBROUTINE  STRMLNE (FOFT, K, NPR, INCRX, INCRY, Z, S, INWELL,    STRM  20
     1   OUTWELL, L1, PLOTFLE, XCOORD, YCOORD)                          STRM  30
C                                                                       STRM  40
C     THIS SUBROUTINE CALCULATES THE VALUE OF STREAMLINES               STRM  50
C     (DIRECTION OF FLOW) OF PARTICLES AT A SUFFICIENT NUMBER OF POINTS STRM  60
C     TO ENABLE CONSTRUCTION OF A CONTOUR MAP.                          STRM  70
C                                                                       STRM  80
      COMMON  /LINES/  ANGLE, RADIUS, NLINES, OUTOPT, MAXID, IPLOT,     STRM  90
     1   DISTME (2)                                                     STRM 100
      DIMENSION   ANGLE (20), COORD (2), INCR (2), PLOTFLE (L1,3),      STRM 110
     1   STREAM(300,3), STRMLST (9), STRMPTS (4), WELL (2), XCOORD (L1),STRM 120
     2   YCOORD (L1)                                                    STRM 130
      INTEGER     OUTOPT, OUTWELL                                       STRM 140
      REAL        INCRX, INCRY, INTRVAL, K, MAX                         STRM 150
      DATA    COORD / 8HX CO-ORD, 8HY CO-ORD  /                         STRM 160
      DATA    INCR / 8HDISTANCE, 8HTIME     /                           STRM 170
      WELL (1)  =  0.0                                                  STRM 180
      WELL (2)  =  S                                                    STRM 190
      IF (DISTME(1) .LE. 0 .OR. DISTME(2) .LE. 0)  CALL ERROR (8)       STRM 200
        DO 1150  JJ  =  1, 2                                            STRM 210
        LNEND  =  0                                                     STRM 220
        MAX  =  0.0                                                     STRM 230
        IF  (JJ .EQ. 1)  DIST  =  DISTME (1)                            STRM 240
        IF  (JJ .EQ. 2)  INTRVAL  =  DISTME (2)                         STRM 250
          DO 1140  I  =  1, NLINES                                      STRM 260
          J  =  1                                                       STRM 270
          SUMINT  =  0.0                                                STRM 280
          IF (WELL(INWELL) .EQ. 0.0)  GO TO 1000                        STRM 290
          IF (ANGLE(I) .LT. 225.0 .OR. ANGLE(I) .GE. 360.0)  CALL ERRORSTRM 300
     1      (4)                                                         STRM 310
          GO TO 1010                                                    STRM 320
 1000     IF (ANGLE(I) .LE. 0.0 .OR. ANGLE(I) .GE. 90.0)  CALL ERROR    STRM 330
     1      (4)                                                         STRM 340
 1010     RADIAN  =  ANGLE (I) * 3.14159 / 180.                         STRM 350
          STREAM (J, 1)  =  STRMPTS (1)  =  WELL (INWELL) + (RADIUS +   STRM 360
     1      1.) * COS (RADIAN)                                          STRM 370
          STREAM (J, 2)  =  STRMPTS (2)  =  WELL (INWELL) + (RADIUS +   STRM 380
     1      1.) * SIN (RADIAN)                                          STRM 390
          STREAM (J, 3)  =  FLOAT (I)                                   STRM 400
          STRMPTS (3)  =  DISTME (1) / 2.0                              STRM 410
          STRMPTS (4)  =  DISTME (1) / 2.0                              STRM 420
 1020     CALL ODDPLOT (FOFT, 1, STRMLST, K, STRMPTS)                   STRM 430
          J  =  J + 1                                                   STRM 440
          IF  (JJ .EQ. 1)  INTRVAL  =  DIST / STRMLST (8)               STRM 450
          IF  (JJ .EQ. 2)  DIST  =  INTRVAL * STRMLST (8)               STRM 460
          STREAM (J, 3)  =  FLOAT (I)                                   STRM 470
          STREAM (J, 1)  =  STRMPTS (1)  =  STRMPTS (1) + STRMLST (6) *STRM 480
     1      INTRVAL                                                     STRM 490
          STREAM (J, 2)  =  STRMPTS (2)  =  STRMPTS (2) + STRMLST (7) *STRM 500
     1      INTRVAL                                                     STRM 510
          SUMINT  =  SUMINT + INTRVAL                                   STRM 520
C     CHECK APPROACH TO WELL.                                           STRM 530
          FARWELL  =  SQRT ((STREAM(J, 1) - WELL(OUTWELL)) *  * 2 +     STRM 540
     1      (STREAM(J, 2) - WELL(OUTWELL)) *  * 2)                      STRM 550
          IF (FARWELL .LE. 1.5*DISTME(1))  GO TO 1030                   STRM 560
          IF (J .LT. MAXID)  GO TO 1020                                 STRM 570
          PRINT  10, MAXID, I                                           STRM 580
          GO TO 1040                                                    STRM 590
 1030     STRMPTS (1)  =  STRMPTS (2)  =  WELL (OUTWELL) + RADIUS       STRM 600
```

```
C////////////////////////////////////////////////////////////////////////PLOT  10
      SUBROUTINE  PLOTLNE (MAX, LNEND, Z, WELL, INWELL, OUTWELL, JJ,    PLOT  20
     1   L1, PLOTFLE, XCOORD, YCOORD)                                    PLOT  30
C***** THIS ROUTINE ALLOWS PRINTER PLOT OF STREAMLINES CALCULATED        PLOT  40
C***** IN STRMLNE.  MAXIMUM OF 5 STREAM LINES MAY BE PLOTTED.           PLOT  50
      COMMON  /LINES/  ANGLE, RADIUS, NLINES, OUTOPT, MAXID, IPLOT,     PLOT  60
     1   DISTME (2)                                                      PLOT  70
      DIMENSION    ANGLE (20), GRAPH (3), PLOTFLE (L1,3), ROW (100),    PLOT  80
     1   UNIT (2), WELL (2), WELLPT (2), XAXIS (12), XCOORD (L1), XVALUEPLOT  90
     2   (12), YAXIS(60), YCOORD(L1), CHAR(20)                           PLOT 100
      INTEGER      OUTWELL, XCOORD, XVALUE, XY, YCOORD, YVALUE           PLOT 110
     1    ,ROW, WELLPT, CHAR                                            PLOT 115
      REAL         INCRE, MAX                                          PLOT 120
      DATA     UNIT / 4HFT. , 4HHRS. /                                 PLOT 130
      DATA     YAXIS / 20 * 1H , 1HY, 1H , 1HD, 1HI, 1HR, 1HE, 1HC, 1HT,PLOT 140
     1   1HI, 1HO, 1HN, 1H , 1H-, 1HF, 1HE, 1HE, 1HT, 1H-, 20 * 1H  /    PLOT 150
      DATA     GRAPH / 1HI, 1H+, 10H+--------- /                        PLOT 160
     DATA CHAR /1H ,1H*,1H2,1H3,1H4,1H5,1H6,1H7,1H8,1H9,8*1H0,1H+,1H*/   PLOT 165
      IF  (JJ .EQ. 1)  SLINE  =  DISTME (1)                            PLOT 170
      IF  (JJ .EQ. 2)  SLINE  =  DISTME (2) / 3600.                    PLOT 180
      PRINT   10, NLINES, Z, (ANGLE(I), I=1, 5), SLINE, UNIT (JJ)      PLOT 190
      IF (JJ .EQ. 1)  PRINT   20                                       PLOT 200
      IF (JJ .EQ. 2)  PRINT   30                                       PLOT 210
       ICOUNT = 0                                                      PLOT 215
        DO 1000  J  =  1, LNEND                                        PLOT 220
      IF ( PLOTFLE(J, 3) .GT. 0.0 )  GO TO 1000                        PLOT 225
        ICOUNT = ICOUNT + 1                                            PLOT 227
         PLOTFLE (LNEND + ICOUNT, 1 ) = PLOTFLE (J, 2) = -PLOTFLE(J, 2)PLOT 230
         PLOTFLE (LNEND + ICOUNT, 2 ) = PLOTFLE (J, 1) = -PLOTFLE(J, 1)PLOT 240
         PLOTFLE (LNEND + ICOUNT, 3 ) = PLOTFLE (J, 3) = -PLOTFLE(J, 3)PLOT 250
 1000   CONTINUE                                                        PLOT 260
      LNEND = LNEND + ICOUNT                                           PLOT 265
       XY  =  INT (MAX / 58. * 6. + 1.0)                               PLOT 270
       YFRAC  =  FLOAT (XY) / 6.0                                      PLOT 280
       XFRAC  =  FLOAT (XY) / 10.0                                     PLOT 290
         DO 1010  J  =  1, 2                                           PLOT 300
           DO 1010  K  =  1, 2                                         PLOT 310
 1010      PLOTFLE (LNEND + J, K)  =  WELL (J)                         PLOT 320
       LNPLUS  =  LNEND + 2                                            PLOT 330
         DO 1020  J  =  1, LNPLUS                                      PLOT 340
         FRACTX  =  AMOD (PLOTFLE(J, 1), XFRAC)                        PLOT 350
         FRACTY  =  AMOD (PLOTFLE(J, 2), YFRAC)                        PLOT 360
         XCOORD (J)  =  IFIX (PLOTFLE (J, 1) / XFRAC)                  PLOT 370
         YCOORD (J)  =  IFIX (PLOTFLE (J, 2) / YFRAC)                  PLOT 380
         IF  (FRACTX .GE. .5)  XCOORD (J)  =  XCOORD (J) + 1           PLOT 390
 1020    IF  (FRACTY .GE. .5)  YCOORD (J)  =  YCOORD (J) + 1           PLOT 400
       WELLPT (INWELL)  =  19                                          PLOT 410
       WELLPT (OUTWELL)  =  20                                         PLOT 420
         DO 1060  K  =  1, 58                                          PLOT 430
           DO 1030  M  =  1, 100                                       PLOT 440
 1030    ROW(M) = 1                                                    PLOT 450
         NUMROW  =  58 - K                                             PLOT 460
           DO 1040  J  =  1, LNPLUS                                    PLOT 470
           IF  (YCOORD(J) .EQ. NUMROW .AND. J .LE. LNEND)  ROW (XCOORD PLOT 480
     1         (J) + 1) = ROW(XCOORD(J) + 1) + 1                       PLOT 490
           IF  (YCOORD(J) .EQ. NUMROW .AND. J .GT. LNEND)  ROW (XCOORD PLOT 500
     1       (J) + 1)  =  WELLPT (J - LNEND)                           PLOT 510
 1040      CONTINUE                                                    PLOT 520
         DO 1045 M = 1, 100                                            PLOT 525
 1045    ROW (M) = CHAR (ROW(M))                                       PLOT 527
```

```
      IF (NUMROW/6*6 .EQ. NUMROW)  GO TO 1050                          PLOT 530
      PRINT   40, YAXIS (K), GRAPH (1), (ROW(M), M=1, 100)             PLOT 540
      GO TO 1060                                                       PLOT 550
1050  YVALUE  =  XY * NUMROW / 6                                       PLOT 560
      PRINT   50, YAXIS (K), YVALUE, GRAPH (2), (ROW(M), M=1, 100)     PLOT 570
1060  CONTINUE                                                         PLOT 580
      DO 1070  I  =  1, 12                                             PLOT 590
1070  XAXIS (I)  =  GRAPH (3)                                          PLOT 600
      PRINT   60, XAXIS                                                PLOT 610
      DO 1080  I  =  1, 12                                             PLOT 620
1080  XVALUE (I)  =  (I - 1) * XY                                      PLOT 630
      PRINT   70, XVALUE                                               PLOT 640
      RETURN                                                           PLOT 650
C                                                                      PLOT 660
  10  FORMAT  ( ///// 30X, 15 * FIRST QUADRANT STREAMLINE(S) PLOTTED *PLOT 670
     1   *WITH THE FOLLOWING DATA* / 40X *HEIGHT IN AQUIFER * F6.2     PLOT 680
     2   * FT.* / 40X *INITIAL ANGLE(S)* 5(2X, F5.2) * DEGREES* / 40X  PLOT 690
     3   *STREAMLINE INCREMENT* F7.2, 1X, A4 )                         PLOT 700
  20  FORMAT  ( 1H1, 30X *F I R S T  Q U A D R A N T  S T R E A M L I *PLOT 710
     1   *N E  P L O T  (DISTANCE INCREMENTS)* / 7X, 121 (1H- ) )      PLOT 720
  30  FORMAT  ( 1H1, 30X *F I R S T  Q U A D R A N T  S T R E A M L I *PLOT 730
     1   *N E  P L O T  (TIME INCREMENTS)* / 7X, 121 (1H- ) )          PLOT 740
  40  FORMAT  ( 2X, 1A1, 4X, 1A1, 100A1, 19X, 1H1 )                   PLOT 750
  50  FORMAT  ( 2X, 1A1, 1X, I3, 1A1, 100A1, 19X, 1H1 )               PLOT 760
  60  FORMAT  ( 8X, 12A10 )                                           PLOT 770
  70  FORMAT  ( 6X, 12(I3, 7X) / 40X * X  D I R E C T I O N  (F E E T)*PLOT 780
     1   )                                                             PLOT 790
C                                                                      PLOT 800
      END                                                              PLOT 810
```

```
C////////////////////////////////////////////////////////////////////////INVE  10
      SUBROUTINE  INVERSE (PERM, POROS, S, ALPHA, BETA, GAMMA, B,       INVE  20
     1   ASSIGN)                                                        INVE  30
C                                                                       INVE  40
C     THIS ROUTINE COMPUTES PERMEABILITY AND POROSITY FROM              INVE  50
C     FIELD OBSNS. OF WELL DRAWDOWN, AT SPECIFIC TIME INTERVALS..       INVE  60
C     A FIVE SPOT PATTERN OF INPUT AND OUTPUT WELLS IS ASSUMED.         INVE  70
C     DISTANCE FROM CENTER WELL TO EACH OF FOUR PERIPHERAL WELLS        INVE  80
C     IS GIVEN BY -S-.                                                  INVE  90
C     AN INPUT WELL OPTION EXISTS WHICH ALLOWS THE SPECIFICATION OF     INVE 100
C     CENTER WELLS OR PERIPHERAL WELLS AS INPUT.                        INVE 110
C     THE ROUTINE INCORPORATES A MODIFICATION FOR COMPUTING PERMEABILITYINVE 120
C     AND POROSITY FROM CENTER WELL AND 1 PERIPHERAL WELL OR FROM       INVE 130
C     THE ENTIRE 5 SPOT PATTERN.  IN THE LATTER CASE THE COORDINATES OF INVE 140
C     OBSN WELLS MUST BE SPECIFIED.                                     INVE 150
C     LIMIT OF  12 TIME PERIOD MEASUREMENTS / WELL.                     INVE 160
C                                                                       INVE 170
      DIMENSION   INPUT (2,12), LOGR (5), R (5), WELL (2)               INVE 180
      INTEGER     ASSIGN, OBWELL, OUTWELL, SAMPLES, WELLUSE             INVE 190
      REAL        INPUT, LOGR                                           INVE 200
      DATA    WELL / 6HCENTER, 6HCORNER /                               INVE 210
      ASSIGN = IABS(ASSIGN)                                             INVE 213
      SUMPOR = 0.0                                                      INVE 215
      SUMPERM = 0.0                                                     INVE 218
        DO 1090  OBWELL  =  1, ASSIGN                                   INVE 220
        SUMDELH  =  SUMTAU  =  SUMTAU2  =  DELTAU  =  0.0               INVE 230
        READ (5,   10)  SAMPLES, WELLUSE, Q, X, Y                       INVE 240
          DO 1000  I  =  1, 2                                           INVE 250
 1000     READ (5,   20)   (INPUT(I, J), J=1, SAMPLES)                  INVE 260
          DO 1030  K  =  1, SAMPLES                                     INVE 270
          IF (WELLUSE .NE. 0)  GO TO 1010                               INVE 280
          FN  =  ALOG (INPUT(2, K) * 60.)                               INVE 290
          GO TO 1020                                                    INVE 300
 1010     FN  =  1.0 / (INPUT(2, K) * 60.)                              INVE 310
 1020     SUMDELH  =  SUMDELH + INPUT (1, K)                            INVE 320
          SUMTAU  =  SUMTAU + FN                                        INVE 330
          SUMTAU2  =  SUMTAU2 + FN *  * 2                               INVE 340
 1030     DELTAU  =  DELTAU + INPUT (1, K) * FN                         INVE 350
        BCONST  =   (SUMDELH * SUMTAU2 - DELTAU * SUMTAU) / (FLOAT      INVE 360
     1    (SAMPLES) * SUMTAU2 - (SUMTAU) *  * 2)                       INVE 370
        BSLOPE  =   (FLOAT(SAMPLES) * DELTAU - SUMDELH * SUMTAU) /      INVE 380
     1    (FLOAT (SAMPLES) * SUMTAU2 - (SUMTAU) *  * 2)                INVE 390
        R (1)  =  SQRT (X * X + Y * Y)                                  INVE 400
        IF (WELLUSE .EQ. 0)  GO TO 1060                                 INVE 410
 1040   F1  =   (X - S) * (X - S)                                       INVE 420
        F2  =   (Y - S) * (Y - S)                                       INVE 430
        F3  =   (X + S) * (X + S)                                       INVE 440
        F4  =   (Y + S) * (Y + S)                                       INVE 450
        R (2)  =  SQRT (F1 + F2)                                        INVE 460
        R (3)  =  SQRT (F1 + F4)                                        INVE 470
        R (4)  =  SQRT (F3 + F2)                                        INVE 480
        R (5)  =  SQRT (F3 + F4)                                        INVE 490
          DO 1050  I  =  1, 5                                           INVE 500
 1050     LOGR (I)  =  ALOG (R (I) *  * 2)                              INVE 510
        TRANS  =  Q / (4.0 * 3.14159 * BCONST) * ( - LOGR (1) + .25 *   INVE 520
     1    LOGR (2) + .25 * LOGR (3) + .25 * LOGR (4) + .25 * LOGR (5))  INVE 530
        STORE  =   (BSLOPE * Q * ( - LOGR(1) + .25 * LOGR(2) + .25 *    INVE 540
     1    LOGR(3) + .25 * LOGR(4) + .25 * LOGR(5)) *  * 2) / ( (BCONST  INVE 550
     2    *  * 2) * 3.14159)                                            INVE 560
        OUTWELL  =  WELLUSE                                             INVE 570
```

```
      GO TO 1070                                                        INVE 580
1060  TRANS  =  Q / (4.0 * 3.14159 * BSLOPE)                           INVE 590
      STORE  =   (Q / (3.14159 * (R(I) *  * 2) * BSLOPE)) * EXP ( -     INVE 600
     1   (BCONST / BSLOPE) - .5772)                                     INVE 610
      OUTWELL  =  I                                                     INVE 620
1070  XTRANS  =  TRANS                                                 INVE 630
      XSTORE  =  STORE                                                  INVE 640
      I  =  1                                                           INVE 650
      IF  (TRANS .GE. 0.0 .OR. STORE .GE. 0.0)  I  =  2                 INVE 660
      TRANS  =  ABS (XTRANS)                                            INVE 670
      STORE  =  ABS (XSTORE)                                            INVE 680
      PERM  =  TRANS / H                                                INVE 690
      POROS  =   (STORE - GAMMA * ALPHA * B) / (GAMMA * BETA * B)       INVE 700
      SUMPERM = SUMPERM + PERM                                          INVE 705
      SUMPOR = SUMPOR + POROS                                           INVE 707
C*****************************************************************     INVE 710
      PRINT   30                                                        INVE 720
      PRINT   40, WELL (OUTWELL)                                        INVE 730
      PRINT   50, OBWELL, WELL (I)                                      INVE 740
      PRINT   60                                                        INVE 750
        DO 1080  J  =  1, SAMPLES                                       INVE 760
1080    PRINT   70, J, (INPUT(I, J), I=1, 2)                            INVE 770
      PRINT   80, STORE, TRANS, PERM, POROS                             INVE 780
1090  CONTINUE                                                          INVE 790
     PERM = SUMPERM / ASSIGN                                            INVE 795
     POROS = SUMPOR / ASSIGN                                            INVE 797
      RETURN                                                            INVE 800
C                                                                       INVE 810
  10  FORMAT  ( 2I5, 3E15.5 )                                           INVE 820
  20  FORMAT  ( 12F6.0 )                                                INVE 830
  30  FORMAT  (1H1   //// 30X *POROSITY AND PERMEABILITY COMPUTED FRO*  INVE 840
    1   *M FIELD OBSNS. OF WELL DRAWDOWN* // 50X *CONFINED AQUIFER CAS*  INVE 850
    2   *E*  )                                                          INVE 860
  40  FORMAT  ( 1H0 / 30X *OUTPUT WELL(S) IS/ARE * A6 * WELL(S)*  )     INVE 870
  50  FORMAT  (  // 40X *MAJOR EFFECT ON OBSN. WELL* IS * IS FROM THE *  INVE 880
    1   A6 * WELL(S).* //  )                                           INVE 890
  60  FORMAT  ( 10X,  *OBSN. NUMBER* 5X *WELL DRAWDOWN* 5X *TIME(MIN.)*  INVE 900
    1   5X *STOREATIVITY* 5X *TRANSMISSIVITY* 5X *PERMEABILITY* 5X      INVE 910
    2   *POROSITY* //  )                                               INVE 920
  70  FORMAT  ( 15X14, 5XE12.5, 4XE12.5 )                               INVE 930
  80  FORMAT  ( 60X, E12.5, 5X, E12.5, 5X, E12.5, 5X, E12.5 )           INVE 940
C                                                                       INVE 950
      END                                                               INVE 960
```

```
C////////////////////////////////////////////////////////////////////////ERRO  10
      SUBROUTINE  ERROR (NUMERR)                                          ERRO  20
      PRINT   10                                                          ERRO  30
      GO TO  ( 1000, 1010, 1020, 1030, 1040, 1050, 1060, 1070, 1080)      ERRO  40
     1   NUMERR                                                           ERRO  50
 1000 PRINT   20                                                          ERRO  60
      GO TO 1090                                                          ERRO  70
 1010 PRINT   30                                                          ERRO  80
      GO TO 1090                                                          ERRO  90
 1020 PRINT   40                                                          ERRO 100
      GO TO 1090                                                          ERRO 110
 1030 PRINT   50                                                          ERRO 120
      GO TO 1090                                                          ERRO 130
 1040 PRINT   60                                                          ERRO 140
 1050 PRINT   70                                                          ERRO 150
      GO TO 1090                                                          ERRO 160
 1060 PRINT   80                                                          ERRO 170
      GO TO 1090                                                          ERRO 180
 1070 PRINT   90                                                          ERRO 190
      GO TO 1090                                                          ERRO 200
 1080 PRINT  100                                                          ERRO 210
 1090 CONTINUE                                                            ERRO 220
      STOP                                                                ERRO 230
      RETURN                                                              ERRO 240
C                                                                         ERRO 250
   10 FORMAT  (  ///// 30X *////////// ERROR STOPS EXECUTION /////////*ERRO 260
     1   */* //  )                                                       ERRO 270
   20 FORMAT  ( 30X *GRID BOUNDRIES ARE NOT LOCATED IN THE FIRST QUADR*ERRO 280
     1   *ANT*  )                                                       ERRO 290
   30 FORMAT  ( 30X *BOTH WELLS ARE NOT LOCATED IN THE FIRST QUADRANT* ERRO 300
     1   )                                                              ERRO 310
   40 FORMAT  ( 30X *AN ATTEMPT WAS MADE TO EVALUATE THE WELL COORDINA*ERRO 320
     1   *TES*  )                                                       ERRO 330
   50 FORMAT  ( 30X *AN INITIAL STREAMLINE ANGLE IS OUTSIDE BOUNDRY CO*ERRO 340
     1   *NDITIONS*  )                                                  ERRO 350
   60 FORMAT  ( 30X *MAXIMUM OF 10 CONTOUR LINES MAY BE SPECIFIED*  )   ERRO 360
   70 FORMAT  ( 30X *A CONTOUR PROPORTION IS GREATER THAN OR EQUAL TO *ERRO 370
     1   *1*  )                                                         ERRO 380
   80 FORMAT  ( 30X *HEIGHT OF ANALYSIS(Z) IS > AQUIFER THICKNESS(B)*  ERRO 390
     1   )                                                              ERRO 400
   90 FORMAT  ( 30X *ERROR IN STREAMLINE SPECIFICATION*  )              ERRO 410
  100 FORMAT  ( 30X *TOTAL NUMBER OF STREAMLINE POINTS EXCEEDS(L1) SPE*ERRO 420
     1   *C.*  )                                                        ERRO 430
C                                                                       ERRO 440
      END                                                               ERRO 450
```

```
C////////////////////////////////////////////////////////////////////////CONT  10
      SUBROUTINE  CONTOUR (INCRX, INCRY, K, XSTART, XFINISH, YSTART,    CONT  20
     1  YFINISH, S, FOFT, Z, M1, XYLIST, VRAD, OUTOPT, INWELL, OUTWELL,CONT  30
     2  NPR)                                                            CONT  40
C*****                                                                 CONT  50
C***** SUBROUTINE CONTOUR CONSTRUCTS ISOPRESSURE AND ISOVELOCITY        CONT  60
C***** PRINTER CONTOUR MAPS.  INPUT TO THIS SUBROUTINE IS READ FROM     CONT  70
C***** TAPE(NPR).  THIS FACILITATES INDEPENDENT OPERATION OF THE CONTOURCONT  80
C***** ROUTINE FOR THE PURPOSE OF OPTIMIZING CONTOUR DISTINCTION.       CONT  90
C***** MAXIMUM OF 10 CONTOUR LINES MAY BE PLOTTED.                     CONT 100
C***** MAXIMUM OF 3000 DATA POINTS / MAP. (WITH MODIFICATION OF COMMON  CONT 110
C***** STORAGE ASSIGNED TO THE PROGRAM.                                CONT 120
C*****                                                                 CONT 130
      COMMON  /CONTR/  LINES (2), PERCNT (10, 2), INTRVL (10, 2)       CONT 140
      DIMENSION   ACCEP (10,2), CONTU (12), GRAPH (3), ODDLIST (9,10), CONT 150
     1  ODDPT (4,10), ROW (100), VRAD (M1,M1), WELL (2), WELLS (2),    CONT 160
     2  XAXIS (12), XVALUE (12), XYLIST (M1,M1), YAXIS (60)            CONT 170
      INTEGER     CONTU, OUT, OUTOPT, OUTWELL, ROW, WELLS, XCOORD,     CONT 180
     1  XFINISH, XSTART, XVALUE, XY, YCOORD, YFINISH, YSTART, YVALUE   CONT 190
      REAL        INCRX, INCRY, INTRVL, K                              CONT 200
      DATA    CONTU / 1H1, 1H2, 1H3, 1H4, 1H5, 1H6, 1H7, 1H8, 1H9, 1H0,CONT 210
     1  1H*, 1H$ /                                                     CONT 220
      DATA    YAXIS / 20 * 1H , 1HY, 1H , 1HD, 1HI, 1HR, 1HE, 1HC, 1HT,CONT 230
     1  1HI, 1HO, 1HN, 1H , 1H-, 1HF, 1HE, 1HE, 1HT, 1H-, 20 * 1H  /   CONT 240
      DATA    GRAPH / 1HI, 1H+, 10H+--------- /                        CONT 250
      WELL (1)  =  0.0                                                 CONT 260
      WELL (2)  =  S                                                   CONT 270
      IN  =  IFIX (WELL(INWELL) / INCRX + 1)                           CONT 280
      OUT  =  IFIX (WELL(OUTWELL) / INCRX + 1.)                        CONT 290
      IF (OUTOPT .GE. 2)  GO TO 1000                                   CONT 300
      READ (NPR,  10)  ((XYLIST(IX, IY), VRAD(IX, IY), IX=XSTART,      CONT 310
     1  XFINISH), IY=YSTART, YFINISH)                                  CONT 320
 1000 XMAX  =  (MAX0(XFINISH, IN, OUT,  - 1) - 1) * INCRX              CONT 330
      XY  =  INT (XMAX / 58. * 6.0 + 1.)                               CONT 340
      YFRAC  =  FLOAT (XY) / 6.0                                       CONT 350
      XFRAC  =  FLOAT (XY) / 10.0                                      CONT 360
        DO 1270  IM  =  1, 2                                           CONT 370
        IMAP  =  5 * IM - 2                                            CONT 380
        IF (LINES(IM) .EQ. 0)  GO TO 1270                              CONT 390
        LOOP  =  IABS (LINES(IM))                                      CONT 400
        IF (LOOP .GT. 10)  CALL ERROR (5)                              CONT 410
        IF (LINES(IM) .GT. 0)  GO TO 1020                              CONT 420
          DO 1010  I  =  1, LOOP                                       CONT 430
          ACCEP (I, IM)  =  PERCNT (I, IM)                             CONT 440
 1010     ODDLIST (IMAP, I)  =  INTRVL (I, IM)                         CONT 450
        GO TO 1070                                                     CONT 460
 1020     DO 1050  I  =  1, LOOP                                       CONT 470
          IF (INTRVL(I,IM) .GT. 1.0)  CALL ERROR (6)                   CONT 480
          IF (IM .EQ. 1)  GO TO 1030                                   CONT 490
          ODDPT (1, I)  =  ODDPT (2, I)  =  INTRVL (I, IM) * ( (XFINISHCONT 500
     1      - 1) * INCRX - S) + S                                      CONT 510
          GO TO 1040                                                   CONT 520
 1030     ODDPT (1, I)  =  ODDPT (2, I)  =  INTRVL (I, IM) * S         CONT 530
 1040     ODDPT (3, I)  =  INCRX / 2.0                                 CONT 540
 1050     ODDPT (4, I)  =  INCRY / 2.0                                 CONT 550
        CALL ODDPLOT (FOFT, LOOP, ODDLIST, K, ODDPT)                   CONT 560
          DO 1060  I  =  1, LOOP                                       CONT 570
 1060     ACCEP (I)  =  ABS (ODDLIST (IMAP, I) * PERCNT (I, IM))       CONT 580
C*********************************************************************CONT 590
 1070   IF (IMAP .EQ. 8)  GO TO 1090                                    CONT 600
```

```
      PRINT   20                                                        CONT 610
      PRINT   30, Z                                                     CONT 620
      PRINT   40                                                        CONT 630
        DO 1080  I  =  1, LOOP                                          CONT 640
1080    PRINT   50, I, ODDLIST (IMAP, I), ACCEP (I)                     CONT 650
      PRINT   60                                                        CONT 660
      GO TO 1110                                                        CONT 670
1090  PRINT   70                                                        CONT 680
      PRINT   30, Z                                                     CONT 690
      PRINT   80                                                        CONT 700
        DO 1100  I  =  1, LOOP                                          CONT 710
1100    PRINT   50, I, ODDLIST (IMAP, I), ACCEP (I)                     CONT 720
      PRINT   90                                                        CONT 730
C*****************************************************************CONT 740
1110  II  =  MAX0 (IN, OUT, YFINISH,  - 1)                             CONT 750
        DO 1120  I3  =  1, 2                                            CONT 760
        FRACTY  =  AMOD (WELL(I3), YFRAC)                               CONT 770.
        WELLS (I3)  =  IFIX (WELL (I3) / YFRAC)                         CONT 780
1120    IF  (FRACTY .GE. .5)  WELLS (I3)  =  WELLS (I3) + 1             CONT 790
        DO 1240  KNUM  =  1, 58                                         CONT 800
        YCOORD  =  58 - KNUM                                            CONT 810
          DO 1130  I2  =  1, 100                                        CONT 820
1130      ROW (I2)  =  1H                                               CONT 830
        Y  =  (FLOAT(II) - 1.) * INCRY                                  CONT 840
        FRACTY  =  AMOD (Y, YFRAC)                                      CONT 850
        NUMROW  =  IFIX (Y / YFRAC)                                     CONT 860
        IF  (FRACTY .GE. .5)  NUMROW  =  NUMROW + 1                     CONT 870
        IF (YCOORD .EQ. NUMROW)  GO TO 1150                             CONT 880
1140    IF (YCOORD .NE. WELLS(1) .AND. YCOORD .NE. WELLS(2))  GO TO     CONT 890
     1    1220                                                         CONT 900
1150    LOOP2  =  MAX0 (IN, OUT, XFINISH,  - 1)                        CONT 910
          DO 1210  J  =  1, LOOP2                                       CONT 920
          X  =  (FLOAT(J) - 1.) * INCRX                                 CONT 930
          IF (J .NE. IN .OR. II .NE. IN)  GO TO 1160                    CONT 940
          KK  =  12                                                     CONT 950
          GO TO 1200                                                    CONT 960
1160      IF (J .NE. OUT .OR. II .NE. OUT)  GO TO 1170                  CONT 970
          KK  =  11                                                     CONT 980
          GO TO 1200                                                    CONT 990
1170      IF (YCOORD .NE. NUMROW)  GO TO 1210                           CONT1000
            DO 1190  KK  =  1, LOOP                                     CONT1010
            IF (IMAP .EQ. 8)  GO TO 1180                                CONT1020
            IF (ABS(ODDLIST(IMAP,KK)-XYLIST(J,II)) .LE. ACCEP(KK))      CONT1030
     1        GO TO 1200                                               CONT1040
            GO TO 1190                                                  CONT1050
1180        IF (ABS(ODDLIST(IMAP,KK)-VRAD(J,II)) .LE. ACCEP(KK))  GO    CONT1060
     1        TO 1200                                                  CONT1070
1190        CONTINUE                                                    CONT1080
          GO TO 1210                                                    CONT1090
1200      FRACTX  =  AMOD (X, XFRAC)                                    CONT1100
          XCOORD  =  IFIX (X / XFRAC)                                   CONT1110
          IF  (FRACTX .GE. .5)  XCOORD  =  XCOORD + 1                   CONT1120
          ROW (XCOORD + 1)  =  CONTU (KK)                               CONT1130
1210      CONTINUE                                                      CONT1140
        II  =  II - 1                                                   CONT1150
1220    IF (YCOORD/6*6 .EQ. YCOORD)  GO TO 1230                         CONT1160
        PRINT  100, YAXIS (KNUM), GRAPH (1), (ROW(N), N=1, 100)         CONT1170
        GO TO 1240                                                      CONT1180
1230    YVALUE  =  XY * YCOORD / 6                                      CONT1190
        PRINT  110, YAXIS (KNUM), YVALUE, GRAPH (2), (ROW(N), N=1,      CONT1200
```

```
     1       100)                                                          CONT1210
  1240      CONTINUE                                                       CONT1220
            DO 1250  MN  =  1, 12                                          CONT1230
  1250      XAXIS (MN)  =  GRAPH (3)                                       CONT1240
           PRINT  120, XAXIS                                               CONT1250
            DO 1260  MN  =  1, 12                                          CONT1260
  1260      XVALUE (MN)  =   (MN - 1) * XY                                 CONT1270
           PRINT  130, XVALUE                                              CONT1280
  1270     CONTINUE                                                        CONT1290
       RETURN                                                             CONT1300
C                                                                         CONT1310
    10  FORMAT  ( 30X, 2E15.5 )                                           CONT1320
    20  FORMAT  ( 1H1 ////// 45X *FIRST QUADRANT ISOPRESSURE(HEAD) CONTO*CONT1330
      1   *UR MAP*  )                                                     CONT1340
    30  FORMAT  (  / 47X *HEIGHT OF ANALYSIS IN AQUIFER* F5.1 * FT.* )    CONT1350
    40  FORMAT  (  // 25X *CONTOUR INTERVAL* 10X *HEAD(IN FEET)* 10X      CONT1360
      1   *ACCEPTANCE REGION(IN FEET) (+,-)*  )                           CONT1370
    50  FORMAT  (  / 32X, 12, 16X, E12.4, 17XE14.7 )                      CONT1380
    60  FORMAT  ( 1H1, 35X *F I R S T  Q U A D R A N T  I S O P R E S S *CONT1390
      1   *U R E  C O N T O U R  M A P* / 7X, 121 (1H- ) )                CONT1400
    70  FORMAT  ( ////// 45X *FIRST QUADRANT ISOVELOCITY CONTOUR MAP*  )CONT1410
    80  FORMAT  (  // 25X *CONTOUR INTERVAL* 10X *VELOCITY(IN FT./SEC.)* CONT1420
      1   10X *ACCEPTANCE REGION (IN FT./SEC.) (+,-)*  )                  CONT1430
    90  FORMAT  ( 1H1, 35X *F I R S T  Q U A D R A N T  I S O V E L O C *CONT1440
      1   *I T Y  C O N T O U R  M A P* / 7X, 121 (1H- ) )                CONT1450
   100  FORMAT  ( 2X, 1A1, 4X, 1A1, 100A1, 19X, 1HI  )                    CONT1460
   110  FORMAT  ( 2X, 1A1, 1X, I3, 1A1, 100A1, 19X, 1HI  )                CONT1470
   120  FORMAT  ( 8X, 12A10 )                                             CONT1480
   130  FORMAT  ( 6X, 12(I3, 7X) / 46X *X  D I R E C T I O N  ( F E E T *CONT1490
      1   *)*  )                                                         CONT1500
```

*U.S. GOVERNMENT PRINTING OFFICE: 1978-703-103/36

INT.-BU.OF MINES,PGH.,PA. 22958

imeter of
successive

SUBJ
MNG
CND

.8 and Br.1

ontact surf
of welds

Br. KhTsr		
00	4000	5000
65	0.70	0.79
57	0.68	0.77
51	0.62	0.83
58	0.69	0.81
68	0.32	0.92
62	0.74	0.82
62	0.72	0.84
72	0.84	0.81
51	0.59	0.73
54	0.63	0.79
67	0.74	0.94
67	0.77	0.91
51	0.63	0.73
52	0.62	0.69
52	0.74	0.85
75	0.68	1.03
55	0.63	0.72
60	0.67	0.80
65	0.79	0.94
46	0.52	0.63

The experimental data were treated by one of the methods of mathematical statistics, i.e. analysis of variance. The effect of all the factors was statistically significant when checked against the F criterion with a confidence probability of 95%. This made it possible to analyse the effect of the treatment regimes on the stability of the electrodes, by comparing the change in the diameter of their contact surface for each level of each factor (table 1). This mainly concerned the stability of the electrodes after 5000 welds.

As a result of analysis of the effect of the treatment regimes on the properties of electrodes of bronze Br. Kh0.8 it is possible to recommend the following scheme for the treatment of the electrodes: quenching + deformation + ageing + deformation. The best treatment regimes in this scheme are given in table 2. The differences from those existing at the present time lie in the fact that, firstly, deformation after quenching is realised at 400°C and not at room temperature; secondly, the ageing temperature must be higher (500 instead of 460°C); thirdly, deformation is required after ageing, and it can be realised either at room temperature or at 500°C.

As a result of analysis of the data on the stability of electrodes of bronze Br. KhTsr it is possible to recommend the following scheme of treatment: quenching + deformation + ageing + deformation. The best regimes of such treatment are given in table 2. The main differences from the existing regimes are as follows: firstly, instead of cold deformation, deformation after quenching is carried out at 450 or 500°C; secondly, one deformation at a temperature of 500°C is required after ageing.

The processes occurring in the electrodes at various stages of treatment and during use are fairly complex, and it is therefore difficult to explain unambiguously the optimum character of the regimes given in table 3. At the same time, certain hypotheses can be put forward on the basis of the existing experimental data[1]). The working surface of the electrode during spot welding is softened as a result of recrystallisation and coagulation of the particles of second phase, and the stability of the electrodes is mainly determined by the amount and size of the segregations. In order to reduce the softening rate it is necessary, on the one hand, that the particle sizes should be as small as possible and that the volume fraction should be as large as possible. On the other hand, the size of the segregations must be stable during the operation of the electrode.

It was shown that deformation between quenching and ageing leads to the result that the rod-like segregated particles becomes spherical and are at the same time refined. In deformation at temperatures of 400-450°C decomposition of the supersaturated solid solution occurs. Here a large number of centres for the nucleation of the second phase appear, and subsequent ageing leads to the formation of a structure characterosed by the optimum combination of the number of particles in unit volume and their size, since redistribution of the dislocations by nonconservative movement and annihilation occurs.

Some of the proposed regimes were tested directly under industrial conditions at the I A Likhachev motor works. For comparison electrodes produced in the tool shop of the ZIL motor works, at the Perovo works, and treated by the standard regime were tested. As stability characteristics of the electrodes we determined the number of welds produced before the electrode was completely worn out. The results from the industrial trial, given in table 3, showed a considerable increase in the stability of the electrodes treated by the proposed regime.

References

1) A I Novikov: Author's Abstract of Thesis: Moscow 1976.

Sov. Non-Fe..
1978 v. 6 N6

UDC 669.2:546.56

Control of the nickel deposition process in the autoclave treatment of pickel-pyrrhotite concentrates

Yu F Markov, V A Ivanov and A F Gravrilenko (Moscow Institute of Steel and Alloys - Department of the Automation of Non-Ferrous and Rare Metals Production)

For the treatment of nickel-pyrrhotite concentrates an autoclave technique was developed[1]), securing an increase in the nickel content of the final product (the sulphide concentrate) of four to six times compared with its content in the initial raw material. Concentration occurs on account of the extraction of the gangue material and a large part of the iron of the pyrrhotite into the tailings and the extraction of sulphur in the elemental form. The extraction of the pyrrhotite iron into the tailings is realised in a set of main operations including the following[2]): aggregation of the elemental sulphur and sulphides undecomposed in the leaching process; the sulphide sulphur granules are separated from the pulp and passed on for the melting of elemental sulphur (in the shortened variant of the technological scheme the oxidised pulp is delivered directly for precipitation, by-passing the aggregation); precipitation of nickel from the pulp in the form of sulphides with metallic iron and elemental sulphur; flotation separation of the sulphides and elemental sulphur from the iron hydroxides and gangue.

The technical operations are fulfilled in succession without intermediate vessels in between them and without recirculation of the solids. The main estimate of the effectiveness of the complex of operations as a whole is therefore provided by the characteristics of the sulphide sulphur flotation (the extraction of nickel and elemental sulphur into the sulphide sulphur concentrate and its quality). The extraction of nickel into the concentrate depends on its content in the tailings and on their yield, and for the technique as a whole it is determined by the losses of nickel with the tailings of the sulphide sulphur flotation. The quality of the concentrate is characterised by the ratio of the nickel to iron content in the concentrate.

By technological investigations it was established that the initial raw material and the leaching regime have a significant effect on the flotation characteristics[2-4]). To determine this effect quantitatively we constructed a nomogram (fig. 1) by means of which it is possible to calculate the quality of the concentrate (K_c) for known contents of pyrrhotite (C_{P_0}) and nickel (C_{Ni}) in the initial raw material, the degree of decomposition of the pyrrhotite (η_{P_0}), the degree of transfer of the nickel into solution (η_{Ni}), and the content of nickel in the flotation tailings C_{Ni}^{t}). (η_{P_0} is equal to the ratio of the amount of oxidised pyrrhotite to its amount in the oxidised pulp; η_{Ni} is equal to the ratio of the amount of nickel in the solution of the oxidised pulp to its amount in the initial concentrate).

The rule for the use of the nomogram is shown in the fig. by lines with arrows, which indicate the sequence of operations. The nomogram was checked against the data from several balancing trials on a pilot plant. (The balancing trials were carried out by a team of investigators under the guidance of Candidates of Technical Sciences, A S Ladygo, V I Goryachkin and Ya M Shneerson). The deviation of the calculated K_c values from the actual values was not greater than 10 rel. %. Consequently, it is possible with an acceptable degree of accuracy for practical purposes to forecast the quality characteristics obtainable

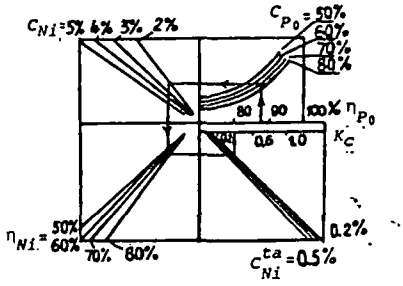

Fig.1 The nomogram for calculation of the quality characteristic of the concentrate (K_C) in relation to the nickel content (C_{Ni}) and pyrrhotite content (C_{P_0}) of the initial raw material, the degree of decomposition of the pyrrhotite (η_{P_0}), and the degree of transfer of nickel into the solution (η_{Ni}) during leaching, and the nickel content of the flotation tailings (C_{Ni}^{ta}).

with a given leaching regime and with ideal realisation of the subsequent operations. Ideal realisation means that sulphide iron or any of its forms extractable into the concentrate are not formed during aggregation, precipitation and flotation.

If the "non-ideality" is characterised by the amount of sulphide iron formed in the given technological operation and is related to a ton of the initial concentrate, it is only necessary to correct the η_{P_0} value in order to predict K_c. In such a way it is convenient to estimate the effect of each of the operations on the formation of K_c in the set of main operations. The contribution from each of them to the resultant value of the degree of decomposition of pyrrhotite (η_{P_0}) is such.

During aggregation 90-98% of the sulphide iron is withdrawn into the granules, irrespective of the degree of decomposition of the pyrrhotite in leaching[5]). Consequently, at the entry to precipitation $\eta_{P_0}^{c} \approx 1$.

A considerable amount of secondary pyrrhotite can form during precipitation[1]), and this can reduce the $\eta_{P_0}^{c}$ value by 0.02-0.15 compared with the input value. During flotation a certain part of the iron hydroxides is extracted into the sulphide sulphur concentration. This may lead to a decrease of $\eta_{P_0}^{c}$ by a further 0.01-0.1 relative unit.

As a result $\eta_{P_0}^{c}$ may be 0.03-0.15 relative unit less than the degree of decomposition of the pyrrhotite during leaching. As seen from the nomogram, the quality of the concentrate is reduced considerably in this case. Here, as shown in the literature[2-6]), the consumption of the reagents on the main operations and on the melting of the solvent increases. Thus, the criterion for control of the precipitation process must be selected with allowance for these peculiarities of the technological scheme.

The set of technological requirements for the precipitation process was formulated as follows: it is necessary to maintain a given nickel content in the solution of the pulp at the outlet from the precipitation process (usually 0.05-0.2g/l) with a minimum consumption of the reagents. Here it is desirable to obtain iron-free nickel sulphides of specific particle size, securing their good flotability, and to realise the precipitation with the pH of the pulp as low as possible. In this case, with other conditions equal, the losses of nickel with the flotation tailings are reduced[6]). The possibility of combining such varied requirements into a single criterion for control of the process is analysed below.

The precipitation process is realised at atmospheric pressure in a cascade of three to four reactors with mechanical agitation at 85-95°C. The average time spent by the pulp in the reactors varies from 40 min to 2 h. The precipitation reagents are metallic iron powder (particle size 100% -0.5mm) and finely ground elemental sulphur, which is delivered with the oxidised pulp or in the form of an aqueous pulp of the various intermediate products from the fusion of the sulphur.

In the mechanism of the precipitation of nickel from acidic sulphate solutions with metallic iron and elemental sulphur[1]) it is possible to distinguish two groups of reactions. The first group is the sulphidisation reactions:

$$Fe^{\circ} + H_2SO_4 \rightarrow FeSO_4 + 2H \quad (1)$$

$$2H + S^{\circ} \rightarrow H_2S \quad (2)$$

$$H_2S + NiSO_4 \rightarrow NiS + H_2SO_4 \quad (3)$$

During reaction according to these equations the consumption of metallic iron and elemental sulphur on the precipitation is minimum and equal to the stoichiometric amount required for the reaction

$$Fe^{\circ} + S^{\circ} + NiSO_4 + NiS \rightarrow FeSO_4 \quad (4)$$

The nickel sulphide does not contain iron, and the pH of the pulp at the outlet from the precipitation stage is equal to the initial value. Consequently, in this case three of the four main technological requirements are fulfilled.

The second group includes the following reactions:

$$NiSO_4 + Fe^{\circ} \rightarrow Ni^{\circ} + FeSO_4 \quad (5)$$

$$Ni^{\circ} + H_2SO_4 \rightarrow NiSO_4 + 2H \quad (6)$$

$$2H \rightarrow H_2\uparrow \quad (7)$$

the overall effect of which can be represented as neutralisation of sulphuric acid by metallic iron:

$$Fe^{\circ} + H_2SO_4 \rightarrow FeSO_4 + H_2\uparrow \quad (8)$$

and leads to unproductive consumption of metallic iron and to an increase in the pH of the pulp. If, however, the rate of reaction (5) is higher than that of reaction (6), the cemented films of nickel which form do not succeed in dissolving during precipitation. In this case increased losses of nickel with the solutions of the concentrate and the tailings are observed in flotation.

Under real conditions the precipitation of iron sulphide is possible, and this leads to the formation of sulphides of the $NiS \cdot nFeS$ type with a variable content of FeS[1]). It is clear that the consumption of the precipitation reagents here exceeds the stoichiometric consumption required for reactions (4).

The task in automatic control of the precipitation process can, therefore, be formulated as follows: it is necessary to organise the control so as to secure the optimum ratio of the rates of the sulphidisation and cementation-neutralisation reactions. The main information about the ratio of these processes is provided by the pH of the pulp, and the criterion for the attainment of the optimum ratio under specific conditions is the minimum excess of metallic iron consumption in relation to the stoichiometric amount required for reaction (4).

These conclusions follow from the analysis of the chemical mechanism of the precipitation of nickel from pure solutions. Their validity for real conditions in the realisation of the precipitation from pulps was checked on a pilot plant. The effect of the excess of the metallic iron consumption on the precipitation characteristics (the nickel content at the outlet, the pH of the pulp) and on the flotation characteristics (the quality of the concentrate and the losses of nickel with the flotation tailings) was investigated. The dependence of the excess iron consumption

on the leaching regime, the main characteristic of which is the degree of decomposition of the pyrrhotite, was also investigated.

The excess ratio of metallic iron consumption (K_{Fe}) was calculated on the basis of experimental data by means of the equation:

$$K_{Fe} = \frac{g_{Fe} \cdot a}{V_p \frac{\gamma_{sd}-\gamma_p}{\gamma_{sd}-\gamma_{sn}} \cdot \frac{M_{Fe}}{M_{Ni}} (C^o_{Ni} - C_{Ni})} \qquad (9)$$

where: g_{Fe} is the consumption of iron powder kg/h; a is the content of metallic iron in the powder; C^o_{Ni} and C_{Ni} are the contents of nickel in the solution of the pulp at the inlet and outlet of the precipitation stage respectively; M_{Fe} and M_{Ni} are the atomic weights of iron and nickel; V_p is the consumption of pulp at the inlet; γ_p, γ_{sd} and γ_{sn} are the densities of the pulp, the solid and the solution respectively.

The excess ratio of the elemental sulphur consumption on sulphidisation is calculated by an analogous formula. As shown by the investigations, the metallic iron consumption depends on the degree of precipitation of the nickel and varies significantly with a variable content of elemental sulphur in the pulp (fig. 2a).

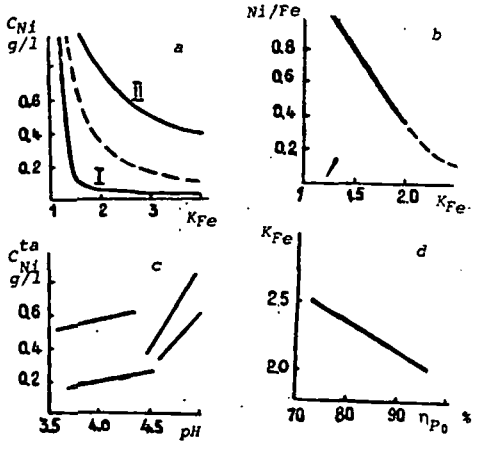

Fig.2 The results from the experimental investigations: a) The effect of the excess consumption of metallic iron on the precipitation of nickel (K_{Fe}) and on the content of nickel in the final solution (C_{Ni}); K_S = 5 (1), $K_S \simeq 0$; b) the effect of the excess metallic iron consumption on the quality characteristic of the concentrate (K_c); c) the effect of the pH of the pulp at the outlet from the precipitation process on the nickel content of the flotation tailings (C^{ta}_{Ni}); d) the effect of the degree of decomposition of pyrrhotite during leaching (η_{P_0}).

Here curve I was obtained with five times the amount. Curve II was obtained with a pulp from which up to 95% of the elemental sulphur had been removed during aggregation. As seen from these data, a specific ratio in the excesses of precipitation reagents delivered to the precipitation reactors is required for the attainment of the minimum iron consumption. The pH of the pulp in the precipitation process also depends on this ratio. Within the range of variation K_{Fe} = 0.1-3.0 and K_S = 0.5-5.0.

$$pH = 4.3 + 0.266 \cdot K_{Fe} - 0.172 \cdot K_S \qquad (10)$$

For the final nickel content of 0.1g/l in the solution a K_{Fe} value of 1.5 is required (curve 1, fig. 2a). The minimum pH value attainable in practice will then be about 3.5 [equation (10)]. As shown in the literature[1]) contamination of the precipitates with sulphide iron hardly occurs at all at pH ⩽ 3-3.5.

The effect of the excess metallic iron consumption on the quality of the sulphide sulphur concentrate is shown in fig. 2b. The significant effect of K_{Fe} on K_c is obvious, and the experimental values for the quality characteristic of the concentrate vary within limits calculated according to the nomogram in fig. 1.

The effect of K_{Fe} on C^{ta}_{Ni} is expressed in terms of the variation of the pH of the pulp during precipitation and is shown in fig. 2c. Depending on a multitude of factors, the nickel content in the solid of the flotation tailings can vary within wide limits but always decreases with decrease in the pH under comparable conditions.

The effect of the degree of decomposition of pyrrhotite during leaching on K_{Fe} is shown in fig. 2d. The K_{Fe} value increases with decrease of η_{P_0}. This is clearly explained by the overall effect of the decrease in the content of elemental sulphur in the pulp and by the variation of its characteristics (activity, particle size, etc.) during the leaching process, a complete assessment of which is provided by the degree of decomposition of the pyrrhotite. Thus the experimental investigations confirm the expediency of formulating the problem of control of the precipitation process as follows:

$$K_{Fe} \rightarrow \min \qquad (11)$$

for a given content of nickel in the solution of the pulp at the outlet from the precipitation stage. In this case all the technological requirements indicated above are best fulfilled.

With unchanged elemental sulphur characteristics formed in the leaching process the condition pH → min is equivalent to the condition (11).

From the presented experimental data it also follows that the absolute values of K_{Fe} and the pH of the pulp at the outlet, as specifications to the local systems of automatic control, cannot be specified arbitrarily. It is only possible to indicate their limiting most favourable values, namely: K_{Fe} = 1.0; pH = 3.5. The search for optimum values of these quantities in the course of the process is the main task in the control of the precipitation as an element of a technological flow chart for the complex of main operations.

References

1) V I Goryachkin et alia: Hydrometallurgical treatment of copper-nickel pyrrhotite concentrates based on autoclave oxidative leaching. Collection: Hydrometallurgy (Ed. B N Laskorin): Nauka, Moscow 1976, p. 48.
2) V I Goryachkin et alia: Tsvetnye Metally 1974, (9), 1.
3) V A Shcherbakov et alia: Byull. In-ta Tsvetnmetinformatsiya, Tsvetnaya Metallurgiya 1974, (1), 24.
4) V V Yakovlev et alia: Tsvetnye Metally 1977, (5), 75.
5) N V Serova et alia: Characteristics of the formation of sulphur-sulphide melt in the pulp from oxidative autoclave leaching of pyrrhotite-containing concentrates: Sb. Tr. Gintsvetmeta No. 41, Metallurgiya, Moscow 1976, 67.
6) V I Goryachkin et alia: Tsvetnye Metally 1975, (1), 11.

SUBJ
MNG
COUO

SPE 7537

SPE
Society of Petroleum Engineers of AIME

CHARACTERIZATION OF THE URANIUM OCCURRENCE IN PRE- AND POST-LEACH ORE SAMPLES FROM SANDSTONE DEPOSITS IN TEXAS & WYOMING

by Susan Wood, Westinghouse

This paper was presented at the 53rd Annual Fall Technical Conference and Exhibition of the Society of Petroleum Engineers of AIME, held in Houston, Texas, Oct. 1-3, 1978. The material is subject to correction by the author. Permission to copy is restricted to an abstract of not more than 300 words. Write: 6200 N. Central Expy., Dallas, Texas 75206.

ABSTRACT

Uranium ore samples from open-pit mines in the Shirley Basin of Wyoming and in Texas are currently being utilized to simulate in situ leaching conditions in laboratory column-leach tests at the W R & D Center. Evaluation of their uranium mineralogies was achieved through analysis of mounted and polished specimens with the electron beam microanalyzer and scanning electron microscope, after first delineating α-active regions by radioluxography. The two ores exhibited both different uranium distributions and mineralogies, but these characteristics were similar for as-received and processed material from each site. No uranium was detected in acid-leached Wyoming ore.

INTRODUCTION

In-situ leaching has become a very attractive method for recovering uranium from secondary arkosic sandstone deposits because of both the relatively low capital costs involved and the amenability of such ore bodies to this leaching technique. To improve and further the understanding of the leaching of uranium by this method, laboratory simulation, utilizing column-leaching apparatus, is currently being exploited at the W R & D Center(1). Although the ores used in these experiments originated in sandstone deposits in Texas and Wyoming, they were obtained from open-pit sites rather than the deeper mineralized roll-fronts normally subjected to in-situ mining. Furthermore, the ore was processed through drying, blending and column-packing operations before being leached. Hence, it is not known, for example, if the uranium distribution in the column truly represents that in the original ore body or if the mineralogies of the open-pit ores are typical of those observed in deposits located at greater depths.

This paper describes the results of a characterization study designed to answer these types of questions. In addition to delineating the uranium mineralogy of both the virgin Texas and Wyoming ores, the uranium distributions in as-received and processed ores were evaluated using a radioluxograph technique. The α-maps thus obtained were also utilized to identify U-rich zones for subsequent examination by use of electron beam microanalysis (EBMA) and scanning electron (SEM) for the delineation of uranium mineralogy. Wyoming ore subjected a sulfuric acid leach was also examined. The low uranium content of the ores prohibits evaluation of uranium mineralogies by petrography and necessitates the use of more sophisticated analytical techniques.

*References and illustrations at end of paper.

EXPERIMENTAL PROCEDURES

A. Selection and Packaging of Ore

Ore samples were obtained from the Lucky Mc mine in the Shirley Basin of Wyoming and the Conquista Project near Falls City, Texas. Material for the pre-leach characterization study was selected from currently-mined areas in the open-pit to be within a grade of 0.05-0.12 Wt% U_3O_8 (as determined by on-site γ-logging techniques). Some of the ore, used only for characterization purposes, was sealed under nitrogen at the mine site, while a larger, bulk sample was merely packaged in a polyethylene bag. This latter material was subsequently dried and processed for column-leach studies.

B. Preparation of Mounted Specimens

In general, both the Texas and Wyoming ores are poorly consolidated, which necessitated packing the as-received material in small cardboard boxes for mounting purposes. Because the Lucky Mc (Wyoming) ore also contained pieces (with a maximum dimension of ~4 cm) which retained their competency, several of these were also selected for mounting. Samples were oven-dried for 24 hrs. at 50°C before vacuum-impregnating with Spurr, a low-viscosity resin cured by baking at 50°C for approximately 16 hrs. Specimens were subsequently ground through 600 grit SiC and polished to 0.5 μm diamond using water as the vehicle. After obtaining both radioluxographs (the procedure for which is discussed in the next section) and mineralogical analyses, a 3 mm section was cut from the polished face of each mount, and all specimens were re-ground and polished at this new plane after re-

impregnating the surfaces with Spurr. Additional EBMA and SEM studies were subsequently peformed at the new sample depths.

Processed (i.e. air-dried, crushed to - 10 m and blended) samples were prepared in a similar manner except rubber molds were utilized to reduce sample size because of the granular nature of the material. Problems were encountered in obtaining acceptable mounts and those finally selected for examination had experienced some pull-out of grains and matrix material during grinding and polishing operations due to poor consolidation of the mounting medium - a problem believed to result from the granular nature of the dry ore. However, the surface condition of the final mounts proved adequate for the characterization studies.

Acid-leached, processed material was received in a moist condition which permitted a mode of preparation identical to that utilized for the as-received ore. Samples were selected from three sections within the column, and no significant pull-out was observed during grinding and polishing operations.

C. Radioluxographs

Radioluxographs, or α-maps, were obtained from all polished sample surfaces prior to their examination with EBMA or SEM. The technique utilizes a ZnS-CdS/Ag activated phosphor which is sandwiched between Type 57 film and the specimen[2] for exposure times of 70 to 73 hrs. Alpha-maps were also obtained from hand-picked pieces of coalified material. These images were used to interpret the distribution of α-emitters on the sample surfaces and to delineate "hot spots", or particularly radioactive zones, for investigation with EBMA and SEM.

D. EBMA and SEM Analyses

All EBMA analyses utilized a MAC 400 microprobe and the SEM was performed on a Cambridge Stereoscan S4.A 20KeV accelerating voltage was used on both instruments. Elemental distributions, obtained by the EBMA mapping mode, were used to characterize U-rich zones in virgin samples of Texas and Wyoming ore. Non U-rich matrix regions were also investigated - in both virgin and leached material. Most areas were subsequently examined with the SEM to identify the morphology of the U-rich phases (in virgin ore) or reaction products (in leached ore). Energy dispersive X-ray (EDAX) analyses were performed concurrently and use of standard operating conditions on the SEM permitted composition comparisons both within one region and from one region to another.

Although most EBMA studies were performed using the mapping mode, 2θ scans were also performed in the matrices of both Conquista and Lucky Mc ores utilizing a beam diameter of ∿20μm. The 2θ scans are significantly more sensitive than the mapping mode (by at least a factor of 10) for the detection of uranium.

RESULTS

A. Radioluxographs

Examples of radioluxographs obtained from the various types of ore samples are given in Figure 1, together with a macro-optical photograph of a typical mounted specimen. Those areas specifically delineated are areas examined in more detail with EBMA and SEM. The radioluxograph or α-map is obtained by permitting the α-particles generated within the ore sample to surface to interact with the phosphor, generating photons of the correct wavelength for exposure of photographic film. A subsequent print of the image is termed a radioluxograph. However, it should be noted that the phosphor does not selectively interact only with α-particles generated by the decay of ^{238}U, but will also produce photons due to all α-particles generated by the decay sequence, including ^{226}Ra. It is now known that ^{226}Ra decay, contributes a significant amount of α-activity and thus, α-maps can only be utilized to monitor U distributions for samples in which the U and Ra are still closely associated and there has been no migration of U.

Figure 1a shows a typical radioluxograph obtained from an unprocessed Lucky Mc specimen. There is a weak background distribution of α-activity plus localized "hot spots", or more radioactive zones. Both disaggregated and competent samples exhibited similar distributions which did not change as a function of depth in the bulk specimen. Comparison of Figure 1a with Figure 1c, which gives a representative α-map from a mount of processed ore, reveals comparable α-activities in the two types of specimens with, perhaps, fewer "hot spots" after processing. All processed Lucky Mc samples were also observed to exhibit an unchanging α-distribution as a function of depth.

Figures 1b and 1e show typical radioluxographs from as-received and processed samples of Conquista ore, respectively. Similar α-activity distributions are again observed before and after the blending operation, but it is apparent that they differ from those in the Lucky Mc ore. There is a higher, more uniform "background" activity with fewer localized hot spots in the Conquista ore; those regions within the specimen boundaries which yielded no exposure on the radioluxographs correspond to zones of resin mounting medium in the sample. Neither type of Conquista specimen exhibited changes in the α-activity distribution as a function of depth.

Additional radioluxographs are presented from coalified wood fragments and H_2SO_4- leached Lucky Mc material (Figures 1d and 1f). The former shows a relatively high overall activity with respect to the bulk samples, even after consideration of the different exposure times, and the latter compares well with the pre-leached material, Figure 1c, but has a somewhat higher background distribution (exposure time for the leached specimen was 72 hr.). Despite the apparent radioactivity of the organic material, it cannot represent a major mode of uranium occurrence because coalified wood was identified only as a minor constituent in these ore samples. The activity exhibited by the leached material is generated primarily by ^{226}Ra decay, and an independent γ-spectroscopy measurement yielded a Ra to U ratio of 3.8±1 (in pci/gm) in one of the mounted specimens. Before leaching this ratio was ∿1.0 (in pci/gm) in the typical mounted specimen.

B. EBMA and SEM Analyses of U-rich Zones in Unleached Lucky Mc Ore

Most investigations were performed in regions within samples which had retained their competency, and thus the original mineral assemblages present in the ore body are still intact. Preliminary optical microscopy observations revealed that most radioactive zones (i.e. hot spots) on the radioluxographs were associated with pyrite, and examples of several different types of such regions are shown in Figures 2 and 3.

The first region (Figures 2a through e) is an assemblage of small pyrite grains surrounded by U-rich matrix material. An EBMA map (Figure 2b) gives the U-distribution within part of the pyrite-matrix aggregate shown in Figure 2a (note the differing manifications of 2a and 2b). The SEM micrograph in Figure 2c presents the typical layered morphology of the U-rich phase, which, in addition to U, also contains Si, Aℓ, K, Ca, Fe and Mg - a composition suggestive of a U-rich clay. EDAX analyses in the matrix region (at 2F and 2G, for example) yield U as the most abundant element present, and close inspection reveals that the structure at 2F is actually a relatively large U-rich precipitate >15μm across, while the morphology and composition of 2G suggest a micaceous mineral such as biotite (nominal composition $(OH)_4K_2(Si_6Aℓ_2)(Mg, Fe)_6O_{20}$).(3) Although biotite does not contain Ca, this element is believed to be in-corporated in the U-rich mineral since EDAX analyses of the larger U-rich zones (e.g. 2F) yielded higher Ca contents than did the bulk matrix.

A second matrix area, represented by Figures 2d through 2f, reveals a U-rich phase in close proximity to pyrite, both of which are cementing quartz clastics. The EBMA UMα scan gives the U-distribution throughout the matrix within the outlined region in Figure 2d while the morphology of the inter-related phases is revealed by the higher magnification SEM micrograph in Figure 2f. EDAX analyses at 1F and 1G show a definite U, Si, Ca and P association (with U and Si present as the most abundant constituents). In contrast, the lower magnification EBMA elemental maps for Ca, K, Aℓ, Si and Fe indicated that they were all associated with U, but it is believed that these analyses simply indicate the presence of matrix clay in addition to pyrite and a uranium phase. (Phosphorus was not scanned by EBMA). No V was detected in the area, and localized Ti concentrations suggested anatase (TiO_2). The U-rich phase is believed to be the primary mineral uraninite, but attempts to extract sufficient material for identification by use of X-ray diffraction techniques were unsuccessful.

Additional U-rich regions whose mineralogy was similar to the two areas discussed previously were also examined in detail with EBMA and SEM and showed similar elemental associations(4). Pyrite was always a common denominator and fine-grained calcite was present in some examples. Large U-rich precipitates (such as those in Figures 2c and 2f) were not always identified, but the existence of a separate U-rich phase was usually established by SEM/EDAX analyses, particularly in biotite regions where the low cation exchange capacity(5) precludes the possibility of having high concentrations of adsorbed uranium.

A third mode of U-occurrence associated with pyrite (for which micrographs are not presented) was observed in weathered pyrite cement surrounding quartz clastics(4). The uranium was associated with montmorillonite clay and observed only in weathered regions, suggesting that U precipitated from the groundwater after pyrite deposition. Numerous scans performed in additional clay matrix areas did not detect U, indicating that if U is present throughout the matrix, its concentration is too low for detection by the EBMA technique.

All results presented previously were derived from surfaces generated by the first grinding and polishing sequence. Only one area was examined in detail after the second sequence since hot spots in the radioluxographs exhibited mineralogies similar to those already investigated. This region, designated B3 in Figure 1a and presented in Figures 3a and 3b, differs from those discussed previously because no pyrite is present. The morphology of the phase throughout which U is distributed is similar to that shown in Figure 2c (at 2G) and is indicative of biotite. Both elemental maps and EDAX analyses showed an association between U, Si, Aℓ, K, Fe, Mg, Ti and Ca, but attempts to delineate the specific morphology of the U-occurrence with SEM were unsuccessful. No discrete U-rich precipitates were identified, but several factors lead to the suggestion that the U is present in a layered morphology sandwiched between the biotite "leaves". Comparison of Ca and P elemental maps indicated localized regions rich in calcium phosphate.

Observations on the processed samples of Lucky Mc ore were restricted to optical and scanning electron microscopy, and evaluation by the former method again revealed that most of the hot spots delineated by the radioluxographs were associated with pyrite, often in close proimity to biotite. SEM/EDAX analyses of one such area, identified in the radioluxograph in Figure 1c, showed it to be both morphologically and mineralogically identical to that represented in Figures 2a through 2c. No large U-rich precipitates were observed, but the U is believed to be present in a fine-grained phase closely intermixed with biotite as EDAX spot analyses yielded compositions representative of this mineral (plus Ca) in addition to U.

SEM/EDAX analyses performed on coalified wood fragments selected from Lucky Mc ore revealed that some had a considerable amount of pyrite, usually with cuboidal morphology, distributed on the outer surfaces, whereas others had only clay (despite having been wet-sieved). The U appeared to be uniformly distributed throughout the coalified wood and no discrete U-rich phase was identified.

C. EBMA and SEM Analyses of U-rich Zones in Unleached Conquista Ore

Evaluation of the uranium mineralogy in these ore samples with EBMA and SEM/EDAX analyses proved difficult because most of the α-active material (and thus, uranium) was uniformly distributed throughout the matrix, and relatively few spots of high α-activity were identified. Two areas examined in detail are represented by Figures 3c throug 3f. The

UM_α distribution shown in Figure 3d was obtained within the clay region shown in Figure 3c and the long (9 min. 31 sec.) scan time required indicates the relatively low level of uranium present (compare this with the 1 min. 54 sec. scan time required for the Lucky Mc specimens). This region is a small clay gall (probably montmorillonite) containing Si, Al, Ca, Mg and K, with small pyrite grains distributed throughout. The U elemental map suggests a background distribution in the clay with some, more localized, higher concentrations. Elemental associations of uranium could not be established and no discrete precipitates were resolved with SEM. Thus, it is suggested that the U is probably adsorbed on the clay.

Two mineralized feldspar grains were evaluated, one of which, designated Al in Figure 1b, is shown in Figure 3e. The uranium is distributed throughout a weathered region within the feldspar which contains clay (probably a calcic-montmorillonite) plus localized areas rich in pyrite, anatase and calcium phosphate. SEM/EDAX analyses were not performed, and the morphology of the U-rich phase was not specifically identified. The second mineralized feldspar grain exhibited a lower level of U but had an otherwise similar mineralogy.

Because of the nature of the uranium distribution in the Conquista ore specimens, additional 2θ scans were performed in the bulk clay matrix. Of 20 areas examined in the specimen of Figure 1b, five were selected for a recorded 2θ-scan because the analyses yielded some counts under the UM_α peak above the normal background level. U was positively identified at two points and was possibly present at the remaining three. Thus, the analyses indicate that U is indeed distributed at a low level throughout the clay matrix as was suggested by the radioluxographs.

D. EBMA and SEM Analyses of Acid-leached Lucky Mc Ore

Several areas associated with hot spots on the radioluxographs were analyzed by use of EBMA for the presence of U, but none was identified. Thus, it was concluded that the residual uranium was too low in concentration to be detected by the EBMA technique.

Another important feature of the ore was characterized - namely the precipitation of gypsum believed to result from the dissolution of calcite. Figure 4 presents an example of a gypsum-rich matrix area (which also contains clay and mounting plastic) between quartz clastics. The SEM micrograph (Figure 4b, reveals the fine-grained nature of the gypsum and the EBMA maps show that not all the Ca is associated with S indicating the presence of residual calcite.

SUMMARY AND CONCLUSIONS

In the Lucky Mc ore, the predominant mode of U-occurrence was in localized biotite regions, often associated with pyrite. Additional modes of mineralization observed were a U-rich phase closely intermixed with pyrite cement, in clay within weathered feldspar, and in coalified wood. Radioluxographs revealed a low background activity with localized hot spots corresponding to the biotite and other U-rich regions. Alpha-activity distributions were similar for all samples of as-received and processed ore indicating that the latter was representative of the former. No U was detected in the bulk clay matrix nor in acid-leached ore. Gypsum precipitation was identified in several matrix areas after acid-leaching.

In the Conquista ore, the predominant mode of U occurrence was in low concentrations in the clay matrix. Uranium was also observed in clay regions within weathered feldspar and in a clay gall. Radioluxographs showed an α-activity distribution distinctly different from that observed in the Lucky Mc; namely, a relatively high, uniform background activity with few localized hot spots. Alpha-maps from processed ore showed the same high background but no hot spots indicating disaggregation of these regions.

Prediction of the relative ore leachabilities in a simulated in situ leach is difficult because of the numerous factors involved, such as the type of lixivium utilized, ore permeability and oxidation state, in addition to uranium mineralogy. However, a comparison of the Lucky Mc and Conquista ores suggested that, for a given lixivium, the former should yield a faster and higher recovery rate because of the availability of the U to the leachant (provided both ores exhibited similar pH and oxidation characteristics). Since the Conquista ore has a higher fines (clay) content[4], and most of the uranium is associated with the clay, it was anticipated that the recovery of U would be more difficult because of permeability problems. Laboratory column-leach experiments did yield lower recovery values for this ore compared to Lucky Mc (for both alkaline and acid lixivia),but the reasons for this are believed to be complex and not limited simply to mineralogical differences. Nevertheless, it is apparent that EBMA and SEM analyses of uranium ores do yield information valuable to the understanding of leaching phenomena.

ACKNOWLEDGEMENTS

This work was performed under U.S. Bureau of Mines Contract #HO262004 in association with D. C. Seidel, Technical Project Officer and W. C. Case, Contract Administrator.

The author wishes to thank C. W. Beck for preparing the mounted specimens, R. W. Palmquist for obtaining the EBMA results and C. J. Spengler for helpful discussion of the results.

REFERENCES

1. P. S. Sundar, "In-Situ Leaching of Uranium Ores - Phases I Through III", W R&D Report #77-9E3-INSIT-R4, June 1977.

2. C. J. Spengler and Susan Wood, "Development of Radioluxography for the Mapping of α-activity in Uranium Ores", to be published.

3. R. E. Grim, "Clay Mineralogy", McGraw Hill (1968), p. 94.

4. Susan Wood, "Characterization of Unleached Uranium Ores from the Conquista Project in Texas and the Lucky Mc Mine in the Shirley Basin of Wyoming", W R&D Report #78-9D2-INSIT-R1, April 1978.

5. Ref. 3, p. 204.

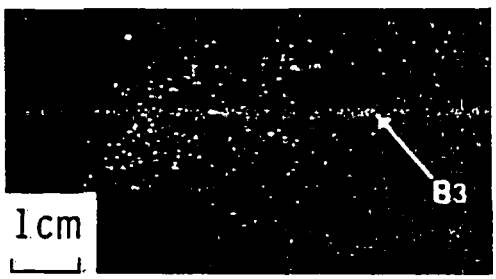

(a) As-Received Sample of Lucky Mc Ore
73 hr. 15 min. Exposure

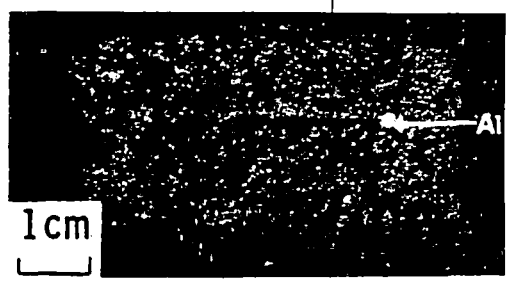

(b) As-Received Sample of Conquista Ore
73 hr. Exposure

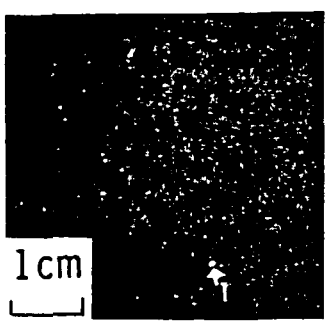

(c) Processed Sample of Lucky Mc Ore
73 hr. 15 min. Exposure

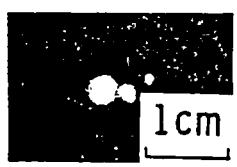

(d) Lucky Mc Organic Material
90 hr. Exposure

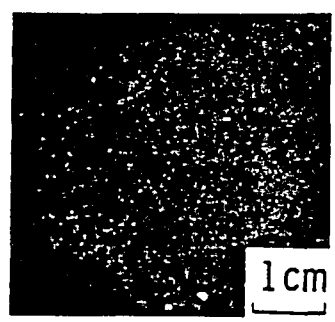

(e) Processed Sample of Conquista Ore.
73 hr. 15 min. Exposure

(f) Lucky Mc Sample After H_2SO_4 Leach

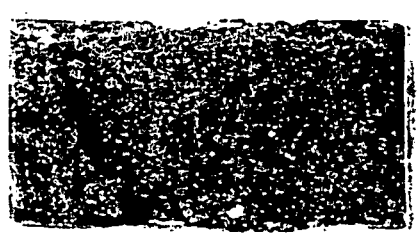

(g) Macro-Optical of a Typical Conquista Sample

Fig. 1 - Radioluxographs and a macro-optical of mounted uranium ore specimens.

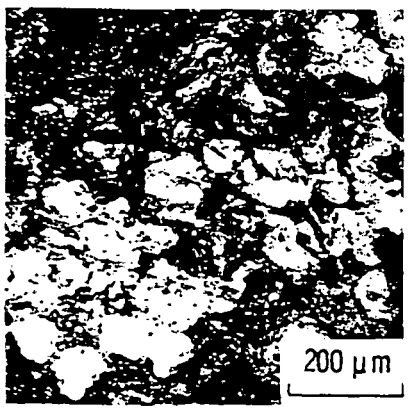

(a) Pyrite - Matrix Aggregate

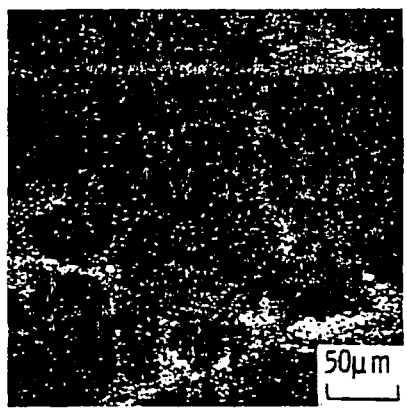

(b) U M_α Distribution in Part of (a). 1 min. 54 sec. Scan

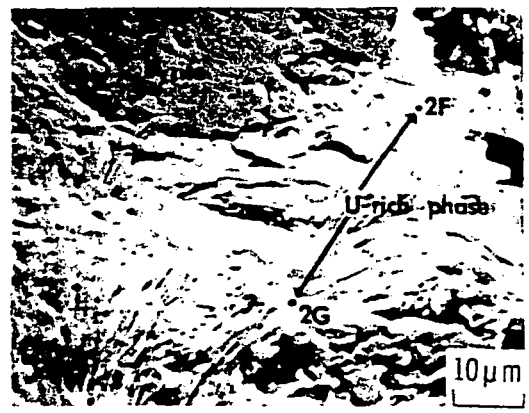

(c) Morphology of Matrix in (a) and (b)

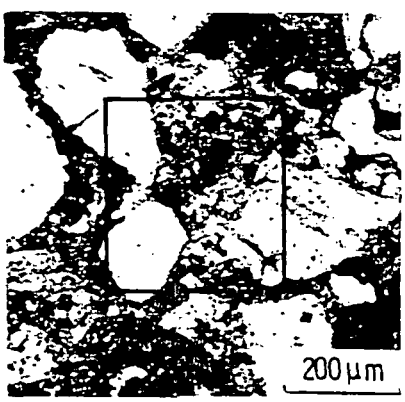

(d) Matrix With Quartz Grains

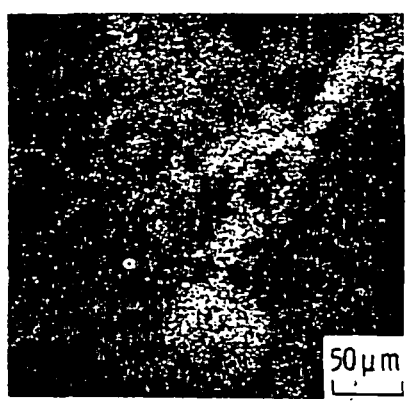

(e) UM_α Distribution from Center of (d). 1 min. 54 sec. Scan

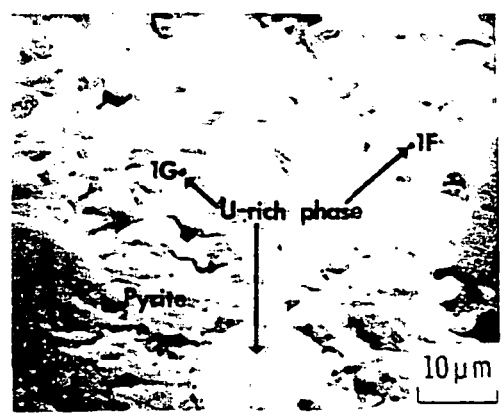

(f) Morphology of Matrix in (d) and (e)

Fig. 2 - U-rich matrix regions in Lucky Mc ore.

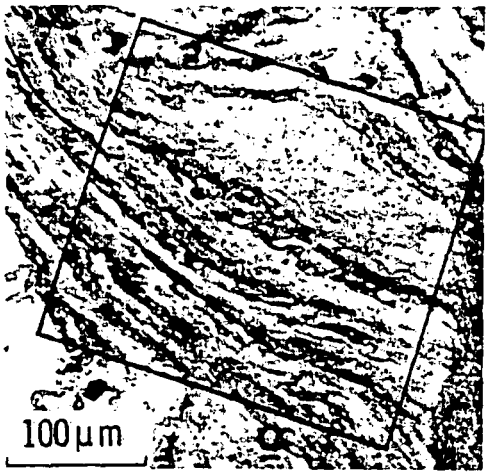

(a) Biotite in Lucky Mc Ore

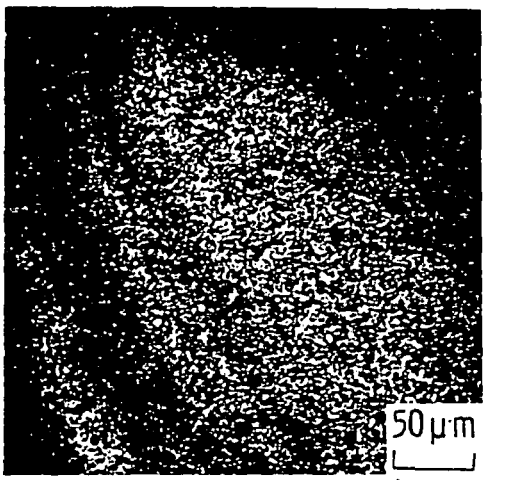

(b) UM_{α} Distribution in Outlined Area of (a). 1 min. 54 sec. Scan

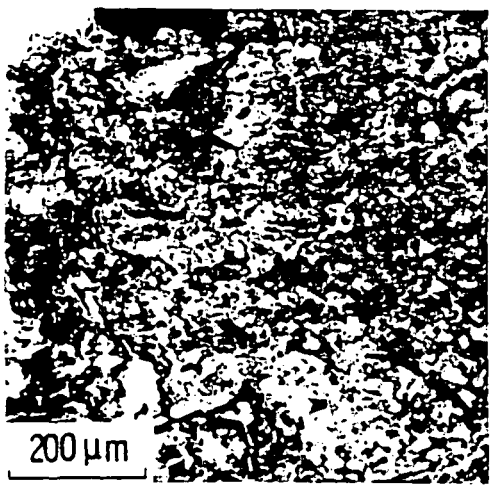

(c) U-rich Clay in Conquista Ore

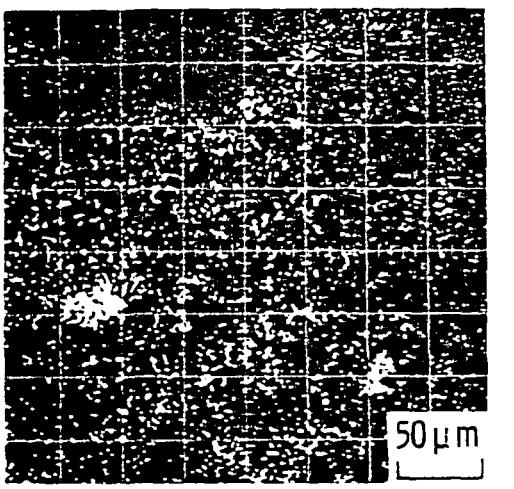

(d) UM_{α} Distribution in Part of Area in (c). 9 min. 31 sec. Scan

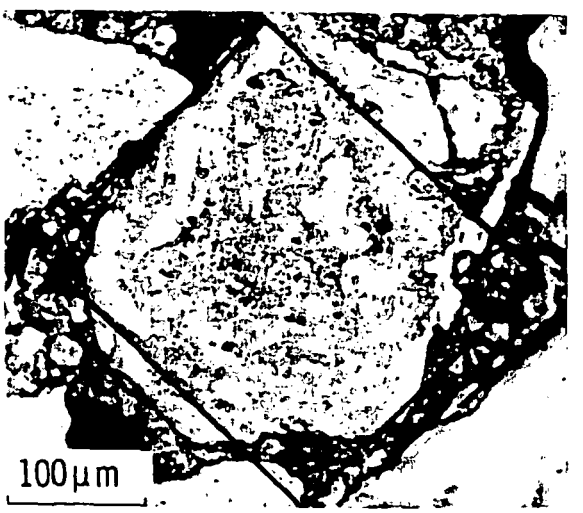

(e) U-rich Feldspar in Conquista Ore

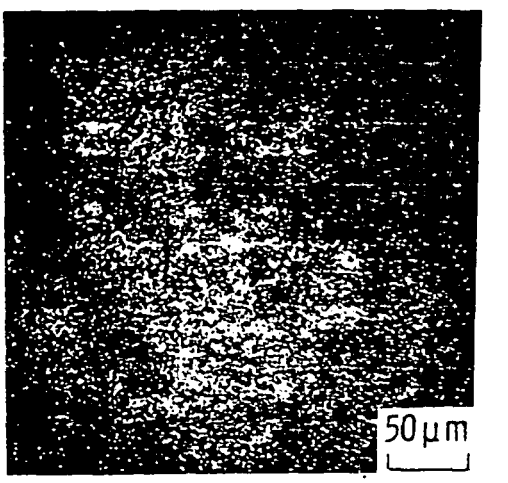

(f) UM_{α} Distribution in Outlined Area of (e). 9 min. 31 sec. Scan

Fig. 3 - Uranium occurrences in Lucky Mc and Conquista ore samples.

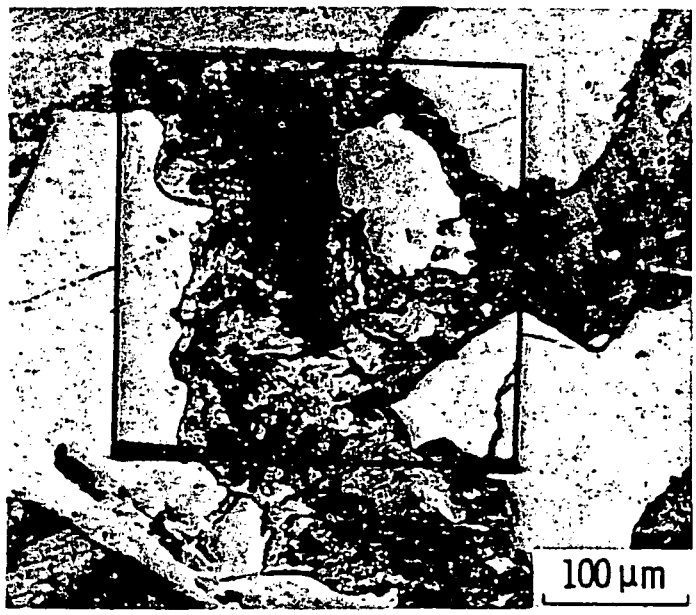

(a) Matrix Containing Gypsum

(b) Morphology of Outlined Area in (a)

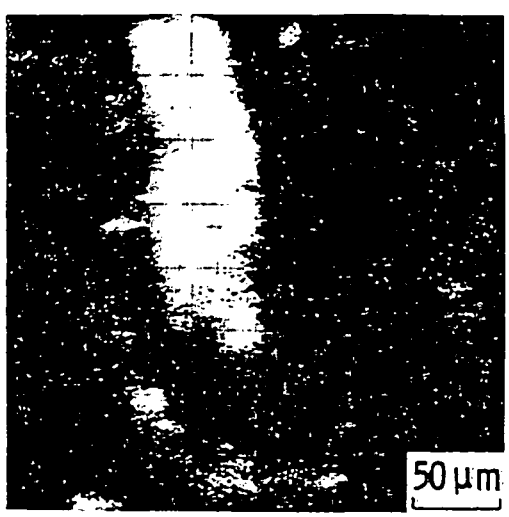

(c) Ca Kα Distribution in (a). 1 min. 54 sec. Scan

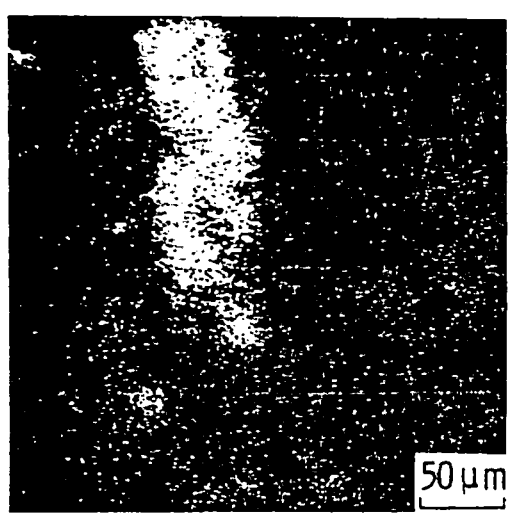

(d) SK_α Distribution in (a). 3 min. 48 sec. Scan

Fig. 4 - Matrix containing gypsum in H_2SO_4 - leached Lucky Mc ore.

IN SITU, 4(2), 111-127 (1980)

CHARACTERIZATION OF THE URANIUM OCCURRENCE IN PRE- AND POST-LEACH ORE SAMPLES FROM SANDSTONE DEPOSITS IN TEXAS & WYOMING

Susan Wood
Westinghouse R&D Center
Pittsburgh, Pennsylvania 15235

ABSTRACT

Uranium ore samples from open-pit mines in the Shirley Basin of Wyoming and in Texas are currently being utilized to simulate in situ leaching conditions in laboratory column-leach tests at the W R & D Center. Evaluation of their uranium mineralogies was achieved through analysis of mounted and polished specimens with the electron beam microanalyzer and scanning electron microscope, after first delineating α-active regions by radioluxography. The two ores exhibited both different uranium distributions and mineralogies, but these characteristics were similar for as-received and processed material from each site. No uranium was detected in acid-leached Wyoming ore.

INTRODUCTION

In-situ leaching has become a very attractive method for recovering uranium from epigenetic sandstone deposits because of both the relatively low capital costs involved and the amenability of such ore bodies to this leaching technique. To improve and further the understanding of the leaching of uranium by this method, laboratory simulation, utilizing column-leaching apparatus, is currently being exploited at the W R & D Center.[1,2] Although

the ores used in these experiments originated in sandstone deposits in Texas and Wyoming, they were obtained from open-pit sites rather than the deeper mineralized roll-fronts normally subjected to in situ mining. Furthermore, the ore was processed through drying, blending and column-packing operations before being leached.

This paper describes the results of a characterization study designed to determine if the uranium distribution in the packed column truly represented that in the original ore body, and if correlations can be made between uranium mineralogy and the overall uranium recovery obtained via column-leaching. In addition to delineating the uranium mineralogy of both the virgin Texas and Wyoming ores, the uranium distributions in as-received and processed ores were evaluated using a radioluxograph technique. The α-maps thus obtained were also utilized to identify U-rich zones for subsequent examination by use of electron beam microanalysis (EBMA) and scanning electron microscopy (SEM) for the delineation of uranium mineralogy. These more sophisticated analytical techniques are now being more widely used for this type of application,[3,4] and were necessitated in the present study because the low uranium content of the ores prohibited evaluation of mineralogies by petrography.

However, petrography did detail some of the basic lithology. The Texas ore was characterized as volcanic in nature and classified as a fine-grained, moderately sorted, feldspathic litharenite.[1] The Wyoming ore was a coarse-grained, poorly sorted lithic arkose in which the rock fragments were predominantly mud balls. Both samples were reduced, containing pyrite, but little iron oxides.

EXPERIMENTAL PROCEDURES

A. Selection and Packaging of Ore

Ore samples were obtained from the Lucky Mc mine in the Shirley Basin of Wyoming and the Conquista Project near Falls City, Texas. Conquista ore came from the Rosenblock formation which is a channel

deposit with a roll character. Material for the pre-leach characterization study was selected from currently-mined areas in the open-pits to be within a grade of 0.05-0.12 Wt% U_3O_8 (as determined by on-site γ-logging techniques). Some of the ore, used only for characterization purposes, was sealed under nitrogen at the mine site, while a larger, bulk sample was merely packaged in polyethylene. This latter material was subsequently air-dried and processed for column leach studies.

B. Preparation of Mounted Specimens

In general, both the Texan and Wyoming ores are poorly consolidated, which necessitated packing the as-received material in small cardboard boxes for mounting purposes. Because the Lucky Mc (Wyoming) ore also contained pieces (with a maximum dimension of ~4 cm) which retained their competency, several of these were also selected for mounting. In order to obtain representative sampling, material was selected on a random basis from the nitrogen-packaged ores to yield at least 6 specimen mounts. Samples were oven-dried for 24 hrs. at 50°C before vacuum-impregnating with Spurr, a low viscosity resin cured by baking at 50°C for approximately 16 hrs. Specimens were subsequently ground through 600 grit SiC and polished to 0.5 μm diamond using water as the vehicle. After obtaining both radioluxographs (the procedure for which is discussed in the next section) and mineralogical analyses, a 3 mm section was cut from the polished face of each mount, and all specimens were re-ground and polished at this new plane after reimpregnating the surfaces with Spurr. Additional EBMA and SEM studies were subsequently performed at the new sample depths.

Processed (i.e. air-dried, crushed to -10 m and blended) samples were prepared in a similar manner except rubber molds were utilized to reduce sample size because of the granular nature of the material. Problems were encountered in obtaining acceptable mounts and those finally selected for examination had experienced

some pull-out of grains and matrix material during grinding and polishing operations due to poor consolidation of the mounting medium - a problem believed to result from the granular nature of the dry ore. However, the surface condition of the final mounts proved adequate for the characterization studies.

Acid-leached, processed material was received in a moist condition which permitted a mode of preparation identical to that utilized for the as-received ore. Samples were selected from three sections within the column, and no significant pull-out was observed during grinding and polishing operations.

C. Radioluxographs

Radioluxographs, or α-maps, were obtained from all polished sample surfaces prior to their examination with EBMA or SEM. The technique utilizes a ZnS-CdS/Ag activated phosphor which is sandwiched between Type 57 film and the specimen for exposure times of 70 to 73 hrs. Alpha-maps were also obtained from hand-picked pieces of coalified material. These images were used to interpret the distribution of α-emitters on the sample surfaces and to delineate "hot spots," or particularly radioactive zones, for investigation with EBMA and SEM.

D. EBMA and SEM Analyses

All EBMA analyses utilized a MAC 400 microprobe and the SEM was performed on a Cambridge Stereoscan S4.A 20 KeV accelerating voltage was used on both instruments. Elemental distributions, obtained by the EBMA mapping mode, were used to characterize U-rich zones in virgin samples of Texas and Wyoming ore. Non U-rich matrix regions were also investigated - in both virgin and leached material. Most areas were subsequently examined with the SEM to identify the morphology of the U-rich phases (in virgin ore) or reaction products (in leached ore). Energy dispersive X-ray (EDAX) analyses were performed concurrently and use of standard operating conditions on

the SEM permitted composition comparisons both within one region and from one region to another.

Although most EBMA studies were performed using the mapping mode, 2 θ scans were also performed in the matrices of both Conquista and Lucky Mc ores utilizing a beam diameter of ∿20 μm. The 2 θ scans are significantly more sensitive than the mapping mode (by at least a factor of 10) for the detection of uranium.

RESULTS

A. Radioluxographs

Examples of radioluxographs obtained from the various types of ore samples are given in Figure 1, together with a macro photograph of a typical mounted specimen. Those areas specifically delineated are areas examined in more detail with EBMA and SEM. The radioluxograph or α-map is obtained by permitting the α-particles generated within the ore sample surface to interact with the phosphor, generating photons of the correct wavelength for exposure of photographic film. A subsequent print of the image is termed a radioluxograph. However, it should be noted that the phosphor does not selectively interact only with α-particles generated by the decay of ^{238}U, but will also produce photons due to all α-particles generated by the decay sequence, including ^{226}Ra. It is now known that ^{226}Ra decay, contributes a significant amount of α-activity and thus, α-maps can only be utilized to monitor U distributions for samples in which the U and Ra are still closely associated and there has been no migration of U.

Figure 1a shows a typical radioluxograph obtained from an unprocessed Lucky Mc specimen. There is a weak background distribution of α-activity plus localized "hot spots," or more radioactive zones. Both disaggregated and competent samples exhibited similar distributions which did not change as a function of depth in the bulk specimen. Comparison of Figure 1a with Figure 1c, which gives a

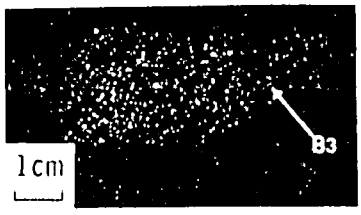

(a) As-Received Sample of Lucky Mc Ore
73 hr. 15 min. Exposure

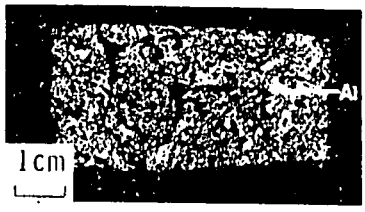

(b) As-Received Sample of Conquista Ore
73 hr. Exposure

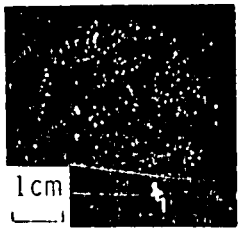

(c) Processed Sample of Lucky Mc Ore
73 hr. 15 min. Exposure

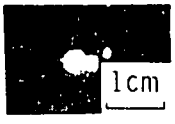

(d) Lucky Mc Organic Material
90 hr. Exposure

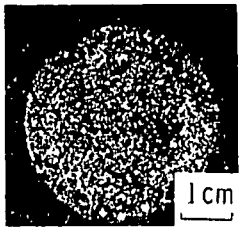

(e) Processed Sample of Conquista Ore.
73 hr. 15 min. Exposure

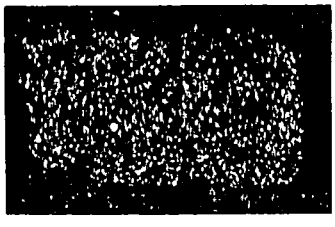

(f) Lucky Mc Sample After H_2SO_4 Leach

(g) Macro-Photograph of a Typical Conquista Sample Mount

FIG. 1 - Radioluxographs and a macro-photograph of mounted uranium ore specimens.

representative α-map from a mount of processed ore, reveals comparable α-activities in the two types of specimens with, perhaps, fewer "hot spots" after processing. All processed Lucky Mc samples were also observed to exhibit an unchanging α-distribution as a function of depth.

Figures 1b and 1e show typical radioluxographs from as-received and processed samples of Conquista ore, respectively. Similar α-activity distributions are again observed before and after the blending operation, but it is apparent that they differ from those in the Lucky Mc ore. There is a higher, more uniform "background" activity with fewer localized hot spots in the Conquista ore; those regions within the specimen boundaries which yielded no exposure on the radioluxographs correspond to zones of resin mounting medium in the sample. Neither type of Conquista specimen exhibited changes in the α-activity distribution as a function of depth.

Additional radioluxographs are presented from coalified wood fragments and H_2SO_4-leached Lucky Mc material (Figures 1d and 1f). The former shows a relatively high overall activity with respect to the bulk samples, even after consideration of the different exposure times (note that the exposed areas on the film are actually slightly greater than the true lateral dimensions of the coalified wood fragments). The leached ore compares well with the pre-leached material in Figures 1a and 1c (exposure time for the leached specimen was 72 hr.). Despite the apparent radioactivity of the organic material, it cannot represent a major mode of uranium occurrence because coalified wood was identified only as a minor constituent in these ore samples. The activity exhibited by the leached material is generated primarily by ^{226}Ra decay, and an independent γ-spectroscopy measurement yielded a Ra to U ratio of 3.8±1 (in pci/gm) in one of the mounted specimens. Before leaching this ratio was ∿1.0 (in pci/gm) in the typical mounted specimen.

B. EBMA and SEM Analyses of U-rich Zones in Unleached Lucky Mc Ore

Most investigations were performed in regions within samples which had retained their competency, and thus the original mineral assemblages present in the ore body are still intact. Preliminary optical microscopy observations revealed that most radioactive zones (i.e. hot spots) on the radioluxographs were associated with pyrite, and examples of several different types of such regions are shown in Figures 2 and 3.

The first region (Figures 2a through e) is an assemblage of small pyrite grains surrounded by U-rich matrix material. An EBMA map (Figure 2b) gives the U-distribution within part of the pyrite-matrix aggregate shown by the reflected light micrograph in Figure 2a (note the differing magnifications of 2a and 2b). The SEM micrograph in Figure 2c presents the typical layered morphology of the U-rich phase, which, in addition to U, also contains Si, Aℓ, K, Ca, Fe and Mg - a composition suggestive of a U-rich clay. EDAX analyses in the matrix region (at 2F and 2G, for example) yield U as the most abundant element present, and close inspection reveals that the structure at 2F is actually a relatively large U-rich precipitate >15 μm across, while the morphology and composition of 2G suggest a micaceous mineral such as biotite (nominal composition $(OH)_4\ K_2\ (Si_6Aℓ_2)(Mg,\ Fe)_6\ O_{20}$).[5] Although biotite does not contain Ca, this element is believed to be incorporated in the U-rich mineral since EDAX analyses of the larger U-rich zones (e.g. 2F) yielded higher Ca contents than did the bulk matrix.

A second matrix area, represented by Figures 2d through 2f, reveals a U-rich phase in close proximity to pyrite, both of which are cementing quartz clastics. The EBMA UMα scan gives the U-distribution throughout the matrix within the outlined region in Figure 2d (reflected light micrograph) while the morphology of the interrelated phases is revealed by the higher magnification SEM micrograph in Figure 2f. EDAX analyses at 1F and 1G show a definite U, Si, Ca and P association (with U and Si present as the most

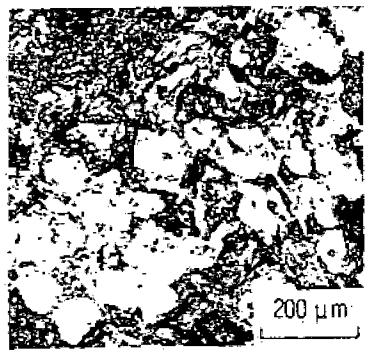

(a) Pyrite - Matrix Aggregate

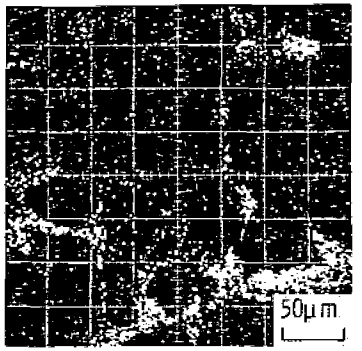

(b) UM_{α} Distribution in Part of (a). 1 min. 54 sec. Scan

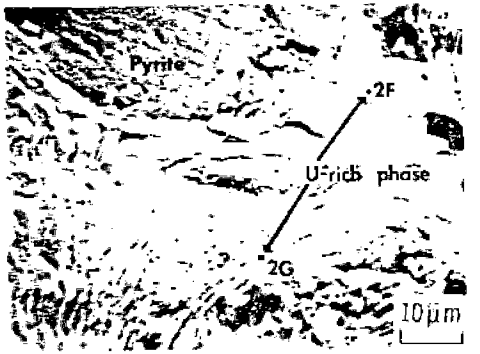

(c) Morphology of Matrix in (a) and (b)

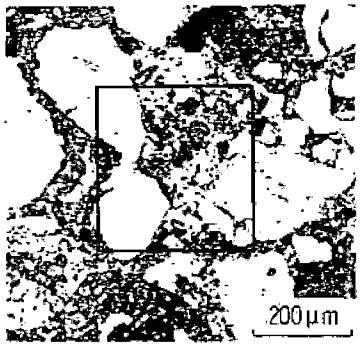

(d) Matrix With Quartz Grains

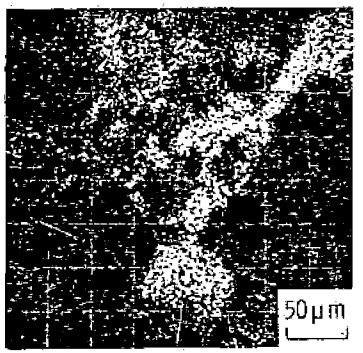

(e) UM_{α} Distribution From Center of (d). 1 min. 54 sec. Scan

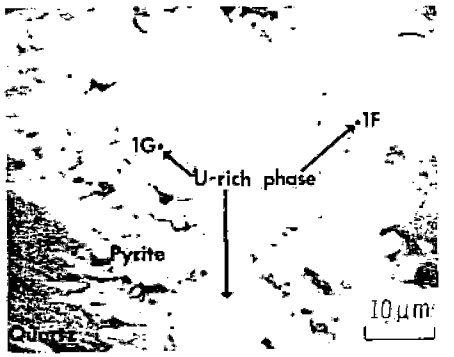

(f) Morphology of Matrix in (d) and (e)

FIG. 2 - U-rich matrix regions in Lucky Mc ore.

abundant constituents). In contrast, the lower magnification EBMA elemental maps for Ca, K, Al, Si and Fe indicated that they were all associated with U, but it is believed that these analyses simply indicate the presence of matrix clay in addition to pyrite and an uranium phase. (Phosphorus was not scanned by EBMA). No V was detected in the area, and localized Ti concentrations suggested anatase (TiO_2). The U-rich phase is believed to be either coffinite of uraninite: the Ca-P association probably indicates apatite. Attempts to identify the uranium mineral by X-ray diffraction were unsuccessful because the volume which could be extracted from the matrix was insufficient to yield a good X-ray pattern.

Additional U-rich regions whose mineralogy was similar to the two areas discussed previously were also examined in detail with EBMA and SEM and showed similar elemental associations. Pyrite was always a common denominator and fine-grained calcite was present in some examples. Large U-rich precipitates (such as those in Figures 2c and 2f) were not always identified, but the existence of a separate U-rich phase was usually established by SEM/EDAX analyses, particularly in biotite regions where the low cation exchange capacity[6] precludes the possibility of having high concentrations of adsorbed uranium.

A third mode of U-occurrence associated with pyrite (for which micrographs are not presented) was observed in weathered pyrite cement surrounding quartz clastics. The uranium was associated with montmorillonite clay and observed only in weathered regions, suggesting that U precipitated from the groundwater after pyrite deposition. Numerous scans performed in additional clay matrix areas did not detect U, indicating that if U is present throughout the matrix, its concentration is too low for detection by the EBMA technique.

All results presented previously were derived from surfaces generated by the first grinding and polishing sequence. Only one area was examined in detail after the second sequence since hot

spots in the radioluxographs exhibited mineralogies similar to those already investigated. This region, designated B3 in Figure 1a and presented in Figures 3a and 3b, differs from those discussed previously because no pyrite is present. The morphology of the phase throughout which U is distributed is similar to that shown in Figure 2c (at 2G) and is indicative of biotite. Both elemental maps and EDAX analyses showed an association between U, Si, Al, K, Fe, Mg, Ti and Ca, but attempts to delineate the specific morphology of the U-occurrence with SEM were unsuccessful. No discrete U-rich precipitates were identified, but several factors lead to the suggestion that the U is present in a layered morphology sandwiched between the biotite "leaves." Comparison of Ca and P elemental maps indicated localized regions rich in calcium phosphate (suggesting apatite).

Observations on the processed samples of Lucky Mc ore were restricted to optical and scanning electron microscopy, and evaluation by the former method again revealed that most of the hot spots delineated by the radioluxographs were associated with pyrite, often in close proximity to biotite. SEM/EDAX analyses of one such area, identified in the radioluxograph in Figure 1c, showed it to be both morphologically and mineralogically identical to that represented in Figures 2a through 2c. No large U-rich precipitates were observed, but the U is believed to be present in a fine-grained phase closely intermixed with biotite as EDAX spot analyses yielded compositions representative of this mineral (plus Ca) in addition to U.

SEM/EDAX analyses performed on coalified wood fragments selected from Lucky Mc Ore revealed that some had a considerable amount of pyrite, usually with cuboidal morphology, distributed on the outer surfaces, whereas others had only clay (despite having been wet-sieved). The U appeared to be uniformly distributed throughout the coalified wood and no discrete U-rich phase was identified.

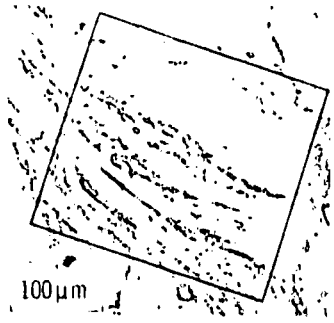

(a) Biotite in Lucky Mc Ore

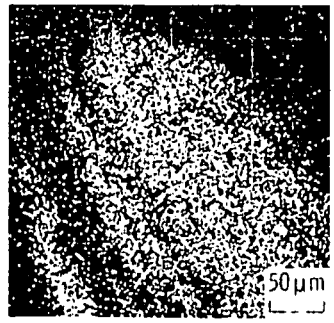

(b) UM_α Distribution in Outlined Area of (a). 1 min. 54 sec. Scan

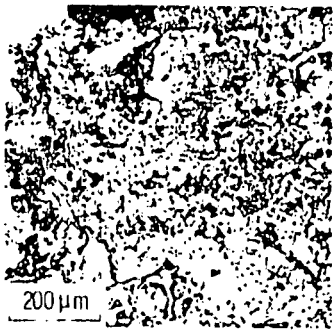

(c) U-rich Clay in Conquista Ore

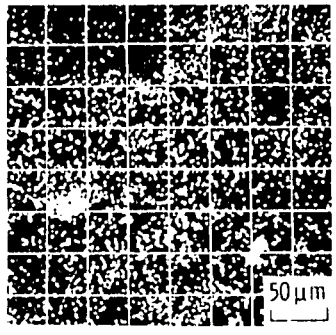

(d) UM_α Distribution in Part of Area in (c). 9 min. 31 sec. Scan

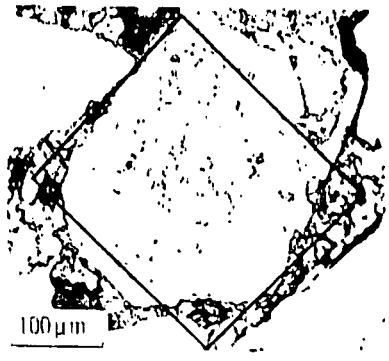

(e) U-rich Feldspar in Conquista Ore

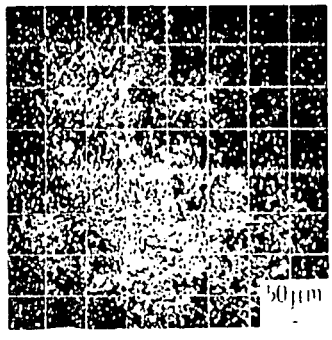

(f) UM_α Distribution in Outlined Area of (e). 9 min. 31 sec. Scan

FIG. 3 - Uranium occurrences in Lucky Mc and Conquista ore samples.

C. EBMA and SEM Analyses of U-rich Zones in Unleached Conquista Ore

Evaluation of the uranium mineralogy in these ore samples with EBMA and SEM/EDAX analyses proved difficult because most of the α-active material (and thus, uranium) was uniformly distributed throughout the matrix, and relatively few spots of high α-activity were identified. Two areas examined in detail are represented by Figures 3c through 3f (3c and 3e are reflected light micrographs). The UMα distribution shown in Figure 3d was obtained within the clay region shown in Figure 3c and the long (9 min. 31 sec.) scan time required indicates the relatively low level of uranium present (compare this with the 1 min. 54 sec. scan time required for the Lucky Mc specimens). This region is a small clay gall (probably smectite) containing Si, Al, Ca, Mg and K, with small pyrite grains distributed throughout. The U elemental map suggests a background distribution in the clay with some, more localized, higher concentrations. Elemental associations of uranium could not be established and no discrete precipitates were resolved with SEM. Thus, it is suggested that the U is probably adsorbed on the clay.

Two mineralized feldspar grains were evaluated, one of which, designated A1 in Figure 1b, is shown in Figure 3e. The uranium is distributed throughout a weathered region within the feldspar which contains clay (probably a calcic-montmorillonite) plus localized areas rich in pyrite, anatase and calcium phosphate. SEM/EDAX analyses were not performed, and the morphology of the U-rich phase was not specifically identified. The second mineralized feldspar grain exhibited a lower level of U but had an otherwise similar mineralogy.

Because of the nature of the uranium distribution in the Conquista ore specimens, additional 2 θ scans were performed in the bulk clay matrix. Of 20 areas examined in the specimen of Figure 1b, five were selected for a recorded 2 θ-scan because the analyses yielded some counts under the UMα peak above the normal background level. U was positively identified at two points and

was possibly present at the remaining three. Thus, the analyses indicate that U is indeed distributed at a low level throughout the clay matrix as was suggested by the radioluxographs.

D. EBMA and SEM Analysis of Acid-leached Lucky Mc Ore

Several areas associated with hot spots on the radioluxographs were analyzed by use of EBMA for the presence of U, but none was identified. Thus, it was concluded that the residual uranium was too low in concentration to be detected by the EBMA technique.

Another important feature of the ore was characterized - namely the precipitation of gypsum believed to result from the dissolution of calcite. Figure 4 presents an example of a gypsum-rich matrix area (which also contains clay and mounting plastic) between quartz clastics. The SEM micrograph (Figure 4b) reveals the fine-grained nature of the gypsum and the EBMA maps show that not all the Ca is associated with S indicating the presence of residual calcite. Figure 4a is a reflected light optical micrograph.

SUMMARY AND CONCLUSIONS

In the Lucky Mc ore, the predominant mode of U-occurrence was in localized biotite regions, often associated with pyrite. Additional modes of mineralization observed were a U-rich phase closely intermixed with pyrite cement, in clay within weathered feldspar, and in coalified wood. Radioluxographs revealed a low background activity with localized hot spots corresponding to the biotite and other U-rich regions. Since the α-activity distributions were similar for all samples of as-received and processed ore, it was deduced that the uranium distribution after processing was indeed representative of that in the original ore body. No U was detected in the bulk clay matrix, nor in acid-leached ore. Gypsum precipitation was identified in several matrix areas after acid-leaching.

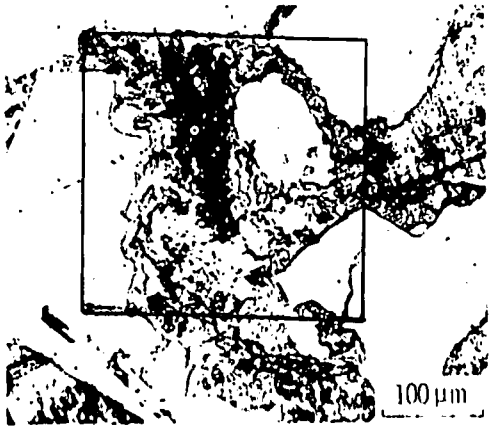

(a) Matrix Containing Gypsum

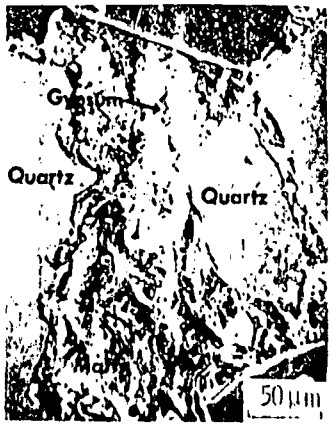

(b) Morphology of Outlined Area in (a)

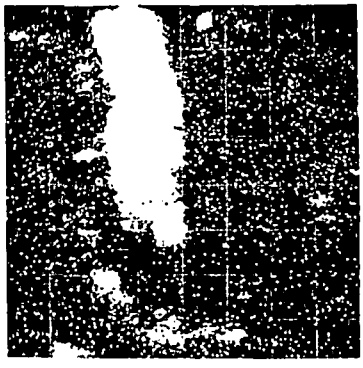

(c) Ca Kα Distribution in (a). 1 min. 54 sec. Scan

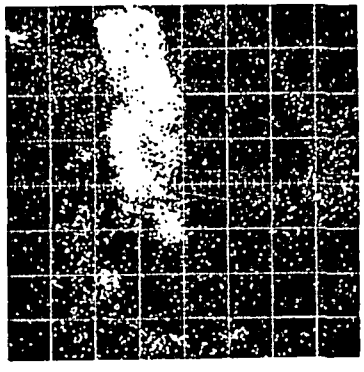

(d) SK_α Distribution in (a). 3 min. 48 sec. Scan

FIG. 4 - Matrix containing gypsum in H_2SO_4-leached Lucky Mc ore.

In the Conquista ore, the predominant mode of U occurrence was in low concentrations in the clay matrix. Uranium was also observed in clay regions within weathered feldspar, and in a clay gall. Radioluxographs showed an α-activity distribution distinctly different from that observed in the Lucky Mc; namely, a relatively high, uniform background activity with few localized hot spots. Alpha-maps from processed ore showed the same high background, but no hot spots, indicating that these regions had been disaggregated.

However, since these hot spots were only a minor source of activity (and thus, uranium), it was concluded that the processed material used for column leaching was representative of the virgin ore. A further conclusion, pertaining specifically to the α-mapping technique, is that this is a good method for assessing and comparing uranium distributions, provided U and Ra are close to equilibrium.

Prediction of the relative ore leachabilities in a simulated in situ leach is difficult because of the numerous factors involved, such as the type of lixivium utilized, ore permeability and oxidation state, in addition to uranium mineralogy. However, the above mineralogical comparison of Lucky Mc and Conquista ores suggests that, for a given lixivium, the former should yield a higher and faster recovery because of the availability of the U to the leachant (provided both ores exhibited similar pH and oxidation characteristics). Since the Conquista ore has a higher clay content,[2] and most of the uranium is intimately associated with the clay, we anticipated that the recovery of U would be more difficult because of permeability problems which would limit access of the leachant to the U. As shown in Table 1, laboratory column-leach experiments did yield lower recovery values for this ore compared to Lucky Mc for both carbonate and acid lixivia, in addition to deionized water. (More

TABLE 1

Summary of Overall Uranium Recovery Values*

Ore	Lixivium	Overall Uranium Recovery, % (Based on lixivia analyses)
Lucky Mc	De-ionized water	62.89
Conquista	"	57.55
Lucky Mc	1.0 g/l NH_4HCO_3/0.5 g/l H_2O_2	86.7
Conquista	"	55.34
Lucky Mc	Sulfuric acid, pH = 1.0	89.24
Conquista	"	75.88

*Obtained from Reference 1.

specific details of the testing procedures and results can be obtained from reference 1.) Although these results were not entirely due to differences in uranium mineralogy, it is believed that this did play a major role. Thus, it is apparent that EBMA and SEM analyses of uranium ores can yield information valuable to the understanding of leaching phenomena, particularly for low grade uranium ores (~0.1 Wt% U_3O_8) whose mineralogy cannot be determined by petrographic techniques.

ACKNOWLEDGEMENTS

This work was performed under U.S. Bureau of Mines Contract #H0262004 in association with D. C. Seidel, Technical Project Officer and W. C. Case, Contract Administrator.

The author wishes to thank C. W. Beck for preparing the mounted specimens, R. W. Palmquist for obtaining the EBMA results and C. J. Spengler for helpful discussion of the results.

REFERENCES

1. P. S. Sundar, "In-situ Leaching Studies of Uranium Ores - Phases I through III," June 1977, NTIS #PB272-717/AS.

2. D. C. Grant, "In-situ Leaching Studies of Uranium Ores - Phase IV," November 1978, U.S. Bureau of Mines Open File #OFR-52-79.

3. D. W. Rhett, "Mechanism of Uranium Retention in Intractable Uranium Ores from Northwestern New Mexico," J. Of Metals, Vol. 31, 1979, p. 45.

4. R. L. Reynolds, M. B. Goldhaber and R. I. Grauch, "Uranium Associated with Iron Titanium Oxide Minerals and Their Alteration Products in a South Texas Roll-Type Deposit." Short papers of the U.S. Geological Survey, Uranium-Thorium Symposium, 1977. Geological Survey Circular 753, p. 37-39.

5. R. E. Grim, "Clay Mineralogy," 2nd edition, McGraw-Hill, New York, NY, 1968, p. 94.

6. Ibid., p. 204.

SUBJ
MNG
CPER

JUN 0 2 1981

ERRATA FOR THE DOE REPORT

The following represent recent errata entries which should be made in the report, "An Assessment of Energy Requirements in Proven and New Copper Processes." produced under contract No. EM-78-S-07-1743 New contract No. DE-AS07-78CS40132 Report No. DOE/CS/40132: — 1981

1. Page 12, Table C-4, Grand total under section 2.6 Outokumpu Flash Smelting should read 18.92; delete incorrect total 20.87.

2. Page 38, para. 1, line 1 - delete 30%, insert 15%. ---- Sentence should read: "Dump leaching accounts for some 15% of the primary copper produced in the U.S."

3. Page 357, Table 3.8-2, Step No. 2, Leach circuit, B (Process Heating Steam). Place asterisk in the 3 columns with the following note at the bottom.

*The minus 4.25 million BTU credit given under 1A represents a balance between roaster recovery and process heating steam. Items 1A and 1B combined provide the net credit indicated in 1A. This credit should be considered tentative since the sulfite reduction process has not been proven commercially.

4. Page 359, bottom of the page - Total Level 1 Energy Requirments: (Table 3.8-3) should read (Table 3.8-2); delete 35.4, insert 17.77. Total Theoretical Level 1 Requirement: delete 33.72. insert 16.09.

5. The following indicated change should be made on Page 54:

TOTAL ENERGY REQUIRED FOR COMMINUTION =

(NET CRUSHING ENERGY/ϵ_C)

+β(NET BALL MILL ENERGY/ϵ_B)

+(STEEL CONSUMED AS MEDIA & LINERS)

x(ENERGY "CONTENT" OF STEEL)

+ ENERGY FOR COMMINUTION CIRCUIT AUXILIARIES

4-10-81

TABLE C-4

ENERGY (MILLION BTU/NET TON COPPER) COMPARING SIMILAR STEPS IN PYROMETALLURGICAL PROCESSES

Section	2.5	2.3a	2.3b	2.15	2.10	2.9	2.11	2.16	2.7	2.8	2.6	2.12
Process Designation	Electric Furnace Copper Smelting	Conventional Smelting, Wet Charge	Conventional Smelting, Dry Charge	Oxy-Fuel Reverberatory Smelting	Mitsubishi Continuous Smelting & Converting	Noranda Continuous Smelting	Queneau-Schuhmann Oxygen Process	Oxygen Sprinkle Smelting	INCO Flash Smelting	Top Blown Rotary Converter	Outokumpu Flash Smelting	AMAX Dead Roast – Blast Furnace
LEVEL 1												
Materials Handling:		.73	.73	.73	.66	.79	.66	.73	.73	.73	.57	
Dry or Roast:	2.67		.66	1.35	1.29	.80	1.47	1.72	1.86	1.86	1.23	1.58
Heat Recovery												-4.73
SMELTING												
Fuel		25.01	14.50	9.27	6.46	3.72		1.38		.40	.80	10.88
kWh	19.03	.64	.64	.64	1.58	1.26		.64	.05	1.16		1.27
Surplus Steam		-10.00	-4.35	-3.71	-8.00	-1.82		-1.09			3.43	-.50
CONVERTING												
kWh	2.92	1.63	1.26	1.63	1.42	.37		1.26	0.94		.64	
Fuel	3.58	.54	.32	.50	.25	.09		.23				
Slag Cleaning					1.35	1.31					1.49	
GAS CLEANING												
Hot Gas	.78	4.03	2.83	1.27	.86	.69	.13	.64	.59	.51	0.42	
Cold Gas	2.21	.25	.40	.48	.32		.05	.24	.31	.34	0.21	.84
Fugitive Emissions		3.57	3.57	3.57	.89	3.57		3.57	3.57	3.57	3.57	
Acid Plant	4.74	2.27	3.87	4.51	4.08	3.10	4.30	3.91	3.19	4.09	3.86	4.18
Water		.10	.10	.10	.10		.10	.10	.10	.10	.10	
Anode Furnace Electrorefining	5.10	5.82	5.82	5.82	5.82	5.82	5.82	5.82	5.82	5.82	5.82	6.03
TOTAL LEVEL 1	41.03	34.59	30.35	26.16	17.08	19.70	12.53	19.15	17.16	18.58	15.28	19.55
LEVEL 2												
Misc. Materials					.63	.65	2.80			0.13	.04	
Oxygen				1.88	1.29	3.17	6.70	2.71	3.53	4.74	3.04	
Electrodes	.86				0.16							
Fluxes	.12	.04	.03	.04	.06	.02	.05	.03	.02	.02	.01	.03
Water		.08	.08	.08	.08		.08	.08	.08	.08	.08	
Anode Furnace Electrorefining	.51	.47	.47	.47	.47	.47	.47	.47	.47	.02	.47	.01
TOTAL LEVEL 2	1.49	.59	.58	2.47	2.69	4.31	10.10	3.29	4.10	4.99	3.64	.04
GRAND TOTAL	42.52	35.18	30.93	28.63	19.77	24.01	22.63	22.44	21.26	23.57	18.92	19.59

1.2.5 Dump Leaching

Dump leaching accounts for some 15% of the primary copper produced in the United States. While much of this comes from the treatment of old existing low grade copper dumps, it is clear that the recovery of some of the copper content of currently mined low grade ore should be taken into consideration in the overall assessment of the energy content of domestic copper production.

For the purpose of this analysis it is assumed that all the low grade ore below the cut-off value will be systematically placed in finger dumps suitable for current acid leaching. (Refer to the mineralization model section 1.2.2.1, and Table 1.2.1.) The base condition for this analysis calls for a cut-off grade of .29% Cu, giving 30% of mineralized ore below cut-off grade sent to the leach dumps at an average value of .22% Cu.

The energy for dump leaching is predominantly required for the circulation of the leacheate solutions; this in turn is essentially a function of the lift and horizontal distance from the cementation plant to the top of the leach dumps. The following specifications are assumed:

Finger Dumps: 150' Vert x 400' flat top x 800 base.
Lift from plant to top of dump 450'
Hor. Dist. from plant to dump 5000'

Tons leached per year (TD in sect. 1.2.2.1)	= 9.0309×10^6 tons @ .22% Cu
$9.0309 \times 10^6 \times .22 \times 20$	= 39.7360×10^6 lbs Cu/year
@ 33% recovery	= 6622.667 tons/year
@ 360 days per year	= 36,792 lbs/day
Leacheate concentration .5 gr/litre	= 4.2 lbs/1000 U.S. gal.
Daily Circulation	= 8.7600×10^6 gal./day
	= 6083 gal./min.

From Ingersoll Rand Hydraulic Data Tables for 14" I.D. pipe we get:

Q	=	3077 gpm
V	=	6.42 ft/sec
H_v	=	.64 ft
H_F	=	1.58 ft/100'

Pumped Flow of barren solution

Gravity Head	=	450 ft
Spray Head	=	50 ft
Velocity Head	=	1 ft
Friction Head	=	79 ft
Fittings	=	40 ft
		620 ft

$Q = 6083 \times .13369$
$= 813\ ft^3/min$

Return flow of pregnant solution

Minm. Head for free flow = (5000 x .0158) + 1 = 80 ft.
Therefore gravity head of 300 ft will effect return flow.

TABLE 3.8-2 ENERGY REQUIREMENTS Level 1

SULFITE REDUCTION PROCESS

STEP NUMBER	PROCESS	UNIT	UNITS PER NET TON CATHODE COPPER	MILLION BTU REQUIRED PER UNIT	MILLION BTU PER NET TON CATHODIC COPPER
1	Roaster				
	A) Waste Heat Recovery	BTU	-4.25	1.00	-4.25
	B) Fuel (Start Up only)	BTU	0.2	1.00	0.20
2	Leach Circuit				
	A) Electrical Power	KWH	59.756	0.0105	0.627
	B) Process Heating, Steam		*	*	*
3	Reduction Autoclaves				
	A) Pumping, Electrical	KWH	8.04	0.0105	0.084
	B) Process Heating, Steam	LBS	8164	0.0014	11.43
4	Filter				
	A) Electrical	KWH	2	0.0105	0.021
5	Melting, Refining, and Anode Casting				
	A) Heating and Melting (Fuel Oil)	GAL	19.5	0.15	2.925
	B) Poling Gas	SCF	225	0.0010	0.225
6	Electrorefining				
	A) Electrical	KWH	272	0.0105	2.856
	B) Process Heating (Fuel Oil)	LBS	1300	0.0014	1.82
7	Gas Scrubber Circuit				
	A) Electrical	KWH	132.43	0.0105	1.39
	Ancillary Loads				
	A) Electrical	KWH	50.0	0.0105	0.525
				TOTAL	17.769

*The minus 4.25 million BTU credit given under 1A represents a balance between roaster recovery and process heating steam. Items 1A and 1B combined provide the net credit indicated in 1A. This credit should be considered tentative since the sulfite reduction process has not been proven commercially.

Energy generated by the reduction-autoclave reactions

(90% of copper is assumed to be reduced by bisulfite [NH_4HSO_4], and the remaining copper is assumed to be reduced by sulfite [$(NH_4)_2\ SO_3$] at a reduction efficiency at 99%)

$$CuSO_4 + NH_4HSO_4 + H_2O \longrightarrow Cu^o + 1/2\ (NH_4)_2\ SO_4 + 1\tfrac{1}{2}\ H_2SO_4 \qquad (3.8.11)$$

In an aqueous solution, this equation can be expressed as

$$Cu^{++} + HSO_3^- + H_2O \longrightarrow Cu^o + SO_4^= + 3H^+ \qquad (3.8.12)$$

$$\Delta H^o_{298} = (15{,}500 - 165{,}000 - 57{,}800) + (-232{,}700)$$

$$= -25{,}400 \text{ cal/mole}$$

$$\text{Energy Generated} = (15.73)\ (.90)\ (.99)\ (25{,}400)\ (3.6 \times 10^{-6})$$

$$= 1.28 \text{ million Btu/ton product}$$

$$CuSO_4 + (NH_4)_2\ SO_3 + H_2O \longrightarrow Cu^o + (NH_4)_2\ SO_4 + H_2SO_4 \qquad (3.8.13)$$

In an aqueous solution, this equation can be expressed as

$$Cu^{++} + SO_3^= + H_2O \longrightarrow Cu^o + SO_4^= + 2H^+ \qquad (3.8.14)$$

$$\Delta H^o_{298} = (15{,}500 - 167{,}200 - 57{,}800) + (-232{,}700)$$

$$= -23{,}200 \text{ cal/mole}$$

$$\text{Energy Generated} = (15.73)\ (.10)\ (.99)\ (23{,}200)\ (3.6 \times 10^{-6})$$

$$= .13 \text{ million Btu/ton product}$$

Total Heat Generated by Processing Reactions = .27 + 1.28 + .13 = 1.68 million Btu/ton product

With some special design features, the heat generated by the processing reactions can be utilized to heat the influents of the reaction vessels and, thus, offset a process heating requirement. Generally, the processing equipment is increased in either size or complexity to accomplish this heat transfer — e.g., employing bulkier continuous-stirred tanks as compared to more efficient tube or staged reaction vessels. The theoretical energy requirement is evaluated as follows:

Total Level 1 Energy Requirement — (see Table 3.8-2) — 17.77 million Btu/ton product

Offset from Heat Generated by Processing Reactions — 1.68 million Btu/ton product

Total Theoretical Level 1 Requirement — 16.09 million Btu/ton product

used by others. The energy requirements for high carbon ferro-chromium is given as 61 x 10^6 Btu per ton (Battelle, 1975). Most of the liners in use today are chromium-molybdenum type while the grinding balls are low alloy steel. In this calculation the value of 18,000 Btu per pound given by H.H. Kellogg for liners and grinding balls is used since it seems to more nearly represent the use of scrap iron, new iron, and alloys. The electrical energy conversion factor is taken from the same article. The energy use, per ton of ore milled, was obtained from private communication with one of the latest copper plants built. Direct kWh meter readings are taken from each step of the process. These total kWh readings are converted to kWh per ton by dividing by the tons processed. The kWh or Btu per pound of copper is directly dependent upon the recoverable copper content of the ore.

1.3.3 Impact of Autogenous Grinding

The significant contribution of iron, and steel consumption to the total energy requirement for conventional grinding is of particular interest in view of the development of autogenous grinding technology in the mineral processing industry. The consumption of iron and steel can be reduced considerably when the ore is self grinding. Many operations in Europe now practice either autogenous or semi-autogenous grinding and the state of the art for this technology was discussed at a recent autogenous grinding conference in Trondheim, Norway, June, 1979. Based on the analysis of this data (Digre, 1979) and the use of standard relationships which have been developed for conventional grinding (Mular and Bhappu, 1978) the energy effectiveness of conventional grinding can be compared to that of autogenous grinding. Figure 1.3-2 presents this comparison for a typical copper ore with a work index WI of 13.1 kWh/ton and abrasion index AI of .095. Here the total energy required for grinding by various methods is plotted versus an autogenous grinding factor. The autogenous grinding factor, β, gives a measure of the energy inefficiency of self-breakage for the ore and is defined as the ratio of the operating work index for autogenous grinding to a standard laboratory ball mill work index as established by a Bond grindability test or the equivalent thereof. The overall energy requirement for each alternative has been calculated as:

$$\begin{aligned}\text{TOTAL ENERGY REQUIRED FOR COMMINUTION} = \\ (\text{NET CRUSHING ENERGY}/\epsilon_C) \\ + \beta\,(\text{NET BALL MILL ENERGY}/\epsilon_B) \\ + (\text{STEEL CONSUMED AS MEDIA \& LINERS}) \\ \times\ (\text{ENERGY "CONTENT" OF STEEL}) \\ + \text{ENERGY FOR COMMINUTION CIRCUIT AUXILIARIES}\end{aligned}$$

Of course, the energy consumption for conventional grinding and pebble grinding is independent of the autogenous grinding factor, whereas the energy consumption in autogenous grinding will reflect the extent to which self-breakage contributes to the energy economy. Available data indicates that the autogenous grinding factor for copper ores is generally between 1.35 and 1.6 with occasional values as low as 0.75. When β is small the energy required for autogenous grinding is less than that required for conventional grinding, since the inefficiency of autogenous breakage is more than offset by the elimination of media requirements, however, when the inefficiency exceeds 45-50% (β = 1.45-1.50) the advantage of no media expense disappears. The comparisons shown in the figure are not indisputable, but are based on the best available data. These data do indicate that for copper ores which are very amenable to autogenous grinding, a reduction in

8 8

SOCIETY OF MINING ENGINEERS of AIME

540 ARAPEEN DRIVE — SALT LAKE CITY, UTAH 84108

PREPRINT NUMBER

76-B-77

CONCENTRATION PROCESSES FOR URANIUM IN SITU LEACH LIQUORS

Geoffrey G. Hunkin
Consulting Engineer
Littleton, Colorado

This paper is to be presented at the AIME Annual Meeting, Las Vegas, Nevada — February 22-26, 1976

INTRODUCTION

This is a brief state of the art paper describing current (1975) Uranium recovery plant flowsheets, some notes on system selection, design philosophies, and materials of construction.

The in-situ, or borehole solution mining, of Uranium is a process which has been developed over recent years to better match Uranium mining and milling technology with the size, shape, grade and territorial distribution of the remaining identified Uranium deposits of western United States.

Solution mining recovery plants are pure hydrometallurgical units ideally suited to automation, modular design, and mobility.

Similar to conventional Uranium mills, two basic flowsheets, one acid and one carbonate, are in use, but the predominance is reversed so that the majority of plants employ the alkaline carbonate flowsheet. All plants incorporate resin bead ion exchange Uranium recovery for both acid and alkaline circuits.

PLANT DESIGN FEATURES

The bulk of conventional Uranium plants is tied up in the ore bins, crushing and grinding, liquid-solid separation and leach tank areas. Because the feed to the solution mining plant is a low turbidity liquid suitable for direct feed to expanded bed or Higgins type resin bead ion exchange adsorption units, even large throughputs — 500 or 1000 gallons per minute IX flows — can be handled in skid or trailer mounted plants. This type of plant is readily automated, the results being generation of interestingly high product values per operator shift, low values of plant construction cost per pound of annual production and short construction lead times.

Future extraction and concentrator plant designs are likely to lean heavily on offshore oil industry experience in design of self contained process plant packages.

Plant tailings are small in volu
ponds or reinjection through disposal

An interesting feature of these
unit of U_3O_8 produced.

SELECTION OF ACI

The choice can seldom be made
recovery or extraction plant charac
the underground sand formation, wit
powerful influence on system select

1. Maintenance of satisfacto
2. Residual reagents and the formation after exploitat affect groundwater qualit

Some years ago, one operator
and sulfuric acid leaching, and r
of sulfuric acid. It appears tha
acid leaching are not a frequent
deposits. While few areas outsi
piloted, the work which has been
studies, (2) (5) and core analys
identified Uranium bearing forma
studies of new projects, and sup

Sulfuric acid treatment te
with clays and calcite and may
The products of reaction with
geochemical cell boundary — Va
the cost of surface processing
water quality compared with th

The carbonate system, und
say 5 to 15 kg/cm^3, temperatu

Plant tailings are small in volume and generally handled by evaporation ponds or reinjection through disposal wells into brine formations (1).

An interesting feature of these plants is the low energy requirement per unit of U_3O_8 produced.

SELECTION OF ACID OR CARBONATE PROCESSES

The choice can seldom be made on the basis of leaching costs, overall recovery or extraction plant characteristics. The leaching process occurs in the underground sand formation, with the result that two new factors exert a powerful influence on system selection.

1. Maintenance of satisfactory permeability in the mineralized formation.
2. Residual reagents and the soluble products remaining in the formation after exploitation is completed, may not detrimentally affect groundwater quality beyond permissible limits.

Some years ago, one operator (3) reported on the successful use of nitric and sulfuric acid leaching, and recently two other (4) (6) confirmed the use of sulfuric acid. It appears that conditions which permit the successful use of acid leaching are not a frequent occurrence in the solution mining of Uranium deposits. While few areas outside of Texas and Wyoming have been systematically piloted, the work which has been done plus the extensive and detailed mineralogical studies, (2) (5) and core analysis data available for a large number of other identified Uranium bearing formations provides satisfactory data for feasibility studies of new projects, and supports the carbonate preference.

Sulfuric acid treatment tends to reduce formation permeability by reaction with clays and calcite and may be associated with the formation of silica gel. The products of reaction with metallic minerals associated with Uranium at the geochemical cell boundary — Vanadium, Molybdenum, Arsenic and Iron — increase the cost of surface processing and of maintaining control over the acquifer water quality compared with the carbonate process.

The carbonate system, under in-situ leach condition of moderate pressure, say 5 to 15 kg/cm^3, temperature 10° to 75°C and low concentration has been

found to have an undetectable effect on mineralized formation permeability, and in particular the ammonium ion may have a beneficial effect on the swelling of some classes of clays. The ammonia form is relatively clear of deleterious side effects and permits acceptable formation water quality control, provided that oxidizer usage is not excessive. The sodium system has the advantage of significantly lower cost — $25.00 per ton for 90/95% Nahcolite ex. Piceance Creek, Colorado (7) — so that increased operator interest in sodium bicarbonate leach solutions can be expected in the future. Each system can be handled effectively in the surface plant with standard ion exchange concentration equipment and commercially available resins.

The selection of process, whether H_2SO_4, NH_4HCO_3, $NaHCO_3$, or other will therefore depend on the performance of these reagents in the underground formation, and not on the extraction plant efficiency demands.

PROCESS TESTING

Standard ore testing procedures tend to be unreliable by virtue of the physical-chemical characteristics of the sandstone formations, limitations inherent in commercial core sampling processes, and the practical difficulties associated with the elimination of or compensation for the natural oxidation effects which occur during sampling, transporation, sample preparation and bench testing of the ores.

It is recommended that process testing be carried out in the field, and methods are available which permit this to be done at costs in the same order-of-magnitude as costs of laboratory tests (8).

PLANT FEED CHARACTERISTICS

Efficiently operated well systems will produce clear fluids, free of significant turbidity, suitable for direct feed to expanded bed or pulsed bed

types of resin bead ion ex
perturbations caused by th
and aerial contamination a
or settling tanks a requir

1975 plant designs ha
bed units (three) and USE
boards at this time are p
pulsed bed units produced
mated adsorption and elut
available in a complete e
South African National In
bed columns marketed by t
Himsley expanded bed colu
offer some improvements i
columns at the cost of a
expanded bed IX equipment
appears particularly sui
(9).

All of these units
fiberglass reinforced pl
use in both acid and alk
to be exhibited by in-si

The feed solution
Uranium Co
Turbidity
Viscosity
Temperatur
Carbonate
Eh
pH
Freezing
Acid Proce
Eh
pH

76-B-77

types of resin bead ion exchange equipment. However, well cleanup operations, perturbations caused by the introduction of new wells to the production line, and aerial contamination at surge tanks make some simple type of filtration or settling tanks a requirement at the input side of all types of IX equipment.

ION EXCHANGE EQUIPMENT

1975 plant designs have been more or less equally divided between fixed bed units (three) and USBM type expanded bed units (four). On the drawing boards at this time are plants incorporating compact package Higgins (11) (12) pulsed bed units produced by Chem Seps. Such units incorporate continuous automated adsorption and elution processes operating at high speed per unit size, available in a complete equipment package. Also under consideration are the South African National Institute of Metallurgy, Cloete-Streat (10) expanded bed columns marketed by the Western Knapp-Arthur G. McKee group, and the Canadian Himsley expanded bed column design. These latter column type units appear to offer some improvements in efficiency over the USBM (Darcy George design) (11) columns at the cost of added complexity. The R. R. Porter design of multi-stage expanded bed IX equipment has inherently high metallurgical efficiency and appears particularly suitable to high solution flow rates and large installations (9).

All of these units have designs which are suitable for construction in fiberglass reinforced plastic and stainless steel so as to be suitable for use in both acid and alkaline circuits over the range of conditions likely to be exhibited by in-situ leach feed solutions.

The feed solution can be expected to have the following characteristics:

Uranium Concentration	50 to 1500 ppm U_3O_8
Turbidity	negligible
Viscosity	1.0 cP
Temperature	10 to 75°C
Carbonate Process	
Eh	-0.15 to +0.4 mV
pH	6.5 to 9.5
Freezing Point	0°C
Acid Process	
Eh	+0.2 to +0.45 mV
pH	1.5 to 5.5

REAGENT HANDLING

Gaseous Reagents

Anhydrous ammonia and liquified carbon dioxide are received in bulk deliveries by tanker vehicles into specially designed storage units available as complete equipment packages. These units incorporate safety features and evaporation equipment designed to maintain constant delivery pressures.

Liquid Oxidizers

Minimum cost H_2O_2 deliveries involve 4000 gallon shipments of 70% H_2O_2 diluted to 50% with client supplied de-ionized water at point of delivery. Packaged storage, metering and pressure injection pump units are available through the major suppliers. Liquid Oxygen and sodium chlorate bulk deliveries require comparable equipment for minimum cost and safe handling.

Other Reagents

Are required in lesser quantities and are generally handled in drum or sack containers.

RADIATION CONDITIONS IN THE CONCENTRATOR

Operator exposure is negligible due to the limited solubility of the daughter products, which are the source of the bulk of radiation present in conventional mills. In most solution mining processes involving an underground leaching stage within the mineralized formation, essentially all daughter products with the exception of minor amounts of Radon 226 remain immobile and do not report in the feed solution.

TAILINGS DISPOSAL

Where continuous recirculation of leach solutions can be practiced, as with carbonate systems, tailings appear to range from near zero to two (2) pounds of waste (1) per pound of Uranium recovered. In acid systems, liquid waste disposal requirement may be higher whenever the circulating load of metal sulfates in solution builds up to unacceptable levels.

The DALCO-ARCO plants inco
system plants rely upon evapora
use at sulfuric acid plants hav

(1) Hunkin, G. G., "The Envi
Mining Congress Journal,

(2) Honea, R. M., Personal C

(3) Anderson, J. S. and Ritc
Mining Congress Journal,

(4) Lang, E. A., Rocky Mount

(5) Garrels, R. M. and Lars
the Colorado Plateau Ur

(6) Bozek, "Uranium Solutio

(7) Nielson, I., Personal C

(8) Hunkin, G. G., "A Revi
Annual Meeting #71-As-

(9) Porter, R. R., U. S. P

(10) Cloete, F. L. D. and S

(11) George, D. R., Ross, J
Recovered with New Ior
Vol. 20, January, 196

(12) Higgins, I. R., Perso

(13) Texas Water Quality B

(14) Texas Water Quality B

(15) Texas Water Quality B

(16) Texas Water Quality B

(17) "New Solution Cuts U
December 24, 1975.

The DALCO-ARCO plants incorporate disposal wells (15), while other carbonate system plants rely upon evaporation ponds. Tailings disposal facilities in use at sulfuric acid plants have not been disclosed at the date of writing.

REFERENCES

(1) Hunkin, G. G., "The Environmental Impact of Solution Mining for Uranium", Mining Congress Journal, Vol. 61, #10, October, 1975.

(2) Honea, R. M., Personal Communication.

(3) Anderson, J. S. and Ritchie, M. I., "Solution Mining of Uranium", Mining Congress Journal, January, 1968.

(4) Lang, E. A., Rocky Mountain Energy Corporation, Personal Communication.

(5) Garrels, R. M. and Larsen, E. S., "Geochemistry and Mineralogy of the Colorado Plateau Uranium Ores", USGS Prof. Paper 320, 1959.

(6) Bozek, "Uranium Solution Mining at HAMR", Czechoslavakia, CSSR.

(7) Nielson, I., Personal Communication.

(8) Hunkin, G. G., "A Review of In-Situ Leaching", AIME Centennial Annual Meeting #71-As-88.

(9) Porter, R. R., U. S. Patent 3,879,287.

(10) Cloete, F. L. D. and Streat, M., U.K. Patent 1,070,251.

(11) George, D. R., Ross, J. R. and Prater J. D., "Byproduct Uranium Recovered with New Ion Exchange Technique", Mining Engineering, Vol. 20, January, 1968.

(12) Higgins, I. R., Personal Communication.

(13) Texas Water Quality Board, Public Hearings, July, 1975.

(14) Texas Water Quality Board, Public Hearings, July, 1975.

(15) Texas Water Quality Board, Public Hearings, Jan., 1975.

(16) Texas Water Quality Board, Public Hearings, Jan., 1975.

(17) "New Solution Cuts Uranium Mining Costs", Chemical Week, December 24, 1975.

76-B-77

7

PLANT CHARACTERISTICS

TEXAS - CARBONATE PROCESS - 1975

	Westinghouse (13)	Mobil (14)	ARCO (15)(17)	DALCO (16)
Leach System	Carbonate Multiple Recirculation	Carbonate Multiple Recirculation	Carbonate Multiple Recirculation	Carbonate Multiple Recirculation
Filtration	Metal Screen	Sand Filter	Carbon Column	Carbon Column
Concentration	Resin Bead IX	Resin Bead IX	Resin Bead IX	Resin Bead IX
IX System Adsorption	USBM Expanded Bed	Fixed Bed	Fixed Bed	Fixed Bed
Elution	Counter Current Column NH_4Cl	Fixed Bed $(NH_4)_2CO_3$	Fixed Bed NaCl	Fixed Bed NaCl
Leach Reagents	NH_3 CO_2 H_2O_2	NH_3 CO_2 Oxidant	NH_4HCO_3 O_2	NH_4HCO_3 O_2
Precipitation	$HCl + NH_3$	NH_3, CO_2 Recovery Steam	NaOH	NaOH
Product	ADU Slurry	U_3O_8 Slurry	Yellow Cake	ADU Slurry
Waste Disposal		Evaporation	Evaporation Deep Well	Evaporation

Cananea's Program for Leaching In Place

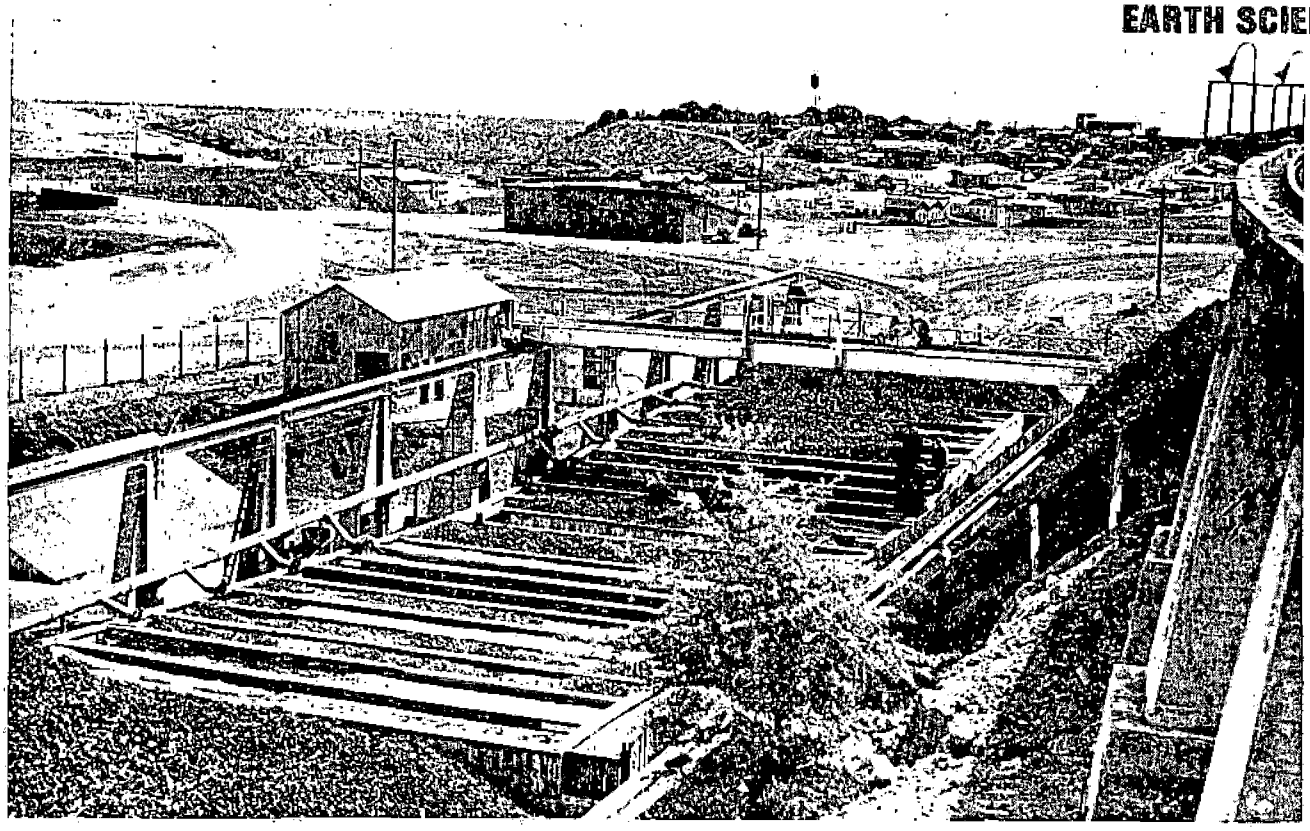

by Robert C. Weed

LEACHING in place at Cananea began in the 1920's on a limited scale. The first plants were small wooden boxes located underground in the Capote and Oversight mines; and output was low. Scrap iron was used as precipitant. Later several other small plants were started up. Leaching was limited entirely to underground areas, and production remained low.

The Veta precipitating plant, the first on a larger scale, was put into operation in the late 1920's. After a period of intermittent service it was rebuilt in 1946 and has since been running continuously.

In 1943 work on the Colorada open pit was started. This produced 40 million tons of waste, which averaged 0.20 pct copper. When these dumps had aged a few years it was decided to leach them on a large scale, and after considerable research and investigation a leaching system of pumps and pipelines was laid out and installed. At the same time the Ronquillo precipitation plant was built to treat the copper solutions from the pit dumps. This plant started operation in March 1953.

Leaching areas consist of the Colorada pit dumps and various mined out and caved underground stopes. The principal mineral, chalcocite, leaches readily in a weak sulfuric acid solution containing ferric iron. Enough pyrite is contained in the areas to produce an acid-ferric iron solution strong enough to dissolve the copper.

Each area is studied to determine the best method of distributing the water over it and the best method of collecting the copper-bearing solutions after leaching has taken place. Water is generally distributed by means of ponds, ditches, and sprays. Spraying has proved the best method of spreading the water evenly; however, in a dry climate some water is lost through evaporation.

After passing through the leachable material the solution is collected underground by dams and bulkheads and on surface by dams. An effort is made to give the maximum storage capacity practicable.

R. C. WEED, Member AIME, is General Superintendent at Cananea Consolidated Copper Co., Cananea, Sonora, Mexico.

TP 42518. Manuscript, Jan. 10, 1956. New York Meeting, February 1956.

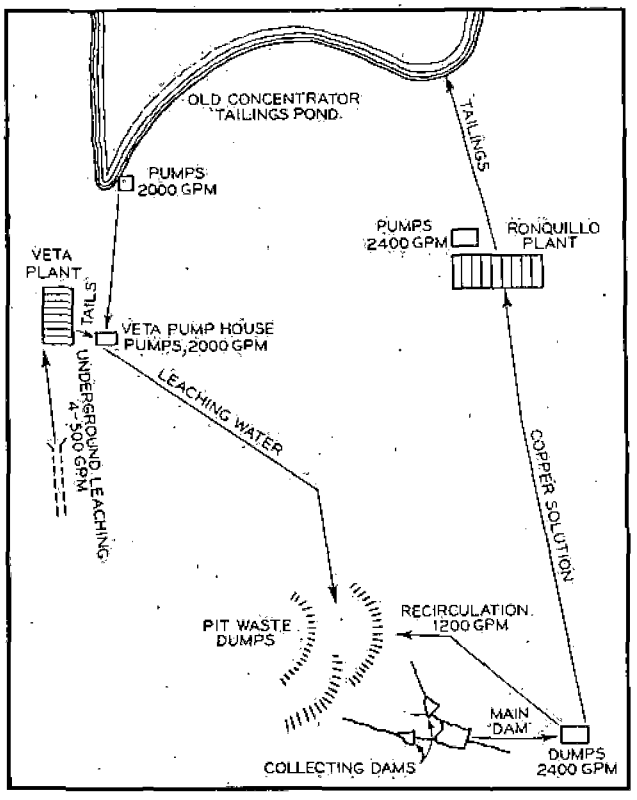

Fig. 1—The surface leaching system at Cananea.

For relatively low pressure (below 150 psi) transite pipe is used. For higher pressures iron pipe lined with wood or rubber is necessary. To facilitate repairs and replacements, pipelines are installed along roads or trails. Each line is equipped with a Y or a lateral to permit the insertion of a *go-devil* for cleaning. Periodic cleanings are necessary to eliminate build-up of iron ochre inside the pipes.

Pumps are mostly of the horizontal centrifugal type, installed wherever possible with a positive feed. Gages on pump discharge lines indicate the head the pump is working against, which can be used to calculate the pump capacity, and also show when the pipelines need cleaning. Nearly all pumps are equipped with automatic start-stop controls. Stainless steel equipment is necessary throughout.

Underground Leaching and Veta Plant: Water for underground leaching is obtained from present mining and from drainage of old mines. Roughly 400 gpm are used. Most of this water is pumped to surface, where it is sprayed over the top of the Colorada cave. From there it percolates down through the mined out sections of the Colorada mine and is collected behind a bulkhead on the Colorada 1300 level. It is then pumped to the 500 level tunnel, through which it flows to the Veta plant. Smaller amounts of water are being used to leach limited areas in the Veta, Oversight, and Republica mines. This solution also goes to the Veta plant.

As mentioned before, the Veta precipitating plant was rebuilt in 1946. Because there were shortages of cement and reinforcing iron at that time, it was decided to make the cells of wood. The plant now consists of 64 cells 4½ ft wide by 10 ft long by 5 ft high and 3 cells 9 ft wide by 16 ft long by 5 ft high. (The latter are for use of scrap iron as a precipitant.) Wooden grids with openings ½x¾ in. are placed horizontally in the cells 3 ft below the top to form a rack for the cans.

After the cell has been charged with burned, shredded cans, the solution is introduced and is directed up and down through the layer of cans by means of baffles. The water usually passes through a pair of cells. When the bulk of the can charge has been consumed, the cell is drained and the copper is washed through the grid with high pressure water. It flows as a sludge out of spigots near the bottom of the cell and down a launder into three large settling tanks with inclined bottoms. The bulk of the water is decanted from the first tank to the second, etc., and the cement copper mud is scraped up the incline with a 54-in. hoe-type slusher bucket. It is then loaded into trucks to be hauled to the concentrator and sluiced into the concentrate thickeners. Cans for the Veta plant are hauled from railroad bins by truck and stockpiled at the plant area. Later they are loaded with a rocker shovel into side dump tram cars, which are used in charging the cells.

Surface Leaching and Ronquillo Plant: Water for leaching the pit dumps is obtained from the old concentrator tailings pond, which collects tailings water from the Ronquillo precipitation plant and a considerable amount of water from the Democrata drainage area. This pond has a surface area of about 75 acres and an average depth of 60 ft. Because the water is acid and contains some ferric iron it makes a good leaching agent. Water is pumped from this pond to the Veta pump house at the rate of 1600 gpm. At this point it is joined by the Veta plant tailings, and the mixture is pumped directly to the Colorada pit dumps where it is distributed by means of ponds. Below the dumps the water is impounded in one of two collecting dams across the mouths of two deep gulches underlying the dumps. If the grade of the solution is too low, it is pumped to the top for a second pass. This solution is caught in the other collecting dam, drained to the main dam, and pumped to the Ronquillo plant, as shown in Fig. 1. After passing through the plant the tailings water is pumped back to the old concentrator tailings pond, thus closing the circuit. Excess iron precipitates out in the pond, probably as basic ferric salts, and the total iron content in leaching water remains about the same.

Table I presents a typical analysis of water in various parts of the circuit.

Table I. Analysis of Water in Circuit

Place	Cu, Gpl	Fett, Gpl	Fettt, Gpl	pH
Old concentrator pond	0.40	9.25	2.00	2.7
Veta plant heads	3.10	1.25	2.10	2.5
Veta plant tails	0.20	6.25	1.00	2.9
On dumps	0.35	7.10	1.80	2.7
Ronquillo heads	3.30	3.00	7.40	2.3
Ronquillo tails	0.25	14.00	1.50	2.9

The Ronquillo plant was constructed in 1952 after a study of a number of operating precipitation plants had been made. Influencing factors in the basic design were flexibility of operation, ease of materials handling, and availability of two overhead cranes, which could be adapted for charging cans into the cells.

The head water passes through a weir box with a recording meter and is distributed to the cells through a 12-in. pipe. This pipe has a number of takeoffs, each equipped with a valve, so that the solution can be controlled both as to location and volume of input to the cells.

THE SOVIET JOURNAL OF NON-FERROUS METALS

COMPOSITION OF PRODUCTS OBTAINED FOLLOWING AUTOCLAVE OXIDATION LEACHING OF PYRRHOTITE CONCENTRATES

UDC [669.243+669.33]:66.046.8

A. G. Kitai, V. I. Goryachkin, V. P. Korneev, A. V. Dolenko, and V. A. Isaev

Autoclave oxidation of the pyrrhotite concentrates of non-ferrous metals, approximately described by the equation

$$Fe_{10}S_{11}+7.5\,O_2+5\,H_2O\rightarrow 5\,Fe_2O_3\cdot H_2O+11\,S^0. \quad (1.)$$

lies at the basis of a series of hydrometallurgical systems developed in the Soviet Union and abroad [1-3].

Various iron oxides, having relatively unstudied compositions, formed during the decomposition of pyrrhotite will in many cases determine the indices for the subsequent separation of the valuable components and the complexity of raw-material use.

This paper will give the results of a study made of the composition and conditions for the formation of iron oxides -- the product obtained following oxidation of the pyrrhotite of Noril'sk copper-nickel concentrates, when processed by the hydrometallurgical technique [3].

Studies were made of the composition of samples selected in laboratory and pilot tests, using x-ray-phase, chemical, and other analyses method.

According to the results of the research into the composition of leaching-product specimens, given in the Table, as the share of oxidized pyrrhotite increases, there will be a steady increase in the amount of goethite and hematite; with the samples in the periodic tests, there will also be an increase in the maghemite. This is clearly confirmed by the Mossbauer spectra (Fig. 1).

Parameters for the Mossbauer spectra of maghemite and hematite are close to each other, which makes it difficult to make a single-valued determination of these compounds. For their identification in the examined samples, the spectra were registered for several specimens which had been placed in an external transverse magnetic field of 20 kE. Since maghemite is ferromagnetic with a spinel structure and the iron in it is found in a tetrahedral and octahedral position, the Mossbauer spectra of the maghemite in the external magnetic field split into two "six-section" lines. Hematite is antiferrimagnetic and its spectra shows almost no change.

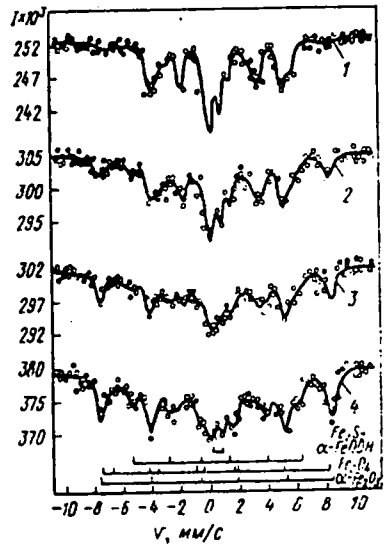

Fig. 1. Mossbauer spectra of specimens (test I): 1 - original concentrate; 2 - specimen 1; 3 - specimen 2; 4 - specimen 3.

As is evident from Fig. 2, the outer lines of the superfine structure are not split in any of the examined leaching-product samples. This makes it possible to assume that there are no perceptible quantities of maghemite in the products obtained after oxidation of the pyrrhotite concentrates; hematite does form.

In test II (see Table), the field on the iron core in hematite is somewhat less than is characteristic for massive hematite, and it increases as the leaching time increases from 491 to 509 kE; moreover, the lines are somewhat wider than in conventional hematite. A similar phenomenon can be caused by the presence of water of crystallization in the hematite structure, the replacement of iron by atomic impurities or by small size hematite particles (superparamagnetic behavior); the latter was noted earlier [4-6] for hematite, maghemite, and goethite.

In our case, the formation of hematite with particle sizes of about 150 A, where they show some increase during oxidation, can be found in spectra of a superfine structure with fields on iron cores changing within specific ranges.

It is interesting to note that no supermagnetic behavior was noted for the magnetite in the examined specimens. This phenomenon -- in conjunction with data on hematite and magnetite distribution by size [7]-- confirms that magnetite is probably concentrated in size class +10 μm, and hematite in size classes of -5 μm.

From the data on the composition of pyrrhotite-leaching products and data in the literature, one can hypothesize the following mechanism of iron-oxide formation.

Composition and Technological Features of Examined Samples

Test no.	Sample no.	Chemical composition, % Cu	Ni	Fe	S_{tot}	S^0	Degree of pyrrhotite decomposition, %	Phase composition of iron oxides, % Fe_2SO_4	α-FeOOH	α-Fe_2O_3	Test conditions
I	1	0,35	2,5	46,1	26,1	5,6	32,0	3,1	2,6	3,2	Periodic test in 15-lit autoclave, at P_{O_2} = 5 atm; 108°C; s:l = 1:1. Oxidizer - commercial oxygen. About 2% Fe_3O_4 in original concentrate
	2	0,34	2,2	42,3	23,8	12,3	68,0	3,0	3,0	5,4	
	3	0,17	0,62	44,3	23,8	19,9	89,0	4,0	5,5	6,8	
II	1	0,51	2,7	54,6	29,8	4,3	43,0	5,4	1,2	2,4	Periodic test in a 1.73 m^3 capacity pilot four-section autoclave, at P_{O_2} = 4 atm; s:l = 1:1. Oxidizer - oxygen-air mixture with 60% O_2. About 1.2% Fe_3O_4 in original concentrate.
	2	0,50	2,6	48,8	28,3	11,1	71,0	7,5	2,5	7,0	
	3	0,40	2,4	45,1	25,9	16,6	92,0	8,2	2,3	9,6	
	4	0,20	2,1	44,9	24,9	17,3	93,0	8,4	3,1	10,6	
	5	0,05	1,6	44,6	24,7	18,1	94,0	8,6	3,2	10,4	
III	1	1,22	2,23	51,0	30,4	7,1	36,0	3,0	1,9	3,5	Continuous test in a 3.46 m^3-capacity pilot eight-section autoclave, at P_{O_2} = = 9 atm; 108°C; s:l = 1:1. Oxidizer - oxygen-air mixture with 60% O_2. <1% Fe_3O_4 in original concentrate.
	2	1,0	1,95	46,5	27,4	15,5	74,0	2,9	4,6	4,1	
	3	0,81	1,61	43,2	26,1	17,2	82,0	3,0	6,3	6,8	
	4	0,39	1,26	42,4	24,8	18,3	88,0	3,0	5,9	6,0	

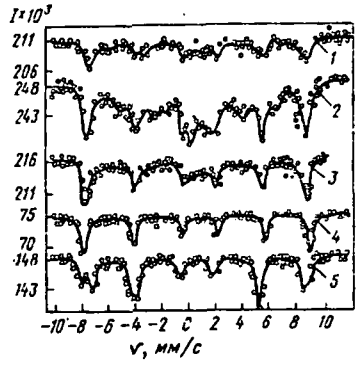

Fig. 2. Mossbauer spectra of specimens which we were placed in a transverse magnetic field of 20 ke:
1 - sample 1; 2 - sample 2; 3 - sample 3; 4 - hematite; 5 - maghemite.

If we accept the dissolution of pyrrhotite (simply represented by the formula FeS) in an electrochemical process, we can assume that the reactions occur as follows:

$$FeS \rightarrow Fe^{2+} + S^0 + 2e^- \quad (2)$$

$$H_2O + 0{,}5\,O_2 + 2e^- \rightarrow 2OH^-, \quad (3)$$

and where the products meet,

$$Fe^{2+} + 2\,OH^- \rightarrow Fe(OH)_2. \quad (4)$$

It is well known that the formation of ferrous hydroxides is possible at pH > 5.5 [8]. During the initial oxidation period, when the free acid concentration is too small, the total pyrrhotite oxidation reaction is:

$$FeS + H_2O + 0{,}5\,O_2 \rightarrow Fe(OH)_2 + S^0. \quad (5)$$

Then, as the pH drops, this reaction can occur only in the adsorption layer at the sulfide-solution boundary.

According to an earlier work [9], the relationship of the phase interface (pH_S) to the pH in the liquid volume (pH_V) and the potential of the sulfide (φ) can be approximated by the equation:

$$pH_S = pH_V \pm 17{,}3\,\varphi. \quad (6)$$

It is well known that the potential for pyrrhotite, for example at a pH 3.2, is about 0.15 V [10]; in the presence of oxygen, the positive value for the potential of this sulfide increases by 50-60 mV [11]. Taking this value into consideration, the pH_S on the pyrrhotite surface -- calculated according to Equation (6) for a pH_V = 3.2 -- is about 7.0; this indicates the possibility of Fe(OH) forming on the sulfide surface, even with a comparatively high acidity which corresponds to the actual continuous leaching process.

The next probable stage is oxidation of amorphous ferrous hydroxide according to the reaction:

$$Fe(OH)_2 + 0{,}5\,O_2 \rightarrow FeOOH + H_2O \quad (7)$$

with the subsequent formation of ferroferrite:

$$Fe(OH)_2 + FeOOH \rightarrow FeOOH\,FeO + H_2O \quad (8)$$

Formation of such a ferroferrite was noted earlier [12].

To confirm the possibility of ferroferrite forming under actual pyrrhotite-oxidation conditions, diffractographs were taken for two specimens obtained at the initial stage of leaching, and prepared according to an earlier described method [12, 13]. The diffractographs of these specimens show a general set of reflections (d_α = 5.69, 4.18, 3.95, and 2.87 A). Comparing the general set of reflections with the interplanar distances for a series of compounds which can be present in the original concentrate or form during the leaching process, clearly showed that the noted set of reflections does not include goethite or hydrogoethite (I = 8, d_α = 2.45 A, I = 10), hydrojarosite (there is no d_α = 5.10, I = 9, hypersthene (no d_α = 3220 A, I = 10), gypsum (no d_α = 3.07 A, I = 10), nor anhdyrite (no d_α = 3.49 A, I = 10).

The above makes it possible to hypothesize the formation of ferroferrite during leaching, especially at the start of the process. Another indirect confirmation of this is the green color of the solid at the start of the oxidation; it is well known

that of all the iron oxides, it is only ferroferrite which has that color.

The next stage in the process is the formation of magnetite:

$$FeOOHFeO+FeOOH\rightarrow Fe_3O_4+H_2O. \quad (9)$$

In the presence of oxygen, a poorly crystallized magnetite can be one of the sources for production of goethite:

$$2\,Fe_3O_4+0{,}5\,O_2+3\,H_2O\rightarrow 6\alpha\text{-}FeOOH. \quad .0)$$

It should be noted that the presence of hydromagnetite and the formation of goethite are probably due to oxidation.

According to some data [14], sulfate- and fluorine-ions contribute to the formation of goethite; this conforms with our results. Goethite is the source of hematite formation:

$$2\alpha\text{-}FeOOH\rightarrow\alpha\text{-}Fe_2O_3+H_2O. \quad (11)$$

The enthalpy of Reaction (11) is about 4 kcal [15]; according to [16], hematite is formed at low pH values. Therefore, completing the leaching at low pH values (1.5-2) will contribute to production of hematite.

As is shown by accumulated experimental data, oxidation of pyrrhotite in water by means of oxygen at about 110°C and a s:1 ratio of 1-1.5 will lead to formation of crystalline forms of oxidized iron; however, at the end of the process, their content is 20-35%. The remaining oxidized iron is represented by x-ray-amorphous forms, which are the sources for the obtainment of various crystalline compounds during the process of further processing of oxidized pulp.

REFERENCES

1. K. Downes and G. Bruce. Canadian Mining and Metallurgical Bulletin, 1955, vol. 48, No. 515, pp. 127-132.
2. W. Kunda, B. Rudyk, and V. Mackey. Canadian Mining and Metallurgical Bulletin, 1968, vol. 61, No. 675, pp. 819-835.
3. V. I. Goryachkin, I. M., Nelen', V. A. Shcherbakov, et al. Tsvetnye Metally, 1974, No. 9, pp. 1-6.
4. M. Rossiter and A. Hodson. J. Inorg. Nucl. Chem., 1965, vol. 27, pp. 63-65.
5. P. Roggwiller and W. Kundig. Solid State Comm., 1973, vol. 12, pp. 901-903.
6. T. Shingo. J. Phys. Soc. Japan, 1966, vol. 21, pp. 917-918.
7. K. N. Galaktionova, Obogashchenie Rud (Byull. Inst. "Mekhanobr"), 1972, No. 6, pp. 6-8.
8. I. I. Ginzburg, Ya. I. Ol'shanskii, and V. V. Belyatskii. Studies into the Experimental and Technical Petrography and Mineralogy. Moscow, AN SSSR, 1961, Vol. 59, No. 4, pp. 114-126.
9. I. N. Plaksin, R. Sh. Shafeev, and V. A. Chanturiya. Influence of Heterogeneity of Mineral Surfaces on Interaction with Flotation Reagents. Moscow, Nauka, 1965, 49 p., ill.
10. I. N. Plaksin, and L. R. Solov'eva. In the book: Beneficiation of Ores and Coals. Moscow, AN SSSR, 1963, pp. 109-120.
11. I. N. Plaksin and L. R. Solov'eva. Scientific Reports from the A. A. Skochinskii Mining Institute, 1962, No. 12, pp. 3-12.
12. W. Feitknecht. Zeitschrift fur Elektrochemie, 1959, vol. 63, No. 1, pp. 34-43.
13. U. Schwertmann. Zeitschrift fur Anorg. und Alg. Chem., 1959. vol. 298, No. 5-6, pp. 337-348.
14. O. Baudisch and W. Albrecht. J. Amer. Chem. Soc., 1932, vol. 54, pp. 943-945.
15. K. Wefers. Ber. der Deutsch. Keram. Ges., 1966, vol. 43, No. 12, pp. 703-708.
16. K. Wefers. Ber. der Deutsch. Keram. Ges., 1966, vol. 43, No. 11, pp. 677-702.

THE CHEMICAL PRINCIPLES OF SOLVENT EXTRACTION[1]

UDC 669.2:66.061.5

Yu. A. Zolotov

Solvent extraction is one of the most modern and progressive methods of separating and extracting non-ferrous metals. It is a universal method, being applicable to all metals over a wide range of concentrations. The process is technologically efficient and is comparatively easy to automate. Solvent extraction of metals has been widely used in the last 15-20 years in nuclear technology and analytical chemistry, linked with the extensive use of efficient extractants (phosphoryl high-molecular amines, especially tributyl phosphate). In recent years solvent extraction has become a normal method in non-ferrous metallurgy, and there is a tendency toward further adoption in this field.

The theory of solvent extraction is based upon a number of different scientific trends: chemical thermodynamics, theory of solutions, coordination chemistry, chemical kinetics, and mass transfer theory. The selection of extractants calls for creative use of the achievements of organic chemistry.

The principal task in solvent extraction chemistry is to convert the metal to a compound which is completely and selectively extracted. It is consequently necessary to select such a compound, to find the optimum conditions for its formation, and to seek a suitable solvent. This calls for wide-ranging preliminary research and for determining the patterns and the mechanism of the process.

The basic condition for the passage of a metal from aqueous solution into organic solvent is that the solubility of the Me compounds in the organic solvent must be higher than in water. It must be borne in mind that in actual systems a metal may exist as various compounds. In addition, forms which were entirely absent from the initial aqueous solution are often produced in the extraction process itself.

The following principle also operates: charged compounds cannot pass into an organic solvent. If the metal is present in the form of ions, they must be converted to an uncharged complex or to an ionic association with a suitable ion of the opposite charge. The absolute magnitude of the ion charge is an important factor in the extraction of ionic associations (salts): all other conditions being equal, singly charged ions are extracted best; extraction of doubly charged ions, and of triply charged ions in particular, is not so good.

It is important as a rule to maintain water-repellent characteristics in the compound being extracted, the molecule of which must contain no free hydroxyl or carboxyl groups. Solvation by extractant molecules very often helps extraction; in these cases the nature of the extractant is the decisive factor. Finally, the size of the molecules of the compound being extracted is important: large molecules which break up the water structure more strongly are usually extracted better.

Extraction is a two-phase heterogeneous process; the phase rule is therefore applicable to it.

The distribution of a substance between two liquid phases must be subject to the law of distribution, which states that at a constant temperature and pressure the ratio of equilibrium concentrations of the substance in the two immiscible phases is constant; this is the so-called distribution constant. This law holds good if the form in which the substance exists in both phases is the same and does not alter with changes in concentration.

Finally there is the law of mass action. The process of solvent extraction can be described as a normal chemical reaction, and most solvent extraction reactions are reversible.

Finding the composition of the compounds being extracted is a vital aspect of research on the chemical mechanism of solvent extraction. Chemical analysis of extracts and a variety of physical methods, especially spectroscopic methods, are used for this purpose in addition to methods based upon the law of mass action.

The principal types of metal compound of importance in solvent extraction can be divided into two large groups: unionized compounds and ionic association. Eight groups of compound can be distinguished with a more detailed classification.[2]

1. The first group is composed of molecular compounds with covalent bonds of I_2, $AsBr_3$, and OsO_4 type. Solubility in the organic phase is of particular importance in their extraction.

[1]Based upon material from the First All-Union Conference on Hydrometallurgy.

[2]This classification is based upon the nature of the compound being extracted.

2. The second group, the chelates, are cyclic complex compounds of metals with organic reagents, the molecules of which are attached to the metal by at least two of their atoms; at least one atom of hydrogen is evolved in the reaction. Metal complexes with β-diketones, hydroxyquinoline, dithizon and oxyoximes. This class of compounds has been thoroughly studied, and the theory of solvent extraction of chelates is very highly developed.

3. The so-called coordination-solvated compounds may be placed in the third group. This means metal complexes with a mixed coordination sphere which includes an inorganic ligand and a neutral extraction reagent. Examples are $[PdCl_2S_2]$, where S is the neutral sulfur-bearing reagent, and $[ScCl_3(TBP)_3]$, where TBP is the tributyl phosphate molecule, or $[UO_2(NO_3)_2(TBP)_2]$. Such compounds are extracted only when solvent-extraction reagents are used which are capable of entering the inner sphere of the complex.

4. Coordination-unsolvated associations similar to that formed by the large tetraphenylarsonium cation with the perrhenate ion (also large and coordination-unsolvated). By stretching a point, salts of quaternary ammonium bases with metal-bearing anions unsolvated in the coordination sphere can also be included.

5. The fifth group includes mineral acids, which are extracted only by solvents of fairly high basicity capable of protonation, for example, by amines, tributyl phosphate, etc.

6. The sixth group includes complex metalliferous acids and their salts. These are primarily compounds of H_nMX_{m+n} type, where M is a metal, X is a singly charged electronegative ligand (fluoride, chloride, cyanide, nitrate), and m is the metal ion charge, for example, $HFeCl_4$, $HCbF_6$, and $HInI_4$. Complex acids are extracted only by highly basic oxygen-bearing extractants: ketones, ethers or esters, or amines.

7. Heteropoly compounds, which are related to complex acids but have features which make it possible to put them into a separate group. Extraction of heteropoly acids is of importance for silicon, phosphorus, and molybdenum.

8. The last group is made up of ionic associations which for some reason or other are not included in the preceding groups, for example, salts of basic dyes.

The proposed classification is neither conclusive nor complete, because extraction chemistry is developing rapidly.

"Synergistic" extraction, when mixtures of extractants take out metal with higher distribution coefficients than might have been anticipated according to the additivity rule, have recently become widespread. So-called substoichiometric solvent extraction, when the quantity of reagent is less than that required in accordance with stoichiometry, is being used in analytical chemistry; this has made it possible to increase selectivity. Substoichiometric extraction is very similar to exchange extraction, which is based upon the displacement of one metal present in the form of a complex in the organic phase by another metal with a higher extraction constant; this is also a very effective way of increasing selectivity. During the last ten years extraction chromatography, which was hitherto regarded as a laboratory method, has become a common routine. The problem now is to introduce it into large-scale production. Study of the mutual effect of metals in extraction has made it possible to give valuable recommendations to increase selectivity.

Selection of extractants is the task of extraction chemistry. The main ways of choosing extraction reagents have been defined in this field, based upon achievements in modern coordination chemistry, organic chemistry, and electrochemistry. Further increases in selectivity of action are essential, based upon thorough development and study of the theory of selectivity.

A series of papers which make a definite contribution to extraction chemistry was presented at the First All-Union Conference on Hydrometallurgy.[3]

Yu. G. Frolov, V. V. Sergeivskii et al. presented a paper on determining the effect of water upon the thermodynamic activity of extractants in triple (extractant-solvent-water) homogeneous solutions.

The results obtained explain a number of the patterns observed in the behavior of substances in solvent extraction.

A paper by E. B. Mikhlin and his co-workers on the extraction of rare earth elements with mixtures of neutral oxygen-bearing extractants was devoted to the use of synergistic effects in solvent extraction; in extraction from nitrate solutions, the metal distribution coefficients are always higher when mixtures of extractants are used than with separate extractants (for example, tributyl phosphate and petroleum sulfoxides). The authors see the reason for the effect as the formation of mixed solvates.

The work of the Polish chemists Sekerski and Fidelis and of the American scientist Peppard has recently attracted the attention of researchers; their subject was the study of the sequence of charges in distribution coefficients of rare earth elements

[3]The Conference materials will be published by the Nauka Publishing House.

with increases in the atomic number. Several groups of elements were found within which the distribution coefficients alter in the same way. The work by A. I. Mikhailichenko and co-workers entitled "The tetrad effect and some peculiarities in the separation of lanthanide mixtures" aroused interest in this respect. The author demonstrated the "universality" of this periodicity in changes in distribution coefficients and indicates ways in which this pattern could be utilized.

In the communication by S. S. Korovin and co-workers, the reaction of rare earth metal chlorides with tributyl phosphate was used as an example to demonstrate the possibility of using infrared spectroscopy to study the solvent extraction mechanism.

Research on the kinetics of the process is a vital but less well-developed line of study in extraction chemistry. This was emphasized in an interesting plenary paper by G. A. Yagodin. In separate communications, G. A. Yagodin and his co-workers have analyzed the results of research on the speed of extraction of zirconium and hafnium from solutions of various compositions, as well as some general aspects of extraction kinetics.

Seeking new extractants which are cheap and readily available, A. M. Reznik et al. studied the extraction of gallium and scandium from chloride solutions with butylbenzylsulfoxide and other sulfoxides, including petroleum sulfoxides. Scandium is extracted fairly selectively from sulfate solutions with petroleum sulfoxides (titanium is extracted at the same time). A group of Novosibirsk chemists (I. M. Ivanov, A. V. Nikolaev, L. M. Gindin, et al.) is systematically seeking chelate-forming reagents for the selective separation of copper. At the Conference they reported on the study of hydroxyazo compounds, hydroxyazomethines, and aminophenols; certain reagents can be used to separate copper and iron, the copper being extracted more quickly than iron.

Branched monocarboxylic acids are relatively new to Soviet specialists: several communications at the Conference were devoted to them. The advantages of these compounds are low solubility in water and low freezing points. The extraction of iron (III), rare earth metals, and alkali metals using such extractants was studied. N. N. Aslanov, A. A. Shepel' et al. have made a detailed study of the compounds themselves.

Various phenols are also used to extract alkali metals. Alkyl phenols were studied in work by A. I. Khol'kin, L. M. Gindin et al. V. I. Bukin and co-workers studied 2-phenyl-2-phenylol-propane. Diantipyrylmethane and its analogs are of interest as extractants for various metals, in particular non-ferrous metals; these compounds have long been studied at the Perm' University by a group led by V. P. Zhivopistsev. New reagents were also suggested for extraction of platinum metals; the previously described compound para-octylaniline (L. M. Gindin et al.) is effective for group extraction of these metals.

Changes in extractive capacity in a series of extractants similar in structure can be achieved by using various correlations, for example, between the electron density on the extractant active atom and the electro-negativity of substitutes in the compound molecule. A. M. Rozen reported on such researches. He drew attention to the features of neutral polydentate extractants with several phosphoryl groups.

The work of the Conference showed that research on the chemical mechanism of solvent-extraction processes is of primary importance in extending the use of solvent extraction in non-ferrous metallurgy.

Int. J. Rock Mech. Min. Sci. & Geomech. Abstr. Vol. 13, pp. 221–223. Pergamon Press 1976. Printed in Great Britain

A Constitutive Relation Describing Dilatant Behavior in Climax Stock Granodiorite

R. N. SCHOCK*

Climax Stock granodiorite was compressively loaded along different paths to failure at a fixed strain rate and at mean pressures to 0.7 GPa. These data are used to develop a constitutive relation. The expression relates dilatant volume strain ϵ_d to mean pressure P and shear stress τ in the form:

$$\epsilon_d = exp\left[\frac{\delta P}{x(\tau)} - A(\tau)\right],$$

where x and A are explicit functions of τ. The equation has the advantage of simplicity and of expressing the actual behavior in terms of measured physical parameters.

INTRODUCTION

Three-dimensional stress–strain data are summarized in a constitutive stress–strain relation that describes compressive loading of Climax Stock granodiorite to 0.7 GPa mean pressure for the condition that the intermediate (σ_2) and minimum (σ_3) principal stresses are equal. Some of the data and the physical processes believed responsible for the observed behavior have been presented before [1, 2].

Failure in this material (to more than 5 GPa mean pressure) is by brittle fracture: a sudden loss of coherency due to a throughgoing fracture (usually accompanied by a loud report) and a drop in the maximum principal stress σ_1 [3]. Failure is always preceded by dilatant behavior: an increase in bulk volume because of an increase in crack volume. Here, dilatant behavior is defined as an expansion when $\sigma_1 \neq \sigma_3$ with respect to the compression observed when $\sigma_1 = \sigma_3$ at the same mean stress.

EXPERIMENTAL OBSERVATIONS

The failure envelope [4] and the envelope denoting the onset of dilatant behavior [1] for Climax Stock granodiorite are, within experimental error, independent of stress path σ_1/σ_3 on compression and in the absence of cyclical loading. If a rock fails or exhibits dilatant behavior at a given shear stress dependent only on mean stress, then these envelopes are each unique (for the experimental condition $\sigma_2 = \sigma_3$ and initial compressive loading). Crack propagation and failure in brittle materials are associated with the accumulation of a critical amount of shear strain energy [5]. This suggests that envelopes representing failure and the onset of dilatancy are unique in terms of shear strain. The uniqueness implies only a constant shear strain at failure at a fixed pressure independent of loading path. Shear strain at failure varies with pressure.

The importance of shear stress and mean pressure in defining the behavior of a brittle rock has been demonstrated [1]. For an isotropic homogeneous body in orthogonal coordinates and with $\sigma_2 = \sigma_3$, the strain $\epsilon_2 = \epsilon_3$. When a brittle rock dilates the volume increase is due to an increase in ϵ_3 such that $d\epsilon_3 \gg -d\epsilon_1$ [6]. Therefore, a volume strain change $d\epsilon_v = 2d\epsilon_3 + d\epsilon_1$ for a dilating sample is related to the change in shear strain $d\epsilon_s = d\epsilon_1 - d\epsilon_3$. Thus, the constitutive relation should involve three parameters: shear stress τ, mean stress P, and either ϵ_v or ϵ_s.

To test this hypothesis we examine the data. Figure 1 is a plot of P as a function of ϵ_v for Climax Stock granodiorite on a variety of loading paths. The data were taken at a strain rate ($\dot{\epsilon}_1$) of about 10^{-4}/sec. The hydrostat is the $P - \epsilon_v$ path followed during loading with $\sigma_1 = \sigma_2 = \sigma_3$, and is shown as a bold line. Values of τ corresponding to specific values of P and ϵ_v are plotted for non-hydrostatic ($\sigma_1 > \sigma_3$) loading paths. These data were selected from the complete data set but chosen to represent dilatant but unfailed rock. For an elastic, non-dilating solid, all values of τ lie on the hydrostat. (The essentials of the figure could also be represented by strain values plotted on a graph of τ vs P.) We plot the data in terms of strain and pressure because they are commonly used as the basis for finite-difference calculations, and because they show the hydrostat as a reference that may be used to generate part of the equation of state through the normal bulk modulus $K = K(P)$. Although inelastic behavior in rocks can occur while material is loading along the hydrostat (e.g. pore collapse), the distinguishing feature of dilatant behavior is that a void space is created as

* University of California, Lawrence Livermore Laboratory, Livermore, CA 94550, U.S.A.

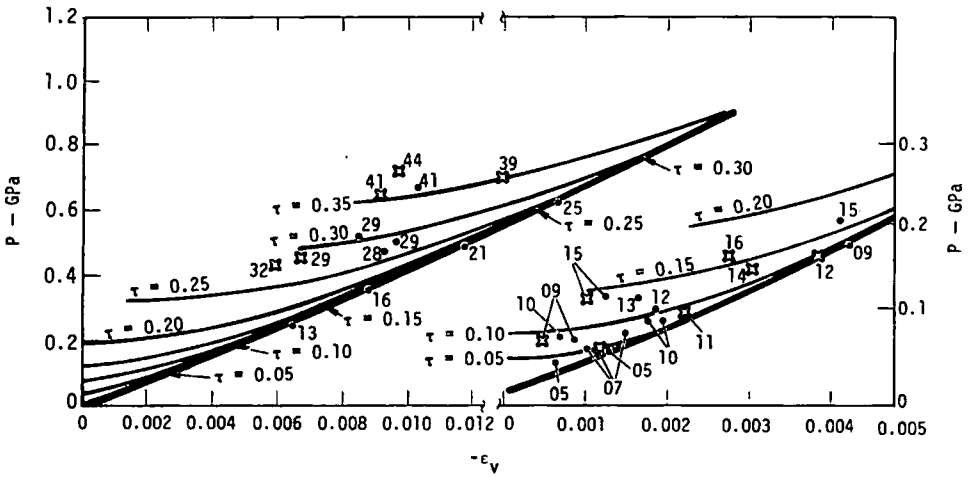

Fig. 1. The behavior of τ as a function of pressure P and volume strain ϵ_v for dilatant but unfailed Climax Stock granodiorite over a variety of loading paths. Numbers represent data ($\tau \times 100$), dots are uniaxial stress ($d\sigma_3 = 0$) loading and x denotes other ($d\sigma_3 \neq 0$) loading paths. Lines represent equation (1) for fixed τ values. Plot on right is enlarged from plot on left.

τ increases. This results in an increased macroscopic volume of the sample with respect to the volume of the solid material which must decrease with increasing mean stress.

For this granite under uniaxial stress compression (where no compaction is observed), low strain-rate uniaxial strain loading is confined along the hydrostat (dilatant strains are precluded) and coincides in $\tau - P$ space with the onset of dilatant behavior [1, 7]. Values of τ for this path therefore define the intersection of isoshear–stress lines (constant τ) with the hydrostat.

CONSTITUTIVE RELATION

To represent isostress (τ) lines in Fig. 1 with an equation, a relationship was chosen to describe the behavior of ϵ_v with respect to P to the left (expansion) side of the hydrostat. This relationship converges to the right (compression) with the hydrostat. When dilatant strains are observed, the data (Fig. 1) are fitted by

$$\epsilon_d = \exp\left[\frac{\delta P}{x(\tau)} - A(\tau)\right], \qquad (1)$$

where ϵ_d is the increase in strain at fixed P due to τ. For the data in Fig. 1, $A = 20(0.7 - \tau)$ and $x = 0.4(\tau - 0.05)$ GPa for $0.1 \leq \tau \leq 0.25$ GPa. At $\tau \leq 0.1$ GPa, x is fixed at 0.2 τ. For $\tau \leq 0.25$ GPa, A is fixed at 9.0 and x at 0.08 GPa. The data for $\tau > 0.25$ GPa are inadequate to fix A and x more closely. The value δP is the difference between the actual pressure P_a (corresponding to a value of τ) and the value of P where the isostress line for that value of τ intersects the hydrostat (P_h), $\delta P = P_h - P_a$. With the relationship $P_h = -0.01 + 2.0\,(\tau + \tau^2)$, P_h is calculated from τ. The $P_h - \tau$ relationship is the envelope that denotes the onset of dilatant behavior [7]. The total volume strain $\epsilon_v(P)$ is obtained from

$$\epsilon_v = -\Delta P/K(P) + \epsilon_d. \qquad (2)$$

The failure surface is commonly used as an envelope in τ and P space as a limit to τ in computer codes. Dilatant strain would be a better indicator because accumulated shear strain is assumed to be directly related to failure. Unfortunately, the experimental data are equivocal (see Figs. 2 and 14 of Ref. [1]), because just before failure the radial strain rate ($\dot{\epsilon}_3 = \dot{\epsilon}_2$ and therefore $\dot{\epsilon}_v$) is very high ($> 10^{-2}$/sec) and strain at the precise moment of failure is often not measured. Until ϵ_3 is more clearly defined at failure, $\epsilon_d = 0.01$ might be used as the failure dilatant strain for this material. Though somewhat arbitrary, this value is in accord with observed data [1]. Furthermore, τ at failure is very insensitive to the chosen value of ϵ_d for $\epsilon_d > 0.005$.

Finally, the need for an explicit relationship including both τ and P is illustrated in Fig. 2. Loading at constant σ_1/σ_3 means that the $\tau - P$ relation is different than for uniaxial stress (constant σ_3) loading. Accounting for this fact is the $P - \epsilon_v$ curvature, which is different if σ_3 is held constant.

CONCLUSIONS

The constitutive relationship at constant axial strain rate for one rock type is expressed as $\epsilon(P, \tau)$. The relationship is simple and expresses the actual behavior

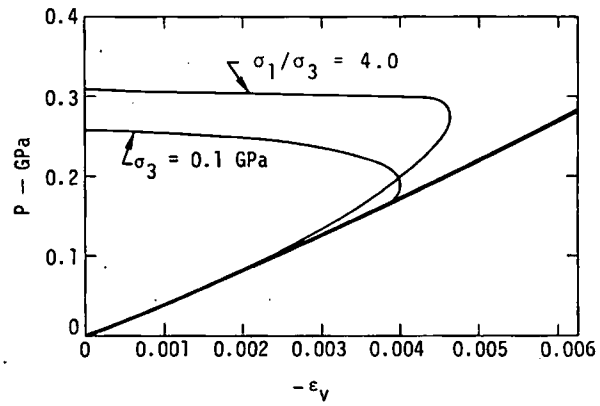

Fig. 2. Predicted pressure P vs volume ϵ_v relationship for loading at constant $\sigma_1/\sigma_3 = 4.0$, compared with the hydrostat and with uniaxial stress loading ($\sigma_3 = 0.1$ GPa).

in terms of experimentally relevant physical parameters. The expression (1) applies only to this rock under the conditions of compression and $\sigma_2 = \sigma_3$. The form should be applicable to other rock types, with different x and A, where dilatancy is exhibited under these conditions.

Brace and Orange [8] have suggested that a simple relation exists between electrical resistivity and crack porosity in dilating rock. Coupled with the ability to calculate crack induced volume changes (ϵ_d), this suggests that electrical measurements might be useful in deducing the magnitude of stress changes in dilating rock bodies. Although no similar relation has been proposed for acoustic velocities, they have been shown [9] to be markedly affected by dilatant strain and might therefore be utilized in a similar manner.

Most holocrystalline granitic igneous rocks exhibit similar physical properties [4], and a constitutive relationship describing their behavior should be similar to that for Climax Stock granodiorite. Another commonly observed inelastic phenomenon, compaction of pores, has been described by constitutive relationships developed in a similar manner [10, 11]. However these relationships do not treat compaction enhanced by shear stress [1]. Nevertheless, the similarity of these relations offers the attractive possibility of treating dilatancy and compaction simultaneously [1]. The form of the compaction relationship as well as that for dilatancy in other rocks is under study.

Acknowledgements—M. Costantino, A. Duba and H. Heard critically reviewed the manuscript and offered many useful suggestions.

This work was performed under the auspices of the U.S. Energy Research & Development Administration.

Received 9 October 1975.

REFERENCES

1. Schock R. N., Heard H. C. & Stephens D. R. Stress-strain behavior of a granodiorite and two graywackes on compression to 20 kbar. *J. Geophys. Res.* **78**, 5922 (1973).
2. Schock R. N., Abey A. E., Heard H. C. & Louis H. Mechanical properties of granite from the Taourirt Tan Afella massif, Algeria., University of California, Lawrence Livermore Laboratory Rept. UCRL-51296 (1972).
3. Griggs D. & Handin J. in *Rock Deformation, Geol. Soc. Am. Mem.* **79** (1960).
4. Swanson S. R. & Brown W. S. An observation of loading path independence of fracture in rock. *Int. J. Rock Mech. Min. Sci.* **7**, 257 (1971).
5. Griffith A. A. The phenomena of flow and rupture in solids. *Phil. Trans. R. Soc.* London, **A221**, 163 (1921).
6. Brace W. F., Paulding B. W., Jr. & Scholz C. Dilatancy in the fracture of crystalline rocks. *J. Geophys. Res.* **71**, 1417 (1966).
7. Schock R. N. & Heard H. C. *J. Geophys. Res.* **79**, 1662 (1974).
8. Brace W. F. & Orange A. S. Electrical resistivity changes in saturated rocks during fracture and frictional sliding. *J. Geophys. Res.* **73**, 1443 (1968).
9. Benzing W. M., Bonner B. P. & Schock R. N. Ultrasonic travel times in a granodiorite under uniaxial compression. University of California, Lawrence Livermore Laboratory Rept. UCRL-51477 (1973).
10. Herrmann W., Constitutive equation for the dynamic compaction of ductile porous materials. *J. appl. Phys.* **40**, 2490 (1969).
11. Carroll M. & Holt A. C. Suggested modification of the $P - \alpha$ model for porous materials. *J. appl. Phys.* **43**, 759 (1972).

Akad. Nauk SSSR 1948.
7) A I Begunov et alia: Izv VUZ Tsvetnaya Metallurgiya 1972, (5), 42.
8) Lapple and Shepherd: Ind Eng Chem, 1940, 32, 605.
9) J Perry: Chemical Engineer's Handbook, Vol. 1, Khimiya, Leningrad.

UDC 669.721.4

Purification of magnesium melts with special additives

V A Kechin, N M Demido, A S Malyugin and I P Vyatkin (North-Caucasian Mining-Metallurgical Institute and the Bereznik Titanium-Magnesium Combine)

Summary

The preferred and most promising method for the refining of magnesium melts is treatment with metallic additives. The aim of the work was to investigate the effectiveness of the reaction of manganese, zirconium and titanium with the impurities in the magnesium melt. The reaction between the additives and the impurities was assessed from the qualitative (phase diagrams) and quantitative (effectiness of the reaction) standpoints.

The phase diagrams for the magnesium-additive-impurity system were analysed with due regard for the metallic and chemical characteristics of the reacting elements in combination with calculated and experimental data on the effectiveness of the reaction. The necessary information was obtained for selection of the additive, its consumption rate, and the technique for purification of magnesium melts in relation to the composition of the initial material and to the requirements made of the final product.

Reaction of iron(II) with cyanide and alkali in solution

L D Sheveleva, A A Golovin and M N Tagil'tseva (Urals Polytechnical Institute - Department of the Metallury of Noble Metals)

Summary

To reduce the losses of cyanide with iron(II) compounds it is necessary to maintain not only the optimum alkalinity in the pulp but also the appropriateconcentration of the oxidising agent in the solution both in the alkaline agitation process and in the cyaniding process. The presence of ferrocyanide in the solution may indicate a deficiency of both alkali and oxidising agent in the pulp.

Increase in the oxidation rate of iron(II) is promoted by better dispersion of the air in the pulp, the delivery of oxygen, the use of surfactants, and the use of strong oxidising agents. The cyanide consumption can be reduced by dissolving the cyanides in a weak solution of acid, followed by treatment of the pulp in an alkaline medium before cyaniding.

UDC 661.877:66.094.235:543.5+543.257.1

Contact reduction of molybdenum from organic media

V I Sherashov, O V Kuz'michev and V M Blavatnik (Yaroslavl Polytechnical Institute - Department of Analytical Chemistry)

Little is known in the literature on the contact reduction of metals from organic media on solid metal cementation reagents. The present report gives the results from an investigation into the reduction of molybdenum(VI) from a series of oxygen-containing solvents: tributyl phosphate (TBP) and its solutions in kerosene and caron tetrachloride, cyclohexanone (CH), acetophenone (AP), methyl isobutyl ketone (MIBK), diethyl ketone (DEK), and butyl acetate (BA), which are good extractants for the extraction of molybdenum from aqueous solutions[1]. All the employed extractants were of pure grade, and the TBP was purified from hydrolysis products by the method described in the literature[2]. Ammonium molybdate of chemical purity was used to prepare the aqueous solutions of molybdenum.

The molybdenum was transferred into the organic phase by extraction from hydrochloric acid solutions with the aqueous and organic phases in a ratio of 1:1. (The volume of the phases amounted to 20ml). The concentration of molybdenum in the aqueous phase amounted to 5g/l. After separation into layers the aqueous phase was separated from the organic phase and analysed for residual molybdenum content[3]. The amount of molybdenum in the organic phase was calculated from the difference between its concentrations in the aqueous phase before and after extraction. The contact reduction of molybdenum was realised in a thermostated cell (±1°C) provided with a magnetic stirrer. At the end of the experiment the residue of the metal reducing agent and the molybdenum reduction products were separated from the organic phase by filtration, washed several times with acetone and distilled water, and dissolved in hydrochloric acid (1:1) with the addition of hydrogen peroxide or nitric acid to oxidise the molybdenum to the hexavalent state. After removal of the excess of the oxidising agent the molybdenum content was determined by the methods described in the literature[3,4].

The effect of various factors on the rate and degree of extraction of molybdenum was investigated. These factors included the nature of the metal reducing agent and the organic extractant, the temperature, the contact time, and the concentration of hydrochloric acid in the organic phase.

The effect of the nature of the metal reducing agent on the degree of extraction of molybdenum was investigated on magnesium, aluminium, zinc and iron (in the form of plates and powders) from a 50% solution of TBP in carbon tetrachloride. The results showed that the highest degree of extraction of molybdenum is observed on zinc and amounts to 92% when zinc powder of grade PTs-2 is used (particle size 45-60μ). At 40°C with a contact time of 20 min the degree of extraction of molybdenum increases with increase in the weight ratio, of the metal reducing agent to molybdenum (fig. 1). All the subsequent experiments on the contact reduction of molybdenum were carried out on zinc powder with a

Zn:Mo ratio of 30:1.

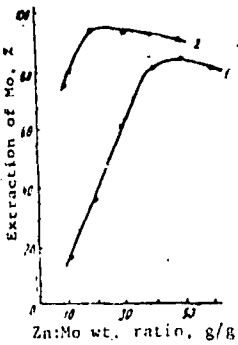

Fig.1
Effect of the weight ratio of zinc and molybdenum (g/g) on the degree of extraction of molybdenum from solutions of 100% TBP (1) and 50% TBP in carbon tetrachloride (2).

The table gives data on the effect of temperature and contact time on the degree of extraction of molybdenum from various organic extractants. The results show a fairly high extraction of molybdenum from ketones (MIBK, AP, CH, DEK) over a wide range of temperatures. For TBP, which has a considerably higher viscosity (η = 3.39cP) than ketones (η = 0.5-1.99cP), the degree of extraction increases with increase in temperature. Dilution of the TBP with inert solvents (fig. 2), which is accompanied not only by a decrease in the viscosity of the solution but also by a decrease in the dielectric constant, leads to a considerable increase in the molybdenum reduction rate. The results from experiments on the reduction of molybdenum from butyl acetate (fig. 2, curve 3), which also has low viscosity (0.732cP) and dielectric constant (4.87), makes it possible to conclude that the viscosity of the organic extractant is one of the important factors affecting rate of the process.

Table: The degree of extraction of Mo during contact reduction from various organic extractants

Temp. °C	TBP			MIBK	AP	CH	DEK
	Time min						
	10	20	30	10	10	10	10
20	3.12	3.70	3.75	93.5	93.5	94.0	80.0
40	3.50	62.9	62.8	91.0	94.5	93.2	85.0
60	72.5	87.5	87.5	93.0	98.8	94.5	80.0

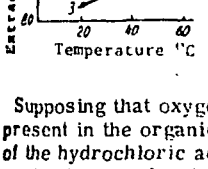

Fig.2
The effect of temperature on the degree of extraction of Mo from butyl acetate (1), a 50 vol.% solution of TBP in kerosene (2), and in carbon tetrachloride (3).

Supposing that oxygen-containing ions of molybdenum are present in the organic phase [1], we investigated the effect of the hydrochloric acid concentration in the organic phase on the degree of reduction and the degree of extraction of molybdenum. For this purpose we used a 50% solution of TBP is ethyl alcohol and molybdenum acetylacetonate, obtained by the method in [6]. An accurately weighed sample of the salt was dissolved in an aliquot portion of the solution of TBP in ethyl alcohol, containing various amounts of hydrochloric acid. The experiments showed that the extraction of molybdenum increases from 25 to 92% with increase in the concentration of hydrochloric acid in the organic phase from 0 to 0.2mole/l. Further increase in the concentration did not lead to a significant change in the degree of extraction. It should be noted that in the absence of hydrochloric acid molybdenum is largely reduced to "molybdenum blue".

To determine the mechanism of the contact reduction of molybdenum from TBP the electron paramagnetic resonance spectra were recorded. The spectra were recorded on a JES-ME-3X 3-cm spectrometer with modulation of 100Hz. The EPR spectrum of the solution of molybdenum in TBP obtained during contact reduction is typical of Mo(V) compounds [7]. The strong central line in the spectrum from the even isotopes of Mo(V) has a g factor of 1.946. The intensity of the EPR signal of Mo(V), which was determined as the distance between the minimum and the maximum of the central line in the spectrum, increases sharply (from $5\cdot10^{-2}$ spin/g to 10 spin/g) with the addition of zinc to the solution of Mo(VI) in TBP (at 60°C). It then decreases for 10-15 min (to $6\cdot10^{-2}$ spin/g), which indicates further deeper reduction of molybdenum (V).

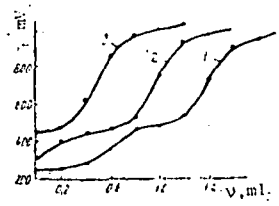

Fig.3
Potentiometric titration curves for the solution containing the products from the reduction of molybdenum: 1 - recorded directly after dissolution of the reduction products; 2,3 - 96 and 240 h after dissolution. Titration with a $7.26\cdot10^{-2}$M solution of cerium sulphate.

The presence of compounds of molybdenum of lower valency in the contact reduction products was established by potentiometric titration. For this purpose the zinc residue with the contact reduction products was thoroughly washed with acetone and distilled water and dissolved in 3N hydrochloric acid without the addition of an oxidising agent. The obtained solution was titrated with a standard solution of cerium (IV) sulphate [8, 9] on an LPM-60M pH-meter with a platinum indicator electrode and a saturated calomel electrode in 3N hydrochloric acid at room temperature. The potentiometric titration curves are given in fig. 3 (curve 1). Quantitative treatment of the experimental data and gravimetric analysis of the solution [4] containing the contact reduction products for total molybdenum content made it possible to conclude that the first potential jump in the titration corresponds to the oxidation of Mo(III) to Mo(IV) and the second corresponds to further oxidation of Mo(IV) to Mo(VI). The average valency of the molybdenum in such a solution, which was established by the published method [10], was found to be +3.5, which shows that ions of molybdenum in various valency states are present in the solution. It was established that the products from the contact reduction of molybdenum are unstable in hydrochloric acid solution (fig. 3, curves 2 and 3).

Consequently, the reduction of Mo(VI) by zinc in a TBP medium takes place in stages:

$$Mo(VI) + \bar{e} \longrightarrow Mo(V)$$

$$Mo(V) + 2\bar{e} \longrightarrow Mo(III)$$

and the formation of molybdenum sesquioxide as one of the supposed products from the contact reduction of Mo(VI) can be described by the reaction:

$$2MoO_2^{2+}{}_{(org)} + 2H^+_{(org)} + 3Zn_{(solid)} \rightarrow Mo_2O_3{}_{(solid)} + H_2O_{(org)} + 3Zn^{2+}_{(org)}$$

Conclusions

1. The possibility of contact reduction of molybdenum(VI) from various oxygen-containing organic extractants with zinc was demonstrated. The effect of various factors on the rate and the degree of extraction of molybdenum was investigated, and the optimum conditions for the extraction of molybdenum from TBP were selected.
2. The stage character of the reduction of Mo(VI) to Mo(III) was demonstrated by the EPR and potentiometric titration methods, and the mechanism of the formation of Mo_2O_3 as one of the reaction products is described.

References

1) Yu A Zolotov et alia: Extraction of metal halide complexes: Nauka, Moscow 1973.
2) M S Milyukova et alia: Analytical chemistry of plutonium: Nauka, Moscow 1965, p. 318.
3) L B Zaichikova: Zavod. Lab. 1949, 15, (9), 1025.
4) V F Gillebrandt et alia: Practical manual of inorganic analysis: Goskhimizdat, Moscow 1957, p. 239.
5) M Mark Jones: J. Amer. Chem. Soc. 1959, 81, 3188.
6) N S Garif'yanov et alia: Dokl. Akad. Nauk SSSR 1963, 150, (4), 802.
7) N S Garif'yanov et alia: ZhETF, 1962, 43, No. 2, (8), 376.
8) M J Farah et alia: Z. Anal. Chem. 1959, 166, 24.
9) A Berka et alia: New redox methods in analytical chemistry: Khimiya, Moscow 1968, p. 212.
10) A S Goncharenko: Zh. Prikl. Khim. 1964, 37, (4), 915.

UDC 669.55.298.621.357.9.298

Anodic dissolution of thorium and thorium-zinc alloys in chloride and chloride-fluoride electrolytes

Yu P Kanashin, I F Nichkov and S P Raspopin (Urals Polytechnical Institute. Department of the Metallurgy of Rare Metals)

Summary

Thorium reacts vigorously with zinc to form stable intermetallic compounds. This must have an effect not only on the decrease in the cathodic deposition potentials of thorium on zinc but also on the kinetics of the anodic dissolution of zinc-thorium alloys. The anodic polarization of metallic thorium and thorium-zinc alloys in chloride and chloride-fluoride electrolytes was investigated. The polarization curves were used to obtain the limiting diffusion currents for the ionisation of thorium during the dissolution of zinc-thorium alloys.

On the basis of data on the current yield and of anodic polarisation measurements it was established that a mixture of divalent and tetravalent ions is formed during the dissolution of thorium and its alloys with zinc. It was shown that an increase in the temperature from 680 to 780°C leads to a decrease in the proportion of tetravalent ions from 90 to 50%.

UDC 669.018.95:621.7.073

Properties of sintered materials based on titanium and chromium carbides and their use under isothermal deformation

S S Kiparisov, V K Narva, B D Kopyskii, I S Zonnenberg, I L Tseitina and A M Tashlykov (Moscow Institute of Steel and Alloys and the All-Union Correspondence Engineering Institute)

One of the most promising trends in the pressure treatment of metals is hot deformation under isothermal conditions[1]). High temperatures (up to 1000-1100°C) and prolonged treatment (up to 10-15 min), which give rise to rapid crushing of the tool, make special demands in the choice of tool materials. The employed heat-resistant nickel casting alloys have substantial disadvantages, i.e. billet at high degrees of deformation and high cost.

As known, compositions based on refractory carbides with various heat-resistant binders have the ability to operate for a prolonged period under high temperature conditions[2]). Since there are no thermal shocks, dynamic loads, or high specific pressures (the main reasons giving rise to crack formation in sintered materials) during hot isothermal deformation, their use under these conditions is promising. The present work was devoted to this problem.

Compositions containing 45-75 wt.% of titanium carbide cemented by the ZhS6-K alloy and also materials containing 70 wt.% of chromium carbide with a binder of the Nimonic type were investigated. The ZhS6-K alloy was used in the form of a powder obtained by joint reduction of the oxides with calcium hydride, and the binder of the Nimonic type was used in the form of a mixture of the powdered alloy components. The investigated materials were obtained by joint mixing of the carbide powders and the cementing binder, subsequent compaction, and liquid-phase sintering under vacuum. The sintered materials were subjected to heat treatment, i.e., quenching from high temperatures with air cooling followed by ageing. The conditions for the production and heat treatment of alloys with density close to the theoretical are given in table 1.

To investigate the possibility of using the obtained alloys under conditions of isothermal deformation the physical and mechanical properties, which characterise the resistance to the main forms of damage under operational conditions, were studied. These included plastic deformation (crushing), adhesion wear resulting from seizure with the surface of the deformed billet, oxidative wear, and the brittle fracture characteristic of sintered materials.

The resistance of the alloys to crushing was evaluated by a combination of two characteristics, i.e., the conditional static yield limit and the index m characterising the effect of the loading time τ or the deformation rate $\dot{\epsilon}$ on the resistance to deformation σ. For the resistance to deformation we used the conditional yield limit at various deformation rates. The dependence of σ on τ is determined by the equation [3]):

$$\sigma = B\left(\frac{\epsilon}{\tau}\right)^m (0 < m < 1) \qquad (1)$$

where B = constant of the material $\tau = \epsilon / \dot{\epsilon}$
ϵ = degree of deformation (const).

The values of the index m can be obtained graphically as the tangent of the slope of the straight line against the coordinates $\log \sigma$ and $\log \dot{\epsilon}$.

The adhesion strength of the materials was determined from their hot hardness. To determine the susceptibility of the alloys towards oxidation during use in air under high temperature conditions the scale resistance was investigated. To characterise the resistance of the alloys to brittle fracture we used the bending strength. The physical and mechanical properties of the sintered materials were compared with the strength characteristics of the best heat-resistant casting alloys ZhS6-K and ZhS6-U[4]).

The resistance to deformation under compression and the bending strength of the materials were determined experimentally on a UMÉ-10TM machine. Samples 8.5 mm in diameter and 25 mm high were upset with deformation rates in the range of $3.3 \cdot 10^{-6}$ to $3.3 \cdot 10^{-3}$ sec^{-1} with a degree of deformation $\epsilon = 0.002$. The conditional static yield limit was determined with a deformation rate of $3.3 \cdot 10^{-4}$ sec^{-1}. The conditional static yield limit was determined with a deformation rate of $3.3 \cdot 10^{-4}$ sec^{-1}. The dimen-

(Continued from p 39)

he short term, the embassy is predicting mport demand in 1981 for $70 million in backhoes, buckets, continuous miners, cutters, dredging machinery, drills, excavators, graders, scrapers, shovels, trenchers and ditchers, and hammers and other pile driving equipment. There will also be a $30 million demand for loaders, truck shovel conveyors, cranes and jacks, and $22 million in pumps and air compressors during that year. Off-highway rear dump trucks and truck-tractor haulers will make up another $30 million in demand. Additional projected demands for 1981 include $11 million in trucking and hauling equipment (including carriers and trailers); $5 million for surveying instruments, and geophysical equipment; $5 million for vibrators, drills, and tools; and $12 million for separators, cyclones, scrubbers, thermal dryers, spirals, thickeners, filters, feeders, washing plants, screening plants, mixers, and crushing-grinding equipment.

The embassy is optimistic that US exporters can hold their own as the market grows because of the leading role US consultants play in mining expansion and new development projects in Chile. The US share of the market in 1978 was an average 48%.

The embassy emphasizes the importance of exporters having an import agent or distributor in Chile. Codelco calls for bids on all projects above $600,000, and takes into account the reputation of the manfacturer and its previous experience with the company as well as the reputation and experience of the local agent with whom Codelco will deal for parts, service, and delivery.

Chilean tariffs, except for automobiles and small trucks, are at 10% across the board, with a 20% value added tax on cif value plus customs duties.

Recent US government measures that cut Eximbank financing and guarantees and Overseas Private Investment Corp. guarantees to Chile will have no effect on the Chilean economy in general or the mining industry in particular, according to Santiago sources. Hardest hit by the measures will be US exporters who want to enter the Chilean market but are not able to supply credits that are supplied by other countries.

Eximbank has extended no loans to Chile since 1970, and has limited guarantees to credits of up to $740,000. OPIC has guaranteed no investment in Chile since 1970, when a Socialist government was elected.■

Cliffs readies uranium solution test in Pumpkin Buttes area

Construction is 80% complete at the Collins Draw uranium solution mining pilot research project managed by The Cleveland-Cliffs Iron Co., and startup is planned for early this year. The project is located in Campbell County, Wyo., about 85 mi northeast of Casper in the Pumpkin Buttes district of the North Powder River Basin. Joint venturers with Cliffs in the project are Pioneer Nuclear Inc., Getty Oil Co., Thunderbird Petroleum Inc., and Texas Eastern Nuclear Inc.

The host sand lies at an average depth of 425 ft, and averages 50 to 55 ft thick. A water-based solution of ammonium carbonate and hydrogen peroxide will be used as the lixiviant.

A fixed-bed ion exchange system and yellowcake precipitation will be used along with a dryer circuit and water purification system. Major components of the process equipment are modular and mounted on skids. The plant has been built on an impervious pad near the well field and housed in a building to permit year-round operation. The well field area occupies 1¼ acres of the 23-acre permit area.

Process description

At Collins Draw, dilute ammonium carbonate and hydrogen peroxide are

(Continued on p 47)

R&D concept for Cleveland-Cliffs Iron Co. uranium solution mining project

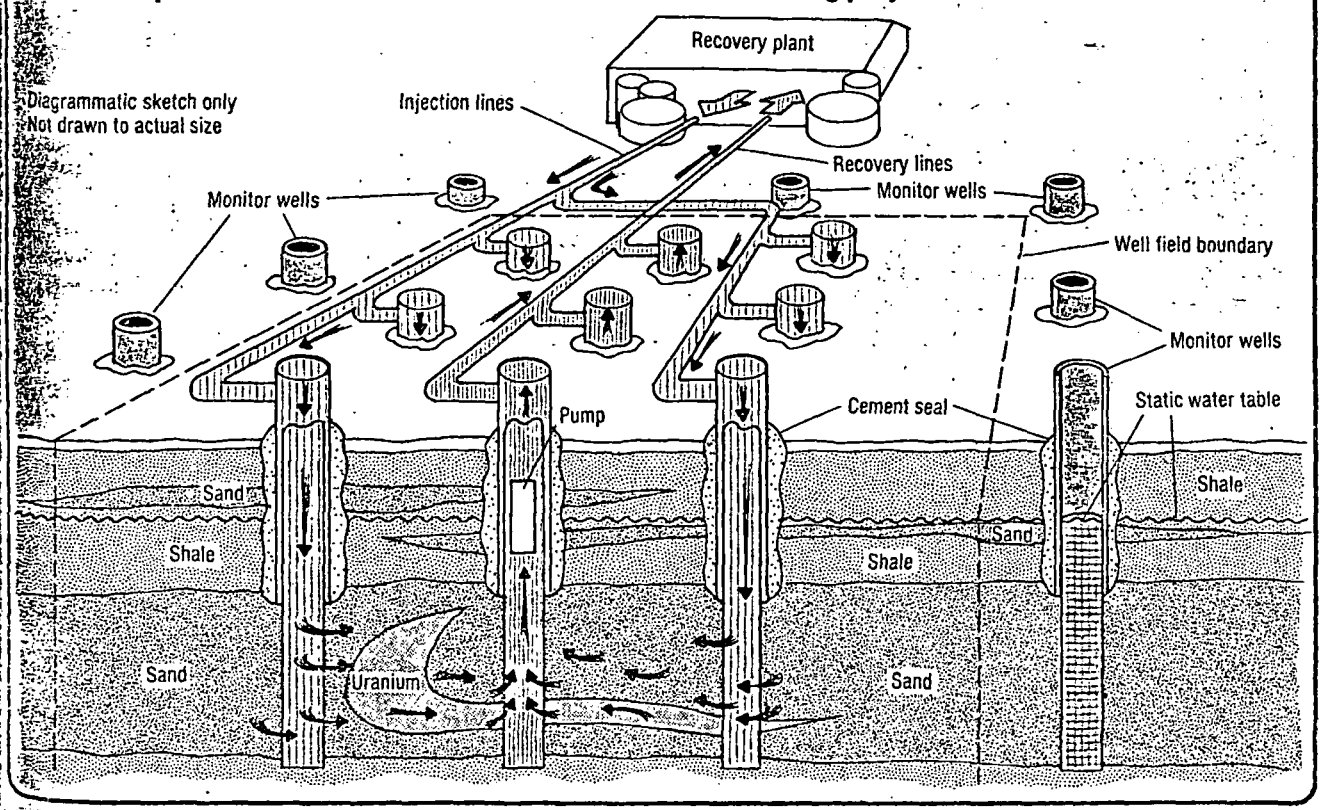

EMJ JANUARY 1980

(Continued from p 43)
introduced into the sandstone host rock to dissolve the uranium. The solution will be extracted by submersible pumps from the production wells and moved to a production surge tank. The solution then passes through an anionic exchange resin that has a strong affinity for the ammonium uranyl tricarbonate complex. A strong solution of ammonium carbonate is then used to strip the uranium complex from the resin. The eluant solution will contain 10 to 20 gpl of uranyl tricarbonate.

The uranium is precipitated with heat to produce a very pure uranyl oxide, gaseous ammonia, and carbon dioxide. The uranyl oxide is pumped to a settling tank, and from there to a rotary vacuum dryer heated by steam. The gas products are recovered and recycled to produce fresh strip solution for re-use in the eluant circuit.

The yellowcake is dried to less than 3% moisture and transferred to drums for shipment. All water vapor and other gases from the drying process are collected and made available as plant makeup water.

Monitoring and detection

A "12-spot" well pattern will be used, with the distance between wells varying from 20 to 30 ft. High-quality flow meters, recording both flow and quantity, will be installed on each production and injection well.

The well field area will be circled with monitoring wells, which will be sampled regularly for uranium, sulphate, ammonium, bicarbonate, alkalinity/acidity, and other factors. Before beginning the injection of lixiviant solution into the sandstone host rock, water purified by a reverse osmosis process is introduced into the pattern area to form a barrier between the well fields and the monitoring wells. Any escape of lixiviant outside the mined area will push this water ahead of it. The mining operator will thus have an early indication of any excursion when sampling of the monitoring well shows a drop in sulphate and bicarbonate. Corrective action can be taken by adjusting the injection and pumping rates within the pattern area. Bromine added to the reverse osmosis water can be used as a tracer to aid in excursion detection.

Should an escape of uranium from the well field pattern occur, the flow of the injection wells nearest the point of excursion can be reversed so that they become extraction wells, drawing the escaping ions back into the well field pattern.■

Chinese iron ore projects are basis for future steel boost

The Sijiaying and Nanfen open-pit mines currently under development in China will be among the world's largest, reaching a final depth of about 500 m, according to a recent article in KAISER ENGINEERS BUILDER. Since August 1978, Kaiser Engineers has been working on the two iron ore mining projects that will play significant roles in China's plans for a substantial increase in steel production during the 1980s.

To remove 3 billion to 4 billion mt of overburden, the mining operations will use some of the largest equipment ever utilized in iron ore mining—13.6-cu-m shovels and 154-mt trucks.

The Sijiaying project requires development of a new mining operation and ore processing facilities to produce iron oxide pellets for blast furnace feed. Sijiaying is in the floodplain of the Luan River in Hebei province, about 300 km east of Peking. Kaiser Engineers is currently providing phase 1 engineering for the mine, concentrator, pellet plant, and auxiliaries, including utilities, tailings disposal, maintenance, and warehousing facilities.

Sijiaying ore is a complex mixture of martite and magnetite. The martite occurs in the upper layers of ore, with predominantly magnetite below. In devising a mining plan, computer analysis was used to coordinate pit development, truck movement, and related factors to achieve the required consistency and optimum operation. Beneficiation will involve a highly complicated flow through three stages of concentration, blending concentrates that have been produced through fine grinding, low-intensity magnetic separation (for magnetite), high-intensity magnetic separation (for martite), and flotation. Iron content of the ore will be upgraded to about 66% from the initial 28%.

The stripping ratio at Sijiaying is unusually large—more than three to one. A variety of options is being examined to handle the problem, including rail haulage, truck haulage, crushing in the pit with conveying, and combinations of these.

Tailings at Sijiaying will be pumped 45-50 km to the coast and impounded in tailings ponds in the sand dunes to avoid disrupting valuable agricultural land in the Luan floodplain.

Nanfen is an operation in Liaoning

(Continued on p 49)

Notes on Zambian mining

Delays in communications prevented the following corrections and additions from being made in the reports on operations at the Chibuluma, Chambishi Div. of RCM and the Broken Hill Div. of NCCM in the November E&MJ.

At Chambishi, the fluid bed reactor at the cobalt plant measures 9.6 m dia at the tuyere bed and 12.5 m dia at the dome. Partially neutralized, spent electrolyte is used to quench hot roaster calcine. The plant is designed to produce 16,800 mtpy of copper cathode. The cobalt is shipped in 200-kg drums. Underground mine production is expected to reach 187,000 mtpm by January 1981. The No. 3 shaft is 1,021 m deep. Reserves at the mine total 39 million mt at 2.9% Cu. Reserves at Chambishi Southwest total 29 million mt.

The flotation circuit consists of three parallel banks of Fagergren 120 cells, 15 cells per bank. The first four cells in each bank produce rougher concentrate. The remaining 11 produce a scavenger concentrate, which is returned to the head of the ball mill circuit for further grinding. The rougher concentrate is upgraded to a final concentrate grading 45% Cu by passing it through four parallel Davcra 180 cells. Normal flotation pH is 8.5.

At Chibuluma, mines are designated Chibuluma and Chibuluma East. Maximum strike length is 700 m, and dip averages 40° at Chibuluma, where reserves measured to a depth of 820 m total 6.8 million mt grading 4.68% Cu. At Chibuluma East, reserves stand at 5.0 million mt of 4.70% Cu and 0.12% Co. The 2A shaft is sub-inclined and hoists from the 730-m level. It is being deepened to 822 m. At the concentrator, the cobalt circuit produces a single concentrate from Denver No. 30 cells, with a Davcra 180 cell functioning as a scavenger but producing final concentrate grade. The combined cobalt concentrates are pumped to the cobalt thickener.

At Broken Hill, current production totals 46,000 mtpy of zinc and 14,000 mtpy of lead. All crushing takes place on the surface. After heavy media separation, grind of the sink product produces a 65% minus-325-mesh feed for the flotation circuit. After galena-pyrite flotation, tailings from the rougher cells report to zinc rougher cells. Cleaner cells produce a zinc concentrate, and cleaner tails return to the roughers.■

SOCIETY OF
MINING ENGINEERS
OF
AIME
CALLER NO. D, LITTLETON, COLORADO 80123

PREPRINT
NUMBER
80-327

CONCENTRATE REGRIND AT THE RAY CONCENTRATOR

J. W. Lowry
Concentrator Operations Superintendent
Ray Mines Division
Kennecott Minerals Company
Hayden, Arizona

For presentation at the SME-AIME Fall Meeting and Exhibit
Minneapolis, Minnesota - October 22-24, 1980

Abstract. After 69 years of processing copper porphyry ores, the Ray concentrator of Kennecott Minerals Company installed a concentrate regrind mill in its flotation circuit. The first cleaner concentrate is reground rather than the usual rougher concentrate. An additional cleaning of the reground product yields an increase in copper content of the final concentrate and a significantly lower insol content. The desired goal of decreasing the energy requirements for smelting the concentrate has been achieved.

The concentrator at the Ray Mines Division of the Kennecott Minerals Company has processed porphyry copper ores for 69 years with many of the techniques described in Taggart's "Handbook of Mineral Dressing." The ore has been reduced in jaw and gyratory crushers, rolls and standard and shorthead cone crushers to feed grinding circuits containing Chilean mills and several sizes of rod and ball mills. Sizing and classification has been accomplished with impact and vibrating screens, Janney hydraulic classifiers, cone tanks, rake and bowl classifiers and hydraulic cyclones. Gravity separations have been made with Garfield and Wilfley shaking tables, jigs and vanners. Flotation separations have been made with Janney flotation machines, pneumatic Callow cells, followed by Fagergren machines for cleaning, and for the past seven years in modern WEMCO 120 cells. A leach-precipitation-flotation circuit was used to process high non-sulfide ores for eleven years.

However, until this year we did not have a concentrate regrind mill installed for that purpose only. To the best of my knowledge concentrate regrind capabilities are included in every other copper concentrator in the southwest, and so it certainly is not a new wrinkle. Yet, our flotation differs sufficiently from the conventional regrind and cleaner circuits to consider it novel.

The Ray flotation circuit consists of six rows--fifteen cells per row--of WEMCO No. 120 flotation machines as portrayed graphically in Figure 1. The roughing circuit consists of five rows that currently process 24,900 metric tons per day. The first nine cells in each row make a rougher concentrate, and the last six cells make a rougher scavenger concentrate that is recirculated to the head of the rougher circuit. The rougher concentrates from each row are pumped to the sixth row that serves as the cleaner row. The cleaner row is identical to the rougher rows in that it contains fifteen cells arranged in banks of four, five and six cells each. The first bank is designated as the final cleaners, the middle bank as the first cleaners, and the last bank as the cleaner scavenger bank.

The rougher concentrate is introduced into the fifth cell at the head of the first cleaner bank of the cleaner row. In the original flowsheet, and whenever the regrind mill is down, that bank makes a first cleaner concentrate that is pumped to the first cell of the final cleaners, and those four cells produce the final concentrate. The tailings from the final concentrate bank flow into the first cleaners where the sulfide minerals have another opportunity to join the first cleaner concentrate. The first cleaner tails flow into the last bank of cells in which a cleaner scavenger concentrate is made. The latter flows back to the rougher concentrate sump for recirculation and upgrading in the cleaner row. Cleaner scavenger tails can be diverted to the rougher tails or sent back to the head of the rougher circuit.

We used the original flowsheet for two and a half years and made concentrates containing 16%-18% insol. Then we were asked to reduce the insol content as much as possible without additional capital expenditures in an effort to improve the smelting process. One of the 7 x 10 ball mills had been outfitted with four D10B Krebs cyclones several years previously for a concentrate regrind test on Row 1 of the sulfide roughers. (This is the test row of WEMCO 120 machines installed in 1968.) The small mill obviously could not handle the tonnage of rougher concentrate from five rows and we doubted that it could handle even the first cleaner concentrate. But we tried it. It didn't. Back to the drawing board.

Sampling of each cell of the cleaner row when the new cells were installed had established that the first two cells of the first cleaner bank made a concentrate grade higher than the final concentrate over 90% of the time. Nothing astounding about that -- the completely liberated mineral particles are fast floating and pop to the surface immediately. So we decided to take advantage of this by routing the high grade froth from the first two cells directly to the final concentrate sump. We hoped that this would reduce the tonnage going to the little mill by as much as one-third. The froth from the last three cells of the bank contained the locked minerals that really needed regrinding. The idea worked beyond our expectations and the insol content was reduced to the 12%-14% level.

We operated the temporary regrind for three years in the expectation that an expansion would be approved that would include sufficient regrind capacity to process the rougher concentrate as in other concentrators. The expansion did not materialize.

Then along came the energy crunch that made a fuel reduction program imperative. The smelter could reduce its fuel requirements if the insol content of the concentrate were reduced still further. As a consequence, approval was received to install one concentrate regrind mill.

It had been calculated that three 670 kW mills would be required to handle the tonnage of rougher concentrate but that only one 450 kW mill would be necessary to treat the first cleaner concentrate. The regrind circuit was designed accordingly with the flow shown in Figure 2.

The first cleaner concentrate is pumped to a cyclone feed sump that also receives the regrind mill discharge. The combined pulps are pumped to a pod of four D20B Krebs cyclones. The cyclone overflow is pumped back to the head of the final cleaner bank and refloated to produce a final cleaner concentrate. The cyclone underflow drops down into the mill feed spout.

The regrind mill is a 3.2 m x 4.27 m Allis-Chalmers overflow ball mill with a 450 kW motor operating at 14.3 rpm. The mill is charged with 2.5 cm ARMCO Moly-Cop forged steel balls.

The D20B Krebs cyclones are fitted with 129 cm^2 inlets, 15.2 cm diameter Ni-Hard vortex finders and 6.35 cm diameter Refrax apexes.

Initially the mill was charged with enough balls to draw approximately 360 kW. The ball load has been increased at times so as to draw as much as 400 kW. The grind improved but was not accompanied by further reductions in insol in the final concentrate.

To date, two cyclones handle the feed most of the time. The cyclone underflow density which is also the mill discharge density, ranges from 70%-75% solids. The overflow density hovers around 15% solids. Although the cyclones are operating well below the design pressure of 100 kPa, screen analyses of the final concentrate averaged 81% minus 44-microns for the first five months of operation.

Overall the regrind circuit is meeting its objectives. The reduction in insol content has been greater than expected. For the first years of operation with the WEMCO cells and no regrind at all the insol level ranged from 16%-18%. The next four years of operation with the temporary regrind circuit yielded insol levels ranging from 12%-14%. The new regrind facility has cut the insol content in half, averaging 7% for the first months of operation.

We are not satisfied that we have yet found the optimum parameters. Wide variations in the ore mix, supply and hardness for the first months of this year have made life interesting, and a steady state operation has been a rather elusive target. Nevertheless, the concentrate produced by a circuit that treats a first cleaner concentrate rather than rougher concentrate is improving the smelting operation. Fuel consumption has been reduced, the lower smelting temperatures should increase the refractory life of the furnace, and less reverberatory slag is produced. The regrind circuit is not conventional, but it works.

Acknowledgements: I would like to acknowledge the assistance of Mr. Marvin Harmer, chief metallurgist, and his metallurgical technicians, for their work in sampling the regrind circuit, and the fact that Mr. Gary Jungenberg, concentrator general foreman, brought the circuit on-line with a minimum of problems.

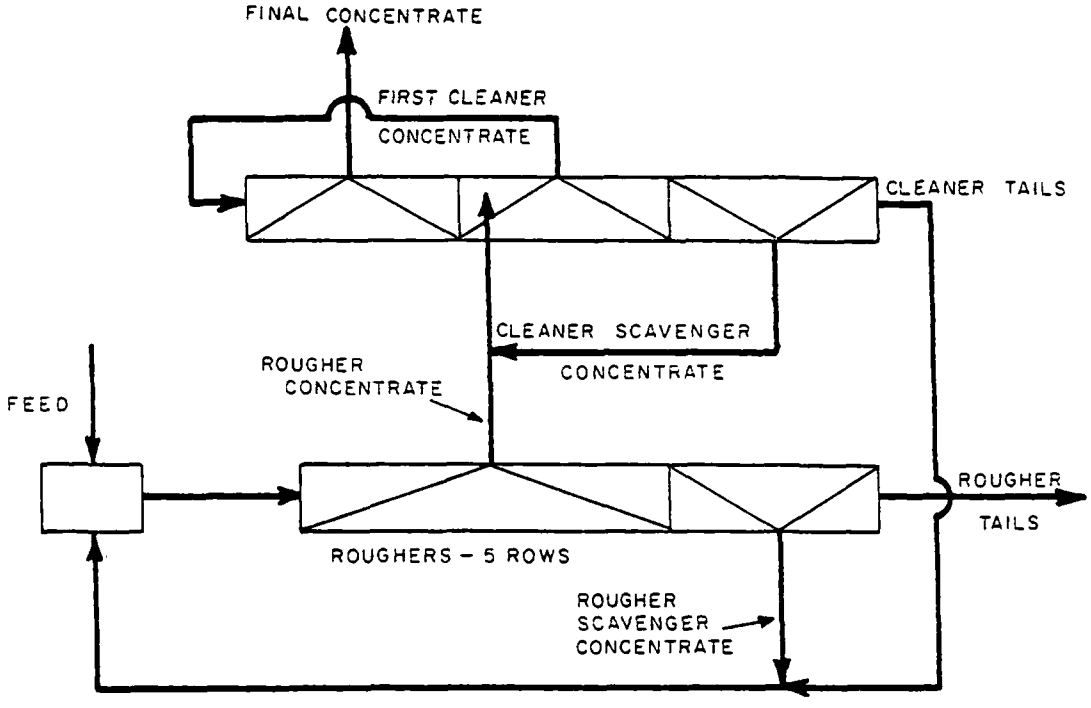

Figure 1. Sulfide Flowsheet

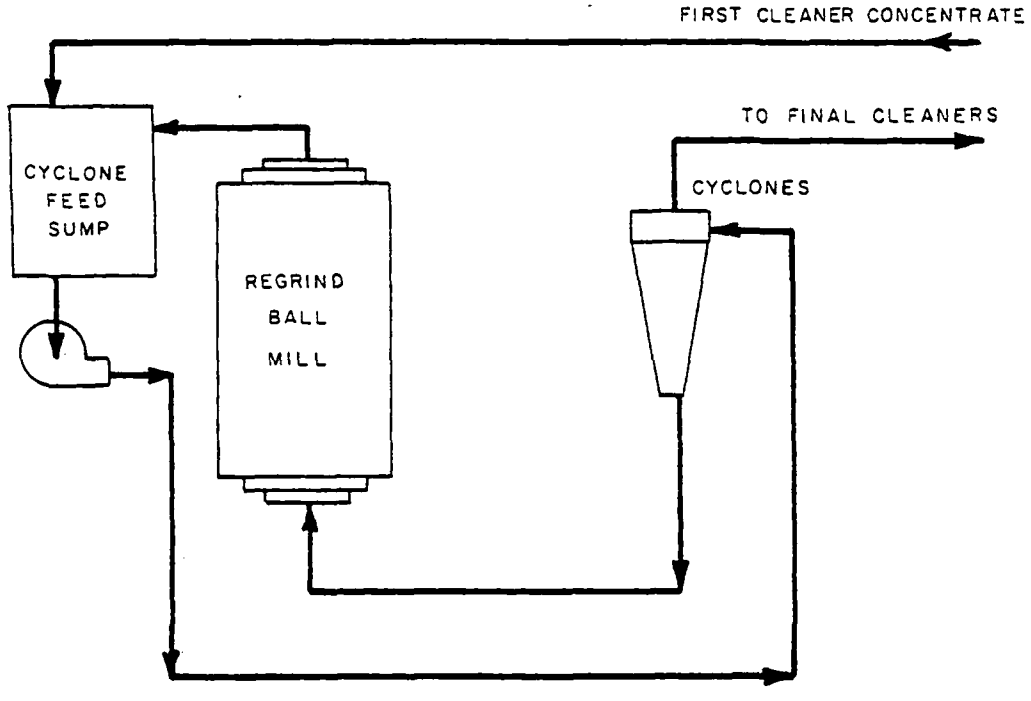

Figure 2. Concentrate Regrind Circuit

PREPRINT NO. 60B61

SOCIETY OF MINING ENGINEERS
of AIME
29 WEST 39TH STREET NEW YORK 18, N.Y.

THE COPPER SEGREGATION PROCESS

Carl Rampacek
Supervising extractive metallurgist

W. A. McKinney
Extractive metallurgist

United States Bureau of Mines
Tucson Metallurgy Research Laboratory
Tucson, Arizona

This paper is to be presented at the Annual Meeting of the American Institute of Mining, Metallurgical, and Petroleum Engineers, Inc., New York, February 14 to 18, 1960.

THE COPPER SEGREGATION PROCESS

60B61

By Carl Rampacek[1]
W. A. McKinney[2]

ABSTRACT

Laboratory and small-scale continuous pilot-plant investigations made at the Tucson Metallurgy Research Laboratory of the Bureau of Mines have demonstrated that the copper segregation process is applicable to the treatment of oxidized and mixed oxide-sulfide copper ores regardless of the gangue constituents. The process comprises heating the ore to a temperature of 750° C. with small quantities of sodium chloride and coke to produce metallic copper, which then is recovered by flotation. Tests were made on 23 copper ores of different types containing 0.8 to 5 percent Cu. The copper recoveries ranged from 73 to 96 percent in concentrates assaying 10 to 62 percent Cu, depending on the grade and type of ore. The direct operating cost for a 1,000-ton-per-day furnace and flotation plant is estimated at about $3 per ton of ore.

INTRODUCTION

The recovery of copper from low-grade oxidized and mixed oxide-sulfide copper ores by acid leaching is standard practice in the Southwest. Some ores, however, are unamenable to this method of treatment owing to excessive acid consumption by calcite or other acid-consuming gangue minerals. Other ores present a handling problem because of the presence of clay or other clime forming gangue minerals. The Tucson Metallurgy Research Laboratory has investigated for the past several years the applicability of the copper segregation process to the treatment of different types and grades of oxidized and partly oxidized copper ores.

This paper briefly outlines the history of the segregation process, discusses the principal reactions involved, and summarizes the results of the bench and pilot-plant research, with the objective of delineating the process conditions for treating different types of copper ore. A more detailed discussion of the process and the results of research completed to date are given in a recent Bureau of Mines report.[3]

1/ Supervising extractive metallurgist, Bureau of Mines, Region III, Tucson, Ariz.
2/ Extractive metallurgist, Bureau of Mines, Region III, Tucson, Ariz.
3/ Rampacek, Carl, McKinney, W.A., and Waddleton, P.T., Treating Oxidized and Mixed Oxide-Sulfide Copper Ores by the Segregation Process: Bureau of Mines Rept. of Investigations 5501, 1959, 28 pp.

THE PROCESS

The copper segregation process, which was discovered in 1923, comprises heating copper ore with a reducing agent and sodium chloride to about 750° C., followed by flotation of the metallic copper produced. By 1931 the process was sufficiently developed so that two plants were constructed in Africa for treating oxidized ores. 4,5/ One plant, having a daily capacity of 50 tons, was constructed in Southern Rhodesia by the Minerals Separation Co. At this plant minus-10-mesh ore was heated and segregated in a seven-hearth, mechanically rabbled furnace. The first five hearths were direct-fired to heat the ore to a reaction temperature of about 700° C. Salt and coal were added to the hot ore and segregation was carried out on the sixth and seventh hearths, which were heated by the exothermic nature of the reaction and by indirect heating with waste gas from the upper hearths. The segregated calcine subsequently was cooled in a rotary cooler, screened, and floated to recover the copper. The small plant operated for 4 months in 1931. About 3,500 tons of ore assaying 5 percent Cu was processed, and recovery of copper was 87 percent.

4/ Moulden, J. C., and Taplin, Bruce, Heat Treatment and Concentration of Copper Ores: U. S. Patent 1,679,337, July 31, 1928.

5/ Rey, Maurice, The Segregation Process for Low-Grade Copper Oxide Ores: 7th Internat. Cong. Min. Met. and Appl. Geol., Metallurgy Sec., vol. 11-3, Paris, Oct. 20-26, 1935, pp. 55-62; Rev. Met., vol. 33, 1936, pp. 295-302.

The other plant was built in 1931 at Katanga in the Belgian Congo by the Union Miniere du Haut Katanga. The plant had a rated capacity of about 350 tons of ore per day. A direct-fired rotary kiln was used to preheat the ore before segregation in a second rotary-reactor kiln. The exothermic heat of reaction maintained the temperature of the reactor kiln between 700° and 750° C. The calcine was cooled in a rotary cooler prior to recovery of the segregated copper by flotation. Operating results in the plant, which had a life of about 4 months, are not available.

The low price of copper that prevailed during the depression was a factor in shutting down the two plants, but mechanical difficulties also may have contributed to the cessation of activities.

REACTIONS INVOLVED

Segregation of copper from oxidized ore minerals probably involves a number of complex reactions. These include: (1) the decomposition of sodium chloride, (2) the volatilization of copper chloride and (3) reduction of the copper chloride to metallic copper. The principal chemical reactions presumed to occur are as follows:

Decomposition of sodium chloride. Hydrochloric acid is produced by interaction of sodium chloride with hydrous clay minerals, such as kaolinite and montmorillonite, according to the following reaction:

$$4NaCl + Al_2O_3 \cdot 2SiO_2 \cdot 2H_2O = 4HCl + Na_4Al_2O_3 \cdot 2SiO_3 \quad (1)$$

in the presence of traces of water vapor released in the furnace by the slow dehydration of the clay or other hydrous minerals, the reaction is rapid at temperatures of 600° C. or higher. Moisture is obligatory for the reaction to take place.

Volatilization of copper chloride. The hydrochloric acid produced by reaction 1 attacks the copper oxide minerals to form volatile cupric and cuprous chlorides. The cupric chloride decomposes into chlorine and cuprous chloride at temperatures well below 500° C.6/ When treating a chrysocolla ore the reaction between the hydrochloric acid and chrysocolla is as follows:

$$2(CuSiO_3 \cdot 2H_2O) + 4HCl = Cu_2Cl_2 + 6H_2O + Cl_2 + 2SiO_2 \quad (2)$$

6/ Maier, C. G., Vapor Pressures of the Common Metallic Chlorides and a Static Method for High Temperatures: Bureau of Mines Tech. Paper 360, 1925, 45 pp.

At the temperature of the reaction cuprous chloride has a vapor pressure of about 20 mm. and diffuses from the mineral grains. The chlorine liberated in reaction 2 also attacks the copper minerals to form more cuprous chloride as shown in reaction 3.

$$2(CuSiO_3 \cdot 2H_2O) + Cl_2 = Cu_2Cl_2 + 4H_2O + 2SiO_2 + O_2 \quad (3)$$

Formation of metallic copper. The cuprous chloride vapor released by reactions 2 and 3 is reduced directly to metallic copper upon coming in contact with the hot carbon particles. Although a number of side reactions occur, the principal reaction taking place is as follows:

$$2Cu_2Cl_2 + C + 2H_2O = 4Cu + 4HCl + CO_2 \quad (4)$$

More detailed discussions of the reactions involved in segregation are presented in earlier reports.[7,8]

7/ Work cited in footnote 3 (p.2)
8/ Work cited in footnote 5 (p.2)

Side Reactions

During segregation, a negligible quantity of metallic copper may be reduced in place as micron-size particles, probably by the small quantity of carbon monoxide and hydrogen that is formed by interaction of the hot carbon and steam. Such metallic copper is generally unrecoverable because it cannot be liberated and froth floated.

A common side reaction that occurs during segregation is the absorption of cuprous chloride by the gangue or by the siliceous skeletons formed from decomposition of the chrysocolla. Enough cuprous chloride is often absorbed by the gangue particles to render them floatable with xanthate after fine grinding.

THE SCOPE AND RESULTS OF THE INVESTIGATION

The initial phase of the investigation was confined to bench-scale research designed to evaluate the segregation method as applied to different grades and types of copper ore. A total of 23 domestic and foreign copper ores that contained 0.8 to 5 percent Cu was tested. The samples were either wholly or partly oxidized ores containing different proportions of chrysocolla, malachite, azurite, cuprite, brochantite, melaconite, chalcopyrite, chalcocite, bornite, and covellite associated with various siliceous, calcareous, and ferruginous gangue minerals.

The laboratory research was sufficiently promising to warrant further evaluation of the segregation process by continuous tests in a small pilot plant having a capacity of 65 to 70 pounds of ore per hour. The ore, salt, and coke or coal were premixed for segregation in an indirect-fired rotary kiln. The rotary kiln was 6 inches in diameter by 14 feet long and consisted of a type-316 stainless steel reactor tube, 6 feet long, enclosed in a natural-gas-fired furnace. A 2-foot length of mild steel tube was attached to the reactor tube at the feed end and a 6-foot length of mild steel tube was bolted to the discharge end for indirectly cooling the segregated calcine by an external water spray. The feed end of the kiln was sealed by a choke feed screw and the discharge end by a ring seal and vented hood open at the bottom. The lower part of the vent hood was immersed below the pulp level in a drag classifier, allowing the partly cooled calcine to drop directly into the pool without coming into contact with the atmosphere. The quenched calcines were wet-ground to pass 100-mesh in a ball mill in closed circuit with the classifier. The ground pulp, after conditioning with amyl xanthate, was floated in a 5-cell rougher flotation machine. The rougher froth was cleaned once. The contact time in the roughing circuit was 28 minutes.

Several grades and types of oxidized ore were successfully processed in the test plant and enough operating and engineering data were obtained to permit making tentative estimates of the direct costs of operating a commercial-size plant.

The results of the laboratory and pilot plant tests demonstrated that different types and grades of ore could be effectively segregated and the metallic copper recovered by flotation. The completely oxidized ores were processed to recover 73 to 96 percent of the copper in rougher flotation concentrates assaying 10 to 62 percent Cu. The mixed oxide-sulfide ores responded equally well to treatment. From 85 to 92 percent of the copper was recovered in concentrates assaying 12 to 27 percent Cu.

The tests made on the oxidized ores showed that those containing 1 percent Cu or less gave low copper recovery in low grade concentrates. The relatively poor

results obtained on such ores can be attributed to the absorption of copper by gangue. Part of the copper so absorbed was lost in the flotation tailing and the remainder activated some of the gangue to xanthate flotation. The copper in low-grade calcareous-type ores proved somewhat difficult to segregate. Apparently the calcite in the ore reacts with some of the salt, hydrochloric acid, and chlorine to form calcium chloride, which is not an effective copper chloridizing agent. Tests using calcium chloride instead of sodium chloride confirmed this hypothesis.

The quantity and ratios of salt and coke required for good segregation of the copper differed for each ore. From 1 to 1.5 percent salt and 0.5 to 1 percent coke gave the best results. Less salt gave incomplete segregation and resulted in a slightly lower copper recovery. Siliceous ores usually required less salt, and the ratio of salt to coke was not as critical as for calcareous or hematitic ores.

The free segregated metallic copper floated rapidly and completely, and the flotation tailings rarely contained any visible flake copper. Microscopic examination of tailings from the better tests failed to disclose any unreacted copper oxide minerals. The copper lost in the flotation tailings from these ores can be attributed principally to copper chloride absorbed by the gangue or by the siliceous skeletons formed from decomposition of chrysocolla. An insignificant quantity of copper occurred in the tailings as micron-size metallic inclusions in the gangue. These particles probably were copper that failed to migrate and was reduced in place.

Some gold and silver in both the oxidized and mixed ores was segregated and floated with the copper. The gold and silver recoveries ranged from 60 to 80 percent from ores assaying 0.2 to 8.2 ounces per ton of total gold and silver. Efforts to identify free gold or silver in the concentrates were not successful. Presumably the precious metals were carried in the segregated copper. Segregation of the silver or gold from ores devoid of copper so far has proved unsuccessful. It appears that copper must be present to serve as a carrier for precious metals.

FACTORS INFLUENCING SEGREGATION AND FLOTATION OF COPPER

Time and Temperature

The time and temperature employed to reduce and segregate the copper were critical process variables. Good segregation was achieved on typical siliceous ores at 600° to 850° C. Calcareous ores required a temperature of about 750° C. for best segregation. Although moderately good segregation was obtained on a few calcareous samples at 700° C., erratic results were obtained on other ores, indicating that segregation at this temperature was sensitive to slight variations in the processing conditions. Oxidized ores with a ferruginous gangue were almost as sensitive to temperature variation as strictly calcareous ores.

The time required for good segregation varied with the roasting temperature. Heating a siliceous ore for 15 minutes at 700° C. gave nearly as good segregation as was obtained with a 60-minute contact time. When calcareous ore was treated, heating for at least 60 minutes was necessary for effective segregation at 700° c., whereas 15 minutes sufficed at 800° C. These and other tests demonstrated that siliceous or high-alumina ores generally are less sensitive to time and temperature than those containing appreciable calcite, limestone, dolomite, hermatite, or magnetite.

Moisture

The free-moisture content of the feed had a pronounced effect on segregation, particularly at low furnacing temperatures. At 750° C. or higher the addition of moisture to ores, which usually contained about 5 percent combined water, had little influence on segregation of charges treated batchwise, but at 700° C. about 1.5 to 3 percent of added water was desirable for good segregation.

The influence of moisture on segregation was more pronounced for charges segregated continuously than for those treated in batches. Continuous segregation of dry charges or feeds low in free moisture gave inferior

results even at a reaction temperature of 750° C. The divergent results obtained on dry or low-moisture charges in the batch and continuous tests may be attributed to a difference in composition of the reaction gas in the furnaces or to a catalytic action of moisture on segregation. In general, a contact time of 40 minutes was desirable when dry charges were segregated, whereas 20 minutes generally sufficed for moist charges.

Coke Particle Size

Segregation was noticeably affected by the upper limiting size of the coke used, particularly on calcareous ore. Coke crushed to pass 20- or 48-mesh gave good segregation, but coarser or finer coke gave poorer segregation. In tests with minus-100-mesh coke the conditions in the retorts probably were too strongly reducing, and some copper was reduced in place within the ore particles. Coke coarser than 20-mesh, on the other hand, failed to provide enough nuclei for rapid and efficient reduction of the volatilized copper chloride, thereby causing incomplete segregation. Apparently the copper chloride must be reduced simultaneously with its migration from the copper mineral to release the chlorine or hydrogen chloride for additional copper volatilization.

Type of Reducing Agent

Tests were made to compare the merits of different kinds of reducing agents. Samples of petroleum coke, two bituminous coals, mesquite charcoal, and a char made from bituminous coal were compared. The results obtained on several ores indicated that satisfactory segregation could be obtained with any of these reductants. Based upon the quantity of coal used and the fixed carbon content, the two coals were more effective as reducing agents than coke, char, or charcoal.

Size of the Furnace Feed

A number of tests were made to define the effect of ore feed size on the segregation of copper. In general, segregation improved with fineness of the feed. In typical batch tests on a calcareous ore, for example, 75 percent of the copper was recovered when using a 3-mesh feed, as compared to 86 percent from a 65-mesh feed. Crushing the ore much finer than 10-mesh did not significantly improve segregation as reflected in the amount of copper recovered by flotation. The data obtained in the study of the influence of feed size also indicated that a relationship exists between the size of the ore feed and the retention time at reaction temperature. The coarser ore feeds required longer retention times than fine ore feeds.

Flotation Feed Size

Under ideal segregation conditions all of the copper migrates from the copper minerals and reports in the calcine as friable nodules about the size and shape of kidney beans and consisting of free flakes of finely divided metallic copper with some coke and gangue particles. Several methods for recovering copper from the calcines were investigated: One was to screen the calcine on a 6-mesh sieve to remove the nodules, followed by flotation of the screen undersize to recover the remaining copper; a second was direct flotation of the minus-10-mesh calcines to recover the flake copper; and a third procedure was to grind the calcine to different limiting sieve sizes before flotation.

A high recovery of copper was obtained only by grinding the segregated product to pass 100-mesh for flotation. Recoveries of copper were lower when coarser feeds were floated. Removing the copper nodules by screening, followed by flotation of the undersize after grinding to minus-100-mesh, gave about the same recovery as fine grinding and flotation of the entire charge. The copper nodules removed by screening assayed about 30 percent Cu and accounted for about 50 percent of the copper in the ore.

CURRENT RESEARCH

A small continuous two-stage segregation plant consisting of a rotary kiln for preheating oxidized and mixed oxide-sulfide ores to about 750° C. and a second fire-brick-lined rotary reactor kiln for segregation is now being tested at Tucson. The hot ore is transferred from the preheat kiln to the reactor by means of a screw feeder enclosed in an insulated transfer box. Salt and coke for segregation are introduced into the reactor through a second screw feeder. The exothermic heat of reaction accompanying the volatilization and reduction of the copper minerals, with a small amount of heat supplied by an auxiliary burner, maintains the temperature of the charge in the reactor at the segregation temperature.

Preliminary tests in the plant have been successful. The two-stage procedure appears to have considerable merit for treating mixed oxide-sulfide ores containing pyrite.

The sulfides are oxidized during the preheating step, which facilitates segregation of the copper and production of a high-grade flotation concentrate substantially free of pyrite.

Tests of an exploratory nature also are in progress at the Salt Lake City Metallurgy Research Center to investigate the feasibility of segregating ore in a fluidized-bed reactor. Tests in an indirectly heated 4-inch unit, using an inert gas for fluidization, have been encouraging, but much research remains to be done to fully evaluate the method. Results of segregation tests in the continuous two-stage plant and fluidized-bed reactor will be presented in a later publication.

ESTIMATED OPERATING COSTS

Based upon the data obtained from the laboratory and pilot plant tests, the direct operating cost of a 1,000-ton-per-day furnacing and flotation plant for treating oxidized or mixed oxide-sulfide copper ores would be about $3 per ton when coke was used as the reducing agent or $2.85 when coal was used. Heat required for furnacing is estimated to be 2,500,000 B.t.u. per ton of ore. At 27 cents per thousand cubic feet of natural gas the cost would be about 70 cents per ton. The estimated cost of furnace maintenance is 40 cents per ton; power and labor are estimated at 15 cents, and salt at 12 cents. The coke or coal costs are estimated at 25 and 10 cents, respectively. Crushing, grinding, and flotation are estimated at $1.35 per ton.

COPPER SEGREGATION PROCESS SHOWS PROMISE AT LAKE SHORE MINE

by G. A. FREEMAN, CARL RAMPACEK and L. G. EVANS

A large aggregate tonnage of oxidized and mixed oxide-sulfide copper ore of the southwestern U.S. is not amenable to conventional flotation concentration or sulfuric acid leach treatment. Most of the ores contain chrysocolla as the principal oxide copper mineral, for which no successful commercial flotation method has yet been developed. Acid leaching some ores is not feasible since they contain substantial quantities of calcite and other acid-consuming constituents. Other ores decrepitate during leaching or contain excessive slime and clay minerals which cause plugging of the ore beds.

Research at the U.S. Bureau of Mines' Tucson Metallurgy Research Laboratory over the past several years demonstrated that the segregation process had merit for treating oxidized and mixed oxide-sulfide copper ores regardless of the gangue constituents present, or the physical characteristics of the feed.[1,2]

Small-scale pilot-plant tests performed by the USBM and by Transarizona Resources, Inc., further demonstrated that the process was applicable to the highly-calcareous and iron-bearing oxide ore occurring in the Lake Shore deposit near Komelik, Ariz. Based on test results, the company began erection of a 175-tpd experimental segregation plant to further test the process in December 1959. Construction of the plant was completed in May 1960, and shakedown operations were started in June 1960.

Briefly described, the segregation process comprises heating and oxidized or mixed oxide-sulfide copper ore with a halide salt and a carbonaceous material, such as coke or coal, at approx 1400° to 1500°F. Segregation produces fine metallic copper which can then be recovered by conventional copper sulfide flotation methods. Although numerous reactions are involved in the process, basically the copper is volatilized from the copper minerals as cuprous chloride and then reduced to metallic copper on the surfaces of the carbonaceous particles. The fine flakes often agglomerate forming nodules as long as ¾-in. and ½-in. in diam. These nodules, however, immediately fall apart with agitation. A more complete discussion of the process and its application to oxide and mixed oxide-sulfide copper ores is given in earlier reports.[1,2]

LAKE SHORE MINE

Lake Shore mine is located at an elevation of about 1800 ft on the southwest piedmont of the Slate Mountains, about 30 miles south of Casa Grande and 3 miles east of Komelik, Ariz. A shaft was sunk in the deposit in the period 1880 to 1884. Ore was produced sporadically from several shafts and three development levels in the deposit in the period between 1884 and 1929, when the last reported production was made. Total production from the mine is reported to have been approximately 280,000 lbs of copper.[3]

Although previous *high-grading* operations employed underground mining, the deposit is now being mined by the open-pit method. Part of the north orebody has been stripped of alluvium down to a depth of about 30 ft to expose enough ore for several years of operation. Drill holes are spaced in a pattern of 5 to 6-ft centers; use of ammonium nitrate readily breaks the ore to about 10-in. in size. Load-

G. A. FREEMAN, Member of SME, is with Transarizona Resources, Inc., Casa Grande, Ariz. C. RAMPACEK, Member of SME, and L. G. EVANS are associated with the U.S. Bureau of Mines. Paper presented at 1961 AIME Annual Meeting.

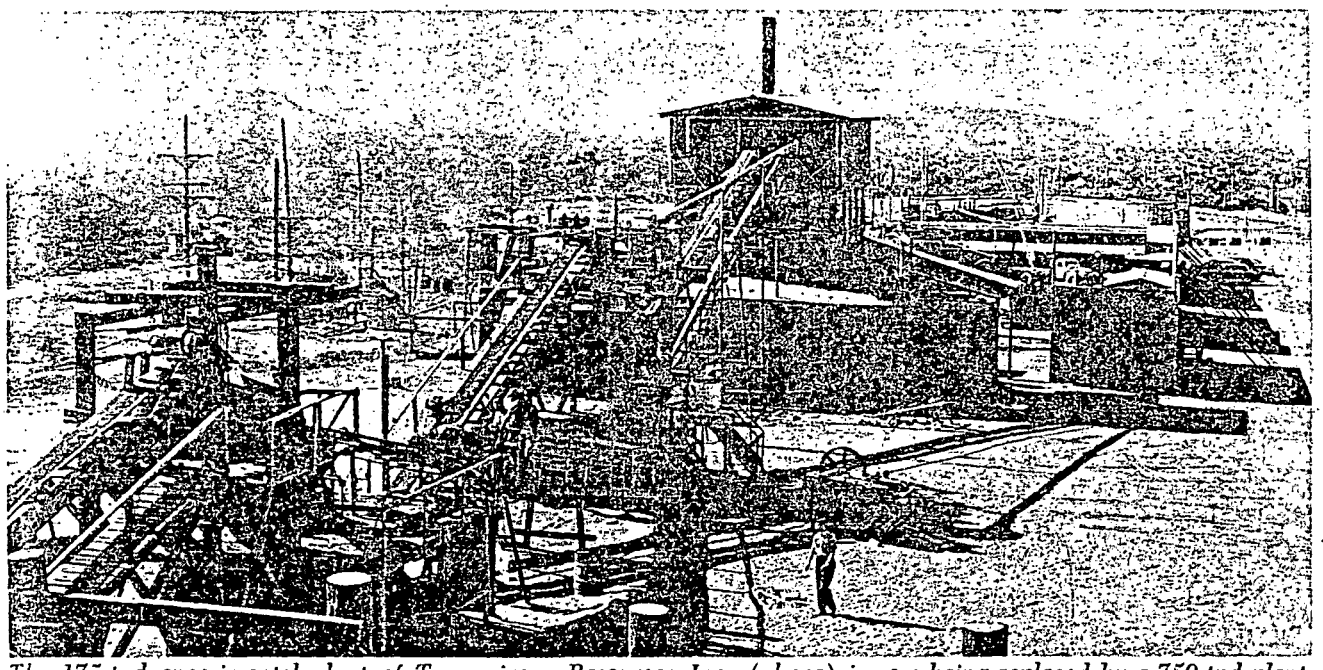

The 175-tpd experimental plant of Transarizona Resources, Inc., (above) is now being replaced by a 750-tpd plant.

ing is done by a 1-yd front-end loader. The ore is hauled in 10-ton trucks to the segregation plant about 1500 ft southwest of the pit.

The ore being treated is a reddish-colored, magnetite-bearing quartzite which has been fractured and recemented with quartz, chrysocolla, hematite, calcite and chlorite material. The ore is devoid of sulfides, and at times, massive magnetite, enriched in chrysocolla, and considerable calcite is encountered. The grade of minable ore varies from about 1.5 to 2.25% Cu. Detailed development work by rotary drilling has assured the mining and delivery of a consistently uniform feed to the plant.

SEGREGATION-FLOTATION PLANT

The segregation-flotation plant has a daily capacity of about 175 tons of ore containing 3 to 4% moisture, the capacity being limited by the segregation furnace. A flowsheet of the plant as of November 1960, is shown below.

Power is supplied at 24,900 v from the lines of the Trico Electric Co., about two miles southwest of the deposit. A 750-kva transformer substation at the plant site drops the voltage to 440 v for plant operation, and a standby diesel-electric plant provides emergency power for the segregation furnace and calcine cooler during power failures.

Water from a 251-ft well about 2.5 miles west of the plant is delivered to the plant through a 5-in. pipe line by means of a 30-hp pump. Pumping facilities are available to produce enough water to treat as much as 500 tpd of ore. In addition to the primary water source, provisions are being made to recover water from the tailing disposal pond and thickeners. It is anticipated that 50 to 60% of the water will ultimately be recovered.

Natural gas, purchased from the Southwest Gas Co. is received at the property through a 4-in line at 150 psig. The high pressure gas is reduced to 20 lbs for plant use.

The ore is dry-crushed to minus 6 mesh for segregation. Coarse crushing is accomplished in a 16x24-in. jaw crusher set at two in., operating in open circuit. The jaw crusher discharge is conveyed and crushed in a 5-ft Tornado impact crusher in closed circuit with a 6-mesh vibrating screen. Rapid and efficient reduction is obtained in the crusher so that the circulating load is light. The undersize particles from the 6-mesh screen are conveyed to a 400-ton, fine-ore storage bin.

Crushing is carried out on the day shift. About 60 tph of ore can be crushed to minus 6 mesh. A typical screen analysis of the minus 6-mesh segregation furnace feed is given in Table I.

SEGREGATION FURNACE

The segregation reactor measures 54-in. ID x 48 ft long with the ends coned to 30 in. inner diam. The segregation unit is fabricated of ½-in. rolled and welded, type-316 stainless steel plate. A refractory brick-lined, natural gas-fired furnace, 31 ft long, encloses part of the reactor. About eight ft of the shell extends from the furnace at the feed end and eight ft extends at the discharge end. Riding rings attached to the reactor shell on either side of the furnace support the reactor. The discharge end outside of the furnace is completely insulated with 4½-in. thick magnesite block to reduce radiation losses to a minimum. Staggered, 3/16-in. stainless steel lifters three in. high and 24 in. long are attached to the inside of the reactor throughout the

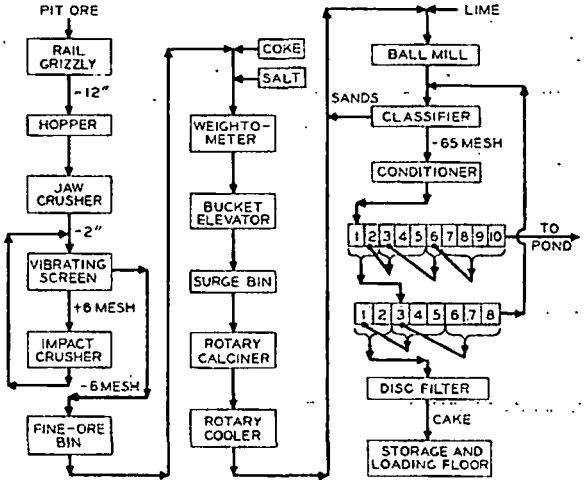

Flow sheet of copper segregation process at Lake Shore.

Table I. Screen Analysis of Segregation Feed

Screen Size, Mesh		Wt Pct
	+6	—
−6	+8	4.6
−8	+10	7.9
−10	+20	18.7
−20	+35	16.9
−35	+48	7.3
−48	+65	7.3
−65	+100	7.5
−100	+150	7.1
−150	+200	4.7
−200	+270	4.6
−270		13.4
Composite		100.0

Table II. Screen Analysis of Tailing

Screen Size, Mesh		Wt Pct
	+48	0.4
−48	+65	1.0
−65	+100	5.3
−100	+200	25.0
−200		68.3
Composite		100.0

54-in. diam section to facilitate mixing of the ore charge as it passes through the unit. The reactor is driven at four rpm by a 20-hp motor connected to a speed reducer which drives a ring gear attached to the reactor shell at the feed end. The furnace has a 74-in. inner diam and is equipped with 14 natural-gas burners complete with spark ignited pilots and auxiliary air and gas valves. The gas burners are located at the side and bottom of the furnace, firing tangentially to the rotating shell. Two dampered flues attached to the top of the furnace and near each end conduct the exhaust gases to a single 2x40-ft stack which discharges into the atmosphere.

The furnace is equipped with a complete temperature control system incorporating flame protection features and safety shut-off valves which automatically cut off the natural gas should the external shell temperature exceed a predetermined figure.

The outside temperature of the reactor tube is measured by five thermocouples equally spaced and riding on top of the reactor shell in the heated zone. Another thermocouple indicates the stack gas temperature. These temperatures are recorded on an eight-point strip chart recorder. A sixth thermocouple, located in the ore bed about 21 ft from the discharge end of the reactor, is the principle furnace control. This thermocouple is connected to a circular chart potentiometer which operates a pneumatic control valve which increases or decreases the fuel to the burners, depending on the temperature of the charge. A second thermocouple is installed in the ore bed about 15 ft from the discharge end and also is recorded on the eight-point recorder.

The minus 6-mesh ore from the fine-ore bin and the required quantities of minus 20-mesh commercial salt and minus 48-mesh petroleum coke are fed on a 18-in. x 20-ft long conveyor belt using Syntron feeders. Some mixing of the salt, coke and ore is achieved on the conveyor belt by means of chains and rubber fingers suspended above the belt which drag in the ore ribbon as it passes beneath. The partly mixed feed discharges into a bucket elevator and then into a 10-ton surge bin ahead of the segregation furnace. Mixing of the ore, salt and coke is completed in the elevator. It was found that a thorough mixing of the salt and coke with the ore was very important.

The salt-coke-ore mixture is fed to the segregation furnace at a rate of about 7.5 tph by means of a variable speed 9-in. spiral screw feeder connected to the bottom of the surge bin and extending about three ft into the reactor. A ring seal between the screw feeder and the reactor prevents escape of the reaction gases. An ore column is maintained in the furnace surge bin for air seal.

The temperature of the reactor charge is increased as rapidly as practicable, the outside shell temperature, or more likely the flame temperatures at shell surface, are 1500° to 1700°F. The desired reaction temperature of 1400°F is reached in the ore bed at a point about 22 ft from the feed end and is maintained at this temperature until the ore leaves the heated section. The temperature then drops to about 1300°F as it moves into the insulated section toward the discharge end.

The normal bed in the reactor occupies a cross sectional volume of about 20%. Under the operating conditions employed, the contact time of the ore charge at the reaction temperature of 1400° to 1500°F is about 18 min.

The segregated calcine discharges from the reactor at approximately 1100°F through a vented hood attached to the shell and feeds into a 4x44-ft Baker-type cooler. Moderately gas-tight connections are maintained between the reactor hood and cooler by means of ring seals. Absolutely air-tight connections are not required because the segregation reaction produces steam and reaction gases which develop a positive pressure and prevent entry of air into the unit.

GRINDING AND FLOTATION

The cooled calcine discharges from the cooler at 200°F onto a 18-in. x 68-ft conveyor belt which feeds into a 6x12-ft Allis-Chalmers ball mill operating in closed circuit with a Dorr Duplex Classifier. The grind is controlled to give a minus 65-mesh classifier overflow. The classifier overflow, containing about 25% solids, is conditioned in a 5x5-ft slow-speed conditioner using potassium amyl xanthate, methylisobutyl carbinol and enough lime to establish a pulp pH of 11.5. The conditioned pulp is floated in 10 No. 24 Denver cells. A rougher concentrate is recovered from the first two cells and gravity-fed to the cleaning section. Froth from the next three rougher cells is returned to No. 2 rougher.

Table III. Summarized Results of Plant Operations, November 1 to November 27, 1960

Product	Assay, Pct Cu	Fe	CaO	SiO_2	Al_2O_3	Distribution, Pct Cu
Heads	1.81	13.7	—	—	—	100.00
Concentrate	50.09	3.2	2.6	13.3	0.8	87.15
Tailing	0.23	—	—	—	—	12.85

Reagents:		
NaCl	lb/ton ore	28.0
Coke	lb/ton ore	18.0
CaO	lb/ton ore	4.8
Potassium amyl xanthate	lb/ton ore	0.5
Methylisobutyl carbinol	lb/ton ore	0.1
Natural gas	Btu/ton ore	1,900,000

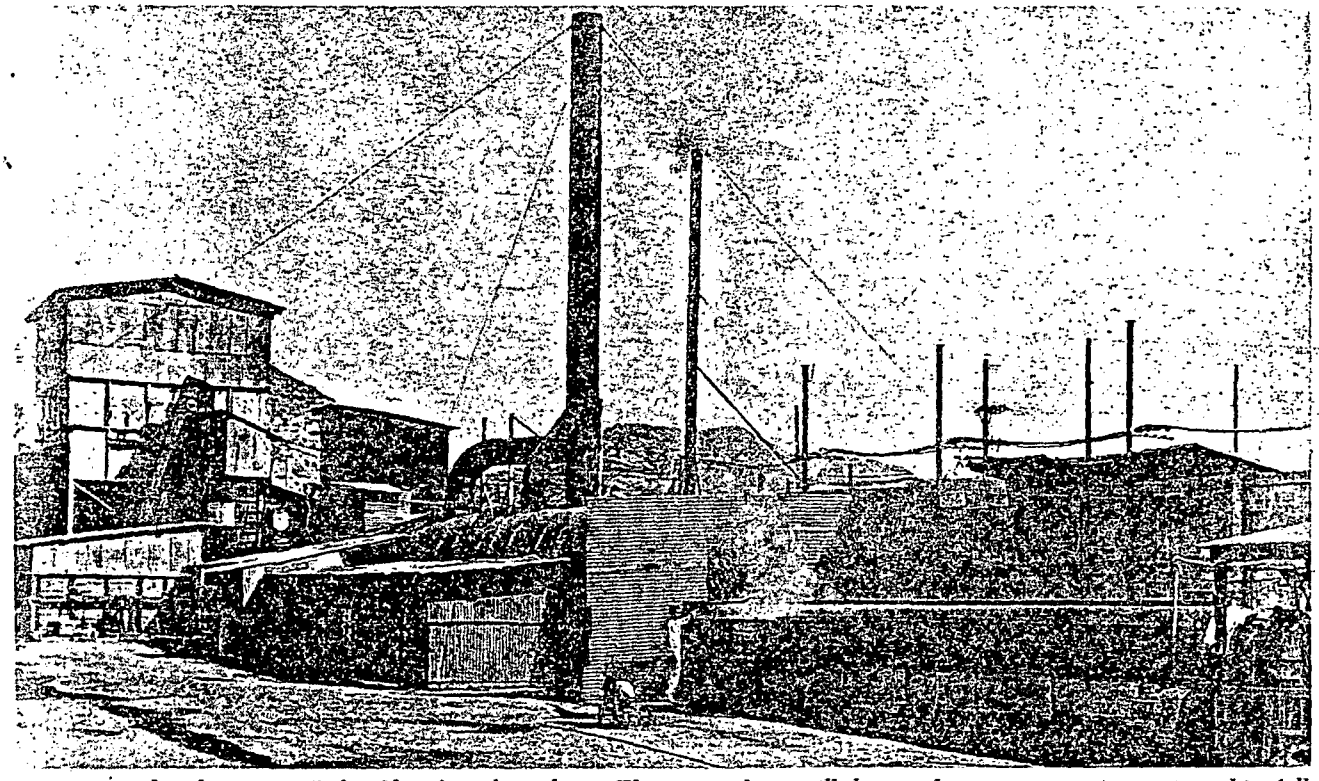

Furnace and calciner at Lake Shore's pilot plant. The new plant will be ready to go into operation this fall.

Froth from No. 6 cell is returned to No. 3 rougher, and a scavenger froth obtained from the final four roughing cells is combined with feed to the No. 6 rougher cell. The final tailing is pumped to a tailings pond 1000 ft away. The average screen analysis of the tailings is given in Table II.

The cleaning section consists of eight No. 18 special Denver cells. The rougher froth is cleaned twice using three cells in the first stage and two in the second. The final flotation concentrate is filtered on a 6-ft disc filter and stored in a bin for periodic shipment to the smelter. The first cleaner tailing is refloated in three additional cells to produce a scavenger concentrate which is combined with the froth from the roughing circuit. These products return to the head of the cleaning circuit, and the tailings from the middling refloat are returned to the Dorr classifier.

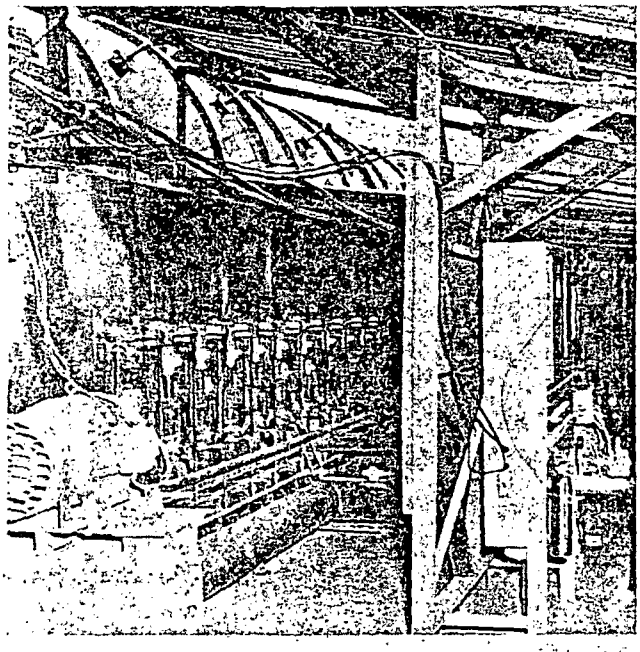

Control panel (right) keeps furnace operating properly.

RESULTS AT LAKE SHORE PLANT

Plant operations have been as good as, and in some instance have exceeded, the results obtained in the laboratory and pilot-plant research. A summary of results obtained during a 27-day period during the month of November 1960, are given in Table III. The grade of concentrates produced has consistently improved since the start of operations, and in some cases has approached 65% Cu. Copper recoveries also have improved, and the gas and reagent requirements have gradually been reduced. The gas consumption will be reduced considerably with the installation of pre-heaters using the waste stack gases.

Considerable experimentation was conducted in the plant and at the USBM station in Tucson during the six months of operation ending in November 1960. A number of changes in the original furnace design and simplification of the hot and cool calcine handling system were made before settling on the final flow sheet.

Based on the plant operation and results, the Lake Shore operations now are being expanded to about 750 tpd. The company will install two new furnaces, each of which will have a capacity of ten tph of ore. The capacity of the experimental reactor also is being increased to ten tons by making a number of modifications in both the reactor and furnace design. Three pre-heaters will also be incorporated into the flowsheet to take advantage of waste heat.

REFERENCES

[1] C. Rampacek, W. A. McKinney, and P. T. Waddleton: Treating Oxidized and Mixed Oxide-Sulfide Copper Ores by the Segregation Process: *USBM* Report 5501, 1959, pp. 1-28.

[2] Editorial Staff: USBM Charts Segregation Process; *Eng. & Mining Journal*, vol. 160, no. 11, 1959, pp. 98-99.

[3] T. M. Romslo: Investigation of the Lake Shore Copper Deposits, Pinal County, Ariz., *USBM* Report 4706, 1950, pp. 1-24.

Report of Investigations 8290

Copper and Silver Recovery From a Sulfide Concentrate by Ferrous Chloride-Oxygen Leaching

By B. J. Scheiner, G. A. Smyres, P. R. Haskett,
and R. E. Lindstrom

UNITED STATES DEPARTMENT OF THE INTERIOR
Cecil D. Andrus, Secretary

BUREAU OF MINES

This publication has been cataloged as follows:

Copper and silver recovery from a sulfide concentrate by ferrous chloride-oxygen leaching / by B. J. Scheiner ... [et al.] [Washington] : U.S. Dept. of the Interior, Bureau of Mines, 1978.

11 p. : ill. ; 27 cm. (Report of investigations - Bureau of Mines ; 8290)

Bibliography: p. 11.

1. Copper. 2. Silver. 3. Leaching. 4. Cyanide process. I. Scheiner, Bernard J. II. United States. Bureau of Mines. III. Series: United States. Bureau of Mines. Report of investigations - Bureau of Mines ; 8290.

TN23.U7 no. 8290 622.06173

U.S. Dept. of the Int. Library

CONTENTS

ILLUSTRATIONS

COPPER AND SILVER RECOVERY FROM A SULFIDE CONCENTRATE BY FERROUS CHLORIDE-OXYGEN LEACHING

by

B. J. Scheiner,[1] G. A. Smyres,[2] P. R. Haskett,[1] and R. E. Lindstrom[3]

ABSTRACT

A ferrous chloride-oxygen leaching system was investigated by the Federal Bureau of Mines to determine its effectiveness for recovering copper and silver from a tetrahedrite concentrate that had been pretreated to remove a majority of the antimony. The pretreated concentrate contained copper, silver, lead, zinc, antimony, and arsenic. Parameters affecting metal extraction (such as temperature, pressure, amount of ferrous chloride, and initial hydrogen ion concentration) were studied. Copper extraction of 98 pct was achieved by leaching 4 hours at 40 pounds per square inch gage (psig) and 100° C. Copper was recovered from leach solutions by cementation with iron, and the resulting ferrous chloride was recycled. Leaching the residue with cyanide followed by electrowinning recovered 99.7 pct of the silver. Iron, antimony, arsenic, and sulfur reported to the tailings.

INTRODUCTION

One of the goals of the Bureau of Mines is to insure that an adequate supply of minerals is available to meet national, economic, and strategic needs. To help reach this goal, the Bureau is conducting research to advance minerals processing technology, which includes investigations for recovering metals from complex sulfide ores and concentrates.

Marketing complex sulfide concentrates that contain a variety of metals along with arsenic and antimony has always presented a problem. This situation has been compounded recently by increasing smelter costs. These factors have stimulated considerable interest in the development of hydrometallurgical procedures for recovery of metal values from sulfide concentrates.

---

[1]Research chemist.
[2]Metallurgist.
[3]Supervisory chemical engineer.
All authors are with the Reno Metallurgy Research Center, Bureau of Mines, Reno, Nev.

Chlorination and acid-oxygen leaching procedures have been investigated for the recovery of metal values from sulfide concentrates (1-3).[4] Favorable metal recovery values are obtained with the chlorination technique. However, the system results in the dissolution of metals such as iron and arsenic; and additional separation schemes are required to separate and remove these metals. The acid-oxygen leaching technique is more selective, but metal extraction is generally less than that obtained by chlorination. Also, some of the iron is extracted into solution and additional processing steps are required to remove it.

More recently, Haver and Wong developed a ferric chloride leaching technique for treating chalcopyrite and galena concentrates (4-7). In this system the metal sulfide is oxidized by ferric chloride to produce metal chloride and elemental sulfur:

$$CuFeS_2 + 4FeCl_3 \rightarrow CuCl_2 + 5FeCl_2 + 2S, \quad (1)$$

$$PbS + 2FeCl_3 \rightarrow PbCl_2 + S + 2FeCl_2. \quad (2)$$

The system successfully treats classical concentrates such as chalcopyrite and galena, but as the concentrates become more complex in mineral composition, the ferric chloride system has several disadvantages. If a galena concentrate containing excessive amounts of iron, copper, and silver is treated, the iron, copper, and silver are coextracted and must be separated. The simplest separation method to remove the silver is to use lead shot to precipitate the silver. The resulting silver-lead product must be fire refined to produce high-grade bullion. A diaphragm cell is required to recover the copper, and a turbo aerator sequence is required to reject the iron that dissolves during leaching and to regenerate the ferric chloride solution for recycle.

The objective of this investigation was to test a ferrous chloride-oxygen leach system as an alternative method for leaching a complex, refractory sulfide concentrate. The proposed ferrous chloride-oxygen leach sequence differs from ferric chloride leaching in that the combined use of ferrous chloride and oxygen effectively converts silver and base metals to chlorides, and simultaneously rejects iron as Fe_2O_3 and sulfur in the elemental form, all in a single step. The leach system operates without excess chloride ion so that copper-silver separation is achieved in the leach step.

MATERIALS AND EQUIPMENT

The composition of concentrate used in experiments described in this paper is shown in the following tabulation. This concentrate is the end product of a leaching sequence with a sodium hydroxide-sulfur mixture to remove the antimony from a tetrahedrite flotation concentrate. During leaching, a portion of the sulfide in the concentrate was converted to sulfate, which accounts for the high sulfate content of the concentrate. The oxygen content

[4]Underlined numbers in parentheses refer to the list of references at the end of this report.

is residual hydroxide remaining after the leach step to remove the antimony from the tetrahedrite.

Concentrate	Analysis
Cu.....pct..	25
Zn.....pct..	2.0
Pb.....pct..	2.8
As.....pct..	0.52
Sb.....pct..	0.44
Fe.....pct..	16.0
S.....pct..	24.8
SO_4.....pct..	8.0
Ag.....oz/ton..	1,266.6
O_2[1].....pct..	10.0
Insol.....pct..	5.8

[1]Oxygen associated with metal hydroxides.

The ferrous chloride-oxygen leaching experiments were conducted in several different sizes of low-pressure glass or Teflon[5]-lined reactors, with titanium, and Teflon agitators. The charge to the reactor ranged from 50 to 4,000 grams of concentrate, depending on the size of the reactor. Larger scale experiments were conducted in a 14-liter reactor constructed from an 18-inch length of 8-inch-diameter steel pipe flanged on both ends. A Teflon liner was employed to protect the pipe and flanges from the corrosive solutions. The bottom and top of the reactor were sealed by bolting 1/2-inch-thick titanium end closures to the pipe flanges. The stirrers, temperature well, and gas inlet were made of titanium, as were the ball valves for emptying the reactor. The apparatus is shown in figure 1. Oxygen was added at 40 psig and monitored by a totalizing mass flowmeter.

The cell consists of a 3-liter Pyrex beaker equipped with an overflow spout. The anode consists of a 35-mesh stainless steel screen, 4 inches in diameter and 7 inches high. The cathode consists of a stainless steel inlet tube with an attached circular bottom and top plates 3-1/2 inches in diameter. The top plate is perforated, and steel wool is wrapped around the inlet tube between the top and bottom plate. The anode and cathode are separated by a tubular, perforated, 3-7/8-inch-diameter plexiglass sleeve. Solution from a holding tank is pumped into the cell near the bottom of the tube and flows upward and outward through the insulating sleeve and anode. The solution exiting the cell container was returned to the holding tank and recirculated through the cell until the silver values in solution were depleted.

[5]Reference to specific brand names is made for identification only and does not imply endorsement by the Bureau of Mines.

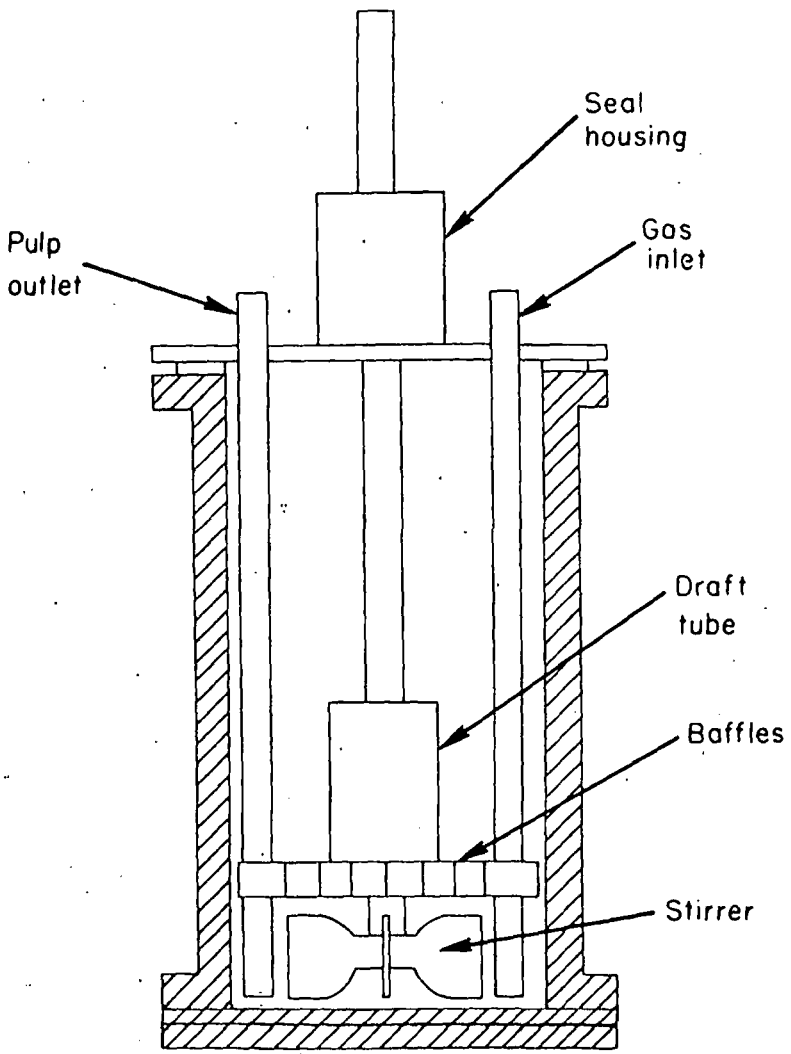

FIGURE 1. - Diagram of a 14-liter-capacity reactor.

Metal extractions were determined by complete material balances. All solutions and residues were analyzed by either atomic absorption or standard chemical techniques.

EXPERIMENTAL PROCEDURES

Experiments were conducted in the following manner: The concentrate and a predetermined amount of $FeCl_2 \cdot 4H_2O$ were slurried together with water in the reactor. Oxygen was added at a predetermined pressure until the system stopped consuming oxygen. The reaction of oxygen with the concentrate is exothermic, and it was necessary to control temperature in the 100° to 110° C range by cooling. At the end of the leaching period, the slurry was cooled to room temperature to allow trace amounts of lead chloride to precipitate. The slurry was then filtered, and the filter cake was washed with a volume of water equal to the initial volume used in the reactor. The pregnant solution and wash solution were combined, and the copper was precipitated by adding iron metal in the form of shredded cans. The silver was extracted from the reaction filter cake by slurrying the solids with a cyanide solution and agitating the slurry for 1 hour. The silver was recovered from the cyanide leach solutions by electrolysis. A drawing of the electrowinning cell is shown in figure 2. This silver-recovery cell was developed by the Bureau of Mines to recover gold and silver values from activated carbon strip solution (8).

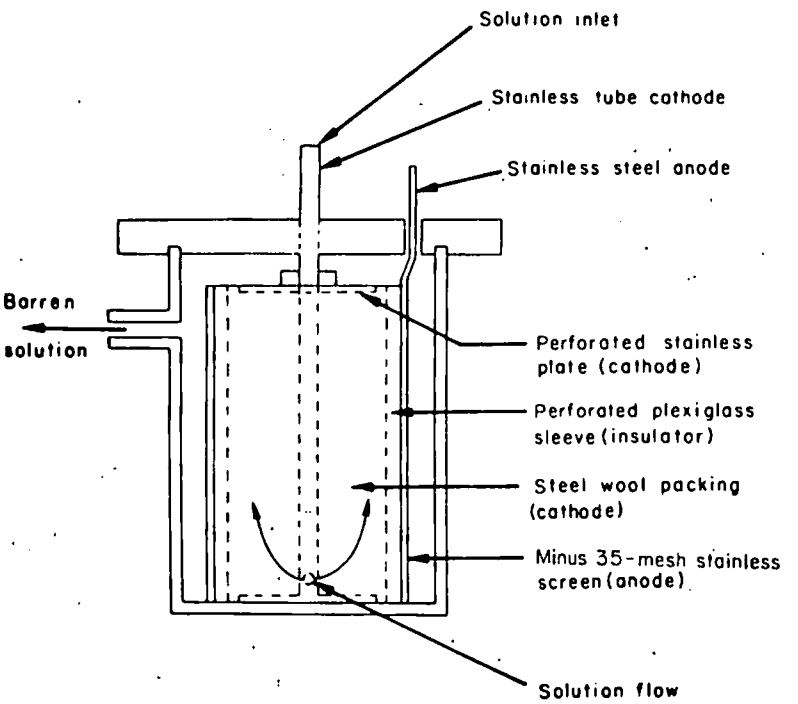

FIGURE 2. - Silver electrowinning cell.

RESULTS AND DISCUSSION

A conceptual flow diagram giving essential details of the ferrous chloride-oxygen leach process as applied to treatment of the silver-copper concentrate is shown in figure 3. Basically, the process consists of reacting the concentrate with oxygen and recycling ferrous chloride for 4 hours at 100° C and 40-psig pressure. Copper is extracted as soluble copper chloride; silver is converted to insoluble silver chloride. Copper is recovered from the leach solution as metal by cementing iron, and the resulting ferrous chloride is recycled directly for additional leaching. Silver is extracted from the original ferrous chloride leach residue by cyanidation and then recovered as metal by electrowinning. Copper and silver recoveries exceeding 98 pct each have been achieved.

The chemistry of the leach step is somewhat difficult to interpret because the original tetrahedrite mineralization was altered to an unidentified mixture of metal sulfides, which was caused by the pretreatment to recover antimony by leaching with a hot mixture of sodium hydroxide and sulfur. Because the feed material to the ferrous chloride-oxygen leach step is comprised of nonstoichiometric compounds, the following generalized equations serve only to give a qualitative description of the chemistry involved:

$$3FeCl_2 + 3/4\ O_2 \rightarrow 1/2\ Fe_2O_3 + 2FeCl_3, \quad (3)$$

$$6FeCl_2 + 3/2\ O_2 + H_2O \rightarrow 2FeO(OH) + 4FeCl_3, \quad (4)$$

$$(CuFe2Ag)S_x + 2XFeCl_3 \rightarrow X(CuFe2Ag)Cl_2 + 2XFeCl_2 + XS. \quad (5)$$

$$(CuFe2Ag)S_x + 4XFeCl_3 + XO_2 + 2XH_2O \rightarrow$$

$$X(CuFe2Ag)Cl_2 + 4XFeCl_2 + 2XHCl + XH_2SO_4. \quad (6)$$

$$(CuFe2Ag)S_x + 2XHCl + X1/2\ O_2 \rightarrow X(CuFe2Ag)Cl_2 + XH_2O + XS. \quad (7)$$

The initial reaction is the conversion of $FeCl_2$ to $FeCl_3$, which reacts with the metal sulfides. All of the reactions, 3 through 7, take place during

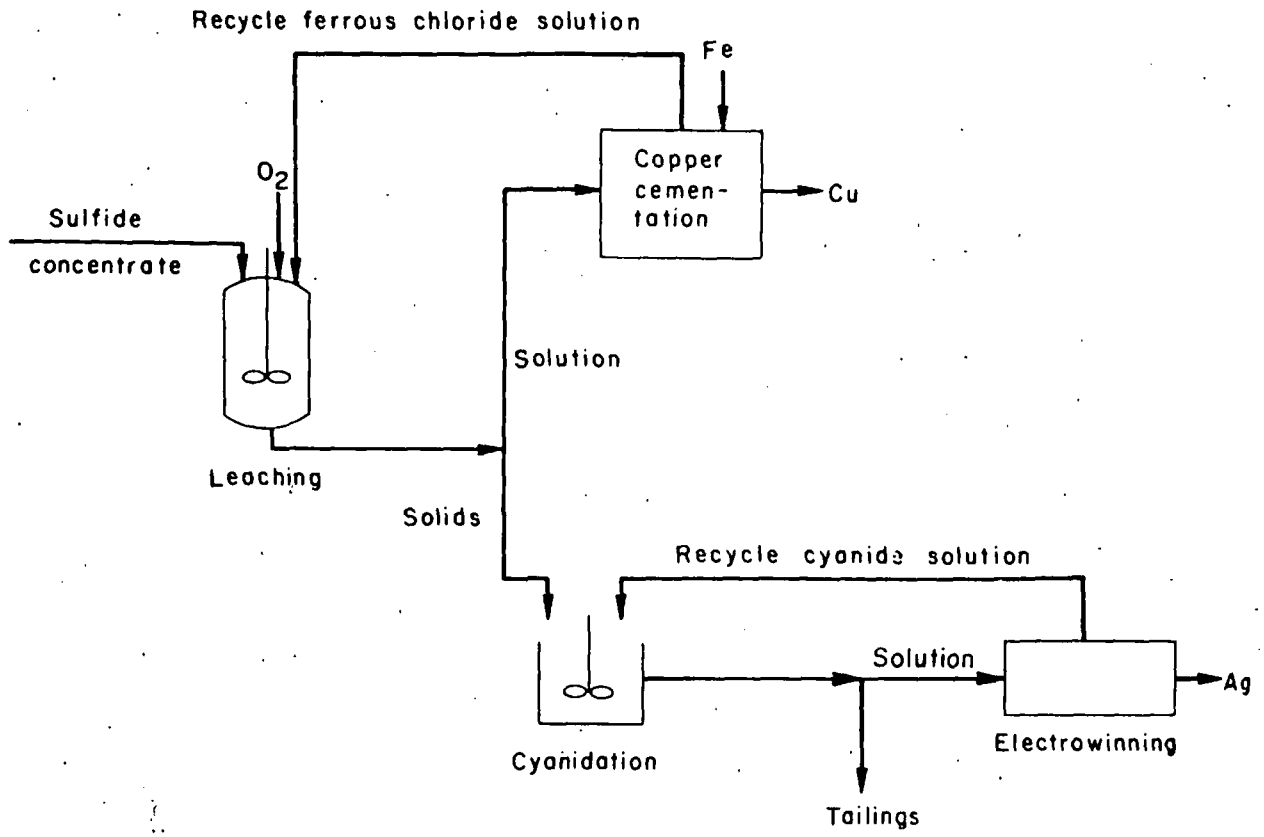

FIGURE 3. - Flow diagram for ferrous chloride-oxygen leaching of silver-copper concentrates.

leaching. The major reactions are those in which ferric chloride is regenerated from ferrous chloride and reacts with the sulfide minerals to produce metal chlorides. The minor reactions are those in which sulfate and hydrogen ions are formed. These reactions account for conversion of 6 pct of the sulfide contained in the concentrate to sulfate during leaching. The major difference between this sequence and ferric chloride leaching is the fact that iron is converted to oxides during leaching and silver remains insoluble in the leach solution.

Initial experiments to establish the leachability of the concentrate and to determine the effect of operating conditions were conducted on a 50-gram scale. The first parameter studied was the effect that the amount of ferrous chloride added to the reaction system has on copper and silver extraction. The amount of ferrous chloride employed in the tests was ranged from 50 to 110 pct of the theoretical amount required to convert all of the cupric copper, lead, zinc, and silver in the concentrate to chloride salts. The results of this series of tests are shown in figure 4.

The data are interesting in that copper extraction increased almost linearly with increasing addition of ferrous chloride up to 97 pct and then leveled off. In contrast, silver extraction by subsequent cyanidation was

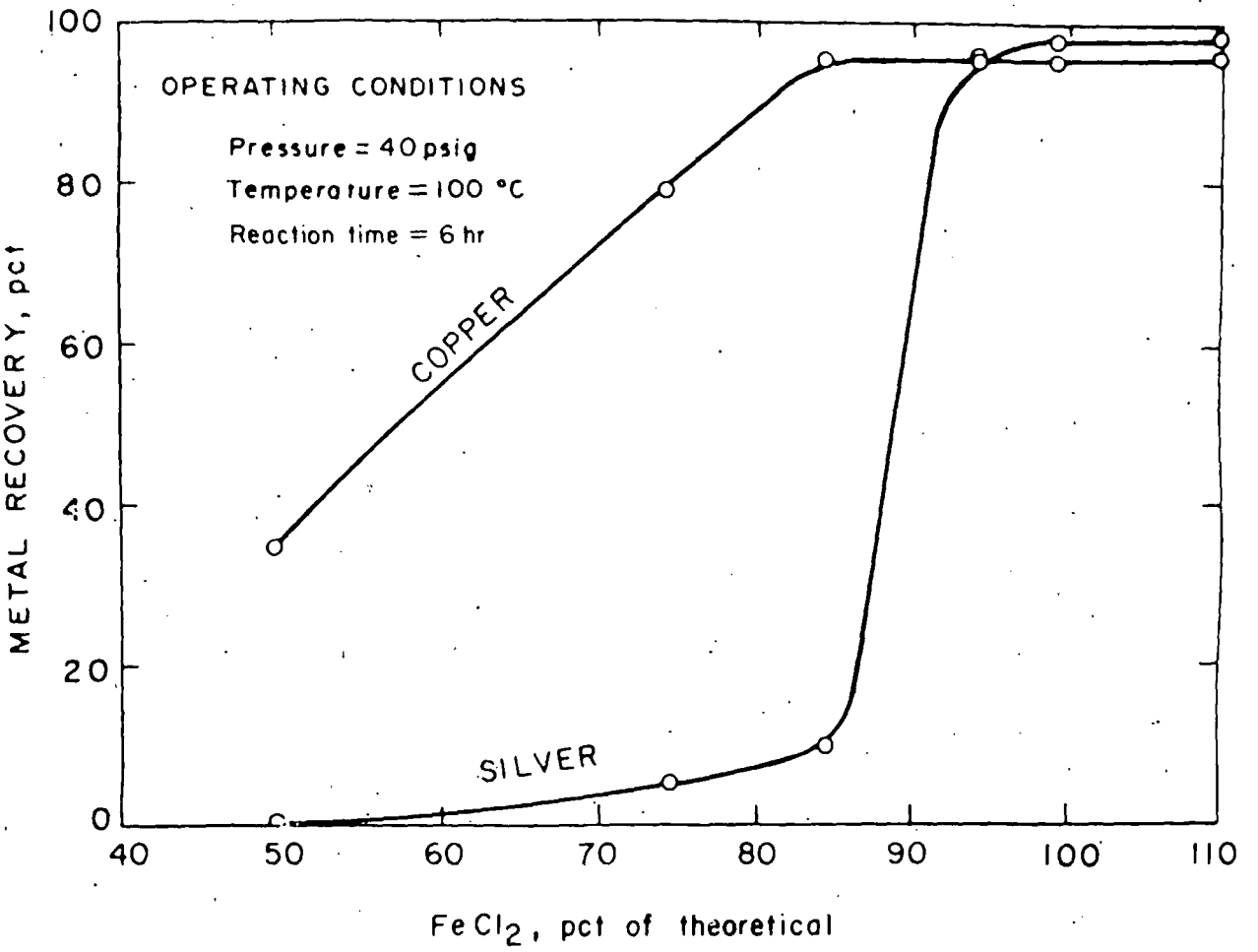

FIGURE 4. - Effect of ferrous chloride addition on copper and silver extraction.

almost uneffected until 85 to 90 pct of the ferrous chloride had been added. When 100 pct of the theoretical amount of ferrous chloride had been added, silver extraction increased sharply to its maximum of about 98 pct. The data illustrate that the copper reaction takes place first, consuming nearly all of the reactants, and thus preventing reaction of the silver.

The operating pressure of the leach system is an important parameter because it affects the solubility of oxygen in the leach solution, which, in turn, affects the rate of reaction. Figure 5 shows the influence of oxygen pressure on the operating time required to reach 97 pct copper extraction and 98 pct silver conversion at 100° C when employing 100 pct of the theoretical amount of ferrous chloride required. As expected, the data show that time required to complete the leach reaction declines at a decreasing rate as the pressure is increased. Under these operating conditions, the reaction time becomes nearly constant at pressures above 80 psig.

The rate of reaction is also affected by temperature. The effect of temperature on the time required to reach a constant extraction of 97 pct copper

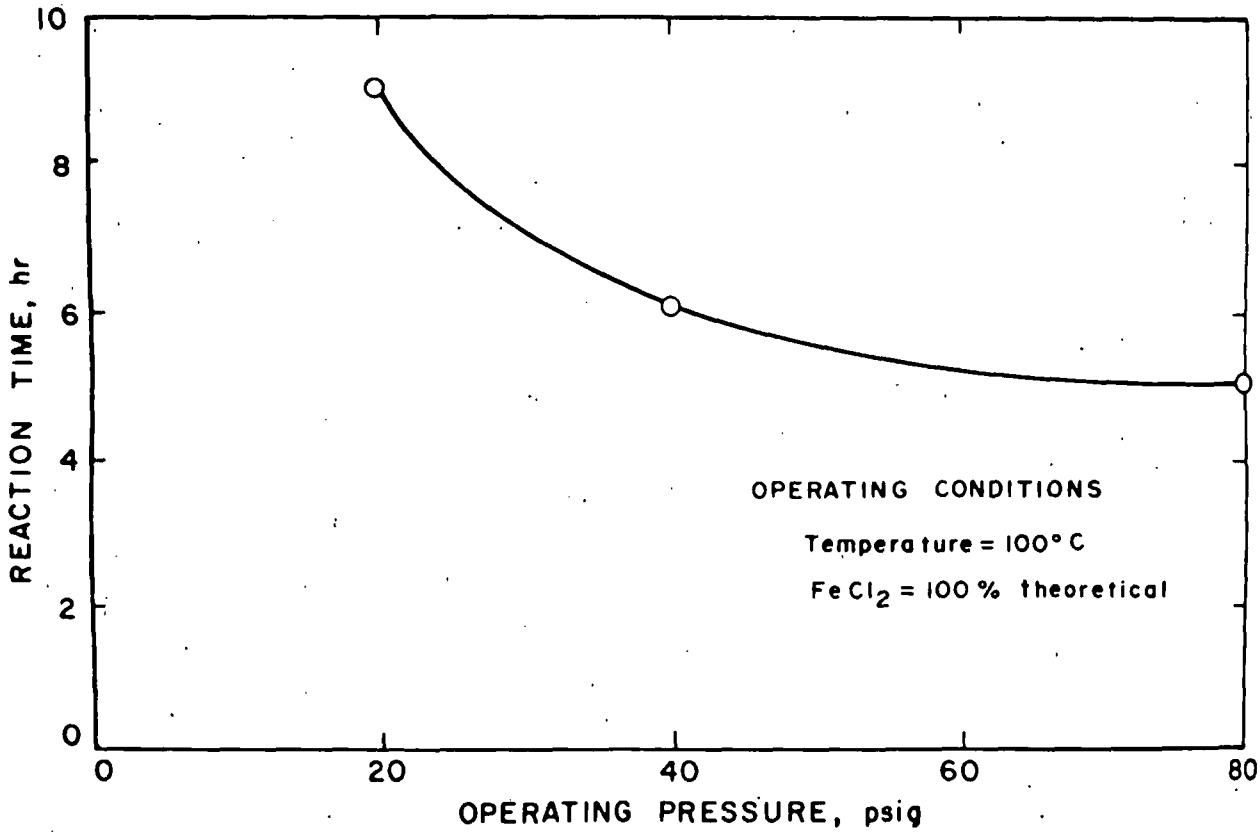

FIGURE 5. - Effect of pressure on reaction time to attain 98-pct silver extraction and 97-pct copper extraction.

and 98 pct silver at 40 psig when using 100 pct of the theoretical amount of ferrous chloride required is shown in figure 6. These effects are similar to those obtained by changes in operating pressure in that the time required to complete the leach reaction declines at a decreasing rate until it becomes nearly constant after 4 hours of leaching.

Also investigated was the effect of hydrogen ion concentration on the leach system because it was felt that this variable could be important in terms of what chemical reaction was predominant during leaching. The pH of the ferrous chloride solution generated during cementation of the copper is 1.74, and the use of this solution as a leachant resulted in a final pH of 1.8 to 2.0. The pH of the ferrous chloride leach solution was lowered to 0.32 stagewise in a series of experiments, and it was found that the copper and silver extraction was independent of hydrogen ion concentration within the range studied.

Based on data obtained in tests using a small reactor, the treatment sequence was scaled up to a reactor 14 liters in size. A charge of 4,000 grams of concentrate, 977 grams of ferrous ion as $FeCl_2 \cdot 4H_2O$, and 8 liters of water were added to the reactor. Pressure in the reactor was held at 40 psig with oxygen. The temperature quickly increased to 100° C, and the temperature

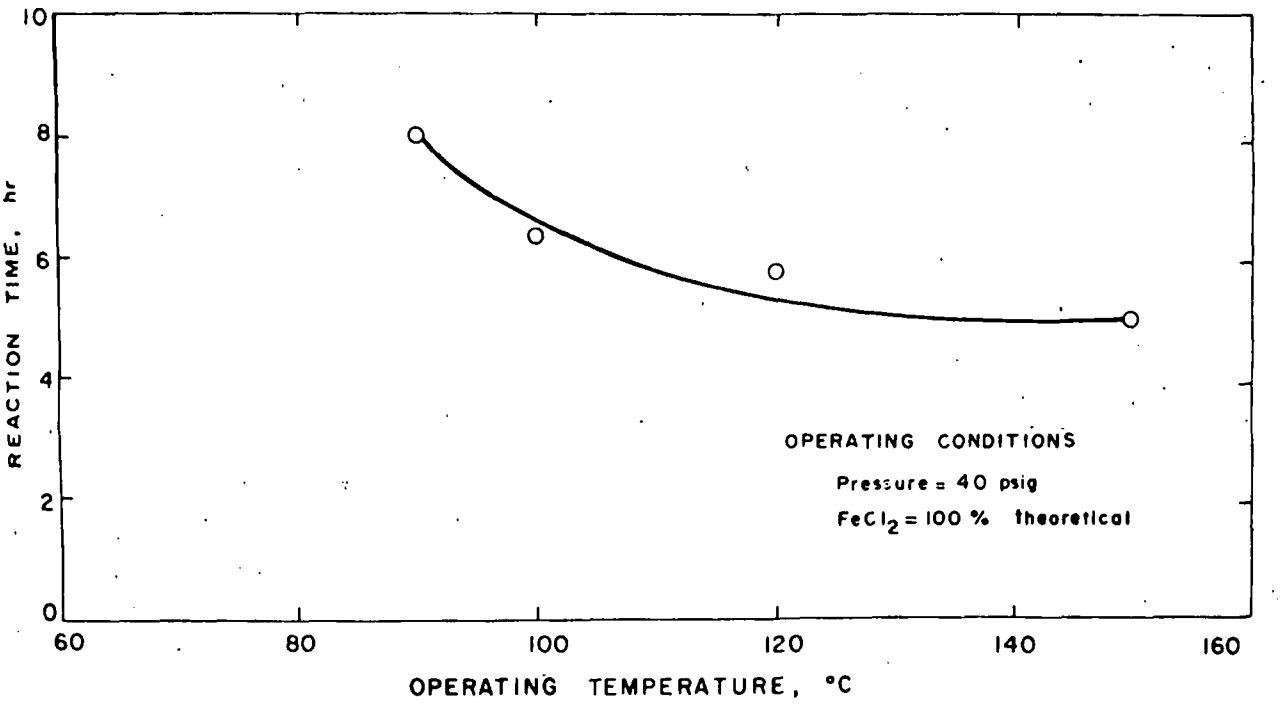

FIGURE 6. - Effect of temperature on reaction time to attain 98-pct silver extraction and 97-pct copper extraction.

was controlled between 100° and 115° C by cooling. The reaction was complete in 4 hours. The oxygen consumption was 300 grams or 150 lb/ton of concentrate. The reaction time of 4 hours is 2 hours shorter than the time required for similar experiments in a 50-gram-capacity reactor. The shorter time is attributed to the more violent agitation achieved in the 14-liter reactor. Silver and copper extractions of 99.4 and 98.6, respectively, were obtained when the pulp was treated by the sequence described in figure 3. Silver and copper extractions were also higher in the larger reactor when compared with those in the 50-gram reactor. The reason for this increase, again, is due to the increased agitation achieved in the larger reactor, which gives better contact between the mineral particles and the oxygen. This experiment was repeated three more times, and silver and copper extractions ranged between 99.1 to 99.7 and 98.2 to 98.6, respectively. The data obtained in these experiments showed that 65 pct of the sulfide portion of concentrate reacted with the ferric chloride, and, of this, 94 pct of the sulfur was oxidized to elemental sulfur with the remainder being converted to sulfate ion. The sulfate originally contained in the concentrate remained insoluble during the ferrous chloride-oxygen treatment. More than 99.9 pct of the iron, antimony, and arsenic were converted to insoluble oxides and reported to the tailings.

CYANIDATION AND ELECTROWINNING

Silver was recovered from the leach residue by cyanidation followed by electrowinning. Experiments conducted at a pulp density of 25 pct, initial cyanide concentration of 33 g/l, and ambient temperature to determine

required reaction times indicated that a constant silver extraction of 99.7 pct could be obtained with only 1 hour of cyanidation.

Silver was recovered from pregnant cyanide solutions by electrolysis in a cell operating at a fixed voltage of 1.8 and an amperage of 2.15 to 4.30. The silver content of the solution was reduced from 14.5 g/l to 0.1 g/l during electrolysis. The power requirements were 0.0224 kwhr/oz of silver recovered, corresponding to a current efficiency of 77.2 pct. After electrolysis, silver was recovered from the steel wool cathode by adding HCl to dissolve the iron and fire refining the residue. The resulting ferrous chloride solution can be used in the ferrous chloride-oxygen leaching step. The barren cyanide electrolyte would be recycled to the cyanidation step. The solid tailings from the cyanidation step would have to be washed for appropriate removal of cyanide prior to disposal or subjected to an oxidation step to destroy the entrained cyanide content.

COPPER RECOVERY

Copper was recovered from leach solutions by cementation with iron as shown by the following equation:

$$CuCl_2 + Fe^\circ \rightarrow Cu^\circ + FeCl_2. \quad (8)$$

A typical copper solution produced by ferrous chloride-oxygen leaching contained 122 g/l copper, 8 to 10 g/l zinc, 15 to 20 parts per million (ppm) lead, 20 to 30 ppm silver, 20 to 30 ppm iron, and 10.2 g/l sulfate ion. The cementation reaction was performed by adding shredded iron cans to the copper solution and agitating vigorously for 20 min. The solution was filtered, and the cement copper was washed with water. Cement copper containing 88 pct copper, 3.1 pct iron, and 0.7 pct chloride ion was produced using 120 pct of the theoretical amount of iron required. The source of chloride ion is cuprous chloride. The resulting barren solution contained 0.009 g/l copper and 125 g/l ferrous ion. This solution in plant practice would be recycled to the reactor to treat a fresh batch of concentrate. With time, the concentration of zinc and sulfate ion would build up in the solution. Ion exchange or sulfide precipitation could be used to remove zinc from the recycle solutions, and sulfate ion could be precipitated by adding calcium chloride.

A 500-lb/day miniplant incorporating the leach and recovery sequence depicted in figure 2 is being operated at the Reno Metallurgy Research Center to quantify reagent requirements and determine optimum operating conditions for extracting metal values from this complex concentrate.

CONCLUSIONS

Silver and copper can be effectively recovered from a pretreated complex concentrate by a ferrous chloride-oxygen leach, followed by cyanidation and electrowinning. Silver extractions of 99.7 pct and copper extractions of 98 pct were obtained in 4 hours of leaching, employing 150 pounds of oxygen per ton of concentrate at a pressure of 40 psig and a temperature of 100° to 110° C. Greater than 99.9 pct of the iron, sulfur, arsenic, and antimony content of the original concentrate reports to the tailings as insoluble products.

REFERENCES

1. Derry, R. Pressure Hydrometallurgy: A Review. Miner. Sci. and Eng., v. 4, 1972, pp. 3-24.

2. Forward, F. A., and I. H. Warren. Extraction of Metal Sulfide Ores by Wet Methods. Met. Rev., v. 5, No. 18, 1960, pp. 137-164.

3. Habashi, F. Recovery of Elemental Sulfur From Sulfide Ores. Montana BuMines Bull. 51, 1966, 31 pp.

4. Haver, F. P., R. D. Baker, and M. M. Wong. Improvements in Ferric Chloride Leaching of Chalcopyrite Concentrate. BuMines RI 8007, 1975, 16 pp.

5. Haver, F. P., and M. M. Wong. Ferric Chloride-Brine Leaching of Galena Concentrate. BuMines RI 8105, 1976, 17 pp.

6. _____. Recovery of Elemental Sulfur From Nonferrous Minerals: Ferric Chloride Leaching of Chalcopyrite Concentrates. BuMines RI 7474, 1971, 20 pp.

7. Murphy, J. E., F. P. Haver, and M. M. Wong. Recovery of Lead From Galena by a Leach Electrolysis Procedure. BuMines RI 7913, 1974, 8 pp.

8. Zadra, J. B., A. L. Engle, and H. J. Heinen. Process for Recovering Gold and Silver From Activated Carbon by Leaching and Electrolysis. BuMines RI 4843, 1952, 32 pp.

INT.-BU.OF MINES,PGH.,PA. 23008

The presence of aluminium nitrate in the solution not only strengthens the contradictory effect of pH and temperature on the solubility of ferric oxide but also increases its solubility by 0.5-1.5 orders of magnitude. There may be several reasons for the specific action of aluminium nitrate. In particular, in the absence of free acid formation of hydroxy complexes of aluminium in the solution may have a large effect on the solubility of iron oxide. Calculations of the ionic composition at various temperatures[8]) show that the area of intense hydrolysis is rapidly shifted towards the acidic region with increase in temperature. Subsequent development of the concept of hydrolytic polymerisation suggests a high probability of the formation of heteropolynuclear hydroxy complexes[9]) having such elements as

$$-Fe\text{-}OH\text{-}Al-;\quad -Fe\begin{matrix}\nearrow OH\\ \searrow OH\end{matrix}Al-;\quad -Fe\text{-}O\text{-}Al-\ \text{etc.}$$

in their composition.

In the presence of free acid ($\mu_{HNO_3} > 6$) the pH of the mother solutions is low. This bears witness to the known salting out action of aluminium nitrate, which leads to an increase in the activity of the nitric acid[10]) and, as a result, to an increase in the equilibrium concentration of iron over the ferric oxide precipitate.

In spite of the negative effect of aluminium nitrate on the degree of hydrolytic separation of iron (III), under the most favourable conditions the iron ratio of the mother solutions exceeded 2000. This demonstrates the fundamental possibility of using hydrolytic purification for the production of commercial alumina meeting the standard in respect of iron.

Conclusions

1. Aluminum nitrate has a considerable negative effect on the degree of hydrolytic separation of iron (III) from nitrate solutions.
2. In the presence of aluminium nitrate the contradictory character of the effects of temperature and pH on the solubility of the products from the hydrolysis of iron (III) is intensified. This reduces the range of favourable values of these parameters.
3. The hydrolytic removal of iron from aluminium nitrate solutions by the autoclave method can be used for the production of standard commercial alumina.

References

1) N A Koryukina et alia: Treatment of mineral raw material and industrial wastes. Izd. UPI Sverdlovsk, 1975.
2) V S Makarova et alia: Investigation of processes in the metallurgy of nonferrous and rare metals, Moscow: Nauka 1969, 195, 200.
3) R Z Karimov: Abstract of Thesis. Tashkent 1969.
4) L A Bogachevn: Abstract of Thesis. Tashkent 1973.
5) Kh R Istmatov et alia: Zh. Neorgan. Khim., 1971, (12)
6) Yu Yu Lur'e: Manual of analytical chemistry. Khimiya, Moscow 1971.
7) Yu A Klyachko et alia: Course of qualitative chemical analysis. Goskhimizdat, Moscow 1960, 114.
8) B I Malyshev: in Geochemistry of hydrothermal ore formation. Nauka, Moscow 1971, 106.
9) Yu I Sannikov et alia: Zh. Neorgan. Khim., 1967, (10), 2651.
10) R Treibal: Liquid extraction. Khimiya, Moscow 1966.

UDC 669.71.053.4

Conversion of sodium sulphate by potassium aluminate solution

A I Lainer, Yu A Lainer and T D Israfilov (Azerbaidzhan Polytechnical Institute)

During the comprehensive treatment of alunites by the reductive-alkaline scheme at the Kirovabad aluminium works a mixture of potassium and sodium sulphate is produced in the evaporation of the recycled aluminate solutions. This mixture is used to compensate the losses of caustic alkali by thermal caustification with aluminium hydroxide in rotating furnaces. However, such caustification is not economically justified, since it involves high production and energy costs. Moreover, it leads to the accumulation of potassium hydroxide in the aluminate solutions, and this leads to a whole series of additional complications in the technological cycle.

The alkali sulphates produced from the aluminate solutions during evaporation contain up to 60-70% of potassium sulphate. This makes it expedient to convert them completely into potassium sulphate, which is a good fertiliser for agricultural purposes and, particularly, for subtropical cultivation.

In recent years G Z Nasyrov at the All-Union Aluminium and Magnesium Institute proposed a method for the conversion of sodium sulphate with potassium hydroxide solution according to the reaction: $Na_2SO_4 + 2KOH = K_2SO_4 + 2NaOH$. This eliminates the production of caustic alkali in the thermal caustification of sulphates. In this case, however, it is necessary to have separate caustic potash production or its provision from outside, which complicates the process.

In the acid-alkali method for the treatment of alunites developed at the Moscow Institute of Steel and Alloys and the A A Baikov Institute of Metallurgy, Academy of Sciences of the USSR, sulphuric acid is added to the main reduction-alkali branch. Provision is made for leaching of the alunite dust with sulphuric acid solution, crystallisation of potassium alum from the solution, and sintering of the alum with coke. After leaching a solution of potassium aluminate is obtained. This is passed on for conversion of the sodium sulphate from the main branch:

$$2KAlO_2 + Na_2SO_4 = K_2SO_4 + 2NaAlO_2$$

The conversion of the sulphate mixture into potassium sulphate involves twofold conversion of the sulphate mixture with potassium aluminate solution from the sulphuric acid branch by repulping in mixers with a counterflow system at a temperature of about 60°C (fig. 1). The sodium hydroxide solution (containing 78.5% Na_2O) obtained as a result of the conversion of the sulphate mixture is used to compensate for the production losses of caustic alkali. To free it from alkali the potassium sulphate after the second stage of conversion is washed by irrigation with a hot solution of sulphates followed by filtration. The wash water is used to dilute the initial potassium aluminate solution. After filtration the washed potassium sulphate is dried and passed to the store in the form of the finished product with a content of 95.5-98.5%

Investigations were carried out into the relationships governing the substitution of potassium in the solution by sodium from the sulphate mixture as a function of the number of moles of K_2O in the initial potassium aluminate solution for one mole of Na_2O in the initial sulphate mixture, the variation of the molar ratio of Na_2O and K_2O in the initial solution, the concentration of K_2O in the initial solution, the caustic ratio of the initial potassium aluminate solution, the time of contact between the solution and precipitate, and

the treatment temperature.

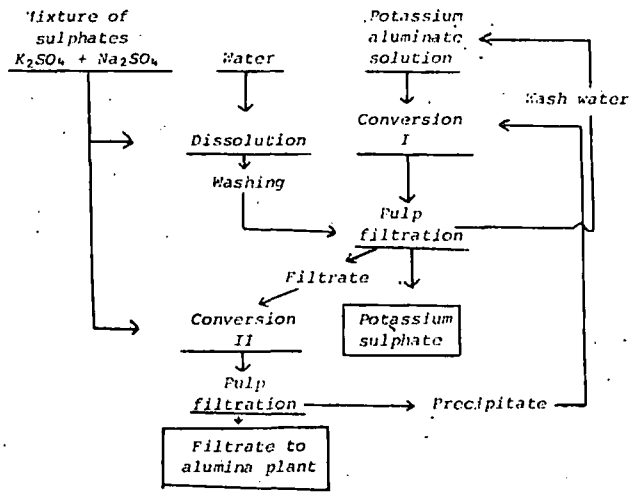

Fig.1 Technological scheme for the conversion of the mixture of potassium and sodium sulphates into pure potassium sulphate with the aid of potassium aluminate solution.

For the initial sulphate mixture we used pure sodium sulphate and potassium sulphate in the ratio of 39% Na_2SO_4 and 61% of K_2SO_4, which corresponds to the composition of the mixture of sulphates produced at the Kirovabad aluminium works in the evaporation of the aluminate solutions. The investigation was carried out with solutions of potassium and sodium aluminates in a beaker fitted with a mechanical stirrer and thermostat. During agitation of the pulp the equilibrium distribution of Na_2O and K_2O between the solution and the precipitate was effectively reached after 30 min. The sulphate precipitate filtered well. After filtration of the pulp the precipitate and the filtrate were analysed for Na_2O, K_2O, SO_3 and Al_2O_3 contents.

It was shown that with a low value of K (0.5), equal to the ratio of the number of moles of K_2O in the initial solution of $KAlO_2$ to the number of moles of Na_2O in the initial sulphate mixture, as a result of conversion a solution rich in Na_2O was obtained with almost complete substitution of the K_2O in the solution (fig. 2). The conversion at the last stage, where the aluminate solution for compensation of the losses of caustic alkali in the main branch is produced, must therefore be carried out with low values of K.

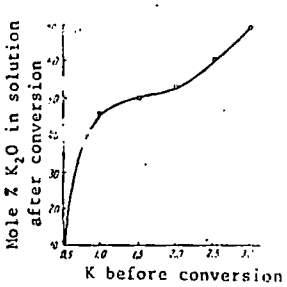

Fig.2 The effect of the initial ratio $K = K_2O_s/Na_2O_{ism}$ on the mole fraction of K_2O in the solution after conversion.

The degree of conversion $(Na_2O)_s/(Na_2O)_{ism} \cdot 100\%$, i.e. the ratio of the amount of sodium alkali which passed into solution as a result of conversion $(Na_2O)_s$ to the amount of sodium alkali in the initial sulphate mixture $(Na_2O)_{ism}$ in the form of Na_2SO_4 (expressed in percentages) (fig. 3), and the mole fraction of K_2SO_4 in the sulphate precipitate after conversion (fig. 4) increase with increase in the K values. This is due to the fact that with increase in K the number of moles of K_2O in the solution for one mole of Na_2O in the sulphate precipitate increases, and this leads to more complete substitution of Na_2O in the sulphate mixture by the K_2O of the solution. This means that in the stage where the sulphate precipitate in the form of the final product (potassium sulphate) is produced the conversion must be carried out with high values of K, e.g. K = 2.

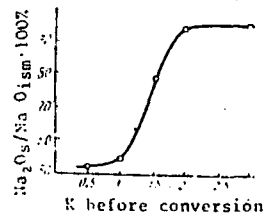

Fig.3 : The effect of the initial ratio $K = K_2O_s/Na_2O_{ism}$ on the degree of conversion.

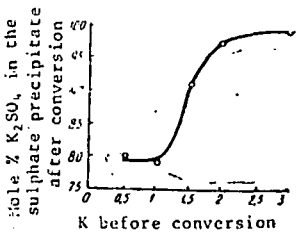

Fig.4 The effect of the initial ratio $K = K_2O_s/Na_2O_{ism}$ on the mole fraction of K_2SO_4 in the sulphate precipitate after conversion.

When the initial solution contains Na_2O in addition to K_2O, the degree of conversion decreases with increase in the fraction of Na_2O with identical K (fig. 5). This clearly leads to an increase in the saturation of Na_2O in the solution and prevents its passage from the sulphate mixture into the solution.

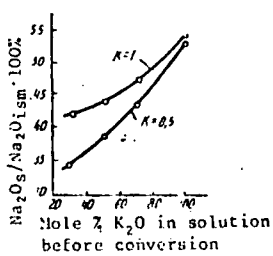

Fig.5 The effect of the mole fraction of K_2O in the initial solution on the degree of conversion.

Consequently, most effective conversion is realised with a purely potassium initial solution. In addition, during development of the conversion technology it is necessary to strive towards a reduction in the number of process stages, since the effectiveness of the succeeding stages decreases with increase in their number.

The amount of SO_3 in the solution decreases with increase in the potassium aluminate concentration, since the equilibrium concentration of the sulphate salts in the solution here decreases sharply (fig. 6). This means that to obtain solutions free from SO_3 after conversion it is necessary to use highly concentrated initial solutions, especially as this has practically no effect on the degree of conversion. The increase in the SO_3 content with variation of the K_2O concentration in the initial potassium aluminate solution from 50 to 100g/l is due to the absence of the necessary amount of sulphate salts in unit volume of solution for its saturation with the latter, since the sulphate salts were used in an amount corresponding to a ratio K equal to unity.

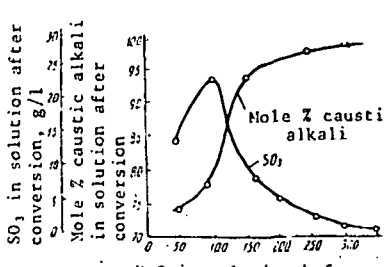

Fig.6 The effect of the K_2O concentration in the initial solution on the mole fraction of caustic alkali and the amount of SO_3 in the solution after conversion.

Table: Composition of the conversion products

Name of products	Composition of products (solution g/l; mixture %)					
	K_2O	Na_2O	SO_3	M % K_2O	M % Na_2O	Al_2O_3
Initial product:						
Aluminate solution	300	-	-	-	-	-
Sulphate mixture No. 1	33.0	17.0	50	56.1	-	-
Sulphate mixture No. 2	41.2	9.85	48.9	73.3	-	-
First stage of conversion:						
Solution before conversion	300	-	-	100	-	-
Sulphate mixture before conversion	40.2	11.2	-	70.3	29.7	1.1
Solution after conversion	142.0	92.5	0.6	50.3	49.7	-
Sulphate mixture after conversion	52.8	1.25	-	96.5	-	0.9
Second stage of conversion:						
Solution before conversion	142.0	92.5	0.6	50.3	49.7	-
Sulphate mixture before conversion	33.0	17.0	-	56.1	-	-
Solution after conversion	59.0	142.0	2.35	21.5	78.5	-
Sulphate mixture after conversion	40.2	11.2	-	70.3	29.7	1.1
Washing:						
Solution for washing	86.3	33.0	110.0	-	-	-
Solution after washing	102.0	41.0	136.0	-	-	3.0
Sulphate mixture after washing	53.2	0.6	-	98.4	-	traces

It was shown that the degree of conversion remains practically unchanged with variation of the temperature in the range from 40 to 95°C and of the time of contact between the solutions and the sulphate mixture in the range from 10 min to 6 h. Variation of the caustic ratio of the initial potassium aluminate solution in the range from 2 to 4 also has no effect on the degree of conversion.

On the basis of the results from the investigations the composition of the products from two-stage conversion of the sulphate mixture from the plant with potassium aluminate solution was determined (table).

The first stage of conversion was carried out twice: the first time with sulphate mixture No. 2 to produce an intermediate solution for the second stage, and the second time with the precipitate from the second stage of conversion.

To eliminate return of the finished product (potassium sulphate) to the beginning of the conversion process the washing of the sulphate precipitate after the first conversion was carried out with a hot solution of sulphates. The washing solution was prepared by dissolving the initial sulphate mixture in hot water.

Conclusion

It was shown that almost pure potassium sulphate and an aluminate solution containing 78.5% Na_2O and 21.5% K_2O are obtained in the two-stage conversion of the sulphate mixture of the Kirovabad aluminium works by means of potassium aluminate solution.

UDC 669.295+66.094.123

Kinetic characteristics of the cementation of aluminium on metallic titanium in a sodium chloride medium

I I Ivanov, R A Sandler and S V Aleksandrovskii (Leningrad Mining Institute)

Summary

The kinetic characteristics of the cementation of aluminium from aluminium chloride on titanium were investigated with high initial contents of aluminium in the melt. The effects of temperature and of the initial concentration of aluminium in the melt on the reaction rate were studied. Increase in temperature leads to an increase in the rate and degree of cementation. Increase in the initial concentration of aluminium leads to an increase in the cementation rate. However, the degree of cementation decreases as a result of the limited amount of cementation agent employed. The time required for the attainment of the same degree of cementation therefore increases with increase in the initial aluminium content. The data obtained show that a secondary process occurs in addition to the main cementation process. This involves reaction of trivalent titanium formed in the cementation process with metallic titanium, giving divalent titanium. Experiments carried out on the cementation of aluminium in melts initially containing titanium dichloride show that in the presence of titanium trichloride the cementation of aluminium only occurs in the initial period. The lower the initial content of aluminium the more rapidly the steady state is reached in the melt. With increase in the initial aluminium content of the melt the degree of cementation decreases somewhat and the amount of the metallic disperse phase and its aluminium content show a tendency to increase. As a rule the aluminium content of the disperse metallic phase is higher, the higher the initial aluminium content of the melt.

For the effective realisation of the cementation of aluminium on metallic titanium the trivalent titanium which forms must be reduced to divalent. For this purpose it is necessary to have an excess of metallic titanium, the surface of which must not be screened by the released cementation product. Since increase in temperature leads to the development of a reaction between titanium and aluminium, a higher degree of purification of a melt containing a small amount of aluminium chloride is secured by a reduction in temperature. With high initial concentrations of aluminium chloride in the melt the positive effect of temperature on the comparatively low degree of cementation is due to greater formation of the dispersed metallic titanium phase in the melt.

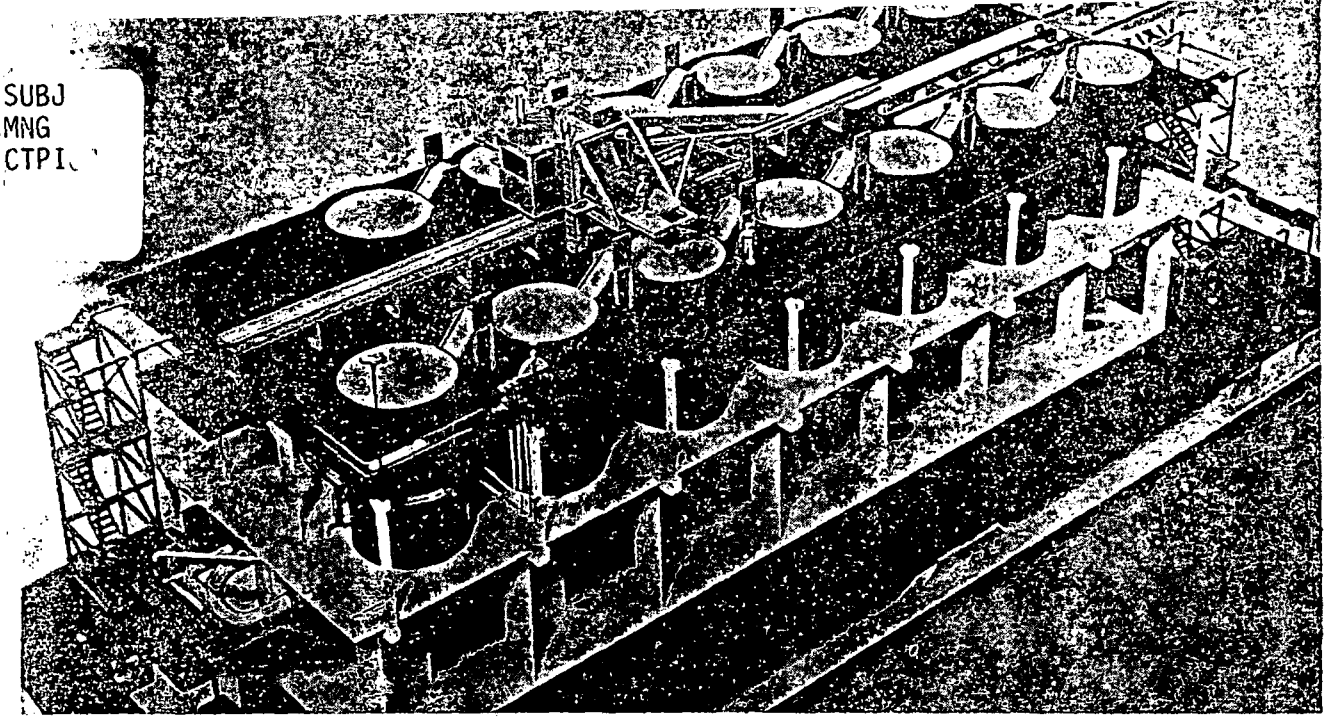

A model of the cone precipitation plant now being constructed by Kennecott Copper Corp. Each module contains 13 cone precipitators. (Photo courtesy Bechtel Corp.)

The problem of recovering copper from copper-bearing solutions has been the subject of research by Kennecott for many years. These investigations have led to the development and use of . . .

Cone-Type Precipitators For Improved Copper Recovery

H. R. SPEDDEN, E. E. MALOUF, and J. D. PRATER

Application of research findings to the old art of leaching copper from copper-bearing mine waste has resulted in a significant contribution of copper to over-all copper production. For example, at the completion of the current expansion program at the Kennecott properties in the United States, copper produced from waste dump leaching will amount to about 25% of the total production, whereas formerly only 2% was derived from this source. This planned expansion of copper leaching focused attention on the problem of developing more efficient methods for the recovery of copper from greatly increased volumes of copper-bearing solutions.[1]

Detailed investigations made in laboratory pilot plant and plant tests for the recovery of copper from copper-bearing solutions have included electrowinning, solvent extraction, ion exchange and cementation with iron in launders, precipitation drums, activated launders, and precipitation cones. The results of these investigations have led to the development of a precipitation cone-type recovery system having advantages over older methods.

Electrowinning: The direct electrowinning of copper from relatively dilute solutions of copper-bearing mine water, namely, solutions containing 10-20 lb of copper per 1000 gal, has always been an attractive possibility.[2, 3] By this method, high-purity copper powder can be recovered with a power con-

The authors, all SME members, are associated with the Western Mining Divisions Research Center of Kennecott Copper Corp., Salt Lake City. H. R. SPEDDEN is Research Director, E. E. MALOUF is Project Development Engineer, and J. D. PRATER is Chief of the Hydrometallurgical Section.

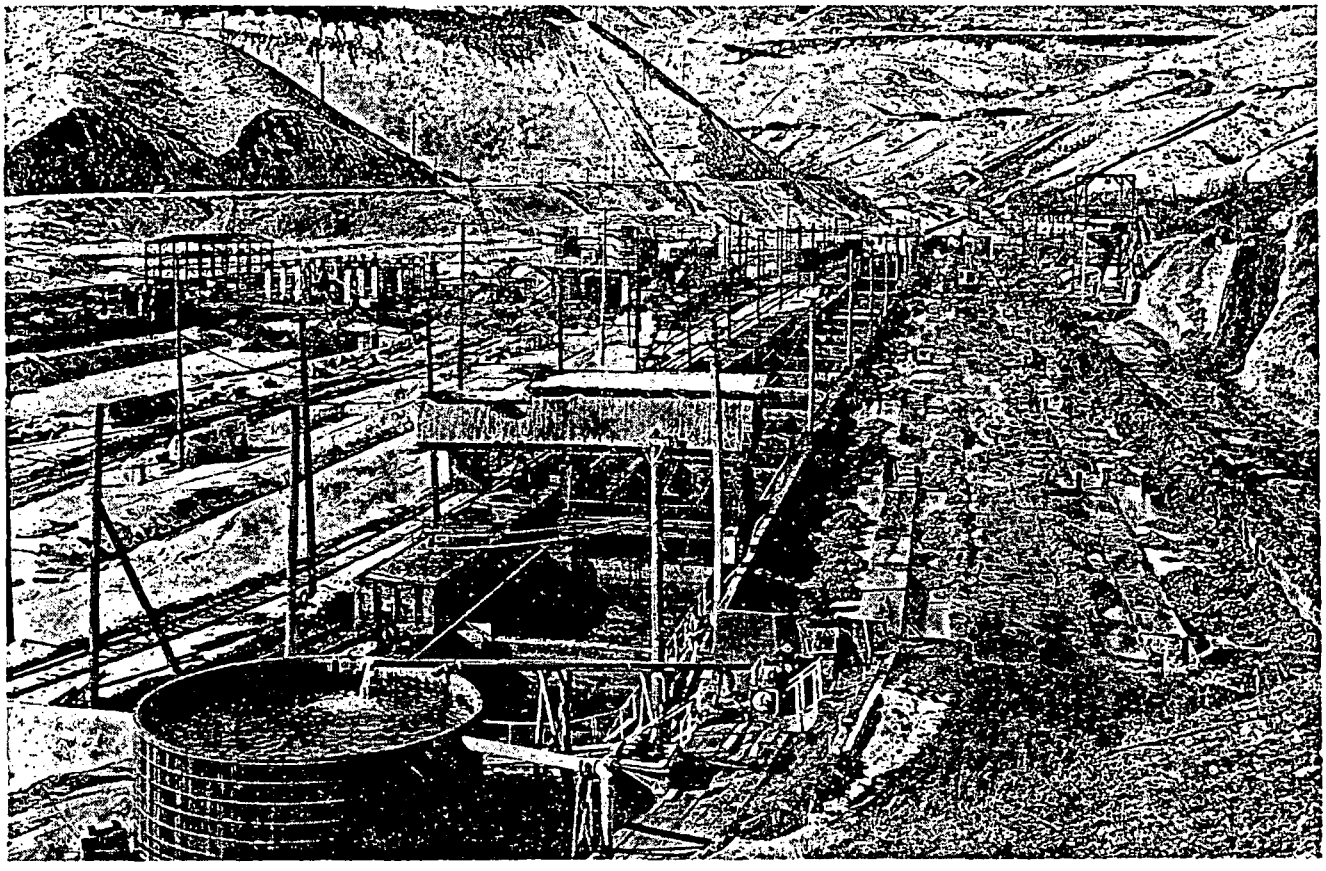

Fig. 1:—*Photograph of gravity launder-type copper precipitation plant at Kennecott's Utah Copper Division Bingham Canyon mine.*

sumption of 3.5 kwh per lb of copper. However, once the solution strength decreases to approximately 5 lb of copper per 1000 gal, current efficiency drops rapidly, requiring the use of other methods to recover the remainder of the copper economically. These results, combined with the high capital cost, make this approach economically unsound under most conditions.

Solvent Extraction: Another technically feasible process is using various organic reagents for the solvent extraction and concentration of copper from dilute acidic solutions.[4] The majority of solutions obtained from leaching rather heterogeneous mine waste dumps, however, contain substantial quantities of ions other than copper as well as suspended insoluble materials. These various ions and suspended gangue can result in a combination that may cause emulsification and costly loss of the solvent. Although substantially improved liquid ion-exchange or solvent extraction reagents which resist emulsification to extremely low levels are now available, enough experience with these new reagents has not yet been obtained to safely justify a major installation. Presently available reagents have a rather low loading factor and thus would require a large capital expenditure for plants of the size now being constructed. A small plant and, in particular, one which does not have a readily available, low-cost source of scrap iron would appear to be the logical next step in this development. The application of the process to copper metallurgy on a significant scale is, nevertheless, a most stimulating goal.

Ion-Exchange Recovery: The use of ion-exchange resins for the concentration of copper from copper-bearing mine solutions has not proven feasible. The non-selectivity of the resins and the fouling of the resins with iron and aluminum ions has precluded the use of this approach. Even the carboxylic-type resins, which are quite specific for copper, display an unsatisfactorily low loading capacity when used for extraction from acidic solutions; thus projected capital costs appear to be unduly high.[5]

Chemical Precipitation: Precipitation of copper from dilute copper-bearing solutions using various chemical precipitants has been a source of continuing investigations by several research groups.[6,7] Consideration has been given to precipitating the copper as a sulfide, as a cyanide, as a thiocyanate, and even as a hydroxide using lime. The recovery of an extremely fine chemical precipitate, with the inherent difficulties of settling and filtering, is a common problem in essentially all processes employing chemical precipitants. The products of chemical precipitation also usually require additional processing steps to obtain the copper in a form readily obtained by cementation on iron.

Precipitation of Copper by Iron: *Gravity Launders*: The oldest, most common method of precipitating copper from copper-bearing solutions has been the gravity-flow launder charged with scrap iron as the precipitant. As a general figure, this type of plant requires 500 ft of launder, 4 ft wide by 4 ft deep, to process 1000 gpm of copper-bearing solution. A launder of this size can effectively recover over 90% of the copper in solutions; however, iron

consumption will vary between 2 to 4 times that amount theoretically required to precipitate the contained copper, depending on the ferric iron and free sulfuric acid contents of the solution. (Fig. 1.)

Launder plants, although simple to construct and operate, require much hand labor and produce an impure cement copper which is usually blended with concentrates as a feed to a smelter. Efforts to improve the method have led to numerous modifications, mostly involving variations in the mechanical handling of the scrap iron or the precipitates.

Drum Precipitators: Rotating drum precipitators have been used industrially in place of launders. The major problem encountered in this system is that of maintaining a large mechanical device in which the total mass of scrap iron is tumbled constantly. Kennecott's test work has shown that the tumbling action breaks the copper precipitates into fine particles, much of it even colloidal in size, thus presenting a further operational problem. Labor requirements for charging scrap iron and for the periodic removal of unconsumed trash likewise make these units generally unsatisfactory.

Activated Launders: Gravity launders have been modified by laying one or more nozzle manifolds along the bottom of the launder to inject the copper-bearing solutions into the mass of iron.[8,9] Studies involving the precipitation of copper in this type of launder have indicated definite improvements over the gravity-type plant, both as to iron factor and volumes of solution treated. However, here again, cleaning of this type of unit requires removing the accumulation of copper precipitates, cans, and trash with consequent high hand labor requirements.

DEVELOPMENT OF A NEW PRECIPITATION SYSTEM

Although most of the recovery methods thus investigated are practical, each one seemed to be lacking in at least one of several desirable features for relatively large scale production. As with most chemical processing methods, an efficient copper recovery system should provide for high volumetric capacity, be able to treat solutions of variable concentrations with high recovery, and be amenable to a substantial degree of mechanical handling and automatic control.

Three chemical reactions, each of which consumes iron, have long been recognized as of importance in copper cementation. These reactions may be shown by the following equations:

$$CuSO_4 + Fe \rightarrow Cu + FeSO_4 \quad [1]$$

$$Fe_2(SO_4)_3 + Fe \rightarrow 3\,FeSO_4 \quad [2]$$

$$H_2SO_4 + Fe \rightarrow FeSO_4 + H_2 \quad [3]$$

Under quiescent conditions, as represented in a launder plant, these reactions will reach equilibrium. If, however, powdered iron of high surface area is used, the copper precipitation reaction is found to be predominant and may be essentially completed before excessive amounts of iron have been consumed by the other two reactions.

Since powdered iron is thus an effective precipitant and may be produced at reasonable cost as a by-product of a base-metal mining and smelting complex, a research program was initiated to develop an efficient vessel in which to utilize such a precipitant. The successful accomplishment of this objective has been reported separately by A. E. Back.[10]

A pressing need for increased copper production required that a further effort be made to improve those precipitation methods which employed available scrap iron, a situation brought about by the absence of an immediately available source of powdered iron. Using the basic cone configuration, a new vessel was designed for a scrap iron feed and this vessel has now been found to have advantages not available in other precipitating processes. Its operation, design, and copper product differ from that of the powdered iron cone. It is a compact unit lending

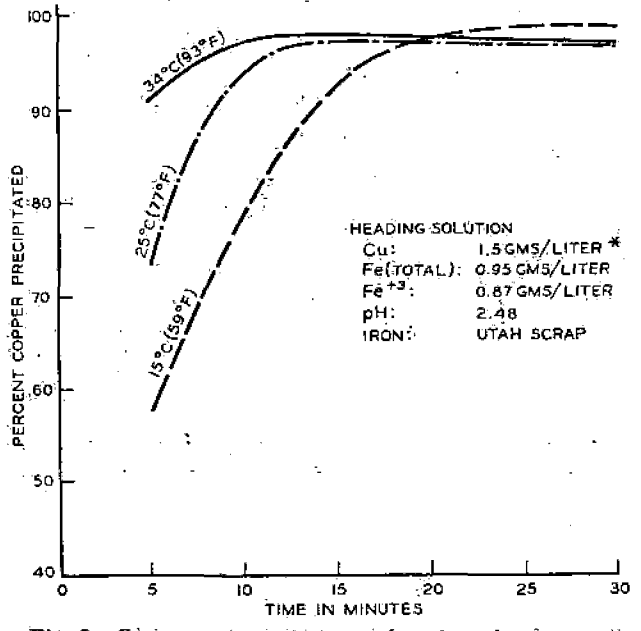

Fig. 2:—*Copper cementation as a function of temperature.* *Conversion factor: 1 gm = 8.345 lb per 1000 gal of solution.

itself to automatic control, low iron consumption, and self-cleaning of copper precipitates. It furthermore results in the production of a higher purity cement copper than that resulting from a launder system. The operating characteristics of the cone precipitator are based on a high-velocity, rapid through-put of copper-bearing solutions and an intimate contact of the solution with clean active iron for precipitation of copper.

Comparison of the relative effectiveness of powdered iron and scrap iron as precipitants clearly indicates that the three basic reactions proceed at different rates. Furthermore, these reactions are temperature dependent, another characteristic of rate reactions. Fig. 2 shows the effect of temperature on increasing the copper precipitation rate. Thus, a rapid contact of solution with iron surfaces promotes the copper precipitation reaction (Eq. 1) by removing the diffusion layer. The resulting sup-

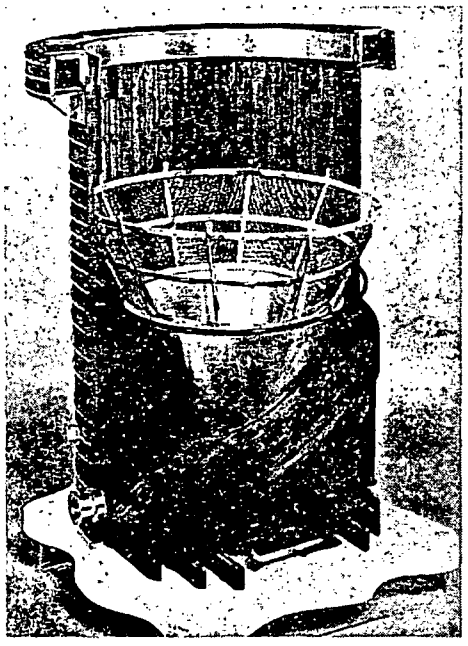

Fig. 3:—*Photograph of a cross-sectional area of Kennecott's cone precipitator (patent pending). Photo courtesy Bechtel Corp.*

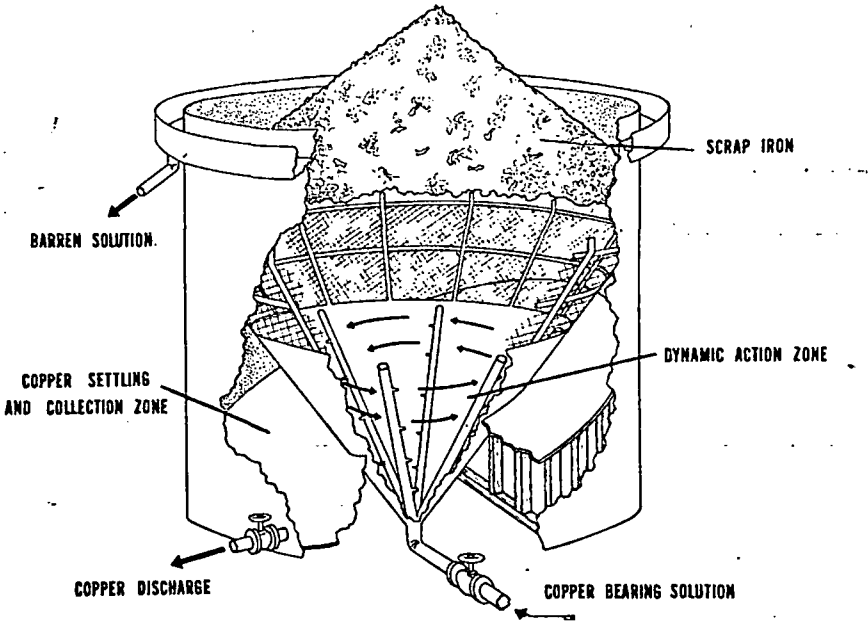

Fig. 4:—*Sketch of cone precipitator showing solution inflow and copper precipitate discharge.*

pression of the acid on iron reaction (Eq. 3) produces a very real reduction in iron consumption.

Wadsworth and co-workers have defined the mechanisms involved in copper precipitation on iron[11] as:

1) Diffusion of reactants to the surface
2) Adsorption of reactants on the surface
3) Chemical reaction at the surface
4) Desorption of products from the surface
5) Diffusion of products away from the surface

They have quantified item 1 for laboratory conditions in the terms of stirring speed of a mechanical agitator. Kennecott has likewise determined an apparent optimum range of conditions in the terms of rate of solution flow through full production size vessels of varying sizes. They further have found that the copper precipitation reaction is a first order rate reaction and that even under some conditions the reaction seems to follow zero-order kinetics. Thus, with adequate agitation, rapid precipitation will occur and acid consumption by iron will be minimized.

The nucleation mechanism has also been studied by Wadsworth[11] with the following conclusion: "The precipitated copper adheres to the iron as a spongy layer at low speeds, peels off in the form of bright strips at medium speeds, and as a fine powder at high speeds." The low speed agitation results defined by Wadsworth correspond to the action in a gravity launder. Medium speed results are of the same magnitude as those found optimum for promoting the precipitation reaction, and thus a dual advantage is gained by dynamic contact of solution with iron.

The theory of diffusional control is further enhanced by experiments employing iron turnings as a precipitant. Clean turnings, extensively laced with sub-micron cracks, present a larger surface area to the small hydrogen ion than to the much larger copper ion. Thus, acid attack by pore diffusion is possible in the cracks. Turnings in this form yielded copper precipitation at a consumption of over 3 lb iron per lb of copper as compared with 1.5 lb per lb of copper when using shredded iron in a precipitation cone.

Table: Typical Data (Daily Average) Comparing The Operating Results of an Experimental Precipitation Cone with a Gravity Launder

CONE PRECIPITATOR			LAUNDER PRECIPITATOR		
Heading lbs Cu/1000 gal	Pct Cu Recovery	Soluble Fe Factor	Heading lbs Cu/1000 gal	Pct Cu	Solution Fe Factor
17.6	92.4	1.13	15.1	98.3	2.85
14.8	93.2	1.45	15.4	89.4	2.15
14.8	88.2	1.83	16.1	85.1	2.04
13.3	94.3	1.60	15.7	87.5	2.26
12.9	91.0	1.49	14.4	85.8	2.30
13.3	92.4	1.77	14.8	90.7	2.17
15.8	93.6	1.86	14.6	93.7	2.16
16.2	93.3	1.74	14.7	91.3	2.22
15.9	95.3	1.54	15.1	91.5	2.25
16.4	96.4	1.74	14.6	84.6	2.40
16.2	95.4	1.10	13.7	84.4	2.47
13.9	94.0	1.72	14.0	95.8	2.70
Average	Average	Average	Average	Average	Average
15.1	93.3	1.58	14.9	89.9	2.33

Another portion of these turnings was crushed in a hammer mill to powder size. In a similar copper-bearing solution, the iron consumption was only 1.2 lb iron per lb of copper. The cracks had thus been opened, exposing all surfaces to the faster copper precipitation reaction.

The granular and dense type of copper produced under dynamic precipitation conditions results in a product that can be filtered readily to a low moisture content, in contrast to the thixotropic-type of precipitates produced in the launder-type plant which, after filtration, may contain 35-40% moisture.

The experimental precipitation cone (Figs. 3 and 4) developed to employ these principles at the Utah Copper Division of Kennecott is capable of processing high volumes of copper-bearing solutions. The vessel consists of a 14-ft diam tank, 24 ft tall, into which is mounted an inverted cone 10 ft in diameter and 10 ft high. The outer 14-ft diam tank contains a 45° sloped false-bottom floor from one side of the tank to a bottom side discharge at the opposite side. The annular space between the inner cone and the tank is covered by a heavy gage stainless steel screen. The screen is mounted as a continuation of the cone and is anchored to the cone and tank. The cone supports a pressure manifold that consists of six vertical legs with each leg containing a series of nozzles directed inward from the tangent to the cone and upward from the angle of the legs of the manifold. The nozzles are arranged in such a manner as to create a vortex when the copper-bearing solutions are pumped through the manifold into the cone. The inner cone and the area of the tank above the stainless steel screens are filled with shredded, detinned iron scrap, such as is commonly used in the precipitation of copper. The shredded iron is "coned" to the top of the tank. This large mass of iron in a confined vessel has proved to be an effective heat retaining medium, thus enhancing the reaction kinetics.

Copper-bearing solutions are pumped through the manifold with the nozzles injecting the copper-bearing solutions into the mass of iron. The injection of the solutions has the effect of not only rapidly precipitating copper, but also removing the metallic copper from the iron surface, thereby exposing clean, fresh iron.

The precipitation cone is a continuously operated unit that is self-cleaning, eliminating the need for fire hoses to wash the copper precipitates from the precipitator, as is the practice in many launder-type plants. The pressure and velocity of the solutions in the lower conical section tend to move the copper precipitates in the same manner as an elutriation column, upward and out of the cone into the reduced velocity zone created by the larger diameter of the holding tank. The copper precipitates settle down through the stainless steel screen and accumulate on the sloped false-bottom of the tank. The copper can then be discharged intermittently with the use of a pneumatically operated valve on a time cycle or bled continuously through a small diameter pipe into a thickener or holding basin. The copper precipitates produced in this

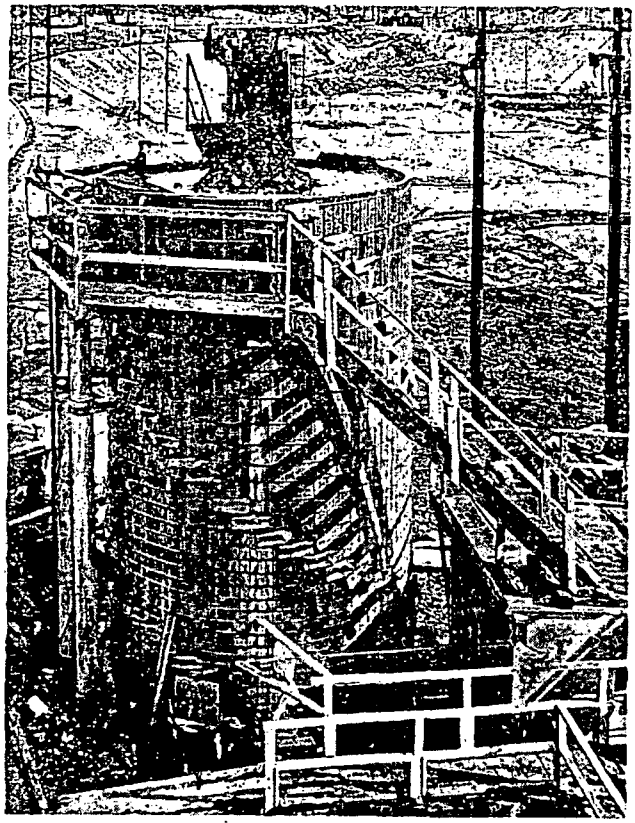

Fig. 5:—*Photograph of experimental precipitator at Kennecott's Utah Copper Division.*

manner are of substantially higher grade than the conventional cement copper produced in a launder-type plant. They typically will analyze 90-95% copper, 0.1-0.2% iron, 0.1-0.2% silica, and 0.1-0.2% alumina with the balance of the impurity being primarily oxygen.

The prototype precipitation cone was operated continuously for seven weeks in one test. After this test run, using commercial shredded iron identical to the material used in the launder plant, the unit was shut down and examined. A total of 18-in. of trash remained in the bottom of the inner cone. This residue consisted of pieces of concrete, rocks, granular copper, and some pieces of copper-plated steel shafting. This small amount of residue was striking evidence that most of the trash inherent in the scrap iron had been masticated by the dynamic action in the cone and discharged in the tailing solutions. In comparison, a launder plant usually requires daily washing with high pressure hoses.

During seven weeks of continuous operation of the experimental cone, copper recovery averaged 89.7% with inclusion of data for periods in which wide fluctuations in the addition of shredded iron was experienced. Sustained periods during optimum operating conditions resulted in copper recoveries exceeding 95% in the single cone.

Results comparing the performance of an experimental precipitation cone operating at approximately double the flowrate of the standard-sized gravity launder with which it is compared are presented in the accompanying Table. These results represent daily averages for the same operating periods.

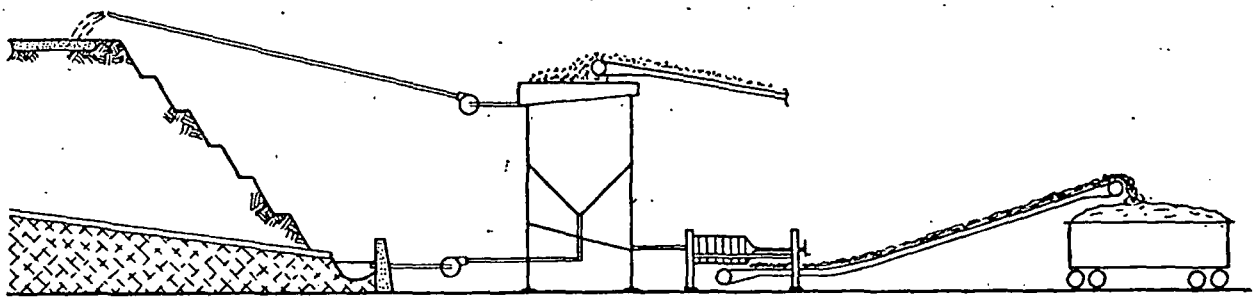

PUMPED ONTO MINE WASTE DUMPS, WATER PERCOLATES THROUGH THE ROCK WHERE IT PICKS UP A COPPER SULPHATE SOLUTION.

THIS SOLUTION IS COLLECTED IN A CENTRAL FLUME SYSTEM AND PUMPED INTO PRECIPITATION CONES.

THE PRECIPITATION CONE, FILLED WITH OLD TIN CANS, PRECIPITATES COPPER FROM THE WATER. THE WATER IS THEN RETURNED TO THE DUMPS.

THE PRECIPITATED COPPER PASSES THROUGH A FILTER PRESS AND THE RESULTANT COPPER PRODUCT IS LOADED INTO RAILROAD CARS FOR SHIPMENT TO THE SMELTER.

Fig. 6:—*Diagrammatic sketch of the copper leaching and precipitation system as used at Kennecott.*

As a result of the successful operation of the experimental cone at the Utah Copper Division, a cone-type precipitation plant is now being constructed which will contain 26 cone precipitator units (Fig. 5). The plant will be of modular construction arranged in a manner to permit the solution flow to pass through two cones in series. This will provide an operational safety factor for optimum stripping. The structure rising above the cone tanks is a movable scrap iron feeder fed by a conveyor belt from the scrap storage yard. Shredded scrap iron is added to each cone intermittently as required (see illustration on title page).

Two cones have been operated in series to determine the effect of the second cone on total iron consumption when only partial stripping has been accomplished in the first cone. This two-stage treatment can provide a better over-all control without increasing iron consumption beyond that required by a single-stage treatment yielding the same recovery. Variations in the copper content of the influent solutions to the second cone have ranged, for test purposes, from 1.5 lb of copper per 1000 gal to as high as 15 lb per 1000 gal, yielding the same low content of copper in the tailing from this second cone. The copper-bearing solutions are chemically conditioned in passing through the first cone, thus resulting in rapid and effective stripping of the remainder of the copper in the second unit.

A further variation of the two-stage system is effectively employed in the recently expanded precipitation plant at the Kennecott Chino Mines Division. Larger cone units, each 20 ft in diam and 24 ft high, and thus capable of processing substantially greater volumes of solution, are used to recover over 80% of the copper in the first stage. The conditioned cone tailing is then passed through the preexisting launder plant for final stripping. A single launder cell which previously had a capacity of 300 gpm, can now strip copper from 1000 gpm of the conditioned solution at a relatively low iron consumption. Thus, the combination of cones and launders has provided the technical advantages of the cone precipitator in a plant of greatly expanded capacity at minimum cost.

Two single-stage cone precipitators, of the same basic design as the Utah cones, are also producing copper at Kennecott's Nevada Mines Division. In addition, a modified cone, using a gravity flow from a hillside head tank at a relatively low injection pressure, is under development at the Kennecott Ray Mines Division. A further variation in this particular design provides for cyclical operation with periodic dumping of the copper through the bottom clean-out valve.

SUMMARY

Kennecott's operating experience with precipitation cones has demonstrated that the application of kinetic principles results in the production of precipitate copper of a more granular, higher purity form and at a lower iron consumption than is possible with the older launder methods. High capacity, versatile, precipitating vessels are now available with features permitting automatic control and mechanized materials handling. An old art has been modernized. ME

References

[1] John C. Kinnear, Jr.: New Developments In The Large Scale Porphyry Copper Operations of Kennecott Copper. Presented to joint meeting Minnesota Section AIME and University of Minnesota Mining Symposium, January 11, 1966.
[2] S. J. Wallden, S. T. Henrickson, et. al.: Electrolytic Copper Refining at High Current Densities. *J. Metals*, 11, 528-34 (1959).
[3] C. B. Kenahan, D. Schlain: Deposition of Copper and Zinc from Sulfate and Cyanide Electrolytes. USBM RI 5890 (1961).
[4] D. W. Agers, J. E. House, R. R. Swanson, and J. L. Drobnick: A New Reagent for Liquid Ion Exchange Recovery of Copper. MINING ENGINEERING, Vol. 17, No. 12, pg. 76, Dec. 1964.
[5] T. A. A. Quarm: Recovery of Copper from Mine Drainage Water by Ion Exchange. *Trans.*, Inst. Mining Met. 64, 109-117 (1954-55).
[6] C. H. Keller: US Patent. 2,390,540. Recovery of Copper from Copper-Bearing Solutions, assigned to The Dow Chemical Co.
[7] P. J. McGauley: US Patent 3,053,651. Treatment of Sulfide Minerals.
[8] F. M. Monninger: Precipitation of Copper on Iron. *Mining Congress J.*, Vol. 49, No. 10, pg. 48-51, Oct. 1963.
[9] John Hutti: Anaconda Adds 5000 TPD Concentrator to Yerington Enterprise at Weed Heights. *E & MJ*, Vol. 163, pg. 74, Mar. 1962.
[10] A. E. Back: Use of Particulate Iron In The Precipitation of Copper from Dilute Solutions. Presented 95th Annual Meeting of AIME, New York, N. Y.
[11] R. M. Nadkarni, C. E. Jelden, K. C. Bowles, H. E. Flanders, M. E. Wadsworth: A Kinetic Study of Copper Precipitation on Iron. Presented 95th Annual Meeting of AIME, New York, N. Y.

by GLEN R. DAVIS and ED L. REED
Manager Texas Uranium, Anaconda Co. Consulting Hydrologist, Ed L. Reed & Associates

Controlling Uranium Solution Mining Operations

Early laboratory experiments with cores indicated that in-situ leaching for uranium recovery was possible. A number of underground pilot leach tests were conducted on different types of ore bodies. The technology was improved with continued laboratory testing and field pilot work and with better understanding and application of chemical and hydraulic principles. The licensing agencies of the various states have developed rules and requirements for leach mining such that mining can proceed with the assurance that ground waters will be protected during the leaching operation and remain safe in future years.

The first large scale commercial operation was undertaken by Atlantic Richfield Co. at George West, Tex., in 1975. This first plant produced 250,000 lb of yellowcake per year and has since been expanded to one million lb per year. The state of Texas has taken the lead in developing comprehensive guidelines to implement the licensing process. Other states are drawing on Texas experience and using Texas guidelines as a framework for writing their own rules. Throughout the leaching process the control of fluids and constant attention to the hydrology is of utmost importance.

The leaching process

No two uranium ore bodies are alike. Differences exist in size, depth, thickness, grade, shape, permeability, chemical characteristics of the rocks and grain size, to name a few. Each ore body is an entity in itself and, to be successful in leaching, a great quantity of technical data must be developed for each prospect.

Fig. 1 depicts a long narrow ore body. It is probable that patterns will cover only a part of the ore body initially. As ore is depleted in early wells, they will be phased out and new ones will be drilled. This will have the effect of gradually moving the active patterns and the mining area from one end of the ore body to the other.

Fig. 2 illustrates the arrangement of wells within a pattern. The nine production wells are located at the centers of the five spots and surrounded by 16 injection wells at the corners of the five spots. Twelve deep monitors surround the pattern and two shallow monitors are completed in the first aquifer above the aquifer to be leached.

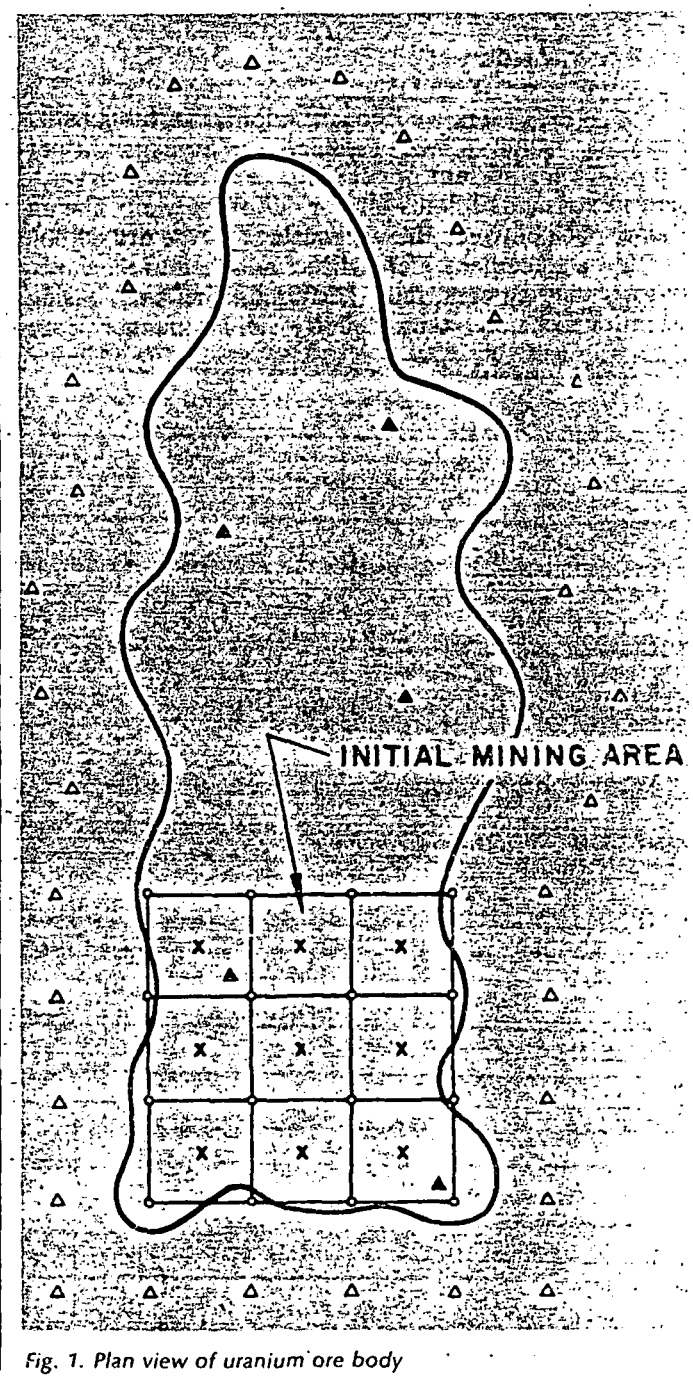

Fig. 1. Plan view of uranium ore body

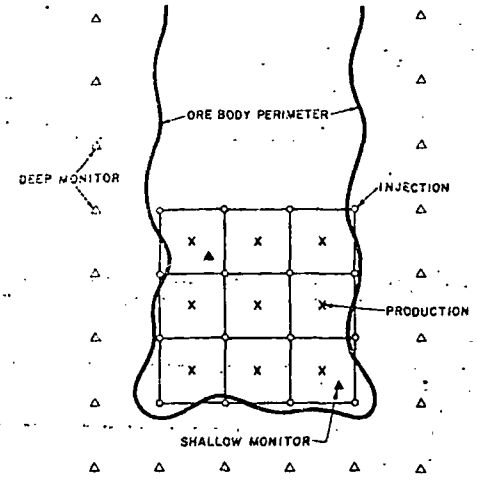

Fig. 2. Arrangement of wells within a pattern

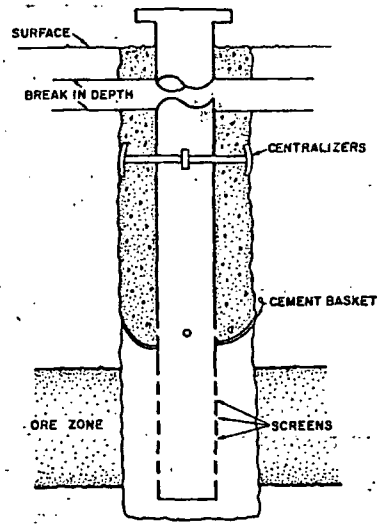

Fig. 3. Well construction

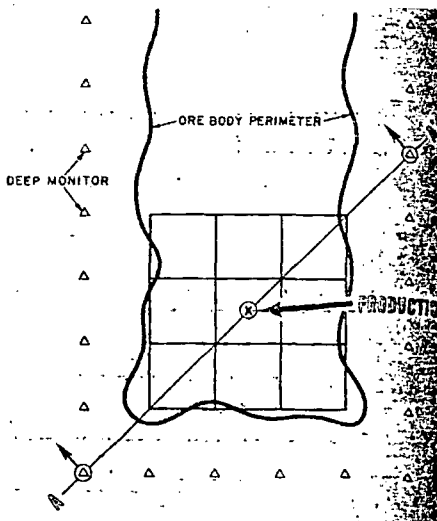

Fig. 4. Pattern area with only center production well completed

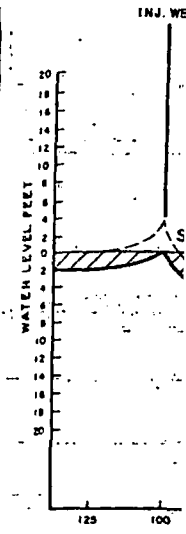

Fig. 8. Multiple w

Well construction

Fig. 3 illustrates well construction. The tubular material is usually PVC or fiberglass. Screens or perforations are present opposite the ore zone interval to permit passage of fluids into or out of the well. The annular space between the well casing and the drilled hole is filled with cement. Centralizers attached to the casing assure that cement fully surrounds the well casing. Monitor wells are completed in a similar manner. Carefully constructed wells minimize the probability that ore zone fluids will migrate upward around the casing and contaminate shallow aquifers.

Fig. 4 represents the same production area as fig. 2 but with only the center production well completed. If this well is pumped, the piezometric surface, along the cross-section A-A, will be as shown in fig. 5. The greater the pumping rate, the greater the drawdown will be. The cone of depression created by fluid withdrawal will cause fluid from the reservoir to flow toward the producing well from all directions as shown in fig. 6. The exterior flow into the mine area resulting from the pressure sink will be the same with one well producing all of the flow or with the same total net volume being produced from a number of wells. To illustrate this, fig. 7 indicates a plan view for the operating well field and fig. 8 shows the piezometric surface. It will be seen that the piezometric surface at the edge of the production zone is below the native or original surface so that the pressure sink in the vicinity of mining will be maintained *provided* production exceeds injection by some amount. When production exceeds injection sufficiently, flow in the reservoir external to the production area will be as shown in fig. 9. In a highly artesian system, an imbalance of one or two percent may be sufficient to control

Fig. 10. Flow line

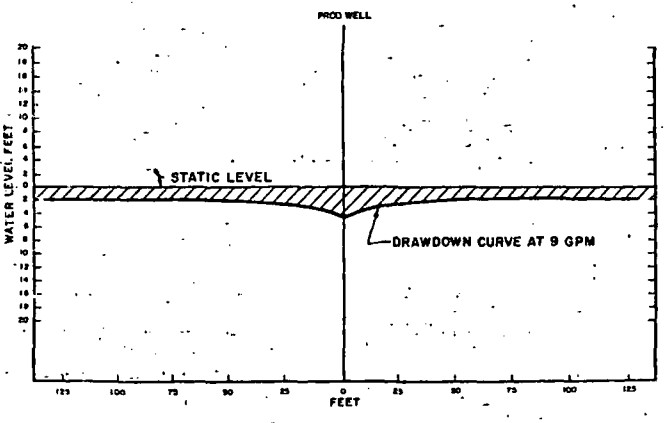

Fig. 5. Single well drawdown profile

Fig. 6. Reservoir flow into a pressure sink

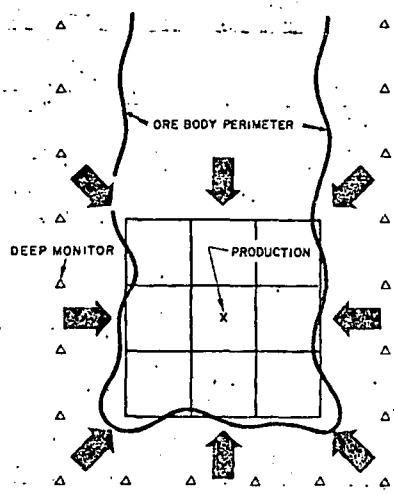

Fig. 7. (far right) Plan view for operating well field

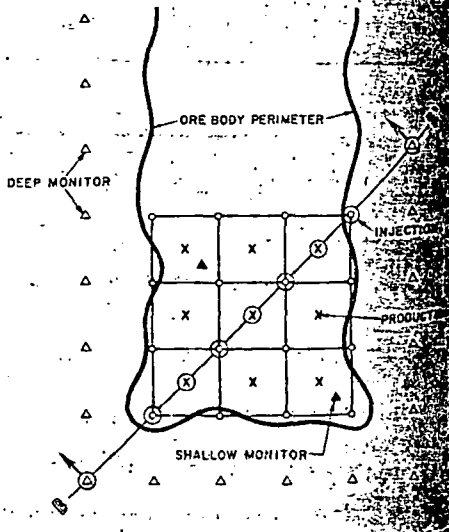

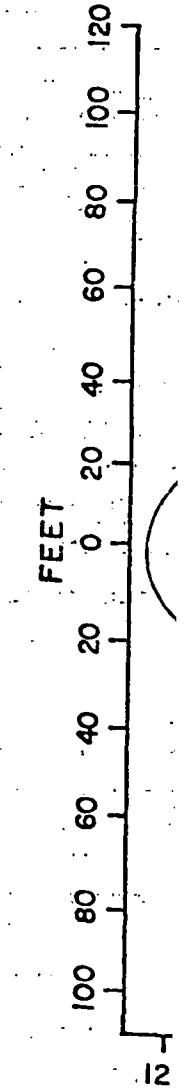

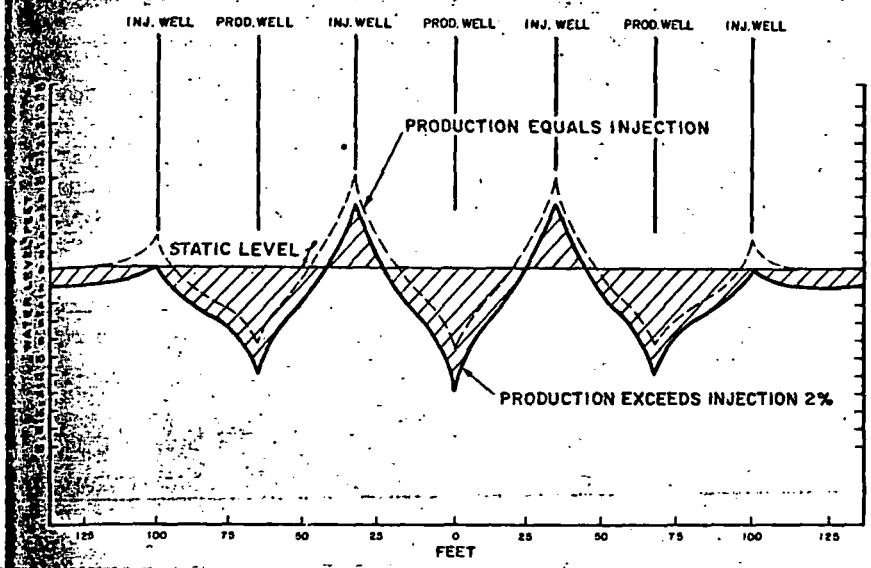

8. Multiple well drawdown profile

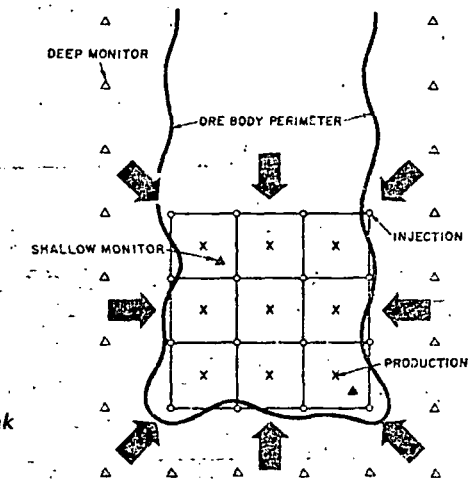

Fig. 9. Reservoir flow into a pressure sink

10. Flow lines of fluid leaving injection well and entering production well

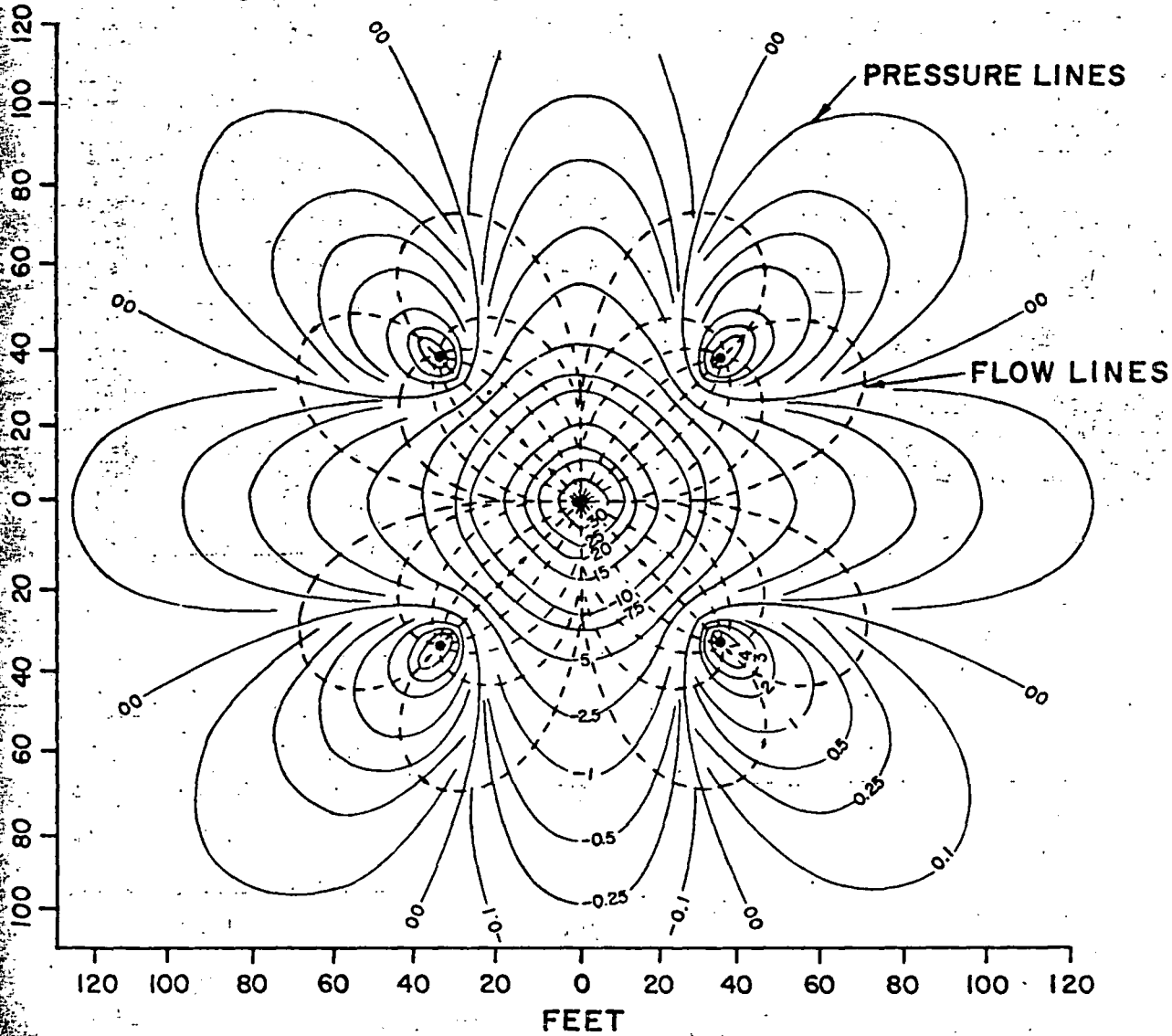

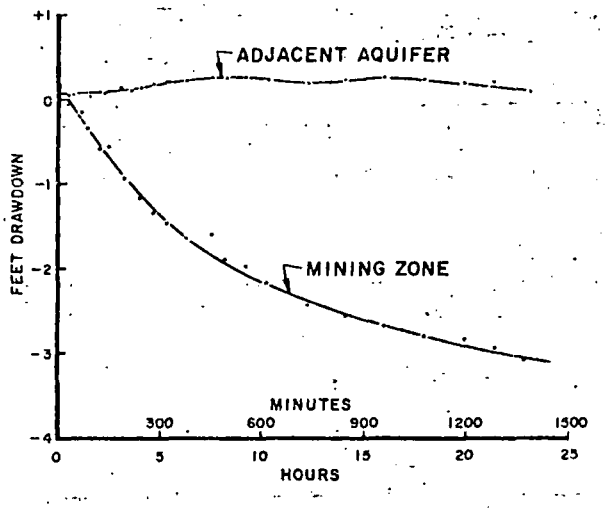

Fig. 11. Drawdown test

the fluid flow. This concept is fundamental to an understanding of fluid retention within the production area "bubble" and when followed carefully will prevent excursions of leach fluid.

Fig. 10 illustrates the flow lines of fluid leaving an injection well and entering a production well. Some of the fluid leaves the boundaries of the pattern and will not return unless an inward fluid flow gradient is superimposed upon the operating 5-spot. This can be done by producing a small amount in excess of the quantity injected.

Environmental considerations

The state of Texas has promulgated rules to be administered by the Department of Water Resources governing in-situ mining for uranium. Basically it is required that pre-existing conditions within the aquifer be determined and that at the completion of mining the reservoir be restored to those conditions. Chemical tests of reservoir waters over a large area are essential to establishing initial baseline conditions. Changes in analyses of monitor well samples during leaching due to the influx of surrounding natural ground waters may indicate that revision of baseline conditions is required.

Aquifers other than that being mined must also be chemically analyzed and hydrologically investigated to guard against their pollution.

A thorough understanding of the geologic framework of the ore zone, together with the super and sub-jacent formations is necessary to a proper evaluation of fluid flow in the mine zone. For example, faults are known to control the accumulation of the uranium and to dictate the direction of ground water flow. Geologic verification of the continuity of sediments and structure is essential to proper placement of mine and monitor wells. As an example, monitor wells drilled across a fault from the mining area may not respond to the mining operation.

Most companies determine the abundance and the nature of the biological chain—the presence of trees, shrubs and grasses, large and small mammals, birds, reptiles and aquatic life. Changes in the abundance, health or habits of biological species may be compared to this baseline by monitoring during the course of the leaching operation. Weather data is required and the extremes of weather data over long periods of time must be known for engineering design.

Ground water hydrology

Proper development of a mine plan for in-situ leach mining must be based upon a determination of the principal hydraulic characteristics of the aquifer. Transmissivity, permeability, storage coefficient and hydraulic gradient can be determined from a properly designed pumping test. The hydrologic study can further show such things as:

1) presence of faults or other boundary conditions
2) continuity of the flow system in the mining zone and to the monitor wells
3) the isolation of the zone to be mined from the overlying and underlying aquifers.

In a simple hydrologic test, fluid is pumped at constant rate from a central well and the water levels (or piezometric surface) at a number of observation wells are monitored. Some of the observation wells should be open to shallower or deeper aquifers where these contain potable water.

Fig. 11 illustrates the manner in which a pumping test from the aquifer to be mined reveals dissimilar responses from an observation well in the aquifer being pumped and another completed in the next overlying aquifer. The failure of the second well to respond to pumping is ample evidence that the wells were cemented properly and the aquifers are hydrologically separated.

Leach mining in areas where external hydrologic stresses may be imposed upon the reservoir require particular hydraulic expertise. Such situations might include:

1) Leach mining next to an irrigation district
2) Two leach mining operations proceeding near each other in the same aquifer
3) Leaching and aquifer restoration proceeding simultaneously in the same zone
4) Leach mining and surface mining operations adjoining and in the same aquifer.

Each uranium ore body is different from any other. It is necessary to gather in great detail a mass of data involving geology, hydrology, geochemistry and ecology. Utilization of this data and the incorporation of laboratory results allows for proper design of the mining facility and the preparation of complete applications for operating permits. Environmental problems can be met and reservoir restoration can be accomplished. ◆

Glen R. Davis is a chemical engineer whose experience ranges from oil and gas engineering and oil reservoir engineering to chemical plant design and Frasch sulfur and uranium production. Currently manager of the South Texas Uranium Projects of the Anaconda Co., he has also worked for Shell Oil Co., Standard Oil Co. of Indiana and Sinclair Oil Corp.

Ed L. Reed is a consulting hydrologist and principal of the firm of Ed L. Reed and Associates. Reed's professional experience includes employment with Atlantic Refining Co. and Standard Oil Co. of Indiana in geology and geological engineering.

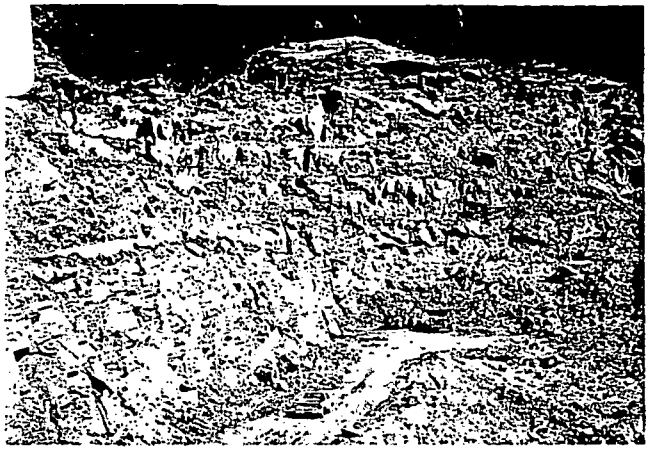

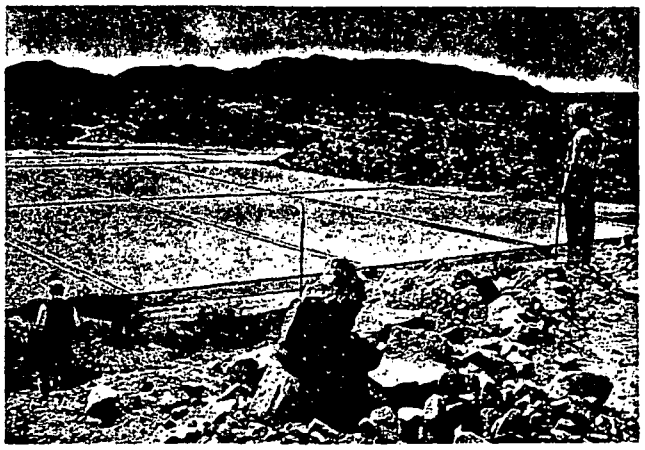

Sierra Pintada uranium deposit, Argentina. Left: Work in progress on the Tigre orebody. Right: View of leaching pad. *(Photos courtesy of Institute of Geological Sciences, London).*

processes is also in preparation. The arsenic content of the concentrates (0.6%) obliges the selection of a process which makes the best use of advanced technology.

Electrical power for the project would be made available through the interconnection of Centromin Peru's system with the national grid (Electroperu). Centromin Peru's lines come within 11km of the Electroperu system which distributes power from the Manataro hydroelectric power station. Centromin has had a feasibility study carried out for a further hydroelectric power station at the Paucartambo II site, which would have a capacity of 126 MW. Adequate water is available in the area, and Centromin has applied for the appropriate water rights. Some labour would be available from the existing town of Morococha, and preliminary plans have been drawn up for a townsite called Pachachaca.

Further details of the Toromocho project are obtainable directly from the Empresa Minera del Centro del Peru, Division Central de Planeamiento, Casilla 4547, Lima, Peru.

Development of Argentinian uranium deposits

BIDS were submitted late last year by two international groups for a 15-year contract to develop uranium deposits at Sierra Pintada in Argentina. The group which wins the contract will work the mines and sell the uranium back to the Argentine National Energy Commission at rates fixed by the Commission.

One bidding consortium consists of Boroquimica SA and Compania Naviera Perez Companc of Argentina, with Noranda Mines Ltd and Rio Algom Ltd. The second consortium consists of the Argentine firms of Alfredo Evangelista y Compania SA, Alianza Petrolera Argentina SA, Sasetru, Inalruco SA, and Petrolera, with the French firms of Uranium Pechiney Ugine Kuhlmann, Societe Technique Enterprise Chimique and the Societe Generale de Recherche et d'Exploitation Mineres.

There are in fact three areas within Argentina where uranium mining is active or under consideration. Sierra Pintada lying in Mendoza province is the largest of these, overall reserves being put at 16,000 tonnes. The district is situated 180km south of Mendoza City and 25km west of San Rafael. Many uranium occurrences have been found in Permian continental cross-bedded sandstone with some conglomeratic intercalations. The sandstone is a member of a very thick sedimentary and volcanic sequence in which tuffs with a high radioactivity are dominant. Many of the occurrences at Sierra Pintada contain less than 200 tonnes of U. The main orebody contains 11,000 tonnes at an average grade of about 1,000ppm. It is a typical stratiform lenticular deposit 14m thick in its central part.

The ore mineral is very fine grained uraninite in sandstone. No other economically interesting minerals are present although about 8-10% calcium carbonate is present. At present only a small satellite orebody is being mined (see photo) and the ore is being sent to Malargue mill 180km away for processing. The main orebody will be exploited by open-pit mining and a new mill will be built closer to the mine by the private companies awarded the contract. Full production is expected to start in 1982/83 with an annual capacity of 400 tons U_3O_8 but will be raised to reach 600 tonnes U_3O_8 in subsequent years, although production potential is put as exceeding 700 tonne/year. Normal grade ores will be processed by conventional methods in the new mill while low grade material containing around 400 ppm will be heap leached. An installation for heap leaching (including the ion exchange plant) is nearing completion (see photo).

Bids have also been received for development and production of uranium concentrate in uranium deposits at Dr. Baulles, Los Reyunos, Sector Tigre 1 and La Terraza — all subsidiary orebodies of Sierra Pintada.

One bidding consortium for development of these consists of Minera Sierra Pintada SA, Sasetru SA, Alianza Petrolera Argentina, Inalruco SA, Alfredo Evangelista SA and Pechiney Ugine Kuhlmann (France). The second group consists of Compania Naviera Perez Companc, Boroquimica SA, Rio Algom Ltd., and Noranda Mines Ltd.

The second of the fairly large Argentinian uranium deposits under active development is that of Los Gigantes, located in the Sierra de Cordoba, Cordoba Province. Sierra de Cordoba is composed of mainly granite batholiths ranging in age from Ordovician to Triassic and intruding Precambrian metamorphic rock. Some plutons contain abnormal uranium (10ppm U and more). The Los Gigantes deposit, which is located about 120km west of Cordoba City, comprises one low grade (300ppm U) orebody.

Exploration was carried out with trenches and galleries and about 10,000m of drilling to an average depth of 70m. Mineralisation, consisting of yellow and green secondary uranium minerals, has proved to be of very recent age with the uranium leached from the granite environment and deposited in brecciated zones. A second important orebody was recently discovered 3km west of Los Gigantes itself. Four companies have reportedly tendered for the exploitation of Los Gigantes.

Argentina's Atomic Energy Commission (CNEA) will buy the uranium concentrate at a price of $72/kg U_3O_8. Total investment in the project is estimated at $8-10 million and production is expected to start in 1981.

In the Cosquin district attention is being given to a deposit at Rudolfo. In the basin of the Cosquin Valley itself, the Eocene member of the Tertiary sequence includes three uranium zones of which one is important. Anomalies were found along a north/south line 20km long. Exploration holes were drilled along the zone to prove the continuity of the mineralisation, and exploration was finally concentrated in the southern 6km of the ore zone. Uranium averaging 550ppm is present as a yellow mineral with a U:V ratio of 1:2 and with a high carbonate content in a mineralised bed averaging 1m thick. Immediately west of the Cosquin Valley a granitic batholith containing large pegmatites rich in beryl and sometimes in uranium crops-out. The uranium potential of the Cosquin district is considered to be high but recovering it will be very difficult because the valley

PLM
for High Voltage Cable Couplers

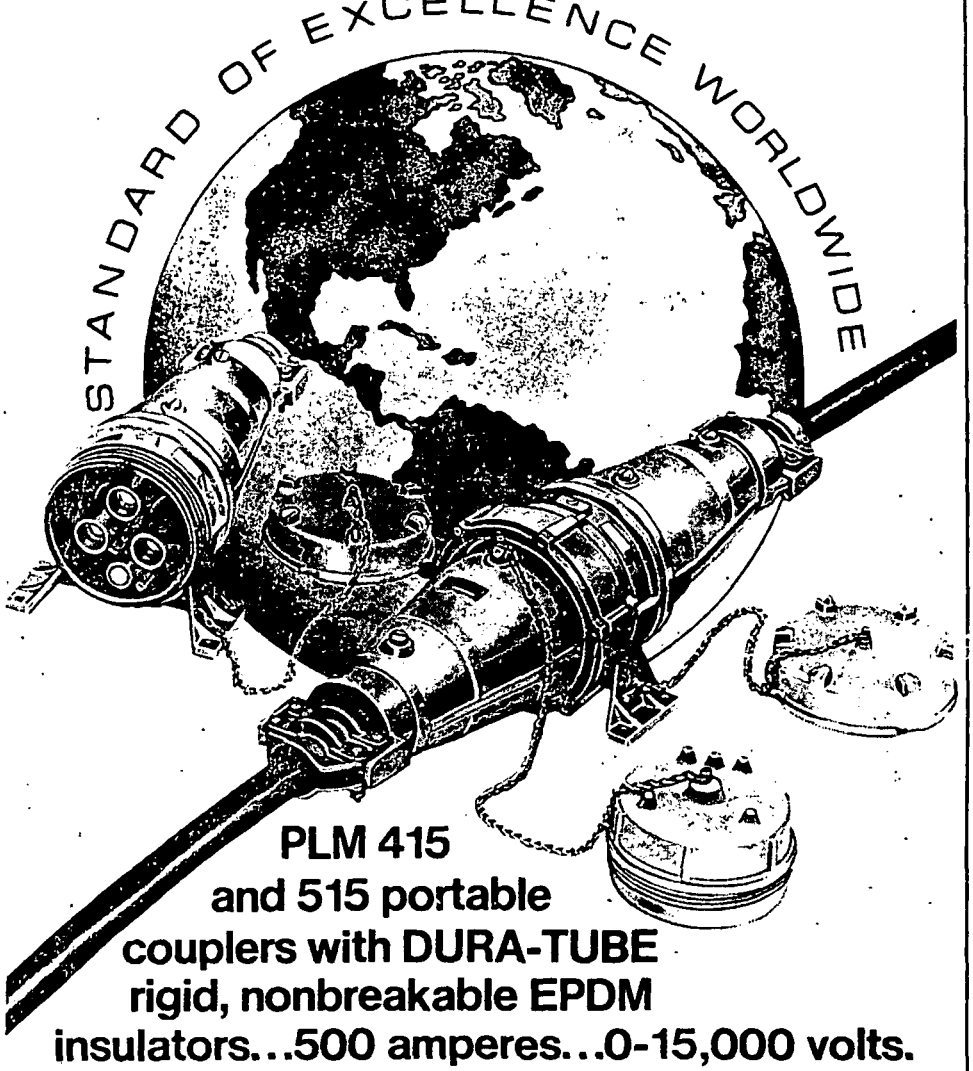

PLM 415 and 515 portable couplers with DURA-TUBE rigid, nonbreakable EPDM insulators...500 amperes...0-15,000 volts.

PLM high voltage couplers are specified worldwide for application in surface and underground mining and portable high voltage power cable applications. 415-515 couplers give superior electrical and mechanical protection. Quik-Thread positive 2½ turn coupling collar eliminates mating problems and makes safe, fast, easy connection.

- Watertight Construction • Corrosion Resistant Aluminum Alloy
- Positive Built-in "First Make Last Break" Ground Connection
- Line or Equipment Mount Types • Ground Check Circuit Contacts

ELECTRICAL CHARACTERISTICS

	No Compound	With Compound
Maximum Voltage Phase-to-Ground	5.5 kV	9.5 kV
1 Minute Dry Withstand AC	35.0 kV rms	45.0 kV rms
6 Hour Dry Withstand AC	25.0 kV rms	35.0 kV rms
15 Minute Dry Withstand DC	65.0 kV aver.	75.0 kV aver
Corona Extinction Level	7.5 kV rms	11.0 kV rms
Basic Impulse Level	75.0 kV crest	95.0 kV crest

All tests per IEEE Standard 48-1962

Ask for Bulletin 894.

ADALET-PLM
Energy related products
4801 West 150 th Street, Cleveland, Ohio 44135
Phone: 216/267-9000
DIVISION OF THE SCOTT & FETZER COMPANY

UNIKAT

Cleans EXHAUST GASES!

The KIRUNA Cleaner

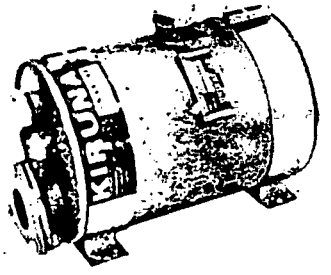

Catalytic exhaust purifier for vehicles

Cleans exhaust gases by after-burning of hydrocarbons, carbon monoxide and aldehydes

Excellent silencer

UNITOX

Portable or mobile exhaust cleaner for workshop use

Solves exhaust problems while starting and running engines indoors

Available both for gasoline and diesel engines

WATER SCRUBBERS

Eliminates black diesel smoke and odors – reduces sulphur and nitrogen oxides

Eliminates sparks

Standard and special models

For the solution to your exhaust problems:

UNIKAT AB
Box 6141, S-20011 Malmö
Sweden • Telex 32546

is a tourist area. The possibilities of exploitation are considered to be limited to a) open pits partly located outside the tourist area and excavated up to a depth of 60m and b) *in situ* leaching processes. The CNEA is studying the possibility of *in situ* leaching to commence in 1981.

Argentina has in fact been looking for uranium for more than 20 years and since the late 1960s has been producing around 180 tonne/year, currently from concentrators at Malargue (mentioned above in connection with Sierra Pintada) — existing production 70 tonne/year; Don Otto (Salta province) 50 tonne/year and Los Adobes (Chubut province) 60 tonne/year. Work is being carried out to double production at Malargue. The first nuclear power plant started up in the country in 1974 and a second is currently under construction. The country's electrical power generation programme is aiming at 3000MW of nuclear capacity by 1990 and 15000MW by 2000. During 1979 $6 million was spent on uranium exploration. Current known reserves are put at around 25,000 tonnes of yellowcake, with additional probable reserves estimated in the region of 16,000 tonnes.

Finance for Dauphin project, Iles de la Madeleine, Quebec

THE government of Quebec recently agreed to a $C51.5 million finance plan to enable SOQUEM (Societe Quebecoise d'Exploration Miniere) to proceed with the implementation of the Dauphin project to develop a salt mine and associated harbour on the Iles de la Madeleine (see map). Quebec anticipates that a further $C17 million will be made available by the federal government's Ministry of Regional Economic Expansion to aid the development of the necessary infrastructure. A new company, "Seleine Mines Inc.", a subsidiary of SOQUEM, has been established to develop and operate the mine.

Of all mineral substances, with the exception of water, salt has the greatest variety of uses. Some 14,000 applications are known in industry, medicine and the household. These range from food preparation to tanning, textiles and chemicals, in addition to its widespread use on roads in winter in the northern latitudes. The province of Quebec has the largest per capita consumption of salt in the world, but currently has no indigenous source it can draw on.

In 1972 a salt bed of uneconomic thickness was discovered at a depth of 148m on the island of Havre-Aubert, the most southerly of the Iles de la Madeliene group. Further exploration using gravimetric surveys revealed in 1974 a massive salt structure under the Rocher-du-Dauphin dunes area of the Grosse Ile at the northern end of the archipelago. Drilling and testwork were undertaken at a number of locations on Grosse Ile, followed by an initial feasibility study in 1976. Construction of preliminary surface works began in 1977 and an exploratory shaft was sunk the following year. Limited underground development and further diamond drilling provided data for the evaluation of the project, which resulted in a decision to proceed.

The salt dome to be mined reaches to within 37m of the surface and drilling has proved its continuation in depth to at least 1,000m. Some 160m below surface it is more or less oval in plan, covering an area 1,600m long by 900m wide. Exploration was carried out by driving more than 910m of 3.5m by 3.5m headings at the 160m level, from which a total of 17,000m of core drilling was carried out. Proved reserves between the 160m and 380m levels have been estimated at 107 million tonnes assaying 95.5% NaCl. Allowing for 25% extraction and a planned annual output of 1.2 million tonnes, this gives sufficient reserves for 20 years.

Production plans call for the mine to use a room and pillar method with a level interval of 50m. Conventional drilling and blasting will be used, the broken salt being loaded by 7.5 or 9m³ load-haul-dump vehicles and carried to an underground primary crusher. To minimise the effects of the diesel powered equipment on the working conditions, the mine ventilation system will be circulating 8,500m³/min of air.

Crushed product will be conveyed to an underground treatment plant housed in a chamber 80m long, 15m high and 15m wide. The crude run-of-mine salt will be further crushed and screened in the 400 tonne/h plant to give a —9.5mm, + 1.0mm product. Fines will be transported back into the mine for dumping in worked-out areas, while the sized product will be stored in bunkers prior to being hoisted in the main No. 2 shaft to surface. The skip loading and hoisting system will be fully automated.

Surface installations at the mine will consist of the winder and headframe, offices, workshops, stores and facilities for the employees.

At surface, the salt will be transported by a series of conveyors a distance of 1.3km to a 15,000 tonne capacity storage silo. This will discharge at rates of up to 2,000 tonne/h by means of belt feeders onto a main conveyor running out to a loading quay. The quay will be constructed on the shore of the Grande Entree Lake, an internal expanse of water almost completely surrounded by the islands of the Madeleine group.

Shipment will be by ocean-going, self-unloading pusher-type barges of 8,000 dwt and 4.9m draught. An access channel 125m wide and at least 6.1m deep will be dredged across the Grande Entree Lake, requiring the removal of more than 2 million m³ of sediments. The channel will be marked by beacons. A 270-day shipping season is anticipated, from April to December, the St. Lawrence being frozen over in the winter.

Numerous studies have been carried out to measure the anticipated environmental impact of the project, to ensure the protection of the unique ecology of the Iles de la Madeleine. In particular it will be necessary to safeguard the other major economic activities of the islands, notably the fishing of lobster, herring and other species. It is believed that the effects of the mine, quay and barge movements on these will be minimal.

The project will create 125 stable jobs in an area where unemployment has been rising. These will be divided roughly as follows: miners 35%, plant operators 10%, maintenance crews 35%, services and supervision 10%, and management and administration 10%. The project will also provide Quebec with a domestic source of a vital product, all of which has at the moment to be imported, and there will consequently be benefits to the finances of the province. (The project is expected to create an added-value of about $C10 million/year compared with the current level of imports evaluated at $C14 million/year). The principal purchasers of the salt are likely to be the Quebec Ministry of Transport, the Quebec Office of Motorways and various municipalities in the province. In addition, there is the possibility of sales outside Quebec.

The first shipment of salt is planned for April 1982. □

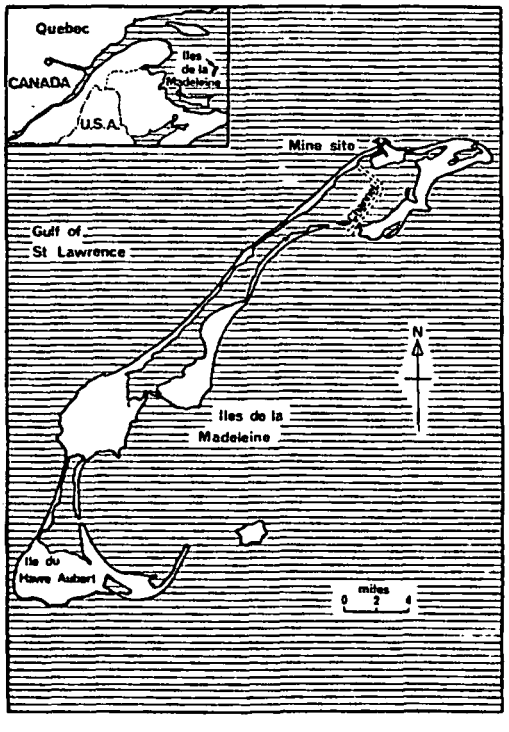

Map showing the location of the proposed mine on the Iles de la Madeleine. Barge movements should aid economic ties between the islands and mainland Quebec, permitting direct return trade.